Investigation of diode-pumped Nd:GdVO4 and Nd:GdYVO4 solid-state lasers

Ng, Siang Ping

2006

Ng, S. P. (2006). Investigation of diode-pumped Nd:GdVO4 and Nd:GdYVO4 solid-state lasers. Doctoral thesis, Nanyang Technological University, Singapore.

https://hdl.handle.net/10356/4962

https://doi.org/10.32657/10356/4962

Investigation of Diode-Pumped $Nd:GdVO_4$ and $Nd:GdYVO_4$ Solid-State Lasers

Ng Siang Ping

School of Electrical & Electronic Engineering

A thesis submitted to the Nanyang Technological University
in fulfilment of the requirement for the degree of
Doctor of Philosophy

2006

ACKNOWLEDGEMENTS

I am grateful first is to my supervisor, A/P Dr. Tang Dingyuan for his valuable advice, continuous guidance, exemplary patience and dedication throughout this period. This dissertation could not have been completed without his great enthusiasm in supervising it. I am especially thankful for his consistent efforts in maintaining a high stimulative environment for research, and this made my graduate life a worthwhile experience.

I would like to express my deep thanks to my co-supervisor, Dr. Xiong Zhengjun (Singapore Institute of Manufacturing Technology, SIMTech) for his enormous support, enlightening advice and discussions. I appreciate having the opportunity to conduct the collaboration project under his supervision. His encouragement, suggestions and full support constitute the crucial factor in the progress and success of this project.

A special acknowledgement goes to Dr. Shen Deyuan (a former fellow in Photonics Research Center) who has inspired me with his knowledge and hands-on experience in laser technology. With his demonstration and guidance, I have been able to initiate my research work.

I am grateful to have had kind help and technical support from technicians in Photonics Lab. 1. Their helping hand has smoothed the progress of this project. Besides this, I would like to thank all the colleagues who have made contributions to my project either in technical support or advice.

Last but not the least, I express my heartfelt appreciation to my parents and friends for their love, care and encouragement accompanying me through this very tough period.

TABLE OF CONTENTS

SUMMARY

Diode-pumped solid-state lasers are under continuous development following the practical demand for compact, high power, as well as pulsed laser sources. In this thesis, general lasing characteristics of two newly developed solid-state gain media, Nd:$GdVO_4$ and Nd:$GdYVO_4$ have been studied. The investigation covers the operation of the lasers in the continuous-wave, passive Q-switching and mode-locking modes, respectively.

Trivalent neodymium doped gadolinium orthovanadate (Nd:$GdVO_4$) crystal is a new gain medium developed after the two commercial Nd^{3+} crystals, Nd:YAG and Nd:YVO_4. Nd:$GdVO_4$ has been studied intensively because of its good optical and thermal qualities for high power laser operation. High thermal conductivity, large absorption and emission cross section, respectively at 808 nm and 1063 nm are some characteristics of Nd:$GdVO_4$ which make it suitable for the advances of laser. Its isomophic mixed laser crystal Nd:$Gd_{0.64}Y_{0.36}VO_4$, possesses the same general features as well. This trivalent neodymium doped mixed-yttrium-gadolinium orthovanadate has only recently been developed, and shows better optical and thermal characteristics than the pure gadolinium orthovanadate. In the present thesis work, the absorption and fluorescent spectra of both laser materials were experimentally characterized. Nd:$GdYVO_4$ was found to have higher absorption coefficient but lower emission cross section than that of Nd:$GdVO_4$ crystal.

Prior to the investigation of the high power laser performance, the thermal effect of both Nd:$GdVO_4$ and Nd:$GdYVO_4$ were explicitly determined. Thermal induced focusing lens is a detrimental factor affecting the cavity stability and mode matching in

the end-pumped laser operation. In this thesis, the thermal focal length of each crystal has been measured to assess its influence in cavity design.

Nd:$GdVO_4$ lasers with different doping concentration were intensively investigated for either the CW or the passively Q-switched operation. Due to its simplicity and compactness, two-mirror cavity was employed for these studies. CW laser was initially constructed with a conventional a-cut Nd:$GdVO_4$ under the proper selection of cavity length. The resonator of the lightly and mildly doped (0.5 at.% and 1.14 at.%) Nd:$GdVO_4$ crystal was kept at about 60 mm in length, while due to the stronger thermal influence, the cavity was shortened to 30 mm for the heavily doped (1.61 at.%) crystal. Experimental results show that Nd:$GdVO_4$ is excellent in CW laser in high power operation. It is particularly efficient for the lightly doped Nd:$GdVO_4$ crystal. A 6.27 W TEM_{00} output power with M^2 of about 1.5 was obtained at the full pump power of 14 W in the laser, giving the average slope efficiency of 62.6%. CW laser performance of the 0.5 at.% doped mixed laser crystal Nd:$GdYVO_4$ has also been confirmed similarly in a 60 mm cavity. Due to smaller emission cross section, the Nd:$GdYVO_4$ laser efficiency laser is poorer than the pure Nd:$GdVO_4$. A 5.2 W output power with $M^2 = 1.53$ was achieved in the laser under the pump power of 12.8 W, at a slope efficiency of about 56.4%.

Under the same cavity configuration, potential of the laser materials in passive Q-switching has been further exploited by using Cr^{4+}:YAG saturable absorber. Nd:$GdVO_4$ laser with the large emission cross section on one hand is good for the CW laser. On the other hand, it could limit the energy storage of a laser during the passive Q-switching process if this is not appropriately designed. To this end, a comprehensive study on the Nd:$GdVO_4$ passive Q-switching with Cr^{4+}:YAG has been conducted. This includes the

influence of laser parameters, such as laser doping concentration, saturable absorption strength, cavity reflectivity, and crystal anisotropy on the passively Q-switched laser performance. The effect of Nd:$GdVO_4$ crystal doping concentration was firstly investigated. It was found that contrary to the CW laser, higher doping concentration of gain medium and saturable absorber is preferable to generate intense Q-switched pulses. By using a Cr^{4+}:YAG of $T_0 = 60\%$, passively Q-switched pulses with the highest pulse energy of 158.2 μJ at a repetition rate of 6.3 kHz were achieved in a 1.61 at.% heavily doped Nd:$GdVO_4$ laser, under the cavity coupling transmission of 40%. The maximum peak power of the Q-switched pulses is 26.4 kW with a pulse width of 6 ns.

Through the natural birefringence of an a-cut Nd:$GdVO_4$ crystal, laser performance was experimentally investigated under different light polarizations. It was then further compared with that of an unpolarized c-cut Nd:$GdVO_4$ laser by using the same experimental parameters. It was found that, though the c-cut Nd:$GdVO_4$ laser could have a good passively Q-switched performance in the low pump power region, the laser performance is influenced by the nonlinear absorptions at the upper energy level, and the thermal induced cavity losses at the high pump power region. Therefore, contrary to the common belief that laser gain media with lower emission cross-section is good for passive Q-switching, the best passively Q-switched Nd:$GdVO_4$ performance has been achieved on an a-cut c-polarized Nd:$GdVO_4$ laser. Stable Q-switched pulses with pulse width of 5.4 ns, single pulse energy of 106 μJ and peak power of 20 kW were achieved in the laser under the cavity transmission of $T = 40\%$, and saturable absorption of $T_o = 60\%$. It is experimentally confirmed that once the Q-switched second threshold is fulfilled, proper combination of the coupling transmission and saturation strength is crucial for

achieving good laser performance. A comparative study of passive Q-switching performance between the lightly doped Nd:$GdYVO_4$ and the pure Nd:$GdYVO_4$ was also conducted. Nd:$GdYVO_4$ passively Q-switched laser successfully showed the highest pulse energy of 111 μJ, and peak power of 14.6 kW with pulse duration of 7 ns under the pump power of 12.8 W. The output is about five times higher than that obtained in the conventional Nd:$GdVO_4$ laser.

High power lasers with bulk crystal commonly have a long cavity length, which limits the generation of narrow Q-switched pulse. In the project, a technique of using the coated GaAs wafer as an output coupler was employed to narrow the passively Q-switched pulses. Based on this simple approach, Q-switched pulses with about three times narrower pulse width were successfully obtained. In such condition, the narrowest Q-switched pulse achieved in the passively Q-switched Nd:$GdYVO_4$-Cr^{4+}:YAG laser is about 2.2 ns, with the maximum single pulse energy of 57.85 μJ and peak power of 26.3 kW. A study on the mechanism of the pulse narrowing showed that the pulse narrowing was not caused by the direct nonlinear absorptions of the GaAs wafer, but could be attributed to the cavity loss variation induced by the free-carrier index grating. The existence of two-photon-absorption (TPA) in the GaAs also introduces a peak limiting effect on the Q-switched pulses, which further stabilized the pulse peak power.

In experiment, it was frequently observed that accompanying the main passively Q-switched pulse, there is a secondary pulse in the Nd:$GdVO_4$ lasers. To find out the forming mechanism of satellite pulse, Q-switching dynamics of the laser was theoretically and experimentally studied. It was firstly revealed that the satellite pulse is caused by the finite relaxation lifetime of the lower laser energy level. By further taking

into account the effective pump rate, and the thermally induced change of the cavity mode size ratio between gain medium and saturable absorber, passively Q-switched pulse properties and the secondary pulse were well reproduced. Based on the good agreement of the simulated result and the experimental observation, the lower energy level lifetime of Nd:$GdVO_4$ is estimated to be about 20 ns.

It is a well-known fact that passively Q-switched lasers normally exhibit strong pulse energy and repetition rate jitters. However, the physical mechanism of the phenomenon has so far been unclear. In this thesis, the dynamics of the CW pumped passively Q-switched Nd-ion doped lasers have also been investigated. Clear period-doubling cascade and route to chaos, as well as an odd number of periodic windows are observed in the Nd-doped lasers, including the passively Q-switched Nd:$GdVO_4$, Nd:$GdYVO_4$, Nd:YAG and Nd:YVO_4 lasers. These experimental results suggest that the time jitters of the Q-switched pulses are an intrinsic property of the lasers, which is caused by the laser dynamics. Experimental studies have revealed that a strong pump could saturate the ion population in the laser ground state. It could cause the chaotic laser dynamics, when combined with the effect of the slow emptying lower laser energy level. Therefore, with an extended rate equations model, which takes into account of these two effects, the observed Q-switching dynamics of the Nd:$GdVO_4$ laser have been simulated.

Compared with the Nd:YAG, Nd:YVO_4 and Nd:$GdVO_4$, the Nd:$GdYVO_4$ laser which has broader gain bandwidth, was further exploited for the generation of narrow mode-locked pulses. Experiments on the passive mode-locking of Nd:$GdYVO_4$ laser were conducted either with the Cr^{4+}:YAG or the GaAs as saturable absorber in a Z-fold cavity configuration. Through proper designing the laser cavity, both Q-switched and

continuous-wave mode-locking were successfully achieved in the lasers. A continuous-wave mode-locking was firstly realized in Nd:$GdYVO_4$ laser with the Cr^{4+}:YAG crystal as saturable absorber, generating the mode-locked pulses of about 2.96 ps in duration and repetition rate of 161.3 MHz. A period-doubling cascade was also observed in the Q-switched mode-locking of the laser. However, it was found that the nonlinear dynamics feature did not affect the mode-locking process. This further confirms that the deterministic chaos is an intrinsic feature of the diode-pumped passively Q-switched Nd-doped lasers. Under the same cavity configuration, Nd:$GdYVO_4$ was also passively mode-locked by GaAs wafer. Continuous-wave mode-locking could be easily achieved by using the GaAs wafer as an output coupler. However, the mode-locked pulses have longer pulse duration which is about 8.8 ps at a repetition rate of about 161.3 MHz.

LIST OF FIGURES

LIST OF TABLES

Chapter 1

Introduction

1.1 Motivation

Nowadays, the laser has found widespread applications from data storage (barcode scanner, CD/DVD players and CD-ROM drivers), industrial microprocessing (scribing, cutting, marking, etching and drilling), medical and cosmetic surgery (LASIK eye surgery, dental treatment, scar and hair removal, wrinkle treatment), to laser light shows, telecommunication and scientific researches. Each of the lasers operates on the same principle of the stimulated emission, which was introduced by Einstein in year 1916 in his proof of Planck's law [1], and experimentally proved by Wefer using microwave transition after almost forty years [2]. Maiman successfully demonstrated the first laser in 1960 [3].

Basically a laser system should consist of three elements: a gain medium for light amplification, an optical pump source to produce the population inversion in the gain medium for stimulated emission, and a cavity to confine light and provide the optical feedback. There are typically four types of laser gain media: gas, liquid, solid-state and semiconductor, with different characteristics for specific applications. Of all of these, solid-state laser materials are doped crystal hosts, which are stable and durable in use compared with the gas and dye materials.

Generally, active ions in the solid-state laser materials determine the lasing wavelengths, while the host materials decide primarily the optical and thermal properties

of the gain medium. The active ions are commonly selected from the transition metal ions and rare earth ions group, which have an incomplete electron shell for optical transition. Rare earth ions with pure narrow electronic transitions and hence less stringent to the temperature are particularly favorable for diode pumping in most of the operations. Of all of these, triply ionized neodymium ion (Nd^{3+}) has received specific attention because of its appropriate four-energy level structure for a creditable lasing performance and the ease of doping. The main Nd-doped lasers emission is in the near-infrared region, in which the sharp fluorescent spectrum and less temperature impact on the lasing action are crucial for many applications. The fixed near-infrared Nd lasers may also be exploited in either visible or mid-infrared wavelength through the nonlinear frequency conversion.

In the early stage, arc lamp and flash lamp are the common pump source of solid-state lasers. The inert gas filled lamps not only has to be replaced after the usage of 500 to 2,000 hours, the major difficulty of these power consuming systems, which require high driving voltage, is the need to remove the waste heat from cavity. Circulating water is thus needed with a separate chiller unit for cooling. Due to the broad emission spectra, bulky physical size and poor beam quality of the light sources, the laser systems generally operate with low efficiency. The solid-state laser progresses greatly with the maturity of laser diode technology. Compared to the flash lamp sources, diode laser has a clearly improved lifetime with operating duration of 30,000 hours up to 500,000 hours in the recent technology. The mass produced high power laser diodes is considerably low cost, and with a continuously falling pricing (with approximately 1 W bare laser diode in US$ 10 range) following the steady development of the semiconductor fabrication technology.

In contrast to the lamp pumped system, the well match spectra between diode emission and solid-state laser absorption band enables a compact fiber coupled laser configuration with high optical transfer efficiency of exceeding 50%. This helps to reduce thermal effects in the gain medium and improve the laser for a stable output and a nearly perfect emission beam. Due to the low heat dissipation, air-cooling is thus possible to further reduce the size and simplify the system maintenance. Besides, to be beneficial with the low electrical power consumption, an efficient laser with diode pumping is also able to operate with just a single phase DC (direct current) power supply. The great enhancement is found in Nd^{3+} doped lasers, whose absorption bands are well matched with the GaAlAs diode emission wavelength at 700 nm - 900 nm. In conjunction with the laser efficiency, beam quality and the marketable running cost, laser diode pumping hence becomes interesting as a replacement for the flashlamp in constructing the compact diode-pumped Nd^{3+} solid-state lasers.

Despite that the diode-pumped solid-state (DPSS) laser operation relies on optical pump source instead of direct current injection, and its cost is also not as cheap as the 'matchbox' size diode arrays, DPSS is apparently exempted from some optical inferiors found in the semiconductor laser. The most advantageous characteristic of solid-state lasers is its coherent and narrow-linewidth emission which is irreplaceable by electrical pumped semiconductor lasers. Compared to semiconductor lasers, the prominent features of the solid-state lasers in giving intense fluorescence and high energy storage capability are essential to develop the laser techniques for pulse generation. High peak power, ultrashort pulses, which are generated through Q-switching or mode-locking technique from the compact lasers are more favorable for applications. The Q-switching method is

widely used to generate the intense pulses with kilowatt to megawatt peak power. Operating on the basis of the simple cavity gain and loss modulation, the Q-switched lasers become interesting light sources in ranging finder application, laser marking and also in the clinical practice of dermatology. The Q-switched laser pulse is normally limited by resonator length to the nanosecond duration. To achieve even short pulses in picosecond to femtosecond regime, mode-locking technique is commonly applied. By phase locking all the longitudinal modes in the cavity, a very short pulse traveling back and forth in the cavity can be generated. The mode-locked pulses are applied in those applications which require the short time resolution or ultrahigh peak power, namely in bioscience, photochemistry and material reaction process studies. It can also be used for material fine processing, surgery, high-speed communication systems and ultrafast data processing.

It is expected that the fields of laser applications will increase in the near future with every breakthrough in understanding. Research on the diode-pumped lasers, which combine the compactness, efficiency, and high optical intensity and energy are crucial to meet a growing number of scientific, medical, and industrial practices. In the present thesis, the diode-pumped laser performance at different operating modes of two newly developed solid-state laser materials, namely the neodymium gadolinium vanadate (Nd:$GdVO_4$) and the neodymium mixed-gadolinium-yttrium vanadate (Nd:$Gd_{0.64}Y_{0.36}VO_4$) will be investigated intensively. The thesis is hence entitled "Investigation of diode-pumped Nd:$GdVO_4$ and Nd:$GdYVO_4$ solid-state lasers".

1.2 Objectives

The dissertation is directed toward the design and development of the diode-pumped high -power solid-state lasers using the newly developed Nd:$GdVO_4$ and Nd:$GdYVO_4$ solid-state laser materials. The research contents are categorized into three portions, which are investigation for continuous-wave, passive Q-switching, and mode-locking operations.

Corresponding to the relatively large emission cross section of the crystals, high efficiency, and low threshold continuous-wave laser output is expected to be obtained in the lasers. The fundamental consideration in achieving the high power laser operation is in the thermal influence in cavity design. Theoretical and experimental investigation on the thermal lensing will be carried out prior to the laser studies. This is on the objective to avoid the thermal induced cavity instability, and to obtain a good cavity mode-matching in gain medium for higher efficiency of the laser output. In order to construct a compact laser cavity, passive Q-switching technique by using Cr^{4+}:YAG as saturable absorber will be selected. Considering the poor passively Q-switched performance of Nd:$GdVO_4$ laser has so far been attributed to the large emission cross section of the laser, attempts to achieve the high peak power pulses in passively Q-switched Nd:$GdVO_4$ laser are expected to be a challenge in the project. Therefore, effects of the laser parameters such as laser doping concentrations, cavity transmission, saturable absorption strength, and crystal anisotropy will be investigated explicitly for the optimum Q-switched output. Since Nd:$GdYVO_4$ is understood to have a slightly smaller emission cross section than the Nd:$GdVO_4$, a comparative study of passive Q-switching is planned between these two lasers. Actually the high power lasers with bulk crystal commonly have a long cavity length, which is expected to limit the generation of narrow Q-switched pulse. In

considering this feature of high power lasers, Q-switched pulse narrowing method is going to be studied to shorten the laser pulse duration and enhance the Q-switched peak power. This study will involve a semi-insulating GaAs semiconductor, which has been widely reported as having strong photorefractive effect and nonlinearities. To understand the diode-pumped passively Q-switched laser behavior, experimental investigation and numerical simulation are planned specifically on the dynamics of passive Q-switching, which has so far not been clearly addressed. For the purpose of ensuring the general dynamical property in the continuously diode-pumped passively Q-switched lasers, besides Nd:$GdVO_4$ and Nd:$GdYVO_4$, dynamic studies will be carried out by using other major Nd^{3+} lasers such as Nd:YAG and Nd:YVO_4. Since Nd:$GdYVO_4$ possesses a broad gain bandwidth, which is favourable for generating ultrashort pulses, the excellent feature of the Nd:$GdYVO_4$ laser is planned to be exploited in the passive mode-locking process. This investigation will be carried out by using Cr^{4+}:YAG crystal and GaAs wafer, respectively in a Z-fold cavity configuration. Through the investigation of the Nd:$GdVO_4$ and Nd:$GdYVO_4$ characteristics in high power laser operations for the continuous-wave, intense and ultrashort pulse generation, their potential as a compact solid-state laser source will be of great interest for wide range of applications in the future.

1.3 Major contributions of the thesis

The optical properties and thermal effect of Nd:$GdVO_4$ and Nd:$Gd_{0.64}Y_{0.36}VO_4$ were determined experimentally prior to the investigation of laser performance. The thermal induced focal lens was measured explicitly for each crystal in order to provide a proper cavity design. Thermal effect incurred in the neodymium mixed-gadolinium-yttrium

vanadate was experimentally found to be weaker than that in the neodymium gadolinium vanadate crystal. Based on the experimental measurement and theoretical calculation, the temperature-dependent refractive index change (dn/dT) of the Nd:$GdYVO_4$ crystal is deduced to be 3.5×10^{-6} K^{-1}.

Based on the measured thermal focal lens, a high efficient CW Nd:$GdVO_4$ laser operating at 1063 nm has been designed and developed. The laser was constructed by a lightly doped a-cut Nd:$GdVO_4$ crystal as gain medium, and was found efficient at high power operation, giving an average slope efficiency of 62.6%. At the full pump power of 14 W, a maximum output power of 6.27 W with M^2 of about 1.5 was obtained in the laser. Comparatively, CW laser performance of the lightly doped Nd:$GdYVO_4$ laser is slightly poorer because of its smaller emission cross section. A 5.2 W output power with M^2 = 1.53 low-order transverse mode was achieved in the laser under the pump power of 12.8 W, at a slope efficiency of about 56.4%.

Under optimized cavity configuration, passively Q-switched Nd:$GdVO_4$ laser with Cr^{4+}:YAG saturable absorber was experimentally characterized. In contrast to the CW operation, Nd:$GdVO_4$ laser with high doping concentration was found to be more favourable in achieving high peak power of Q-switched pulses. By using a 1.61 at.% heavily doped Nd:$GdVO_4$ crystal, maximum Q-switched peak power of 26.4 kW with pulse width of 6 ns was successfully achieved in the laser, which is known as the best result in the passively Q-switched Nd:$GdVO_4$ laser. Through the study of the crystal anisotropic effect on the passive Q-switching, the a-cut Nd:$GdVO_4$, which has a large emission cross section, was found to be efficient in generating the intense Q-switched pulses. This shows that the common belief that lower emission cross-section is good for

passive Q-switching is not absolute to each laser in every condition. According to the demonstration, proper combination of laser parameters was found to be most crucial to generate high peak-power Q-switched pulses in such a large gain cross section laser.

A comparative study of passive Q-switching performance between the lightly doped Nd:$GdYVO_4$ and Nd:$GdVO_4$ was also conducted. Nd:$GdYVO_4$ passively Q-switched laser successfully showed the highest pulse energy of 111 μJ, and peak power of 14.6 kW with pulse duration of 7 ns under the pump power of 12.8 W. The output is about five times higher than that obtained in the conventional Nd:$GdVO_4$ laser. In the same cavity configuration, a technique of using the coated GaAs wafer as an output coupler was employed to narrow the passively Q-switched pulses. Based on this simple approach, Q-switched pulses with about three times narrower pulse width were successfully obtained. The narrowest Q-switched pulse achieved in the passively Q-switched Nd:$GdYVO_4$-Cr^{4+}:YAG laser is about 2.2 ns, with maximum single pulse energy of 57.85 μJ and peak power of 26.3 kW. A study of the pulse narrowing mechanism showed that the Q-switched pulse narrowing was not caused by the direct nonlinear absorptions of the GaAs wafer, but could be attributed to the cavity loss variation induced by the free-carrier index grating. The existence of two-photon-absorption (TPA) in the GaAs also introduces a peak limiting effect on the Q-switched pulses, which further stabilized the pulse peak power.

Generally, a secondary pulse has been observed in the passively Q-switched pulse profile under certain conditions. The formation mechanism of satellite pulse in the passively Q-switched Nd:$GdVO_4$ laser was firstly investigated in the numerical simulation. The finite relaxation lifetime of the lower laser energy level is found to be

detrimental to delaying the laser extraction from the upper energy level. This results in two stages of relaxation to fully release the stored energy at the upper energy level, and forms a satellite pulse subsequent to the main Q-switched pulse. Based on the good agreement between the calculated and the experimentally measured pulse properties, relaxation time of the lower energy level in Nd:$GdVO_4$ is determined to be about 20 ns.

Dynamics of the CW pumped passively Q-switched Nd-ion doped lasers has been investigated to understand the physical mechanism of the Q-switched pulse energy and repetition rate jitters, which are so far unclear. Clear period-doubling route to chaos, as well as odd number of periodic windows are observed in the Nd-doped lasers, including the passively Q-switched Nd:$GdVO_4$, Nd:$GdYVO_4$, Nd:YAG and Nd:YVO_4 lasers. By using an extended rate equations model, which takes into account the saturation of ground state population, and the slow emptying lower laser energy level, the observed Q-switching dynamics of the Nd:$GdVO_4$ laser have been simulated. These experimental results suggest that the time jitters of the Q-switched pulses are an intrinsic property of the lasers, which is caused by the laser dynamics.

The passively mode-locked Nd:$GdYVO_4$ operation has been firstly demonstrated. Cr^{4+}:YAG crystal and GaAs wafer were respectively used as saturable absorber for the mode-locking. Both Q-switched and continuous-wave mode-locking were successfully achieved. In particular, the first continuous-wave mode-locking was demonstrated by using the Cr^{4+}:YAG crystal. The mode-locked Nd:$Gd_{0.64}Y_{0.36}VO_4$-Cr^{4+}:YAG laser has a pulse width of about 2.96 ps at a repetition rate of 161.3 MHz. While using the GaAs output coupler, mode-locked pulses of 8.8 ps were obtained in the laser under the same cavity configuration.

1.4 Organization of the thesis

This thesis describes the experimental and theoretical investigation on the diode-pumped Nd:$GdVO_4$ and Nd:$GdYVO_4$ lasers. The properties of the Nd:$GdVO_4$ and Nd:$GdYVO_4$ laser materials are firstly discussed in Chapter 2. In addition, fundamentals of the passive Q-switching and passive mode-locking are reviewed, including the basic principles of the Cr^{4+}:YAG and GaAs saturable absorber. Chapter 3 contains the investigation of the CW operation of the diode-pumped Nd:$GdVO_4$ and Nd:$GdYVO_4$ lasers. These include the thermal effect on the laser, cavity design, and the experimental characteristics of the lasers performance. Detailed experimental studies on the diode-pumped passively Q-switched lasers are given in Chapter 4. The chapter begins with the investigation on determining the factors for the optimized Nd:$GdVO_4$ Q-switched laser output. It is followed by the comparative study of the Nd:$GdYVO_4$ laser in passive Q-switching, and the proposed pulse enhancing method, which is employed to further improve the generated Q-switched pulse peak power. The investigation of the passively Q-switched pulse profile of Nd:$GdVO_4$ laser under different laser parameters is explicitly shown in the last portion of the Chapter 4. Chapter 5 deals with the numerical simulation on the Q-switched satellite pulse generation in Nd:$GdVO_4$ lasers which is observed in the experiments. Both the experimental observation and the numerical simulation on the chaotic dynamics in various Nd-doped passively Q-switched lasers are presented in Chapter 6. Experimental studies on the passive mode-locking of the diode-pumped Nd:$GdYVO_4$ are discussed in Chapter 7. Chapter 8 presents the conclusion of the work in the thesis. Included in this chapter are suggestions for future work that needs to be undertaken for further development.

CHAPTER 2

Fundamentals of laser materials and operations

Solid-state laser materials are understood to be a solid-state host doped with a small quantity of active ions, which provide the optical transition within the free-ion electronic states. Rare earth ions, particularly the Nd^{3+} doped solid-state laser materials, with an intense luminescence and a relatively long fluorescent lifetime, are of great interest for laser operation. Laser gain medium is the basic component that affects output efficiency and performance of a laser under certain operating conditions. For instance, a gain medium with a large stimulated emission cross section is preferred for the continuous-wave laser, but might not be prominent for the Q-switched laser operation if the laser is not appropriately designed. The effect of the optical property is more apparent in condition where the laser performance is solely dependent on the interaction between radiation and matter. Therefore, background studies of the gain medium, and the understanding on the laser mechanisms are essential to this thesis.

This chapter begins with a review on the characteristics of Nd^{3+} solid-state laser materials to bring out the optical and thermal features of the newly developed Nd:$GdVO_4$ and Nd:$Gd_{0.64}Y_{0.36}VO_4$ crystals. The fundamentals of passive Q-switching and mode-locking are discussed. The relevant experimental parameters and criteria for the effective pulsed laser operations are derived. This provides important guidelines for laser design and optimization. Consequently, properties of the Cr^{4+}:YAG and GaAs saturable absorbers that are used for pulse generation will be described.

2.1 Properties of trivalent neodymium ion

Trivalent neodymium ion is the most successful and commonly used rare earth ions in solid-state laser materials. The 780nm and 810nm absorption bands of the Nd ions are particularly suitable for the AlGaAs laser diode pumping to excite the Nd^{3+} ions in the ground state to either $^4F_{7/2}$ (~ 760 – 780 nm) or $^4F_{5/2}$ (~ 795 – 815 nm) energy levels. The rapid non-radiative decay brings the excited ions to the metastable $^4F_{3/2}$ level before further relaxing down to the lower terminating levels. This metastable lifetime is typically in the microsecond range, and varies according to host material and ions doping concentration. There are two main photon decays from the metastable level are the $^4F_{3/2} \rightarrow {}^4I_{11/2}$ transition, which produce near infrared radiation at 1.06 μm, and the $^4F_{3/2} \rightarrow {}^4I_{13/2}$ transition for the radiation at about 1.34 μm. Without the significant population in the lower lasing level that results in reabsorption, both of these optical transitions are four level systems, giving an efficient laser operation at 300K and above. Another two possible transitions take part between $^4F_{3/2} \rightarrow {}^4I_{9/2}$ and $^4F_{3/2} \rightarrow {}^4I_{15/2}$ for the fluorescent at 0.94 μm and 1.82 μm, respectively. After the fluorescent relaxation, there is then a fast phonon decay to complete the ion transition cycle from the terminating level back to the ground state.

For crystalline materials the fluorescence efficiency from the metastable state is typically greater than 99.5% [4]. This indicates that the excited state absorption is less significant in the Nd-doped lasers. Intense emission lines of Nd^{3+} ions generally yield a relatively large stimulated emission cross section in the order of $1 - 10 \times 10^{-19}$ cm^2 for efficient lasing. In the transitions, 1064 nm fluorescent transition is the most used wavelength. The highest branching ratio from the metastable level and the four-level

nature energy level make it the standard wavelength for many high power laser systems. Since interaction between the crystal field and the active ions is a significant factor to alter the Nd-doped laser characteristics, there is a continuous interest in developing new crystalline host with higher quality for the prominent lasing action.

Up to now, Nd^{3+} ion has been successfully used to lase in many kinds of laser hosts. Among them, Nd:YAG is the famous Nd-doped laser. The isotropic YAG host has a good thermal conductivity of 11.1 W/meter K, which can be used for either the high power CW or pulsed operation. With an effective emission cross section of 2.8×10^{-19} cm^2 [5], Nd:YAG is advantageous to produce the intense Q-switched pulse. The small emission gain, on the other hand, is the cause of the high lasing threshold in laser operations.

Ever since the 70's when the neodymium yttrium vanadate crystal (Nd:YVO_4) was invented, it was found to have some better optical features over Nd:YAG. Spectroscopic studies showed that the emission cross-sections of Nd:YVO_4 at 1064 nm and 1342 nm are much larger than those of the Nd:YAG [6, 7]. Benefiting from the larger stimulated emission cross-section at the lasing wavelength, Nd:YVO_4 laser is able to maintain strong single line emission at lower lasing threshold. With broader absorption bandwidth [8], Nd:YVO_4 can be efficiently pumped, without the influence of the temperature induced wavelength shift in laser diode. Since the a-cut vanadate crystal is uniaxial, polarized laser output can be obtained. Following the development of reliable high power laser diodes, the first demonstration of an efficient, end-pumped Nd:YVO_4 laser was achieved in the 1980's [9]. Strong absorption coefficient and high emission gain of Nd:YVO_4 shows higher output power than Nd:YAG laser in the low pumping

regime. However, the poor thermal quality of Nd:YVO_4 limits its application in high power laser operation. This shows the need for the development of a higher quality new crystal host with similar excellent optical properties as provided by Nd:YVO_4.

In year 1992, the first Nd:$GdVO_4$ crystal was developed using the Czochralski method [10]. Results showed that this new crystal possesses good optical and thermal properties indicating that Nd:$GdVO_4$ has good potential to replace the commercial Nd:YAG and Nd:YVO_4 for many applications [11 - 13]. The development of Nd:$GdVO_4$ was obstructed by difficulties in growing high quality crystal due to the interface instability and scattering problem [14]. In the recent several years, the Nd:$GdVO_4$ crystal quality has been improved intensively. A liquid synthesis approach was reported to replace the conventional solid-phase reaction method in growing Nd:$GdVO_4$ through the Czochralski pulling method [15]. This liquid phase synthesis could effectively purify the polycrystalline materials and minimize the solid impurities for a large dimension of crystal growth. Nd:$GdVO_4$ has hence attracted great attention for high power lasers.

Based on the close similar melting point of Nd:YVO_4 and Nd:$GdVO_4$ at about 20 ^{0}C, very recently, the excellent potential of Nd:$GdVO_4$ has been further improved through the mixture of Gd^{3+} and Y^{3+} ions in vanadate crystals by using the same liquid-phase synthesis Czochralski method. Initial studies revealed that the Nd:$Gd_xY_{1-x}VO_4$ crystals have higher potential in high power laser applications compared to the pure Nd:$GdVO_4$ crystal. Because of the flexible vary of the Gd/Y mixing concentration, this Gd/Y ratio becomes crucial in determining the thermal and laser properties of the crystals [16, 17], such as absorption and emission cross section, fluorescent lifetime and gain bandwidth. In particular, Nd:$Gd_xY_{1-x}VO_4$ with x = 0.64, has been experimentally

characterized. It possesses a relatively lower emission cross section, larger laser emission bandwidth and slightly longer fluorescent lifetime compared with the pure neodymium gadolinium vanadate crystal [18], therefore, it is more attractive for pulsed laser operation.

2.2 Development of Nd:$GdVO_4$ and Nd:$GdYVO_4$ mixed crystals

Based on above considerations, this thesis concentrates mainly on the development of diode-pumped solid-state lasers of the newly developed vanadate crystals, Nd:$GdVO_4$ and the mixed Nd:$GdYVO_4$. Each of these hosts modifies the characteristics of the doped Nd^{3+} ions according to the crystal field. The properties of these laser materials compared with their isomorphous Nd:YVO_4 and the versatile Nd:YAG are discussed, after a brief historical overview of the development of each of the hosts. The absorption and fluorescent spectra of Nd:$GdVO_4$ and Nd:$Gd_{0.64}Y_{0.36}VO_4$ samples have also been checked in the experiment

2.2.1 Crystal structure and orientation

Vanadate crystals like yttrium, gadolinium or the mixed-godolinium-yttrium vanadate compounds are in the same oxide group crystallizing in a zirconium silicate ($ZrSiO_4$) structure [19 - 21] as shown in Fig. 2.1. They all belong to tetragonal space group of $I4_1/amd$. As for a pure $GdVO_4$ crystal host, the Zr^{4+} and Si^{4+} in lattice respectively represent the Gd^{3+} and V^{5+} ions. Each vanadium ion V^{5+} is coordinated by four oxygen ions O^{2-} to become vanadate. While Gd^{3+} ion is surrounded by eight O^{2-} in the crystal host. For better understanding, the simplified structure is schematically shown in Fig. 2.2.

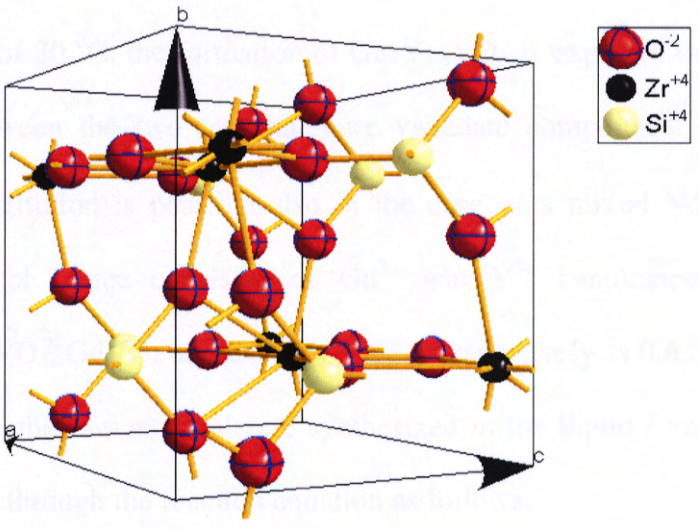

Fig. 2.1: The typical zircon (zirconium silicate) structure.

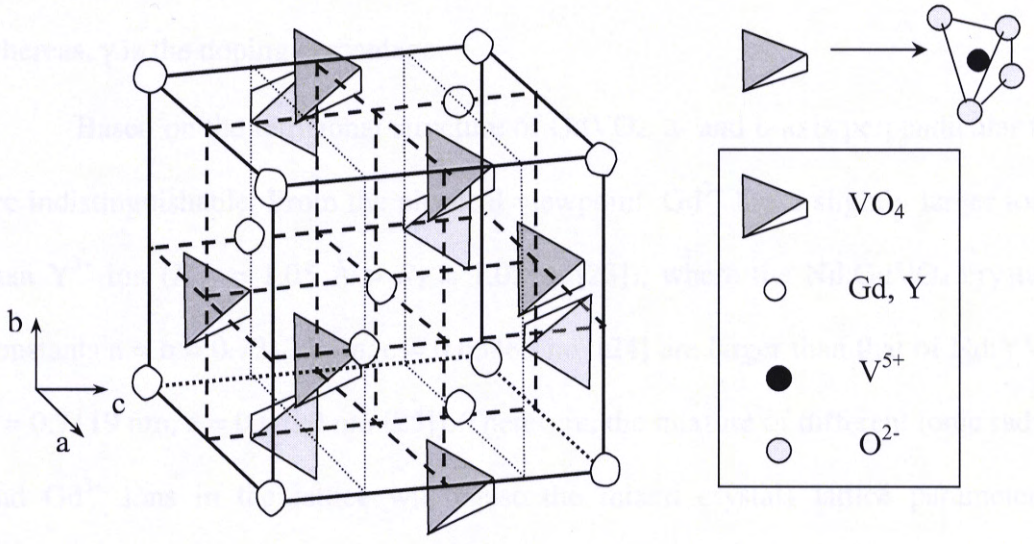

Fig. 2.2: Schematic diagram of the Nd:$GdVO_4$ or Nd:$GdYVO_4$ crystal structure.

When the pure YVO_4 or $GdVO_4$ crystal host is doped by the rare earth Nd^{3+} ions, Nd^{3+} ions will substitute some of the Y^{3+} or Gd^{3+} in the lattice following its doping percentage.

Typically, 1.0 at.% of Nd^{3+} doping level yields population density of about 1.38×10^{-20} ion/cm^3. Since both $GdVO_4$ and YVO_4 compounds have the same structure and with a melting point difference of 20 ^{0}C, the formation of $Gd_xY_{1-x}VO_4$ is expected over a wide range of $0 \leq x \leq 1$ between the two terminal pure vanadate compounds. The same mechanism of Nd^{3+} substitution is possible also in the case of a mixed Nd:$GdYVO_4$ crystal, where the crystal lattice consisted of Gd^{3+} and Y^{3+} simultaneously. The segregation of Nd^{3+} in YVO_4, $GdVO_4$ and $Gd_{0.5}Y_{0.5}VO_4$ is respectively as 0.63, 0.78, and 0.80 [22]. In preparation, the raw materials are synthesized in the liquid form, the ions reaction can be described through the reaction equation as follows.

$$\gamma Nd^{3+} + (1-\gamma)M^{3+} + VO_3^- + 2OH^- = Nd_\gamma M_{1-\gamma}VO_4 \downarrow + H_2O \qquad (2.1)$$

where $M = Y, Gd$ for pure vanadate crystals, or $M = Gd_xY_{1-x}$ for the mixed vanadate crystals. The value of x is a ratio of the mixture between Gd and Y ions in the material, whereas, γ is the doping percentage.

Based on the tetragonal structure of $GdVO_4$, a- and b-axis perpendicular to c axis are indistinguishable. From the physical viewpoint, Gd^{3+} has a slightly larger ionic radii than Y^{3+} ion (R_{Gd} = 1.05 Å > R_Y = 1.02 Å [23]), where the Nd:$GdVO_4$ crystal lattice constants a = b = 0.72126 nm, c = 0.63483 nm [24] are larger than that of Nd:YVO_4 (a = b = 0.7119 nm, c = 0.6290 nm [25]). Therefore, the mixture of different ionic radii of Y^{3+} and Gd^{3+} ions in the lattice will cause the mixed crystals lattice parameters in an intermediate range between the Nd:$GdVO_4$ and Nd:YVO_4. The lattice parameters will become larger with the increase of Gd/Y ratio in the mixed crystal. It has been reported that for the mixed crystal with concentration of Gd = 0.18, Y = 0.82, its lattice constants at a- and c-axis are respectively about 0.71401 nm, 0.63028 nm, whereas, the

Nd:$Gd_{0.64}Y_{0.36}VO_4$ has a slightly longer lattice constants of a = 0.71801 nm, c = 0.63290 nm [16]. By taking advantage of the tetragonal structure, natural crystal facets will be formed as if the growth direction were along the crystallographic axis. For instance, two [100] planes will be easily developed to be the crystal surface if crystal growth direction is perpendicular to the c-direction, whereas, no intrinsic facets are expected, and large diameter of crystal rod will be obtained if the growth direction is [110] [26]. Similarly, Nd:YVO_4, Nd:$GdVO_4$ and the mixed crystals can be a uniaxial crystals depending on the crystal growth direction. Corresponding to the natural birefringent characteristics the physical and laser properties differ depending on the light traveling direction along a- and c-axis.

For a better understanding, the light propagation in relation to one crystal lattice is illustrated in a simple diagram, with lattice axis denoted as a, b, and c-axis, respectively (Fig. 2.3). Commonly for the light propagation direction, which is in parallel with the a-axis, the crystal is denoted as an a-cut crystal. This is so to name a c-cut crystal following light propagation direction along the c-axis. As in Fig. 2.3a, for the a-cut crystal, light will experience the anisotropy of the crystal because of the different lattice constants along the b- and c-axis. Specifically, the polarization of light along the c-axis will have a larger refractive index than that of light polarized along the a-axis (for instant, Nd:$GdVO_4$: $n_e = 2.19 > n_o = 1.97$ [27] at 1.06 μm) . The absorption cross-section and stimulated emission cross section for the c-polarized light is also larger than the a-polarized light [28]. When the crystal is put in a laser resonator, the light polarized parallel to the c-axis (optical axis) survives, giving a linearly polarized e-ray, and the weak o-ray is suppressed due to the gain competition. While for the c-cut crystal, light propagating along the c-axis

cannot experience any difference between the symmetrical a- and b-axis (Fig. 2.3b). Hence, c-cut crystal laser output is unpolarized, which is similar to the case of the Nd:YAG laser.

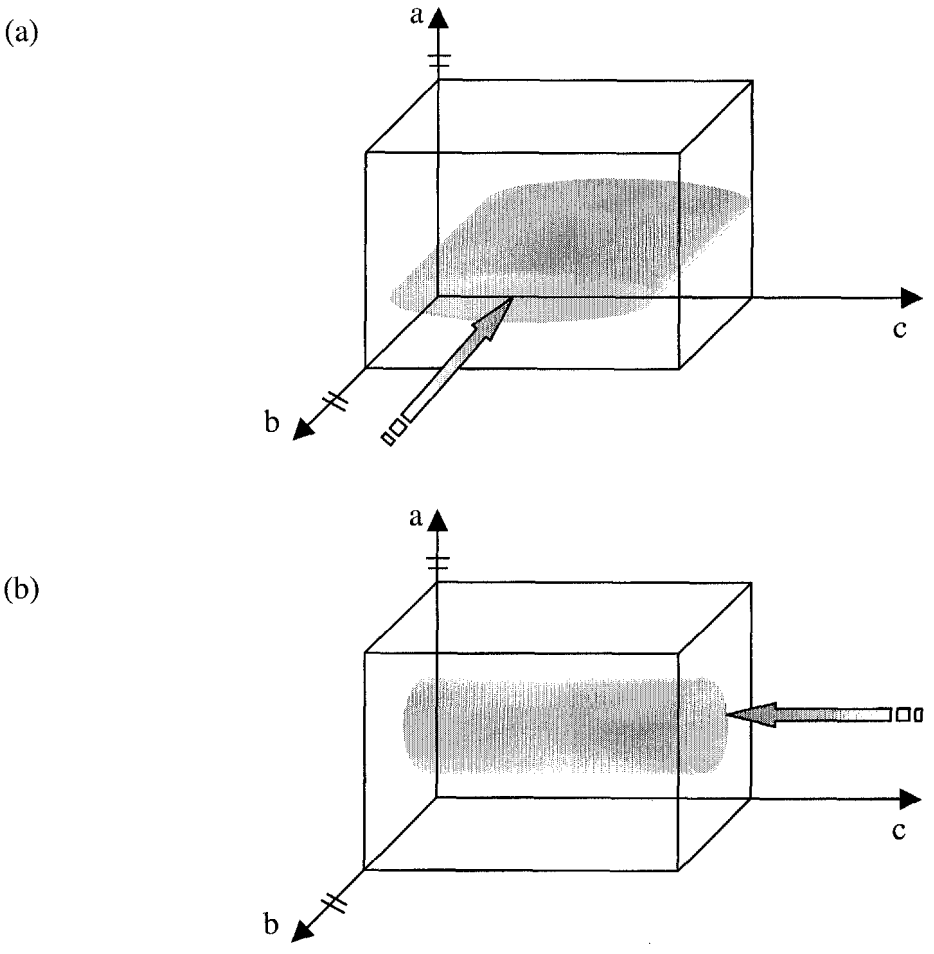

Fig. 2.3: Schematic illustration of the light propagation in the a-cut and c-cut tetragonal Nd-doped vanadate crystal, respectively. (a) a-cut case, (b) c-cut case. The solid shape in the crystal represents the wavefront of the light in the unit crystal cell.

2.2.2 Material characteristics

2.2.2.1 Absorption and fluorescence properties

Due to the anisotropic crystal field, the absorption and emission coefficient of the uniaxial Nd:$GdVO_4$ and Nd:$GdYVO_4$ crystals differ from each other at the two perpendicular axes. Typically for a 1.2 at.% Nd:$GdVO_4$ crystal, the peak absorption coefficient for c (π)-polarized light at 808.4 nm is 78 cm^{-1}, deducing an effective absorption cross section of 5.2×10^{-19} cm^2 as reported by Jensen *et al.* [29], whereas, the absorption coefficient of the a (σ)- polarized direction is about 17 cm^{-1}, which is about 4.6 times lower than that of its perpendicular absorption, giving an absorption cross section of 1.1×10^{-19} cm^2. The Nd:$GdVO_4$ laser is more susceptible to the wavelength variation of the diode pump source following the homogeneously broadened absorption linewidth at 808 nm of 1.6 nm. The a- and c-polarized absorption spectra of a 1.2 at.% doped Nd:$GdVO_4$ sample are shown in Fig. 2.4 [29]. One can clearly see that the absorption peak of c-polarization is several times greater than that of the a-polarization.

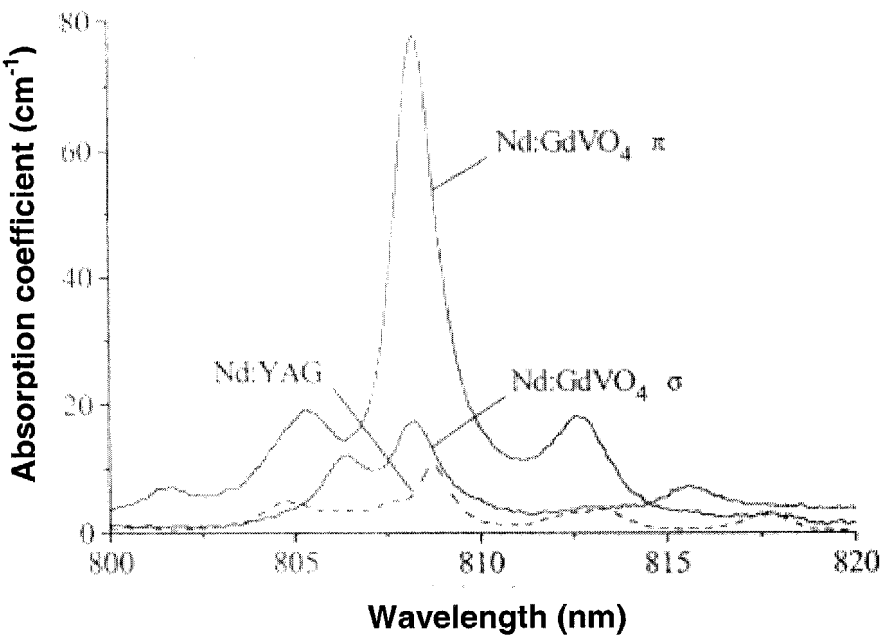

Fig. 2.4: The polarized direction scanned of absorption spectra for Nd:$GdVO_4$ crystal. Absorption spectrum of Nd:YAG is given as a reference.

The absorption spectrum of an a-cut, 0.5 at.% doped Nd:$Gd_{0.64}Y_{0.36}VO_4$ sample was experimentally compared with a Nd:$GdVO_4$ crystal of the same doping level. The spectra measured by using a UV spectrophotometer (HP 8453) show the same absorption peaks in both Nd:$GdVO_4$ and Nd:$GdYVO_4$. It is shown in Fig. 2.5 that Nd:$Gd_{0.64}Y_{0.36}VO_4$ mixed crystal with thickness of 5 mm has a slightly (about 6%) higher absorption peak.

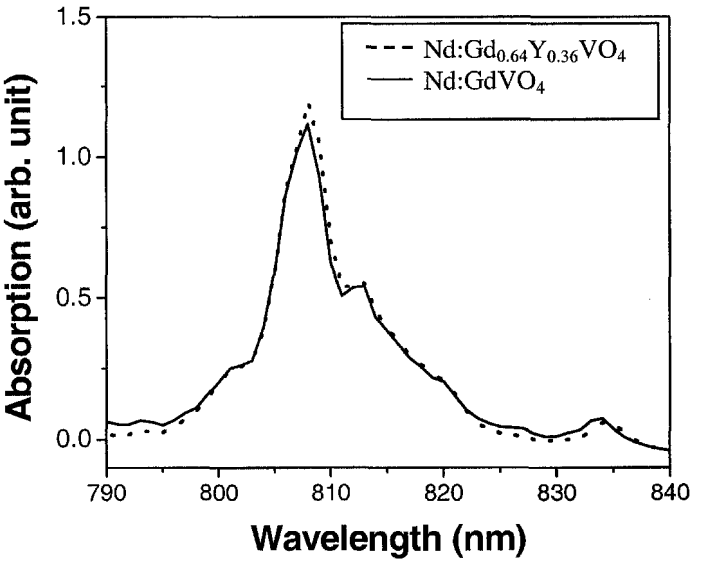

Fig. 2.5: Absorption spectra of Nd:$Gd_{0.64}Y_{0.36}VO_4$ and Nd:$GdVO_4$ measured with UV spectrophotometer.

Similar to the higher absorption coefficient along the c-direction, the c-polarized fluorescence emission coefficient of Nd:$GdVO_4$ is also higher than its a-polarized light. The difference between the a-polarized and c-polarized emission peak intensity at 1063 nm gives a good measure of their stimulated emission cross section ratio. Following the analysis of Jensen *et al.* on the Nd:$GdVO_4$ polarized fluorescence spectra as given in Fig. 2.6 [29], the c-polarized fluorescence peak is about 2.3 times higher than the a-polarized emission peak. From this relation, the a-polarized emission would have a cross section of

3×10^{-19} cm^2, while the c-polarized emission cross section is 7.6×10^{-19} cm^2. The same parameter was reported by Zagumennyi *et al.* [30].

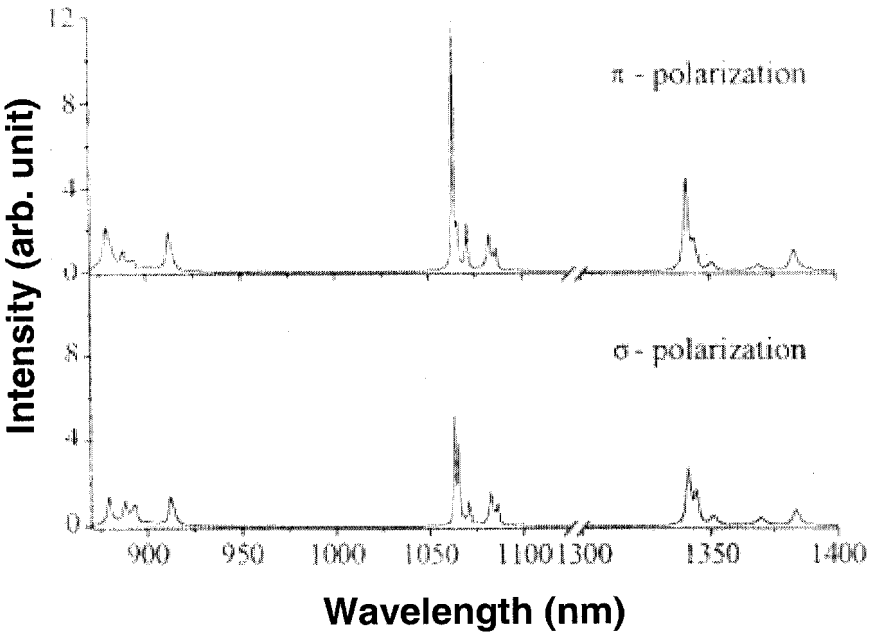

Fig. 2.6: The c- and a-polarized fluorescence spectra of Nd:$GdVO_4$ crystal.

The polarization-dependent fluorescence spectra of a Nd:$GdVO_4$ and a Nd:$Gd_{0.64}Y_{0.36}VO_4$ crystal with 0.5 at.% Nd^{3+} doping concentration were analyzed with an optical spectrum analyzer (Ando, MS9710A). As shown in Fig. 2.7, in the range of 900 nm to 1400 nm, there are three emission peaks at 1063 nm, 1342 nm, and 913 nm, corresponding to the Stark energy transition between $^4F_{3/2}$ with $^4I_{11/2}$, $^4I_{13/2}$, and $^4I_{9/2}$. Referring to the enlarged spectra for the dominant emission at 1063 nm (Fig. 2.8), 1065 nm, 1070 nm, 1082 nm, and 1086 nm transition lines are found mainly caused by the total Stark splitting of the $^4I_{11/2}$ energy level corresponding to the multiplets at 1987 cm^{-1}, 2035 cm^{-1}, 2137 cm^{-1}, and 2165 cm^{-1}.

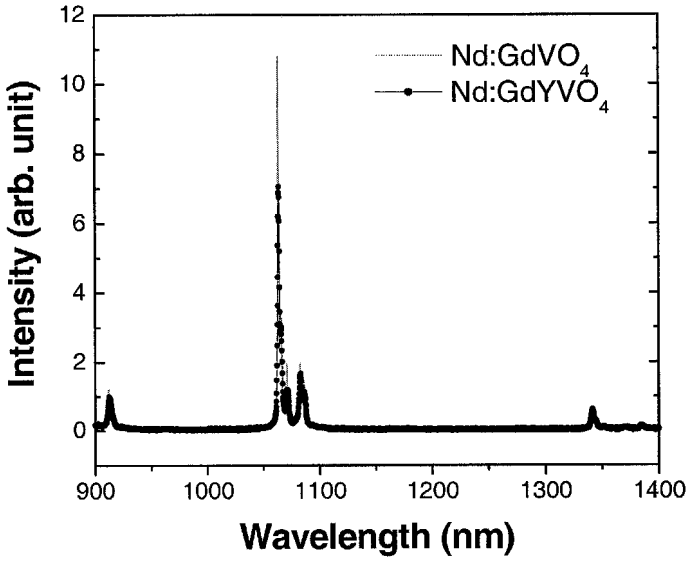

Fig. 2.7: Experimental measured fluorescence spectra of Nd:$Gd_{0.64}V_{0.36}VO_4$ and Nd:$GdVO_4$ crystals.

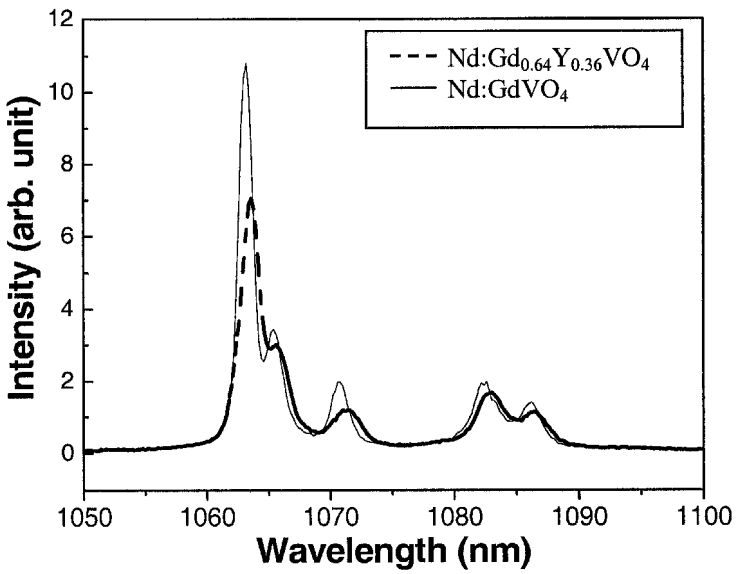

Fig. 2.8: Enlarged of the measured dominant emission spectra of Nd:$Gd_{0.64}V_{0.36}VO_4$ and Nd:$GdVO_4$ crystals in near infrared regime.

According to the spectra shown in Fig. 2.8, the emission peak ratio between the Nd:$GdVO_4$ and Nd:$Gd_{0.64}Y_{0.36}VO_4$ is about 1.57. Stimulated emission cross section of the mixed crystal is thus calculated to be about 4.8×10^{-19} cm^2 if 7.6×10^{-19} cm^2 is taken as

the emission cross section of Nd:$GdVO_4$. The estimated emission cross section of mixed crystal agrees well with the reported measurement [31]. From the figure, the fluorescence linewidth of Nd:$GdVO_4$ is about 1.3 nm, whereas the mixed crystal Nd:$Gd_{0.64}Y_{0.36}VO_4$ has a broader spectrum of about 3.5 nm. These values are the same as those measured by other researchers [31, 32].

2.2.2.2 Visible fluorescence

Besides the dominant atomic transition between $^4F_{3/2}$ - $^4I_{11/2}$ and $^4F_{3/2}$ - $^4I_{13/2}$, it has also been reported that luminescence is possible in Nd:$GdVO_4$ laser. The visible fluorescence is most probably associated with excited-state absorption (ESA) and energy transfer upconversion (ETU) in the metastable $^4F_{3/2}$ level. The processes were even found to have effect at the low pump power levels [33], as which the yellow fluorescence was detected under 500 mW of 808 nm excitation [29]. According to Fornasiero *et al.*, the ESA cross section at Nd:$GdVO_4$ upper energy level is about few 10^{-20} cm^2 [34]. Whereas the ETU rate is 1.2×10^{-15} cm^3s^{-1}, which is about one order magnitude higher than that in other Nd^{3+} crystals such as Nd:YAG and Nd:YLF [35]. Therefore it is expected that such nonlinear interactions will become significant when the stored population inversion is high in Nd:$GdVO_4$ laser. This condition could be fulfilled when the laser is operating in Q-switched regime.

2.2.2.3 Thermal properties

The thermal quality of laser crystals is critical for a laser to achieve good laser beam quality and output performance, particularly for high power lasers. Heating on the laser

material is normally due to the thermalized terminal laser levels, absorption pump photons by the laser medium, optical quenching, and quantum defects. Gain medium may be physically distorted or damaged in the laser operation with the existence of thermal loading. The low thermal conductivity will cause thermal focal lensing, stress induced birefringence, and further degrading of the laser beam quality and output. In principle, there are two independent thermal parameters in relation to the anisotrpic characteristic of Nd:$GdVO_4$ and Nd:$GdYVO_4$. Table 2.1 gives the available thermal parameters of Nd:$GdVO_4$ and Nd:$Gd_xY_{1-x}VO_4$ crystals. As a reference, the related parameters of Nd:YAG and Nd:YVO_4 are shown together in the table.

Table 2.1: Thermal parameters of Nd:YAG, Nd:YVO_4, Nd:$GdVO_4$ and Nd:$Gd_xY_{1-x}VO_4$ crystals.

Crystal	Thermal expansion coefficient ($\times 10^{-6} K^{-1}$)		Thermal conductivity ($Wm^{-1}K^{-1}$)		Specific heat
	a-axis	c-axis	a-axis	c-axis	($Jg^{-1}K^{-1}$)
Nd:YAG [36]	7.8 <111>		11.1 <111>		0.59
Nd:YVO_4 [37, 38]	2.2	8.4	5.1	5.23	0.5022*
Nd:$GdVO_4$ [39, 24]	1.5	7.3	10.7	11.4	0.5016*
Nd:$Gd_xY_{1-x}VO_4$ [16]					
[x] = 0.12	1.48	7.94	-	-	0.73
= 0.42	1.32	7.72	-	-	0.63
= 0.50 [22]	-	-	-	12.5	-
= 0.64	1.32	7.72	-	-	0.55

The specific heat data marked with asterisk (*) are converted from that in unit of cal./(mol K) in [24] for the purpose of comparison. From the table, the mixed laser crystals generally have a large thermal conductivity and specific heat as compared with Nd:YAG, while Nd:$GdVO_4$ has also a relatively good thermal conductivity, indicating that both laser materials are excellent for the high power lasers or for pulsed applications.

For clearer comparison and understanding on the material characteristics in lasing action, basic spectroscopic parameters of the Nd:$GdVO_4$, Nd:$GdYVO_4$ and two other major hosts of Nd-ion doped lasers are summarized in Table 2.2 as a reference.

Table 2.2: Summary of the spectroscopic parameters of the pure and the mixed gadolinium vanadate from the literatures.

Crystal	Absorption cross section @ ~808 nm (× 10^{-19} cm^2)		Stimulated emission cross section @ ~1064 nm (× 10^{-19} cm^2)		Emission linewidth, E ‖ c (nm)	Fluorescent lifetime ‖ c (μs)
	a-axis	c-axis	a-axis	c-axis		
Nd:YAG (1 at.%) [40, 41]	0.7		2.8		0.45	230
Nd:YVO_4 (1 at.%) [42]	0.91	3.1	2.95	14.4	0.8	96
Nd:$GdVO_4$ (1.2 at.%) [29, 43]	1.1	5.2	3	7.6	1.3	90
Nd:$Gd_{0.36}Y_{0.64}VO_4$ (0.5 at.%) [31]	-	5.5*	-	4.8	3.5	138

* Experimental estimate.

Optical properties differ significantly for different laser hosts, with pros and cons to offer for different laser operating condition. Nd:YAG with its relatively long fluorescent lifetime and small emission cross section is beneficial for Q-switching. Narrow emission linewidth allows Nd:YAG laser to be used in longer cavity before the free spectral range is comparable to the gain bandwidth. However, it is unfavourable to mode-locking for ultrashort pulse generation. In addition, weak absorption places limitations on Nd:YAG in diode pumping. In contrast, Nd:YVO_4 is more suitable for CW laser action with the large emission cross section. Its strong and broad absorption band provides ease of diode pumping. In contrast, the relatively short upper state lifetime associated with the large emission cross-section seriously limits the applications of Nd:YVO_4 in passively Q-switched lasers.

Compared between these two commercial laser crystals, Nd:$GdVO_4$ has a much larger absorption cross-section, which reflects its suitability to the diode pumping. With an average emission cross section in between that of the Nd:YAG and Nd:YVO_4, and a fluorescent lifetime which is comparable with Nd:YVO_4, there is potential to apply Nd:$GdVO_4$ in both high power CW and Q-switched operations, whereas, as checked in experiment, the newly developed mixed crystal Nd:$Gd_{0.64}Y_{0.36}VO_4$ has even higher absorption than Nd:$GdVO_4$. The relatively smaller emission cross section as well as the longer upper state lifetime, might make it attractive in the diode-pumped passively Q-switched operation. Because of the random distribution of Gd^{3+} and Y^{3+} in crystal lattice, Nd:$Gd_{0.64}Y_{0.36}VO_4$ has a non-homogeneously broadened emission linewidth, which is preferable to generate narrow mode-locked pulses. All these potential features are the

drive in choosing Nd:$GdVO_4$ and Nd:$Gd_{0.64}Y_{0.36}VO_4$ as gain media for laser development and studies in this thesis.

2.3 Laser operation modes

Besides operating in continuous wave (CW), a laser can also operate in pulsed mode. From a practical viewpoint, optical pulses are required in many applications. High peak powers are advantageous for scientific studies, medical, industry and as a pump source for nonlinear wavelength conversion [44 - 46]. Generally, intensity modulation techniques arise from the introduction of time-varying loss into a cavity. Q-switching is a technique widely used in laser engineering to generate high peak power pulses by altering cavity Q factor, where Q value is defined as the ratio of energy stored to energy dissipated in the cavity. The higher quality factor implies the lower losses. Basically cavity length of the high power Q-switched laser using the bulk laser crystal is the limitation that restricts the pulse duration in the order of nanoseconds. Mode-locking is the common technique for generating picoseconds or subpicoseconds pulses in solid-state lasers. The cavity longitudinal modes are coupled in phase and are emitted from the cavity in each cavity round trip. Laser gain bandwidth determines the locking number of axial modes, and therefore the individual mode-locked pulse duration is inversely related to the bandwidth of laser emission.

Q-switching and mode-locking are categorized into active and passive. In the first approach the radiation in the laser cavity is controlled by a signal derived externally, such as acousto-optics (AO) or electro-optics (EO). While in the passive mode, the laser radiation itself generates a modulation through the mechanism of a non-linear device in

the laser cavity. Commonly, a saturable absorber is employed in the passive approach for both Q-switching and mode-locking incorporated with the laser diode pump source to construct a compact and simple pulsed laser system, which is suitable for many applications.

2.3.1 Mechanism of passive Q-switching

Passive Q-switching is the simplest approach in practice, which requires no external circuitry. This process is controlled purely by the interaction of light with the gain medium and the saturable absorber. Formation of Q-switched pulses can be explained as the interplay between gain and saturable loss in the laser. When the laser gain exceeds the cavity loss and the saturable absorber losses, the photon density starts to build up and saturate the saturable absorber. In other words, laser cavity is kept from oscillating during pumping by the saturable absorption loss in order to build up larger population inversion. When the inversion strikes its peak to saturate the saturable absorber, cavity Q is restored abruptly to its usual high value and dumps the accumulated population inversion in a single short laser pulse. The peak power in the Q-switched pulse can be three to four times higher than the CW oscillation level that would be created in the same laser using the same pumping rate. The repetitive change of the resonator loss yields series of pulses following the cavity switching time.

An analytical model describing the passive Q-switching was derived even in the early period of laser development. The first theoretical study on laser Q-switching was published in year 1963 by Wagner and Lengyel [47]. After two years, Szabo *et al.* first derived the relevant rate equations for the passively Q-switched lasers [48]. Since then,

extensive studies regarding the Q-switched laser parameters have been carried out for further comprehensive description and optimization [49 - 52]. A good reference for the simple analytical description for passive Q-switching is in the well known "laser bible" by Siegman [53], which has been employed intensively by Kuo *et al.* and coworkers in theoretical studies of passive Q-switching of various solid-state lasers [54 - 56]. In the passively Q-switched laser, the process of transferring the potentially stored energy to the kinetic photon energy is nonlinear by involving the loss intensity dependence of saturable absorber. Ideal laser operation is the basic assumption for the qualitative analysis, as which the lower laser state in a four-energy-level system is simplified because of the rapid relaxation to the laser ground state. The analytical solutions are useful to determine the governing experimental parameters for the appropriate considerations in designing an effective passive Q-switching. The rate equations describing the ideal Q-switched laser mechanism are given as below [53, 54],

$$\frac{dn(t)}{dt} = \left[K_g N_g(t) - K_s N_s(t) - \beta K_s (N_{s0} - N_s) - \gamma_c\right] n(t) \tag{2.1}$$

$$\frac{dN_g(t)}{dt} = R_p - \gamma K_g N_g(t) n(t) - \frac{N_g}{\tau_f} \tag{2.2}$$

$$\frac{dN_s(t)}{dt} = -\gamma_s \left[N_s(t) - N_{s0}\right] - K_s N_s(t) n(t) \tag{2.3}$$

where $n(t)$ is the cavity photon number, $N_g(t)$ and $N_a(t)$ are population difference in gain medium and in saturable absorbing medium. Coupling coefficient for laser gain and saturable absorber are denoted as K_g and K_s respectively. $K_g = 2\sigma_g/t_r A_g$ and $K_g = 2\sigma_s/t_r A_s$ whereas, t_r is the cavity round trip time. γ_g and γ_s mean the population recovery rates for the gain and the saturable absorber. γ_s here indicates the ground state recovery rate in the

saturable absorber which is effective for changing the cavity Q factor. τ_f is the laser fluorescent lifetime, and γ_c is the cavity photon decay rate. N_{s0} is the unsaturated population density at the equilibrium state. γ is the population reduction factor ($\gamma = 1$ for the four-level laser, but 2 for the three-level laser). As focusing on the laser pulse evolution process in which the time scale is in the nanosecond range, pumping term and the spontaneous decay are ignored in the population inversion. Eq. (2.2) is then to be

$$\frac{dN_g(t)}{dt} = -\gamma K_g N_g(t) n(t) \tag{2.4}$$

N_{g0} represents the initial laser inversion at the onset of the pulse evolution. The growth rate of N_{g0} is denoted as γ_{g0}. Following the increase of photon numbers, the growth of cavity gain is determined by the saturation sequence of either gain medium or saturable absorber, which is defined as the second threshold condition. Just as, if the gain saturation occurs earlier than the saturable absorber, the intracavity photon number will decrease after a certain period, so the obtained laser pulse will be degraded. In other words, the effective Q-switched pulse can only be achieved if the saturable absorber can be saturated before the gain medium. This critical criterion is crucial in particular for the slow saturable absorber to generate a good quality of Q-switched pulse. The condition is expressed analytically in the equation below.

$$\frac{K_s^2 N_{s0}}{K_g^2 N_{g0}} > \frac{\gamma_s}{\gamma_{g0}}. \tag{2.5}$$

The ratio between the saturable absorber decay rate and the initial laser growth rate is essentially similar to the ratio of the unsaturated loss factor in saturable absorber ($2\alpha_{s0} l_a$) to the initial gain factor in laser medium ($2\alpha_{g0} l_g$).

$$\frac{K_s N_{s0}}{K_g N_{g0}} \equiv \frac{2\alpha_{s0} l_s}{2\alpha_{g0} l_g}.$$

Since $K = c\sigma$, where σ is the cross section, and

$$\frac{K_s}{K_g} = \frac{\sigma_s}{\sigma_g} \times \frac{A_g}{A_s}.$$

Therefore, the condition for good passive Q-switching, which is also denoted as the second threshold condition, can be expressed as follow.

$$\frac{\gamma_{g0}}{\gamma_s} \times \frac{\sigma_s}{\sigma_g} \times \frac{A_g}{A_s} \times \frac{2\alpha_{s0} l_g}{2\alpha_{g0} l_a} > 1. \tag{2.6}$$

This case makes sense with the assumption that the gain is depleted by the cumulative effect when photon flux passes through the gain medium, whereas the saturable absorber is saturated instantaneously. So the ideal passive Q-switching is to let laser intensity grow rapidly at the early stages and saturate the saturable absorber before the laser inversion is burnt up. The ratio of initial gain to unsaturated loss factor is usually close to unity; hence, when the cavity mode size is unity, the basic physical term to be considered for selecting a saturable absorber is to ensure that the absorption cross section is greater than the laser emission cross section. Nevertheless, with the occurrence of thermal focal lens in the laser crystal, the effective mode size in the gain medium and the absorber will directly determine the Q-switched laser performance. It is essential to consider A_g/A_s in designing the laser cavity configuration. Wisely utilizing the thermal lens effect to increase the A_g/A_s ratio will effectively enhance the Q-switched output properties.

Besides the basic Q-switched criteria and enhancement, further analysis on the dynamic change of cavity photon number with respect to the population inversion is required to characterize the Q-switched pulse properties. Turning to the laser dynamical

change on the evolution of a single Q-switched pulse; analysis is separated into three stages: before, at the maximum and after the Q-switched pulse evolution for the estimate of the Q-switching threshold, pulse peak power, single pulse energy, and pulse duration. For the considerations in designing an optimum passive Q-switching, the dominant laser parameters are expressed in terms of the photon number, laser inversion and saturation loss.

At the accumulation of population inversion before the opening of passive Q-switch, intracavity light intensity is low $dn/dt \approx 0$, where all the population of the saturable absorber can be assumed are in the equilibrium ground state $N_s = N_{s0}$. With this term substituted into Eq. (2.1), the initial population inversion for the Q-switching action is written as

$$N_{g0} \approx \frac{K_s N_{s0} + \gamma_c}{K_g} \approx \frac{\ln\left(\frac{1}{T_0^2}\right) + \ln\left(\frac{1}{R}\right) + L}{2\sigma_g l_g}. \tag{2.7}$$

As pointed out by the physical terms in Eq. (2.7), laser with larger emission cross section σ_g would have a lower storage of energy due to the smaller initial population inversion, whereas, higher saturation strength of the absorber (lower T_0) and lower reflectivity R of the cavity mirror are conducive to enhancing the initial population inversion for higher energy storage. L in Eq. (2.7) is the dissipative cavity loss; l_g is the laser crystal length. Using the same Eq. (2.1), when the ground state population of the saturable absorber is strongly excited, the population inversion threshold for building up a Q-switched pulse can be estimated, where $N_s = 0$ is for the depleted absorber.

$$N_{Th} \approx \frac{\beta K_s N_{s0} + \gamma_c}{K_g}. \tag{2.8}$$

The cavity photon flux at the moment is assumed by substitute Eq (2.7) and Eq. (2.8) into Eq. (2.1).

$$\frac{dn}{dt} \approx K_g (N_g - N_{Th}) n . \tag{2.9}$$

Dividing Eq. (2.9) by Eq. (2.4), yields

$$\frac{dn}{dN_g} \approx -\frac{1}{\gamma}(1 - \frac{N_{Th}}{N_g}) . \tag{2.10}$$

The integration of Eq. (2.10) against N_{g0} to N_g gives n as a function of the N_g.

$$n(N_g) \approx \frac{1}{\gamma}\left[- \int_{N_{g0}}^{Ng} 1 - N_{Th} \int_{Ng}^{N_{g0}} \frac{dN_g}{N_g} \right],$$

$$n(N_g) \approx \frac{1}{\gamma}\left[N_{g0} - N_g - N_{Th} \ln \frac{N_{g0}}{N_g} \right]. \tag{2.11}$$

Eq. (2.11) visualizes the dynamic changes of the photon flux in relation to the population inversion as illustrated in Fig. 2.9. It is useful to generate analytically the dependence of Q-switched pulse properties on the experimental parameters.

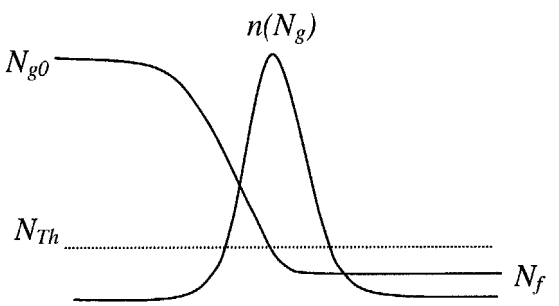

Fig. 2.9: Dynamic changes of the population inversion during a single Q-switched pulse evolution.

As can be seen in Fig. 2.9, photon number n is at its maximum when the saturable absorber is bleached at the point when $N_g = N_{Th}$. Therefore the peak photon number is

$$n_{peak}(N_{Th}) \approx \frac{1}{\gamma}\left[N_{g0} - N_{Th} - N_{Th}\ln\frac{N_{g0}}{N_{Th}}\right], \tag{2.12}$$

$$n_{peak}(N_{Th}) \approx \frac{N_{g0}}{\gamma}\left[\frac{\frac{N_{g0}}{N_{Th}} - 1 - \ln\left(\frac{N_{g0}}{N_{Th}}\right)}{\frac{N_{g0}}{N_{Th}}}\right].$$

Define $\frac{N_{g0}}{N_{Th}} = r$; $n_{peak}(N_{Th}) \approx \frac{N_{g0}}{\gamma}\left[\frac{r - 1 - \ln r}{r}\right]$.

Therefore r is the ratio of the initial inversion to the threshold inversion that proportionally determines the Q-switched laser output. As the initial population follows the pump inversion, the ratio value depends directly on the pumping rate. At the start of the pulse build-up moment, $dN_{g0}/dt \approx 0$, Eq. (2.2) is thus to be

$$R_p - \gamma K_g N_{g0}(t)n(t) - \frac{N_{g0}}{\tau_f} = 0,$$

$$N_{g0} = \frac{R_p}{Kn + \frac{1}{\tau_f}}.$$

From this R_p and N_{g0} relationship, it is found that at the low cavity photon number, before the emission of the Q-switched pulse, initial population inversion grows linearly with the pumping rate.

$$N_{g0} \approx R_p\tau_f \approx rN_{Th}. \tag{2.13}$$

In order words, the r-value is proportional to R_P. Because of the practical limitation on the average pump power in CW pumping condition, r in the continuous pumped passive

Q-switching is much more modest than the pulsed pumping. This results in a lower Q-switched laser output. Nevertheless, following the CW pumping characteristics, CW pumped passively Q-switched laser is advantageous with the good transverse and axial mode stability, which maintain the average output power without the perturbation of the strong pump laser fluctuations.

The laser pump rate that determines the excited volumic ions is a ratio of the absorbed pump power and the volumic pump energy in the laser crystal. By considering the pump mode has a uniform distribution throughout the gain medium, R_P is estimated to be

$$R_p = \frac{P_{in}(1-\exp(-\alpha l_g)}{h\nu_p V_p}, \tag{2.14}$$

where P_{in} is the input pump power, ν_p is the pump frequency, and V_P is the pump focusing volume. $\alpha = \sigma_{abs} N_{total}$ is the absorption coefficient of the laser crystal, which equals to the product of crystal absorption cross section and the total dopant. This implies that laser with higher doping concentration is preferable for higher pump rate.

After the release of the Q-switched laser pulse, population inversion decreases to the value N_f for starting another cycle of the pulse build-up mechanism. The photon number at this moment becomes $n \approx 0$ again. In order to obtain the relation of the population inversion after the pulse relaxation, let $N_g = N_f$ in Eq. (2.12)

$$n(N_f) \approx \frac{1}{\gamma}\left[N_{g0} - N_f - N_{Th}\ln\frac{N_{g0}}{N_f}\right] \approx 0,$$

$$1 - \frac{N_f}{N_{g0}} - \frac{N_{Th}}{N_{g0}}\ln\frac{N_{g0}}{N_f} \approx 0. \tag{2.15}$$

Eq. (2.15) is a transcendental equation, which can only be solved numerically for the value of N_f. The population inversion before and after the evolution of the Q-switched pulse is necessary to determine the single pulse properties, such as energy, peak power and the pulse width.

$$\text{Q-switched pulse energy, } E_{pulse} = \frac{N_{g0} - N_f}{\gamma} h\nu\eta_c$$

$$= \frac{N_{g0} - N_f}{\gamma} h\nu\eta_g \ln\frac{1}{R}.$$

$\gamma = 1$ in the Nd^{3+} laser (four-level system), so pulse energy is written as

$$E_{pulse} = r - \frac{N_f}{N_{Th}} h\nu\eta_g \ln\frac{1}{R}, \tag{2.16}$$

where η_c is the output coupling efficiency and η_g is the laser coupling efficiency involving the effective beam area in the gain medium. In practice, R should be low, so that the higher coupling transmission is able to extract more pulse energy and prevent it from being dissipated by the internal cavity loss. Normally, R is about 50% to 60% depending on the lasing threshold of the system. Clearly, Q-switched output energy is higher with a larger inversion ratio, r as mentioned above.

By defining total cavity losses, α_L = coupling loss + dissipative cavity loss, the cavity decay time, $\tau_c = t_r/\alpha_L \equiv$ cavity round trip time/total cavity losses,

$$\tau_c = 2\left[\frac{d + (n_g - 1)l_g}{c\alpha_L}\right],$$

where d is the cavity length, n_g is the refractive index of the gain medium and c is the light speed. The pulse peak power at the n_{peak} can be written as

$$P_{peak} = \frac{n_{peak} h\nu}{\tau_c} \eta_c$$

$$= \frac{h\nu}{\tau_c} \eta_g \ln \frac{1}{R} \left[N_{g0} - N_{Th} - N_{Th} \ln \frac{N_{g0}}{N_{Th}} \right] \tag{2.17}$$

As we have seen, the fast cavity decay time will generate a higher peak-power pulse. Besides increasing the pumping rate for larger initial population inversion N_{g0}, stronger saturable absorber is also possible to achieve the same effect. On the other hand, passive improvements to the cavity condition by reducing cavity length and increasing coupling loss within an allowable range are also effective to achieve higher peak power.

Q-switched pulse width is ratio of the output energy to the peak power, so from the derived pulse energy and peak power, the Q-switched pulse width is

$$t_{pulse} = \frac{E_{pulse}}{P_{peak}},$$

$$= \tau_c \frac{N_{g0} - N_f}{N_{g0} - N_{Th} - N_{Th} \ln \frac{N_{g0}}{N_{Th}}}. \tag{2.18}$$

At a given pulse energy, narrower pulse width will have higher level of the Q-switched peak power.

2.3.2 Mechanism of passive mode-locking

Passive mode-locking is the desirable method to generate ultrashort pulses. For solid-state lasers with longer upper state lifetime (in the range of microseconds to milliseconds) than the cavity round trip period (typically in the nanosecond regime), passive mode-locking with fast recovering saturable absorber is the simple approach. The saturable absorber

provides a periodical change to the laser radiation at the cavity round trip time by varying loss. Cavity energy can be transferred between the adjacent modes when the modulation period is equal to the cavity period. Hence the modes become coupled together and oscillate in the same phase.

Similar with passive Q-switching, passive mode-locking with fast saturable absorber works without external control, but utilizes the nonlinearity of absorber to create the amplitude instability and provides the gain an intense initial peak to background noise ratio. The fast absorption recovery time in picoseconds is preferentially used in solid-state lasers to compress the fluctuation of the CW laser following the pulse intensity profile until its duration is of the order of the absorption recovery time, or to the gain bandwidth limit. Depending on the laser gain emission linewidth, mode-locked pulse duration can go down to picoseconds or femtoseconds. If the pulses were frozen in space, the mode-locked pulse would be in micrometer lengths, which is much shorter than the Q-switched pulse. This implies that detection resolution in space has about 1000 times difference between both cases.

Considering the temporal characteristic of a passively mode-locked laser, incorporation of saturable absorber has a tendency to drive the laser into Q-switched mode-locking regime, instead of the continuous-wave mode-locking pulse train. Such a laser consists of mode-locked pulses underneath a Q-switched envelope. This laser is interesting for the applications that require high peak power, e.g. nonlinear frequency conversion, micromachining, microsurgery. However, for those that need constant pulse energy, continuous-wave mode-locking is the alternative.

The analytical treatment of Q-switched mode-locking in solid-state laser was first undertaken by Kärtner *et al.* [57] and further extended by Hönninger *et al.* for soliton mode-locked femtosecond lasers [58]. The derivation for the criterion of stability against Q-switched mode-locking is also from the coupled rate equations involving cavity photon number, gain and saturable absorption as shown in Eq. (2.1) – Eq. 2.3. Based on the assumption that saturable absorber has excited state absorption, and is fully recovered before the next pulse in the round trip hits it, mode-locked laser at the cavity full trip period is hence only described by the cavity photon number and laser gain. Since the cavity photon number equates to the intracavity pulse energy, Eq. (2.1) and (2.2) can be rewritten in term of the pulse energy.

$$\frac{dE(t)}{dt} = \left[K_g N_g(t) - K_s N_s(t) - \gamma_c\right] E(t)$$

$$\frac{dN_g(t)}{dt} = R_p - K_g N_g(t) n(t) - \frac{N_g}{\tau_f}$$

By taking $(K_g N_g) \times t_r = g/t_r$ as gain coefficient per round trip; $(K_s N_s) \times t_r = q/t_r$ as saturable absorption coefficient per round trip; $\gamma_c/t_r = L$ as cavity linear loss, $R_p \equiv g_0/\tau_f$, and saturation fluence of gain $E_{sat,L} = h\nu/2\sigma_g$, the equations above are further simplified to describe mode-locked laser.

$$\frac{dE_p(t)}{dt} = \frac{[g - q - L]E_p(t)}{t_r} \tag{2.19}$$

$$\frac{dg(t)}{dt} = \frac{g_0 - g}{\tau_f} - \frac{g}{E_{sat,L} t_r} E_p \tag{2.20}$$

Based on Eq. (2.19) and (2.20), the conditions to achieve mode-locking without Q-switched instability are derived to be

$$\left|\frac{dq}{dE_p}\right| E_p < \frac{t_r}{\tau_f} r = \frac{t_r}{\tau_f} + \frac{E_p}{E_{sat,L}} \tag{2.21}$$

The left side of Eq. (2.21) indicates the bleaching of saturable absorber per round trip. The intracavity pulse energy increases following the loss reduction. The saturation of the absorber results in the raise of pulse energy for saturating the gain. The right side of the equation determines the strength of gain saturation per round trip. The mode-locked laser is only stable against self-Q-swiching if the gain saturation is sufficient to stop the increase of pulse energy and keep the intracavity fluence as a constant. From the physical terms in Eq. (2.21), Q-switching instability in mode-locked laser can be more easily suppressed by using a saturable absorber with large saturation intensity, a gain medium with short upper state lifetime and with a long cavity length. Laser operation at high pump parameter is certainly preferable to easily fulfill this physical interpretation. However, when the laser operates far above the threshold, saturation of the gain medium becomes the governing factor to laser instability. Therefore, a laser material with larger stimulated emission cross section or with a non-homogeneously broadened gain would tend to reduce the gain saturation fluence for achieving the continous-wave mode-locking [58, 59].

2.4 Saturable absorbers

There is a continued interest in finding the novel optical materials with saturable absorption properties to efficiently Q-switch or mode-lock the solid-state lasers. The basic requirement of using the saturable is to match the absorption transition frequency with the laser radiation frequency. Several materials have been used as saturable

absorbers for the lasers operating in the near infrared spectral region. In early stage, bleachable dye cells are commonly employed in the passive Q-switching and mode-locking studies [60]. Due to its poor durability and complex in handling, dye cells have been gradually replaced by the bulk materials such as GaAs semiconductor [61, 62], Cr^{4+} doped crystals like Cr^{4+}:YAG [63 - 66], Cr^{4+}:YSGG [67, 68], Cr^{4+}:LuAG [69] and the multiple quantum well materials [70 - 73]. Among them the epitaxially grown quantum well semiconductor saturable absorber mirrors (SESAMs) [72] and saturable Bragg reflectors (SBRs) [73] represent those that are most popular nowadays. Such structures can be engineered with appropriate absorption saturation fluences and recovery times, as well as sufficiently broad bandwidth characteristics to cover the spectral range of lasers in ultrashort pulse operation. Specific designs on the material characteristics enable them to be incorporated into different critical resonator configurations. However, the prominent molecular beam epitaxial grown materials are relatively expensive in fabrication since specific lattice matching conditions have to be satisfied.

In contrast, bulky materials are cheaper for a reliable and robust pulsed laser output. Compared to the critical grown quantum well semiconductors, mechanism of the bulk saturable absorbers in optical pulse generation is restricted by their own material characteristics. Laser systems become passively dependent on the saturable material. Proper consideration is therefore required in design for the output optimization. Two common and low cost saturable absorbers, Cr^{4+}:YAG crystal and GaAs semiconductor wafer are selected for the studies in this project.

2.4.1 Cr^{4+}:YAG crystal

Cr^{4+}:YAG crystals are used in the pulse pumped [74, 75] and continuously pumped [63 - 65] Q-switched lasers. For certain applications, Cr^{4+} ions are even codoped with amplifying ions in a monolithic structure for self-Q-switching lasers [76]. Besides the renowned Q-switching ability, Cr^{4+}:YAG has been reported for passive mode-locking [77]. Indeed, since the first Q-switched mode-locking was realized with the Cr^{4+}:YAG in a flashlamp-pumped Nd:YAG laser [78], passive mode-locking with the crystal has also been obtained in the Nd:YVO_4 and Nd:$GdVO_4$ lasers [79, 80]. Affected by the ground state absorption to the cavity Q-factor, passively Q-switched mode-locking (QML) has so far been demonstrated in a laser with Cr^{4+}:YAG saturable absorber. Picoseconds mode-locked pulses within a Q-switched envelope are the laser output feature.

Cr^{4+}:YAG crystal is grown with the Czochralski pulling method. The Cr^{4+} concentration in the melt usually ranges between 0.1 at.% and 0.25 at.% to substitute the Al atoms in tetrahedral sites of YAG (60% of Al atoms). Charges compensating impurities such as Mg^{2+} or Ca^{2+} is added to induce the Cr^{3+} from its normal valence to Cr^{4+} in an oxidizing atmosphere [81]. Cr^{4+}:YAG have several broad absorption bands centered at 410, 480, 640 and 1050 nm. The high absorption cross section in near infrared region enables it to Q-switch the Nd^{3+} ion-doped lasers. The saturable absorption strength of the Cr^{4+}:YAG is easily determined through the doping concentration of Cr^{4+} ions. Usually it is controlled by the thickness of the crystal.

The energy level of Cr^{4+}:YAG saturable absorber can be represented by a simple four-energy level system as shown in Fig 2.10a. It has appreciably large ground-state $^3A_2$ absorption cross section σ_{gs} and a long enough first excited-state ^1E lifetime (4.1 μs) for a

considerable depletion of the ground-state $^3A_2$ upon illumination. As a comparison, the excited-state absorption cross section σ_{es} is about 4 times smaller than σ_{gs} with its short second excited state $^1A_1$ lifetime of about 0.1 – 0.5 ns. According to literature, σ_{gs} ranges from 8×10^{-19} - 7.8×10^{-18} cm^2, associated with the σ_{es} value of 2×10^{-19} – 2.3×10^{-18} cm^2 [82 - 84].

The Cr^{4+} ions transition within the energy levels can provide physical insight into the Q-switching and mode-locking laser dynamics. According to the energy level, the rate equations describing the Cr^{4+} ions populations are

$$\frac{dN_{s1}}{dt} = -c\phi_{TL}\sigma_{gs}N_{s1} + \gamma_{gs}N_{s2} \tag{2.22}$$

$$\frac{dN_{s2}}{dt} = -c\phi_{TL}\left(\sigma_{gs}N_{s1} - \sigma_{es}N_{s2}\right) - \gamma_{gs}N_{s2} + \gamma_{es}N_{s3} \tag{2.23}$$

$$\frac{dN_{s3}}{dt} = c\phi_{TL}\sigma_{es}N_{s2} - \gamma_{es}N_{s3} \tag{2.24}$$

The total absorption in Cr^{4+}:YAG saturable absorber is

$$\alpha_{Cr:YAG} = \sigma_{gs}N_{s1} + \sigma_{es}N_{s2}$$

$N_{si\ (i\ =\ 1,2,3)}$ respectively represents the Cr^{4+} ions population in the ground state $^3A_2$, first excited state ^1E, and second excited state $^1A_1$. σ_{gs} and σ_{es} are the absorption cross section of the ground state and excited state, while the corresponding relaxation rate are γ_{gs} and γ_{es}, respectively. c is the light speed. Cavity mode size is a main factor to alter the saturation characteristics. Consideration of thermal lensing effect of laser gain medium is to be taken into account for the light interaction with the absorber. The effective incident photon density $\phi_{TL} = \phi(\omega_g/\omega_s)^2$ on the saturable absorber after taking into account the

cavity beam cross section is crucial to the saturation of Cr^{4+}:YAG crystal, in which ω_g, ω_s are the effective beam size in gain medium and saturable absorber.

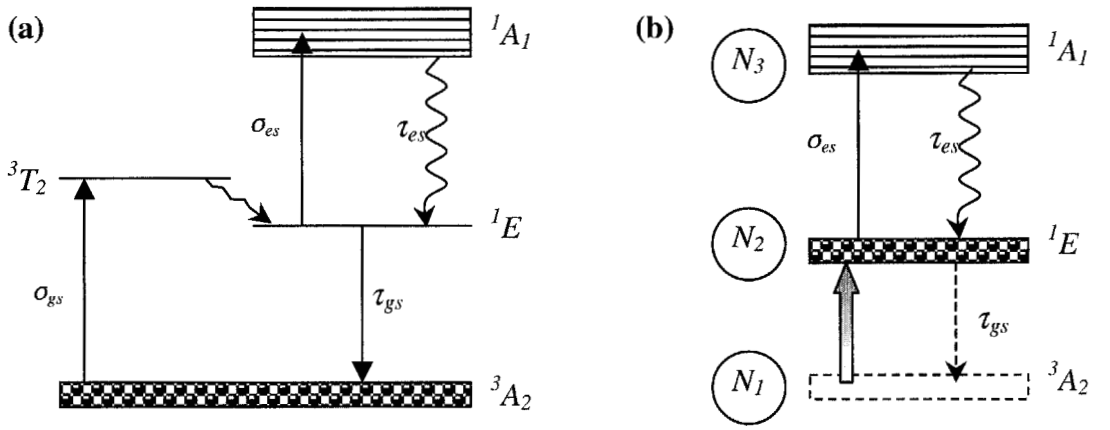

Fig. 2.10: Schematic diagram of the Cr^{4+} ions transition with the interaction of light. (a) The energy levels involved in the absorption in Cr^{4+}YAG crystal. (b) ESA is surmised to be dominant in a ground state depopulated Cr^{4+}:YAG crystal.

The coupled rate equations also determine the influence of cavity photon density to the ion kinetics in each level. When intracavity light intensity is low, Cr^{4+} ions are basically at the equilibrium in the ground state $^3A_2$. Following the increase of photon density, ions are excited and mainly populated in the ground state and the first excited state ^1E. This intensity dependent transition between these two levels contributes to the Q-switching effect to a laser, whereas, the slight influence of the excited state absorption that might occur at the first excited state is considered as additional loss to the passive Q-switching. When the cavity fluence is above the Cr^{4+}:YAG ground state saturation fluence, all the Cr^{4+} ions in the ground state are excited up to the first excited state (Fig. 2.10b). In other words, the Cr^{4+}:YAG saturable absorber is bleached at the ground state,

and the transition between the excited state and the higher lying levels $^1A_1$ become dominant to control the laser dynamics in cavity. The rapid ions transition provide the property for passive mode locking in a laser.

Besides the appropriate optical parameters of Cr^{4+}:YAG, photochemical and thermal stability are the other features that render this material as a long life durable saturable absorber.

2.4.2 GaAs semiconductor wafer

Semi-insulating GaAs is a compound III-V semiconductor. It is a material with good photochemical and thermal stability, as well as high damage threshold. The fundamental feature of this material is its photorefractive effect, which involves both electrons and holes participation in the charge transport process [85]. The dominant defect in an undoped GaAs is the deep donor level $EL2/EL2^+$ within the band gap. This intrinsic defect, which is located 0.82 eV below the conduction band is believed as a cause of photorefractive effect. Because of the intrinsic defect caused by the contamination during the wafer fabrication, GaAs is able to have saturable interaction with the light emission of about 1 μm wavelength.

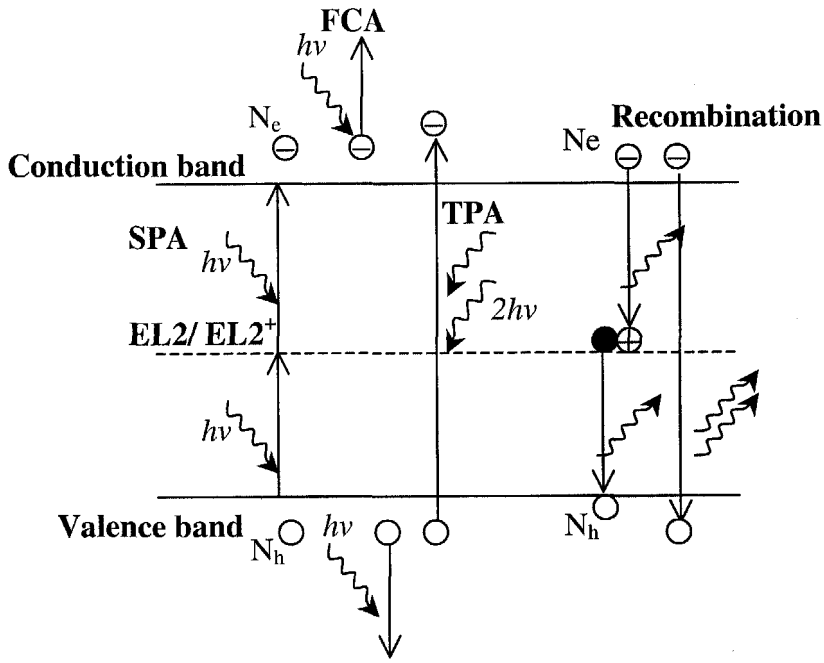

Fig. 2.11: Energy-level diagram for the absorption process in an undoped semi-insulating GaAs semiconductor. ⊖ is electron, ○ is hole, ● is neutral EL2 level and ⊕ is ionized EL2 level.

As in Fig. 2.11, the light-material mechanism is slightly complicated in GaAs compared to the ion transition in the crystalline saturable absorber. Single photon absorption (SPA) mainly takes part under weak illumination. It is simply the transition from *EL2* donor to conduction band to produce free electrons (N_e), and the transition from valence to $EL2^+$ to create free holes (N_h) and neutral *EL2*. The absorption coeffiecient through this process is saturable with the increase in the laser irradiance [86]. The electron-hole recombination time is the absorption recovery time. The exact recombination lifetime may be distinct in each GaAs wafer depending on the fabrication process, but it is commonly estimated within 0.5 to 1 ns in a semi-insulating GaAs

semiconductor [87]. Following the stronger light fluence, nonlinear two-photon absorption (TPA), and TPA-generated free carriers absorption (FCA) become significant to increase the absorption in GaAs. FCA excites electrons higher into the conduction band, and holes deeper into the valence band. These intensity dependent processes are dominant to affect the absorption mechanism in GaAs.

As it is realized that the impurities density in GaAs is the key of the absorption processes, this means the defect density of a sample rigidly determine the absorption coefficient in the semi-insulating GaAs. Basically, a semi-insulating GaAs has total EL2 density of about 1.2 x 10^{16} cm^{-3}, and *EL2* absorption cross section of 1 x 10^{-16} cm^2 [88]. Hence, linear absorption of GaAs should be about 1.2 cm^{-1}. In other word, GaAs is weak to provide the linear absorption, and GaAs saturable absorber would become trivial for laser energy storage in passive Q-switching. This can be confirmed through the commonly reported weak pulse energy from lasers, which are passively Q-switched by the GaAs wafer [89, 90]. The strong pulse jitters could also be understood by the inability of GaAs to Q-switch the laser. Even so, following the saturation of linear absorption at the pulse fluence of about 1.6 mJ/cm^2 [86], nonlinearity taking place in GaAs is detrimental to the laser dynamics. FCA, which always occurs for the energetic nanoseconds long pulses, has been found possible to increase the loss to Q-switched pulse decay edge for narrow pulses [91, 92], whereas, the limiting action from TPA in GaAs has been reported playing a role for laser pulse train stabilization [93]. Normally GaAs wafer is employed as a simultaneous saturable absorber and cavity output coupler to shorten the cavity length and reduce the pulse build up time. The ability of GaAs in passive mode-locking was firstly realized by Zhang *et al.* [94]. TPA process is believed

to be the key to generating the narrow mode-locked pulses. In the studies, the nonlinear TPA of the GaAs wafer was exploited to extend the Q-switched laser pulse width for the realization of continuous-wave mode-locking [95].

The energy transfer and absorption process in GaAs can be illustrated with rate equations as given by Smirl *et al.* [86], which describe the change of density for electrons, holes and ionized *EL2* impurity, respectively. Corresponding to the absorption processes, the electron-hole recombination process in the undoped GaAs is categorized into hole-donor (hole-*EL2*), electron-trap (electron-*EL2*) process and bimolecular electron-hole (direct electron-hole) recombination. The model represents the absorption process in GaAs is as below.

$$\frac{dN_e}{dt} = c\phi_{TL}\sigma_e\left(EL2^0 - EL2^+\right) + Bc\phi_{TL}^2/12 - \gamma_{et}N_e EL2^+ - \gamma_{eh}N_e N_h \tag{2.25}$$

$$\frac{dN_h}{dt} = c\phi_{TL}\sigma_h EL2^+ + Bc\phi_{TL}^2/12 - \gamma_{hd}N_h\left(EL2^0 - EL2^+\right) - \gamma_{eh}N_e N_h \tag{2.26}$$

$$\frac{dEL2^+}{dt} = c\phi_{TL}\left[\sigma_e\left(EL2^0 - EL2^+\right) - \sigma_h EL^+\right] - \gamma_{et}N_e EL2^+ + \gamma_{hd}N_h\left(EL2^0 - EL2^+\right) \tag{2.27}$$

The total absorption in GaAs is hence

$$\alpha_{GaAs} = \sigma_e\left(EL2^0 - EL2^+\right) + \sigma_h EL2^+ + \sigma_{fc}N_e + B\phi_g/2 \tag{2.28}$$

The first two terms in Eq. (2.28) are from SPA, last third term is from FCA process, while TPA contributes to the last term. In the coupled equations above, ϕ_{TL} is the thermal lens affected incident photon density on GaAs and ϕ_g is the photon density in laser gain medium. $B = \beta hvc(\omega_g/\omega_s)^2$ is the coupling coefficient of TPA, with β is the TPA absorption coefficient. σ_e, σ_h, σ_{fc} are respectively the absorption cross section of *EL2*, $EL2^+$ and FCA, while N_e, N_h and $EL2^+$ are the density of free electrons, free holes

and positively charged EL2 defect. γ_{hd}, γ_{et}, γ_{eh} are the recombination coefficients of hole-*EL2*, electron-*EL2* and direct electron-hole, respectively. The material parameters from the literature, which are related with the light interactive processes in GaAs, are summarized in Table 2.3.

Table 2.3: Parameters for light intensity dependent processes and absorption in GaAs.

Material parameters	Values
β TPA absorption coefficient	26×10^{-9} cmW^{-1} [85]
σ_e EL2 absorption cross section	1×10^{-16} cm^2 [85]
σ_h EL2$^+$ absorption cross section	2.3×10^{-17} cm^2 [96]
σ_{fc} FCA absorption cross section	6×10^{-18} cm^2 [85]
γ_{hl} Hole-EL2 recombination coefficient	3.4×10^{-11} cm^{3}s^{-1} [85]
γ_{et} Electron-EL2 recombination coefficient	1.9×10^{-8} cm^{3}s^{-1} [85]
γ_{eh} Direct electron-hole recombination coefficient	2×10^{-10} cm^{3}s^{-1} [85]
$EL2^0$ Total EL2 density	1.2×10^{16} cm^{-3} [85]
$EL2^+$ Initial ionized EL2 density	1.4×10^{15} cm^{-3} [85]

2.5 Summary

This chapter has reviewed the fundamentals of lasers from gain media to saturable absorbers materials characteristics. The optical pulse generating in passive Q-switch and mode-locked processes was analyzed. Understanding on the basic properties of each optical element in the lasers is essential for the development of laser systems.

CHAPTER 3

Continuous-wave lasers performance

Laser performance is closely related to the pump source, thermal or lasing quality of gain medium and the cavity design. For high power lasers, thermal lens influence is detrimental to laser stability and output efficiency. The really crucial parameter in this regard is thermal conductivity of laser material, and certainly the effective pump power that generates the heat for thermal lens, which is dependent on the focusing pump power and pump power absorption coefficient in the gain material. As reviewed in previous chapter, Nd:$GdVO_4$ and Nd:$GdYVO_4$ are categorized as a laser material of high thermal conductivity, and large absorption cross section. The absorption feature of these birefringent crystals is strongly affected by the polarization of pump source and varied with the dopant level of the sample. The thermal lens effect is different for each gain medium under different pump condition. Therefore, thermally induced laser focal length must be identified for proper design of an efficient laser.

This chapter begins with a brief introduction and performance of a commercial laser diode pump source, and then moves to the absorption coefficient measurement of different crystal samples of Nd:$GdVO_4$ and Nd:$GdYVO_4$ that are employed in the studies. Experimental identification of thermal focal lengths based on the concept of cavity stability is compared with theoretical modeling. It is followed by the calculation on cavity design using the experimental measured thermal focal lengths. In the following section, CW laser performance is studied from the perspective of different doping concentrations and emission cross sections in Nd:$GdVO_4$ laser. Under the same

experimental parameters, mixed crystal Nd:$Gd_{0.64}Y_{0.36}VO_4$ laser performance is also identified and compared to the pure Nd:$GdVO_4$ whose has the same doping level.

3.1 Diode laser pump source

A 15W fiber bundle coupled CW dioded-array (OPC-B015-FCPS) was used in the course of this research. The laser pumping system is an integrated package consisting of the drive electronics, thermal electric cooling apparatus and diode source. The fiber bundle end of the pump laser is 1.16 mm in diameter with a numerical aperture of 0.22. The radiation from the fiber tip was collimated and focused by an optical reimaging unit (OPC-ORU-03) to a spot size of approximately 400 μm in diameter. The center emission wavelength of the diode is 807 nm ± 3 nm depending on each degree Celsius of temperature tuning. In order to ensure the wavelength stability associated with the varying of pump power, diode emission spectra were checked at different pumping level. Fig. 3.1 (a) and (b) are the experimental records for the relation of wavelength and pump power, respectively at the fixed diode temperature of 23.5 ^{0}C and 24.5 ^{0}C. These graphs were obtained with optical spectrum analyzer (Ando, MS9710A). The wavelength resolution was set at 0.1 nm with the variation bandwidth of 1 kHz.

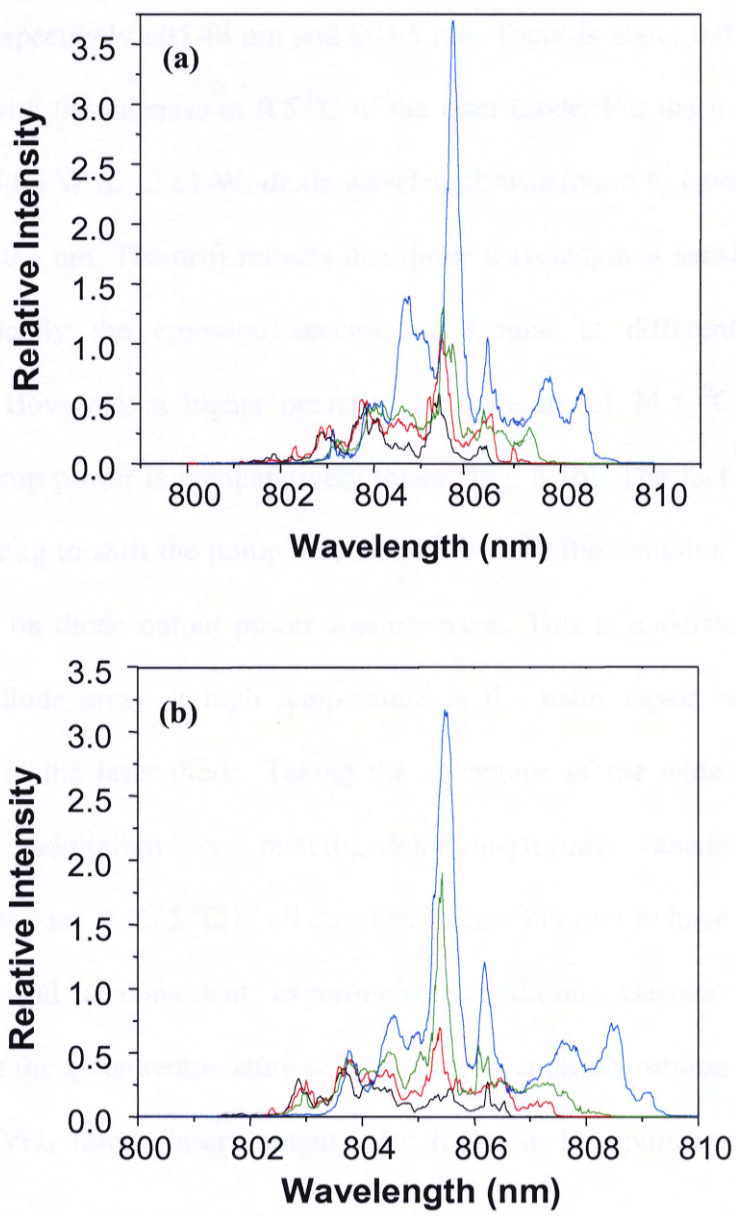

Fig. 3.1: The experimental determined pump and wavelength relationship at diode operating temperature of (a) 23.5 ^{0}C and (b) 24.5 ^{0}C. The spectrum from low to high is respectively for the pump power of 4.06 W, 6.56 W, 8.96 W, and 12.81 W.

At the diode temperature of 23.4 ^{0}C and 24.5 ^{0}C, peak wavelength of full pump power was respectively 805.48 nm and 805.5 nm. There is about 0.02 nm change in the wavelength with the increase of 0.5 ^{0}C of the laser diode. For the increase of the pump power from 4.06 W to 12.81 W, diode wavelength was found to have a thermal induced increment of 0.1 nm. The drift reflects that diode wavelength is sensitive to temperature change. Basically the emission spectra are similar at different values of diode temperature. However, at higher operating temperature of 24.5 ^{0}C, emission peak at maximum pump power is comparatively lower (Fig. 3.1b). The fact is more significant while attempting to shift the pump wavelength towards the emission peak of 807 nm. A rapid decline on diode output power was observed. This is understood as that induced heat in the diode array at high temperature is the main factor, which degrades the performance of the laser diode. Taking the advantage of the wide absorption band in neodymium gadolinium or mixed-gadolinium-yttrium vanadate crystal, diode temperature was set at 23.5 ^{0}C in all the experiments in order to have a better diode laser performance and a consistent experimental condition. Despite the fact that the wavelength at the given temperature was not exactly at the absorption peak of Nd:$GdVO_4$ and Nd:$GdYVO_4$ lasers, lasers output were found to be optimized in term of power stability.

After the diode pump source has been used intensively for a long term, periodic checking on the diode pump power revealed that power emission tending to fall. The measurement was obtained with a CW power meter head (Melles Griot, 30-Watt broadband power/energy meter), which was located slightly away from the tight focusing area in order to avoid the damage on the sensor head. Fig. 3.2 shows a current-to-power

(P/I) curve for the pump laser at the initial of the project (year 2001). About 9% of decrease was found at the maximum of output pump power after a year of usage. The P/I conversion efficiency dropped from 92% to 80%. The limitation of the operating lifetime of diode array is inevitable after long-term use. Therefore the diode output power was recorded frequently as a reference to estimate the laser efficiency in the relevant CW, Q-switched and mode-locked experiments.

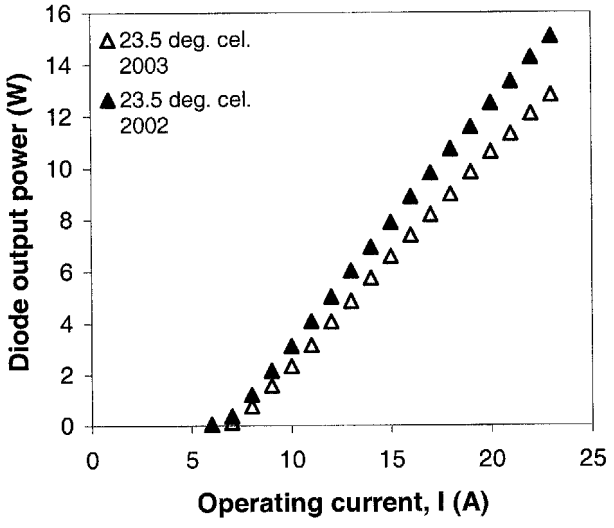

Fig. 3.2: Current-to-power curve of the laser diode array showing the laser performance at different period.

3.2 Crystal features for cavity design

The absorption coefficient and thermal focal lens of the gain medium, which could be affected by the pump source, are required to be well characterized for cavity design. In addition, these parameters are crucial to the laser numerical simulation in the coming chapter.

3.2.1 Pump absorption coefficient

The use of the unpolarized pump beam and the offset of wavelength from the laser peak absorption band might result in lower absorption in the birefringent vanadate crystals. It is necessary to carry out the measurement before starting the laser operation. The basic relation between incident intensity (I_0) and transmitted intensity (I) for an absorbing medium with uniform pump profile is expressed as

$$I = I_0\left[\exp\left(-\alpha_g l_g\right)\right]. \tag{3.1}$$

Based on the assumption that there have no other losses (such as scattering loss) during the transmitting of light through the crystal, the absorbed light is written as

$$I_{abs} = I_0 - I\ .$$

Absorption coefficient α_g can then be determined from the slope efficiency of the linear plot between I_{abs} versus I_0

$$\frac{I_{abs}}{I_0} = 1 - \exp(-\alpha_g l_g)$$

$$\alpha_g = \frac{1}{l_g}\ln\left(\frac{1}{1-\frac{I_{abs}}{I_0}}\right) \tag{3.2}$$

The saturation absorption was demonstrated by measuring the transmission of the pump radiation through the crystal with a power meter. Fig. 3.3 shows the simple arrangement for measuring the transmitted pump light after an anti-reflection coated laser crystal. The input mirror is for coupling the pump beam into the crystal. Considering the mirror loss, the incident pump light was measured after the input mirror.

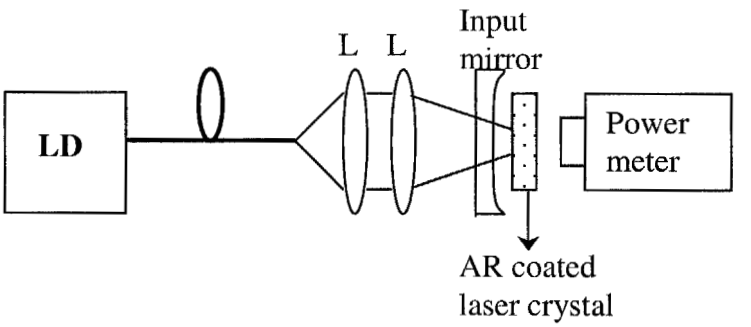

Fig. 3.3: Experimental setup for determining absorption coefficient in laser crystals. L: coupling lens, LD: laser diode.

Pump saturation absorption differs according to the crystal doping concentration. Fig. 3.4 shows the absorbed power against the incident power on the crystals through an input mirror for different doping levels (0.5 at.%, 1 at.% and 1.61 at.%) of a-cut Nd:$GdVO_4$ crystals (hereby onward, the unstated crystal cutting is a-cut). Thickness of the samples is 6 mm, 4 mm, and 3 mm, respectively from the light doping to the heavy doping concentration. The incident power was reduced with the measured input mirror loss of about 10%. From the linear portion of the curve, absorption coefficient is experimentally found for each crystal. They are respectively 2.53 cm^{-1}, 4.06 cm^{-1}, and 9.36 cm^{-1} for the doping level of 0.5 at.%, 1 at.% and 1.61 at.%.

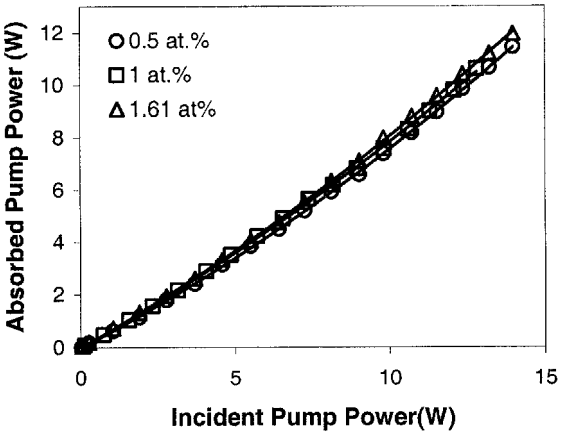

Fig. 3.4: Absorbed power curve for different doping levels of Nd:$GdVO_4$ crystals.

Similar measurement was carried out on the 0.5 at.% Nd:$Gd_{0.64}Y_{0.36}VO_4$ crystal. It was found that the mixed crystal possessing a slightly higher absorption coefficient of 3.46 cm^{-1} compared to the Nd:$GdVO_4$ crystal at the same doping concentration. This effect had also been observed in the absorption spectra between these two laser crystals as in Fig. 2.5. From that, better absorption characteristic of the mixed laser crystal has been further confirmed. Doping concentration level is definitely still the governing factor in increasing the pump light absorption in the crystal.

3.2.2 Thermal focal lens

In the diode end-pumping configuration, gain medium is heated by the focused pump beam at the center of the crystal and cooled by the circulating chilled water along its periphery. Heat flows from the hotter pumped region to the cooler edges of the crystals, resulting in a temperature gradient. This temperature gradient in turn induces a refractive index and thermal expansion profile. Generally, the combination of these effects makes

the crystal act like a lens. Increasing of refractive index provides a net increase in the optical path length with increasing temperature. The presence of the thermal lens is equivalent to a concave mirror at one end of the cavity. How strong a laser being affected by the heat is strongly related with the material parameters, pumping geometry and the cooling system. For the longitudinal CW diode pumping, the effective thermal focal lens is given as [97]:

$$f_T = \frac{\pi k \omega_p^2}{P_{ph}(dn/dT)(1-\exp^{-\alpha_g l})}, \tag{3.4}$$

where k is the thermal conductivity of the gain medium, ω_p is the $1/e^2$ Gaussian radius of the pump beam, P_{ph} is the pump power converted to heat, and α_g is the absorption coefficient.

Thermal lensing is particularly important in designing the cavity configuration. Laser resonator will operate in the optically stable regime if it satisfies the condition:

$$0 < g_1 g_2 < 1,$$

where g_1, g_2 are the cavity parameters, which can be described in terms of cavity length L and radii curvature of the two end mirrors R_1 and R_2,

$$0 < \left(1 - \frac{L}{R_1}\right)\left(1 - \frac{L}{R_2}\right) < 1. \tag{3.5}$$

Based on Eq. (3.5), one could also determine the thermal lens of a longitudinally pumped laser based on the stability of a plane-plano-cavity laser [98]. When the thermally induced focal length is longer than the cavity length, the cavity becomes unstable and results in a decline in the power emission. Therefore, by adjusting the distance of cavity output mirror and observing the dip of output power, one can predict

the effective thermal focusing lens formed in the laser crystal. In practice this method can also be used by fixing the cavity length and increasing pump power to avoid the cavity misalignment from shifting the output coupler. Fig. 3.5 shows the setup scheme for the thermal lens measurement. For the cavity where input mirror is needed, laser crystal should be positioned closely to the mirror to enhance the accuracy of estimating the thermal focal length.

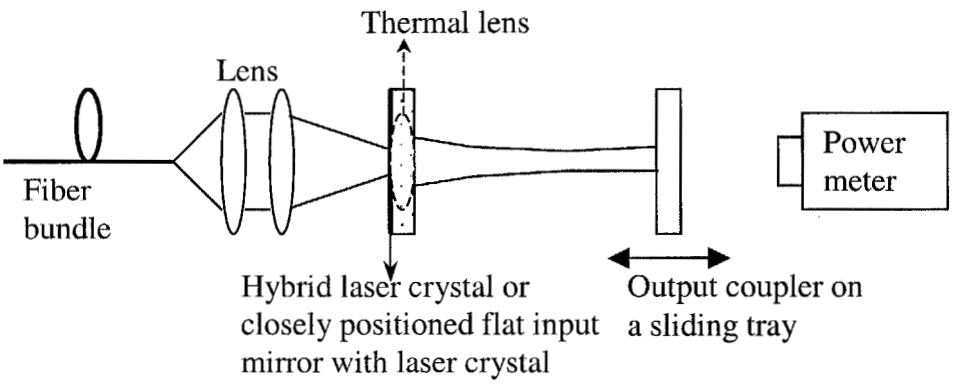

Fig. 3.5: Setup of measuring the thermal focal lens in the crystal.

Practically, the pump power was increased at a given resonator length and it was recorded at the full decrease of the output emission. All the measured thermal focal lengths for three different doping of laser crystals are plotted in Fig. 3.6 with respect to the theoretical calculation. The data are in agreement with Eq. (3.4) in which the calculation is shown by the solid line. The graph was produced by employing $k = 11.4 \times 10^{-2}$ $Wcm^{-1}K^{-1}$, $\omega_p = 0.2$ mm, $P_{ph} = 1-(808/1064) = 0.24$, $dn/dT = 4.7 \times 10^{-6}$ K^{-1} [24].

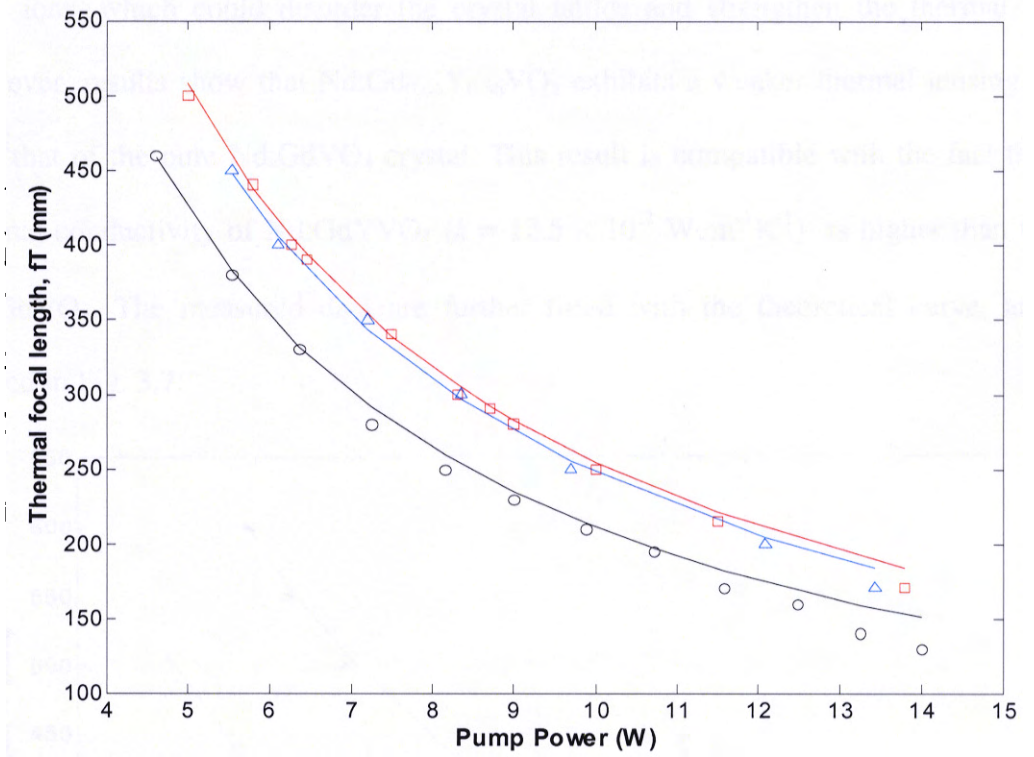

Fig. 3.6: Experimental measured (data points) and calculated (line) thermal focal length for Nd:$GdVO_4$ crystal with doping concentration of 0.5 at.% (triangle), 1 at.% (square), and 1.61 at.% (circle).

The laser crystals showed a distinguishable thermal lens effect between each doping level. Heavily Nd^{3+} doped crystal (1.61 at.%) is expected giving the strongest thermal induced lens, while the remaing two (1 at.% and the 0.5 at.% crystals) have a close similar thermal effect with respect to certain pumping level. The influence of doping level on the thermal characteristics that observed in Nd:$GdVO_4$ is similar to that observed in the mixed gadolinium vanadate crystal, Nd:$GdYVO_4$. The main concern with this newly developed mixed crystal, Nd:$GdYVO_4$ is its thermal lens effect, compared to the pure Nd:$GdVO_4$ crystal. As the mixed crystal has random distribution of Y^{3+} and

Gd^{3+} ions, which could disorder the crystal lattice and strengthen the thermal effect. However, results show that Nd:$Gd_{0.64}Y_{0.36}VO_4$ exhibits a weaker thermal lensing effect than that of the pure Nd:$GdVO_4$ crystal. This result is compatible with the fact that the thermal conductivity of Nd:$GdYVO_4$ (k = 12.5 × 10^{-2} $Wcm^{-1}K^{-1}$) is higher than that of Nd:$GdVO_4$. The measured data are further fitted with the theoretical curve, and are plotted in Fig. 3.7.

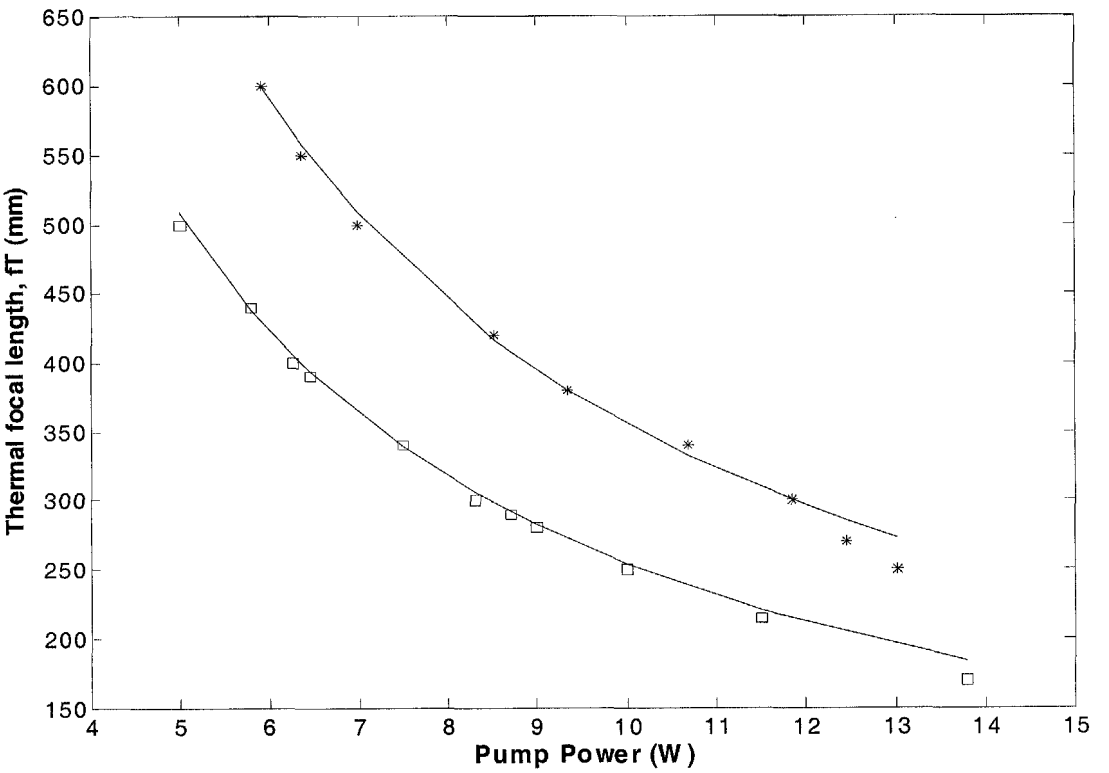

Fig. 3.7: Comparison of thermal focal length between Nd:$GdVO_4$ (square) and Nd:$Gd_{0.64}Y_{0.36}VO_4$ (asterisk) at the same doping level of 0.5 at.%. Solid line is the fitting curve through calculation.

From the fitted result, the temperature-induced refractive index change of Nd:$Gd_{0.64}Y_{0.36}VO_4$ crystal is about 3.5 × 10^{-6} K^{-1}. It is worth pointing out that from the

fitting curve of all laser crystals, the measured thermal focusing data are markedly stronger than the calculation at high pumping regime. Thermal conductivity of crystals reduces with the increase of temperature. It is to note that the proposed model used for the fitting did not consider the effects of thermally induced expansion and mechanical deformation. The crystal surface would be distorted as a result of the high power absorption. The stress and strain effect would also increase refractive index in material and further reduce the thermal focal length. An appropriate description of the thermooptic coefficient χ in a crystal should contain not only the term of thermal induced refractive index change (dn/dT), but also the axial expansion and stress-induced change of refractive index [99].

$$\chi = \frac{dn}{dT} + (n-1)(1+\upsilon)\alpha_T + n^3\alpha_T C_r$$

where υ is the Poisson's ratio, α_T is the thermal expansion coefficient, and C_r is the photoelastic coefficient. The thermo-mechanical sensitivity due to the photoelastic effect in the last term is negligible in lots of materials because it is normally about ten times smaller compared with other terms. At high pumping level, the striking feature of the fast decrease thermal focal length in both Nd:$GdVO_4$ and Nd:$GdYVO_4$ crystals which occurred in a relatively short resonator is believed yielding from the impact of different thermal properties in anisotropic crystals. The thermooptic coefficient of each polarization in the vanadate is considered to be $\chi_{a,c} \approx \frac{dn_{a,c}}{dT} + (n_{a,c}-1)(1+\upsilon)\alpha_T$ for a-polarization and c-polarization respectively, where χ_a should be greater than χ_c because the thermal expansion and temperature dependent refractive index are higher along a-axis, and this hence leads to stronger thermal lensing in a-polarization. During the

determination of thermal lens, cavity length was gradually shortened to measure the thermal focal length at higher pump power. Thermal property of the a-polarization could start to affect and increase the thermally induced diffraction loss when the resonator length was reduced to its stability zone. This would further cause a drastic change of the measured thermal lens and seriously affect the stability of laser output, particularly for those lasers operating close to the edge of the optical stable region. In this model, pump beam is assumed to be constant. Nevertheless, pump beam variation in relation with different drive current could also affect the measurement. Limited by the incertitude material parameters, the thermal lensing of the crystals cannot be further quantified. Even so, this simple model has well satisfied the measurement at most of the power levels within the studied range though there is about few to ten percent of deviation in the calculation at pump power of more than 11 W. Therefore, detailed investigation on the crystal thermal effect is necessary for higher power scaling in future.

3.3 Two-mirror laser cavity design

Attainment of cavity stability criterion requires calculation of the beam parameters inside the cavity. Once the criterion is satisfied, the propagating ray has a minimum spread when it is bounced back and forth between the cavity mirrors. The consideration upon the resonator sensitivity to the optical perturbation is of utmost importance to a cavity that contains a pump-dependent thermal lens in gain medium. The thermal lens perturbs the mode and leads to the change of mode size and beam diffraction. An estimate of the stable laser operating range and the relative cavity mode will be useful as a guideline to design the optimum cavity configuration. This can be done by Gaussian beam *ABCD* law,

which is able to determine the beam propagation through a set of optical elements. Through *ABCD* law, one is allowed to calculate numerically the beam parameters at every position in laser cavity.

The complex beam parameter for a Gaussian beam after passing through an optical system is transformed to

$$q_2 = \frac{Aq_1 + B}{Cq_1 + D} \tag{3.6}$$

where $q_1 = \frac{1}{R} - j\frac{\lambda}{\pi n \omega^2} = \frac{1}{R} - j\frac{1}{z_0}$; R is the radius of curvature of the wave front, ω is the radius of the beam. λ is the propagation beam wavelength and n is the index of refraction. The real part represents the divergence of the surface with constant phase, while the imaginary part is as a degree of power concentration in the beam axial region, z_0 is Rayleigh range, as the distance where the beam remains collimated expanding in radius by less than a factor of 1.41. *A*, *B*, *C* and *D* are the characterizing elements for the optical system [100]. One can calculate the mode size and the position of the next collimated beam systematically by multiplying together the *ABCD* ray transfer matrices for the elements in the cavity. Actually the cavity stability parameter of Eq. (3.5) can also be written in terms of the characterizing elements from the transformation matrix for the system.

$$-1 < \frac{(A+D)}{2} < 1. \tag{3.7}$$

The Rayleigh range of the beam after travelling one complete round trip in cavity is given by

$$z_0 = \frac{|B|}{\sqrt{1-(\frac{A+D}{2})^2}}, \tag{3.6}$$

where *(A+D)/2* should fulfil Eq. (3.7) for a stable laser operation. According to Eq. (3.6), it should be noted that z_0 is dependent on the transformation matrix. Therefore from the determined z_0, beam spot radius in the cavity can be calculated through

$$\omega = \sqrt{\frac{\lambda z_0}{n\pi}}. \tag{3.7}$$

Matlab program is used for the *ABCD* calculation of the experimental cavity design and beam spot estimation. By taking into account the measured thermal lens effect in the laser crystal, three optical elements are included in the calculation for a two-mirror cavity as shown in Fig. 3.8. The front mirror is a concave mirror with radius of curvature of 500 mm, whereas the output coupler is a flat mirror. Transformation matrices of each optical component are also given in the figure. The distance L_1 between M_1 and thermal lens is fixed, while L_2 is varied to characterize the laser stability and beam spot in the simulation.

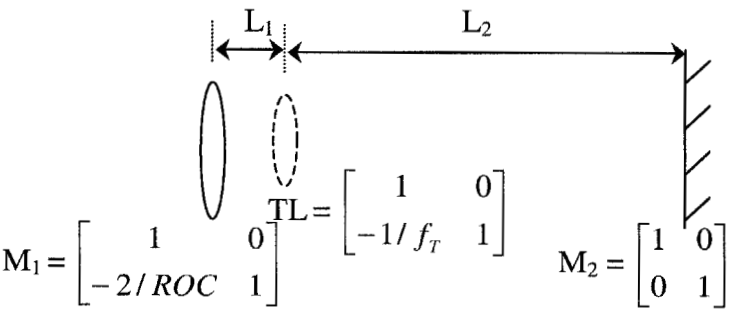

Fig. 3.8: Schematic of a linear laser cavity with intracavity focusing lens. M_1: Input mirror, TL: thermal lens in laser crystal, M_2: output coupler. *ROC*: radius of curvature.

Fig. 3.9 shows the maximum stable cavity length determined from the numerical calculation at full diode pump power. This estimate is inclusive of the laser crystals of different doping concentrations, which respectively exhibit different levels of thermal effect. The thermal induced lens used in the calculation was taken from the experimental measurement. As expected, the allowable stable cavity length for the higher doped crystal is shorter, corresponding to the stronger thermal focusing effect in gain medium.

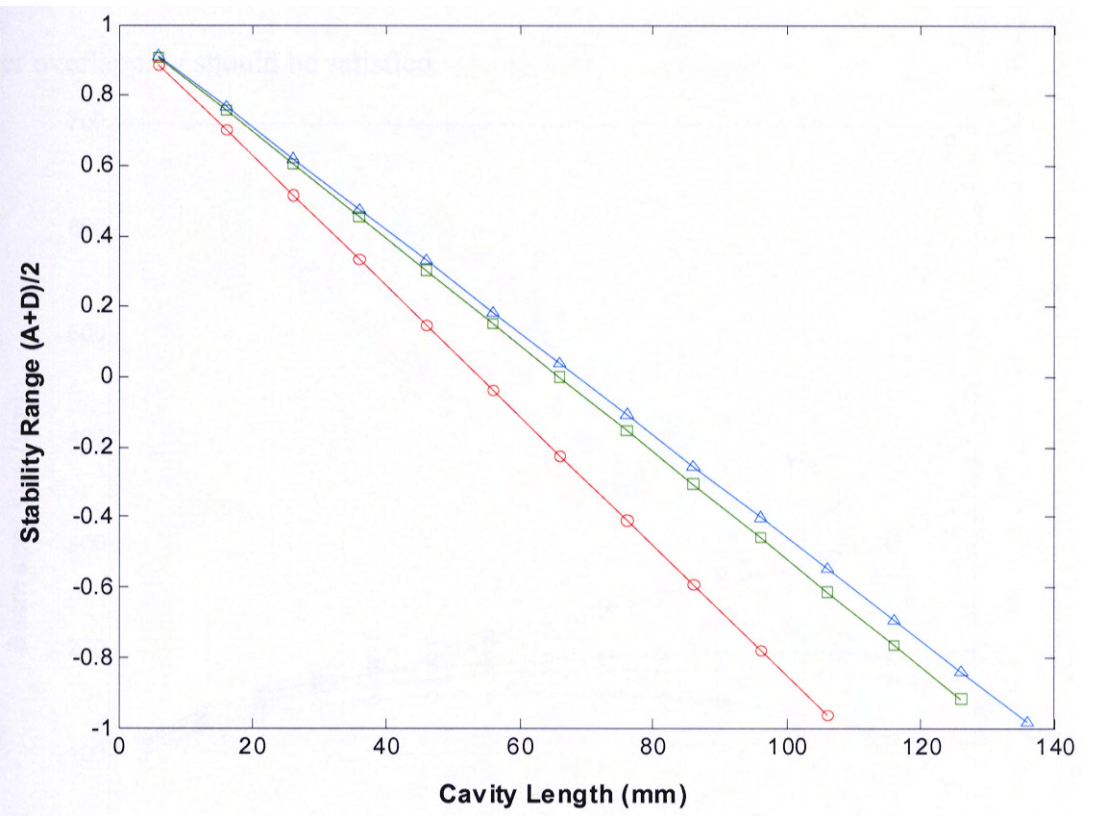

Fig. 3.9: Acceptable cavity lengths for laser operation within the optical stability range. Calculation is made of the crystals with doping concentration of 0.5 at.% (triangle), 1 at.% (square), and 1.61 at.% (circle).

Since the cavity mode size varies with the pump dependent focal length, cavity spot size at different resonator length differs from each other. Fig. 3.10 shows one example of the calculated cavity beam waist with respect to the beam spot size at laser crystal center for three different sets of thermal lens in Nd:$GdVO_4$ laser crystal. Under a strong focusing lens, spot size in crystal shows a significant change. The abrupt decrease of mode size following the increasing of pump power crucially affects the laser performance. For optimal laser output, mode-matching conditions with proper pump to laser overlapping should be satisfied.

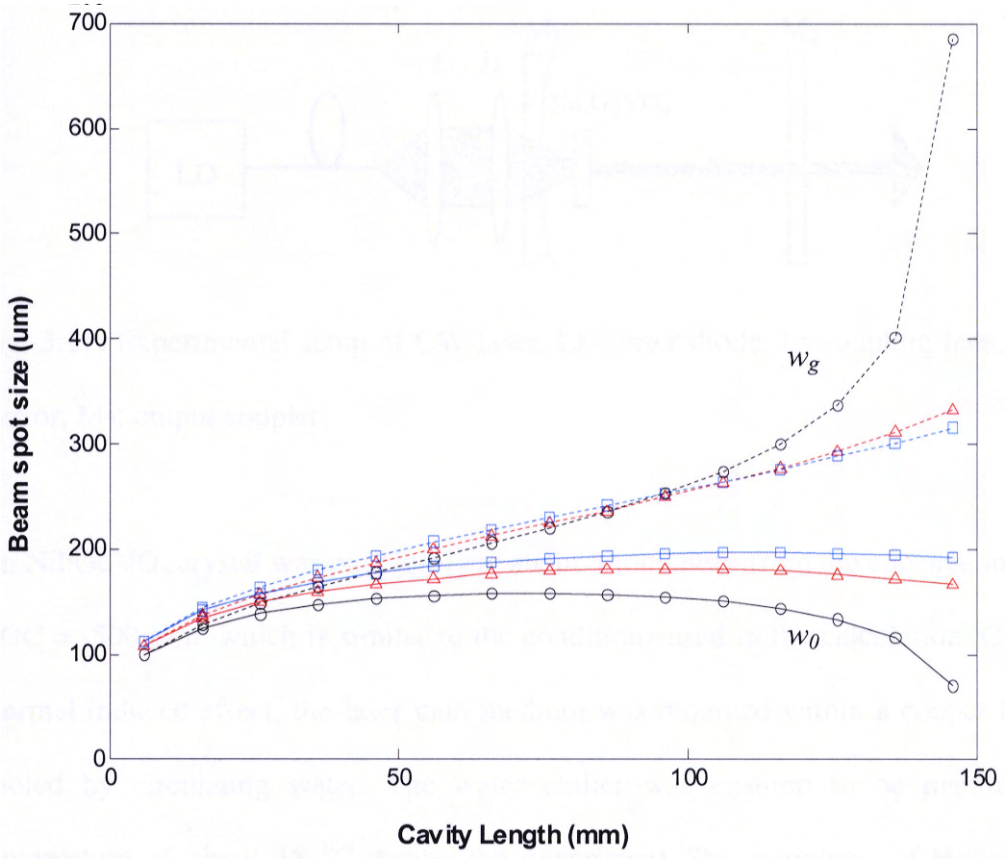

Fig. 3.10: Estimated beam spot size at laser crystal center, w_g (dash line) and cavity beam waist, w_0 (solid line) for thermal focal lens f_T = 200 mm (circle), 300 mm (triangle) and 400 mm (square).

3.4 CW laser performance

3.4.1 Nd:$GdVO_4$ lasers

3.4.1.1 Effects of crystal doping concentration

The CW laser operation was initially studied with different doping concentration of Nd:$GdVO_4$ crystals (0.5 at.%, 1.14 at.%, 1.61 at.%). The crystals are anti-reflection coated on both surfaces at 808 nm and 1.06 μm. Fig. 3.11 shows the experimental plano-concave cavity configuration.

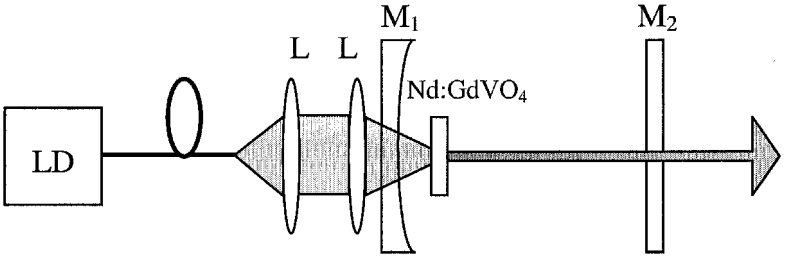

Fig. 3.11: Experimental setup of CW laser. LD: laser diode, L: coupling lens, M_1: input mirror, M_2: output coupler.

An Nd:$GdVO_4$ crystal was put closely at about 5 mm away from the concave input mirror *ROC* = -500 mm, which is similar to the conditions used in the calculation. Considering thermal induced effect, the laser gain medium was mounted within a cooper holder and cooled by circulating water. The water chiller was ensured to be maintained at a temperature of about 18 ^{0}C during the experiment. The periphery of the crystal was wrapped with indium foil in order to have better heat dissipation from crystal to metal holder. The collimated diode laser was focused into Nd:$GdVO_4$ through a dichroic coated input mirror. The mirror surface facing to the diode laser is high transmission (HT)

coated at 808 nm and highly reflective (HR) at 1064 nm, whereas the other side of the mirror is anti reflection coated at 1064 nm. The laser resonator was completed by using a partially transmission plane mirror as coupler.

A proper cavity length selection was selected to obtain the optimal mode matching in the laser for linear increase of the highest average output power within the available pumping regime. Fig. 3.12 depicts the laser output power at different cavity lengths for a given pump power of 13.5 W. The coupling transmission used in the measurement is 30%.

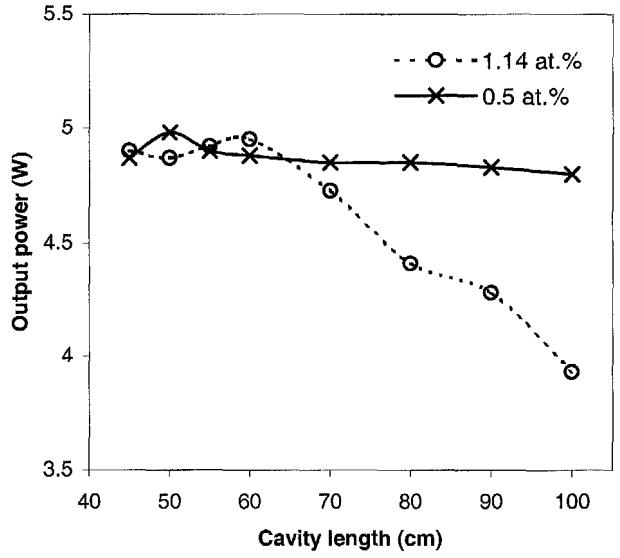

Fig. 3.12: The recorded laser output power at different cavity lengths for the crystals with doping of 0.5 at.% (cross) and 1.14 at.% (circle).

It was found experimentally that the optimal cavity length for the 0.5 at.% and 1.14 at.% Nd:$GdVO_4$ lasers are 50 mm and 60 mm, respectively. Due to the thermal focusing, at longer cavity length, laser output power was prone to drop down from its linear relation with the increasing of pump power.

Sensitivity of the laser output power to the thermal effect is clear following the increase of cavity length. This fact is reflected from the dip of the power, which is significant in the 1.14 at.% doped laser, which has stronger thermal focal lens. As has been pointed out in Fig. 3.10 that at shorter resonator, cavity mode radius at the crystal center would be far below the pump beam size (≈ 0.2 mm). This deduces that the low output from a shorter cavity would be from the inefficient mode matching between the pump beam and cavity mode. On the other hand, stronger thermal lens in the heavily doped 1.61 at.% laser crystal was prone causing a drastic change on cavity mode size, resulting in sudden decline of laser output power especially in the longer cavity length. It was found in experiment that the cavity could only be shortened to 30 mm for the linear increasing of optimum output power. Fig. 3.13 shows the output power with respect to the pump power for these three different doping level of Nd:$GdVO_4$ with the output coupler of 70% reflectivity. For better comparison, both 0.5 at.% and 1.14 at.% doped lasers were kept at the same cavity length of 60 mm, while the heavily doped laser was operating at 30 mm cavity length.

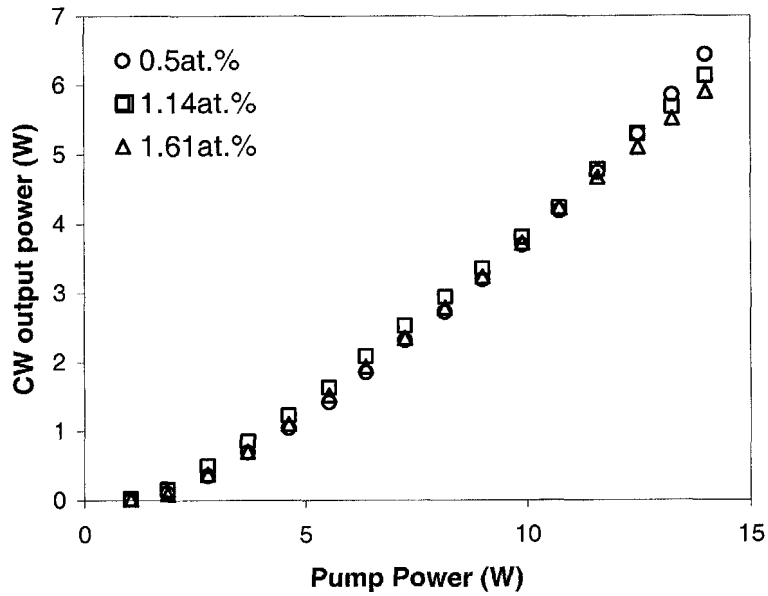

Fig. 3.13: Output power versus incident pump power for three different doping levels of Nd:$GdVO_4$ lasers.

The 0.5 at.% Nd:$GdVO_4$ crystal showed the optimal CW laser performance at the high pumping regime. The average slope efficiency from each linear power curve at pump power range of over 9 W was determined to be 62.6%, 56% and 53.4%, respectively for the lightly doped to the heavily doped laser crystals. Note that the total incident pump power was used in estimating the laser efficiency instead of the absorbed pump power. From the increase tendency of the laser output, it is believed that higher output power will be attainable in the laser.

After investigated the influence of output coupling to the CW laser performance in the 0.5 at.% Nd:$GdVO_4$ laser, output coupler with transmission of 20% was experimentally determined to be the optimum for the laser system. Fig. 3.14 shows the CW output versus pump power for each cavity output coupling. Limited by the pump power of 12.8 W, CW laser emission of 6.27 W was achieved at the slope efficiency of

63%, giving the optical conversion efficiency of about 50%. Based on the slightly curve up laser slope efficiency at high pumping regime, it is expected that higher conversion efficiency could be obtained if higher pump power is available.

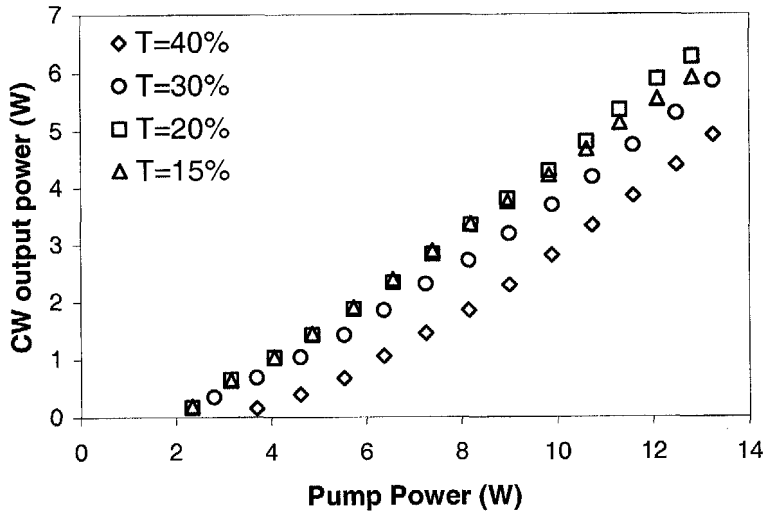

Fig. 3.14: Laser efficiency of the 0.5 at.% Nd:$GdVO_4$ laser at different coupling transmission.

Laser output beam quality from the optimized 0.5 at.% Nd:$GdVO_4$ laser was further characterized through M^2 measurement. The M^2 factor is determined through the ratio of the far-field diameter to the diffraction-limited beam diameter.

$$M^2 = \frac{\pi w_0^2}{z_0 \lambda},$$

where z_0 is the distance of one Rayleigh range from the focal spot, w_0 is the focal beam waist radius and λ is the laser wavelength. Using the moving knife-edge method [101], the laser beam quality factor could be estimated. Laser beam spot diameter is measured through the knife edge moving distance for which the beam intensity is respectively cut off 10% and 90%.

$$2w = 1.561 \mid X_{90\%} - X_{10\%} \mid,$$

where w is the beam spot radius, $X_{90\%,\ 10\%}$ is the knife edge scanning position where the beam intensity is cut off 90% or 10%.

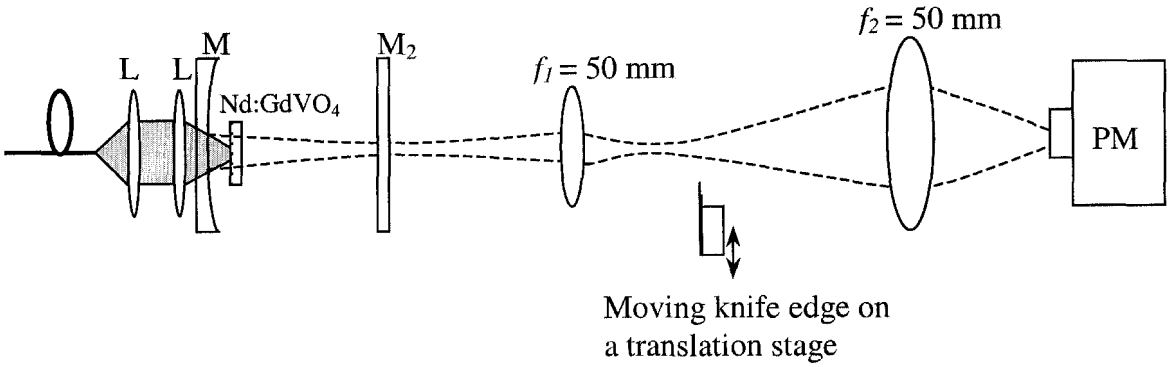

Fig. 3.15: Experimental setup for the laser beam quality measurement. PM: power meter.

Fig. 3.15 shows the simple setup for determining the laser M^2 parameter. Laser output was propagated through a focusing lens (f_1), placed at 135 mm from the output coupler. The lens acts like an expander to diverge the beam into larger beam spot and reduce the knife-edge beam cutting error. For proper power collection, the diverged beam spot was focused with a large diameter lens (f_2, with 4 inches in diameter) into a power meter. From the experimental determined focal beam waist radius and Rayleigh range, laser beam quality parameter under the full pump power was calculated to be about M^2 = 1.5. Based on this result, the laser beam spot size near the coupler, before the focusing lens was calculated to be about 145.6 μm. By removing the beam expander, transverse laser beam spot is further characterized. Fig. 3.16 depicts the spatial intensity distribution of a far-field output beam spot, measured by knife-edge scanning at 0.1 m from the output coupler.

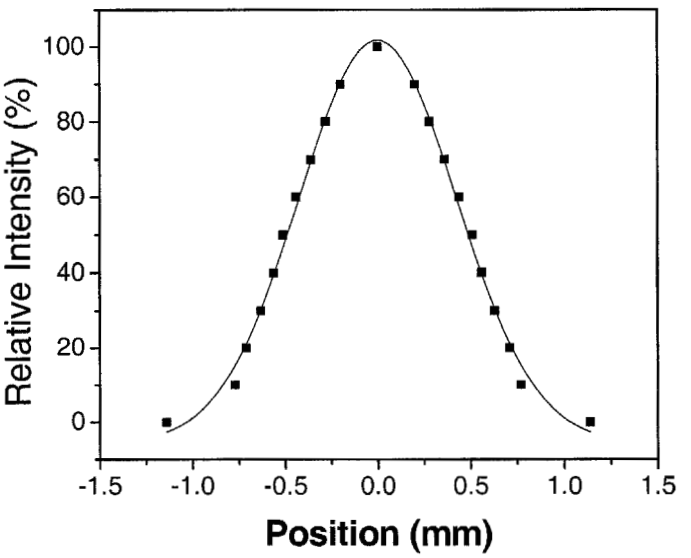

Fig. 3.16: Spatial transverse intensity profile for the laser operation at 11.3 W. Dot: experimental measured data. Line: Gaussian function fitting.

From the Gaussian beam profile, the spot radius was found as about 0.387 mm, which is close to the theoretical estimated beam radius of 0.37 mm at that position. Scanning along the vertical beam spot diameter showed a similar result. These experimental results hence confirm the laser operation was in the low-order transverse-mode.

3.4.1.2 Effects of crystal anisotropy

As has been discussed in Chapter 2, Nd:$GdVO_4$ crystal is a uniaxial crystal. Due to the influence of the crystal birefringence, its absorption and stimulated emission cross-sections are actually dependent on the polarization of light. In order to achieve the optimum laser output in a given operating condition, a comprehensive study on the crystal anisotropy to laser performance is required. By using the natural birefringence of a-cut Nd:$GdVO_4$ crystal, CW Nd:$GdVO_4$ laser has been experimentally operated either in

the ordinary wave (a-polarized) emission or the extraordinary wave (c-polarized) emission state. Comparison was made between their CW performance and with that of an unpolarized c-cut Nd:$GdVO_4$ laser using the same laser parameters.

The extraction of birefringent a- and c-polarization from an a-cut Nd:$GdVO_4$ laser is on a basis to angularly separate the e-ray and the o-ray from the crystal. In the experiment, this is realized by intentionally created a wedged surface on one of the crystal facets. Light passing through the crystal will deviate from normal axis following their respective refractive index, as e-ray with larger refractive index in Nd:$GdVO_4$ will show a larger deviation than the o-ray. Therefore, by changing the resonator longitudinal axis according to the deviated angle of each polarization, it is easy to experimentally select the laser polarization state (Fig. 3.17). As it is understood that the lateral separation between these two polarizations is dependent on the wedge surface ($[n_e - n_o] \times$ wedged degree), the wedge angle should be within the allowable range of cavity misalignment in order to achieve the laser operation for both emissions.

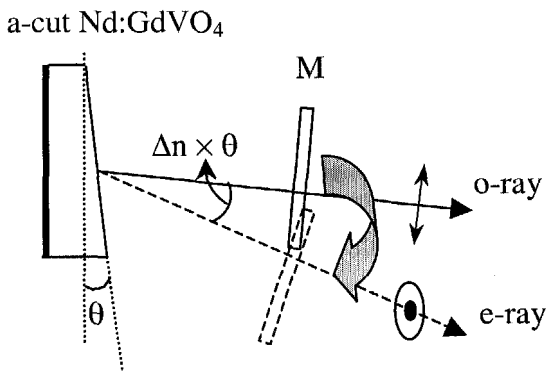

Fig. 3.17: Schematic illustration of the experimentally selective polarization states in a wedged a-cut Nd:$GdVO_4$ laser.

In this case, an a-cut Nd:$GdVO_4$ crystal in dimensions of $3.5 \times 3.5 \times 4$ mm^3 was doped at 1.0 at. % Nd^{3+}. The end of the crystal facing to the pump source has a flat surface, while the other end has a wedged surface with an angle of 3 degrees. The e-ray (c-polarized) and o-ray (a-polarized) from the a-cut Nd:$GdVO_4$ crystal is thereby separated with an angle of about 0.66^0 or 11.52 mrad. With a cavity length of 40 mm, the lateral separation between the two rays at the output mirror is about 0.46 mm. The flat surface of the crystal is high reflection coated at the fundamental wavelength of 1064 nm and anti-reflection coated at the pump wavelength of 808 nm, whereas the wedged surface is *AR* coated at 1064 nm. The c-cut crystal was also doped at 1.0 at. % Nd^{3+} ions and cut into dimensions of $3.5 \times 3.5 \times 4$ mm^3. Both ends of the crystal are flat surfaces and are coated in the same way as those of the a-cut crystal. In experiment, each laser was operated in a normal plane-parallel cavity with the hybrid coated of input mirror on the crystal facet. The plane cavity was stabilized with the existence of thermal focal lens in the laser crystal. In order to efficiently dissipate the generated heat, the crystals were wrapped in a thin layer of indium foil and mounted within a water-cooled copper holder. The water temperature was maintained at about 12 ^{0}C during the experiment to avoid the crystal fracture. Although the Nd:$GdVO_4$ crystal has a better thermal conductivity along the c-axis (11.4 $Wm^{-1}K^{-1}$) than along the a-axis (10.7 $Wm^{-1}K^{-1}$), the cooling temperature for both lasers was fixed at the same value to keep the experimental conditions the same. The laser cavities were completed with a flat output mirror of either transmission T = 20% or T = 30%. Cavity length of 40 mm was found to be optimum for the a-polarized laser, whereas 60 mm was optimal for the c-polarized laser. Nonetheless, in order to have a consistent investigation on the polarization influence to the laser performance, the

experiment was carried out in the same way as possible in all the lasers. Therefore, throughout the study, laser cavity length was kept at 40 mm for all polarized a-cut lasers and the unpolarized c-cut laser. In the experiment of using the wedged a-cut lasers, laser output mirror was mounted on a precise rotation stage. The polarization state of the laser emission could be swapped in between by making a small mirror orientation change. Alternatively, it was found that by fixing the output coupler but tuning the laser crystal within a small angle could also select the polarization of the laser emission. The output power obtained with each of the methods was experimentally checked and they were similar.

The CW performance of the lasers was investigated with an output coupler of T = 20%. Fig. 3.18 shows the CW output power via the pump power of the lasers. For the a-cut Nd:$GdVO_4$ laser the output of the a- and c-polarization components were measured separately.

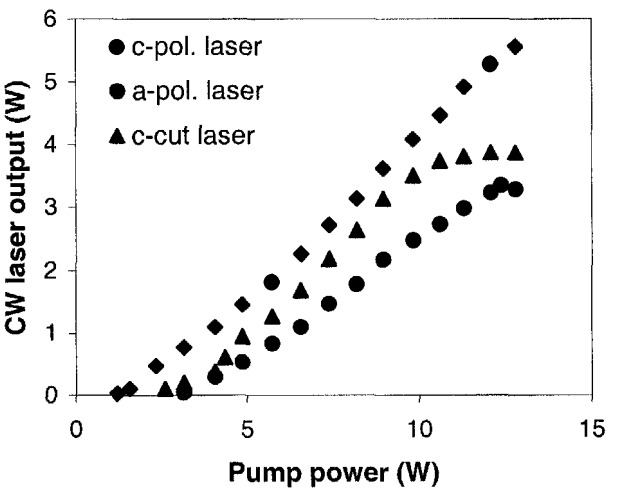

Fig. 3.18: CW output power versus the pump power of the unpolarized c-cut laser and the polarized lasers at each respective direction. The output coupling is at T = 20%.

The highest output of the a-polarized emission was 3.34 W at close to the maximum available incident pump power of 12.39 W. Slope efficiency of the laser is 36.4%. Whereas, the c-polarized component has a maximum output power of 5.56 W at the maximum available pump power, giving a slope efficiency of 50%. The c-cut Nd:$GdVO_4$ laser achieved its highest output of 3.5 W at the pump power of 9.83 W with a slope efficiency of about 49.7%. The laser was saturated with further increase of the pump power. The pump-induced thermal effects are considered to be one of the causes leading to the laser output power saturation. As a plane-parallel cavity was used in the experiment, the thermal lens induced diffractive losses should be strong in the lasers to cause the decrease of the pump efficiency. Since Nd:$GdVO_4$ crystal has a better thermal conductivity along the c-axis than along the a-axis, the pump induced thermal lens in the a-cut laser is consequently weaker than that in the c-cut laser. It was seen that under the same pump power no such pump efficiency decrease appeared in the a-cut laser. The lasing threshold for the a- and c-polarized emission of the a-cut laser, and the c-cut Nd:$GdVO_4$ was measured to be 3.3 W, 1.5 W and 2.93 W, respectively. Based on the same cavity losses in the a-cut lasers, lasing threshold difference between the a-polarized and c-polarized emission gives a good measure of their stimulated emission cross section ratio. From the experimental result, gain cross section of the c-polarized laser is deduced as about a factor of two higher than that of the a-polarized emission. This agrees well with the ratio of the peak emission cross section at c- and a-polarized direction as stated in Chap. 2.

Although the a-cut Nd:$GdVO_4$ crystal has a larger absorption cross-section than the c-cut crystal, it is seen in Fig. 3.18 that the a-polarized emission of the a-cut crystal

laser has lower slope efficiency than that of the c-cut laser before the thermally induced diffraction becomes significant in the c-cut laser. This result can be explained by the unpolarized c-cut Nd:$GdVO_4$ laser being exempted from the polarization losses in it. Since the comparison between the thresholds of the a-polarized emission in the a-cut laser and the unpolarized emission in the c-cut laser gives an indication on their cavity loss difference, this result is also in agreement with the lower lasing threshold of the c-cut laser than the a-polarized laser. For the CW operation of the lasers the advantage of using the conventional a-cut crystal is clear, based on the experimental result of the c-polarized laser. It is expected that with a better mode matching in the crystal and the use of a cavity with low diffraction loss, higher laser slope efficiency as achieved in the conventional a-cut Nd:$GdVO_4$ laser could be obtained.

It is noted that a slightly decrease of output power occurred for the a-polarized component at the full pump power, while there is no such output power decline observed on the c-polarized light. This seems rule out the possibility that it is caused by the thermal induced cavity diffraction losses. The most likely reason could be the excited state absorption and energy transfer upconversion effects, as will be discussed in the passively Q-switched laser section. For the a-polarized light with smaller stimulated emission cross-section than the c-polarized light, the excited state nonlinear effects could be more plausible to appear under a high pumping strength.

3.4.2 Nd:$GdYVO_4$ laser

A similar experiment as used in determining the laser performance in Nd:$GdVO_4$ was conducted on an a-cut 0.5 at.% doped mixed Nd:$Gd_{0.64}Y_{0.36}VO_4$ crystal. For a

comparison made with a lightly doped Nd:$GdVO_4$ laser, the mixed crystal was operated in a 60 mm cavity length as illustrated in the setup in Fig. 3.11. Variation of output coupling transmission was attempted in the laser for the highest output power. Fig. 3.19 shows the experimentally obtained laser average powers under different cavity transmission. The output coupler with reflectivity of 80% was found showing the optimal output with average slope efficiency of 56.4 % in the range that incident pump power is over 9 W.

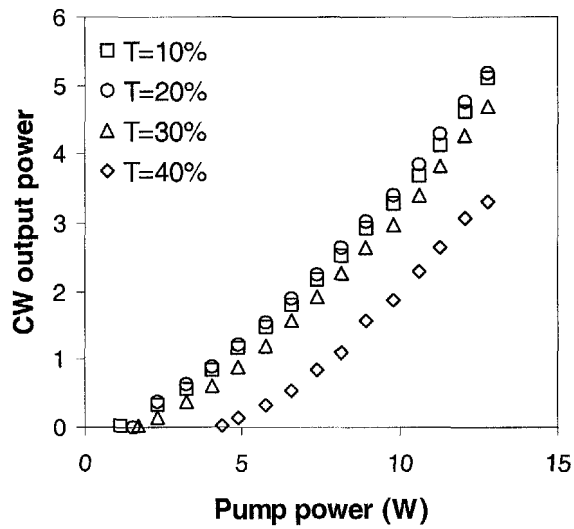

Fig. 3.19: Nd:$Gd_{0.64}Y_{0.36}VO_4$ CW laser performance obtained from different set of coupling transmissions.

For comparison on the laser performance between the mixed and the pure gadolinium vanadate crystals, their CW average power measured at the optimum coupling transmission of T = 20% is plotted in Fig. 3.20, respectively. Despite the fact that the cavity loss of the lasers might slightly differ from each other, comparison of their lasing threshold would reflect the difference of their laser stimulated emission cross

section. According to the plot, the mixed crystal was found having a lasing threshold of about 1.3 times higher than that of the Nd:$GdVO_4$ laser. This value agrees well with their emission cross section ratio (≈ 1.58).

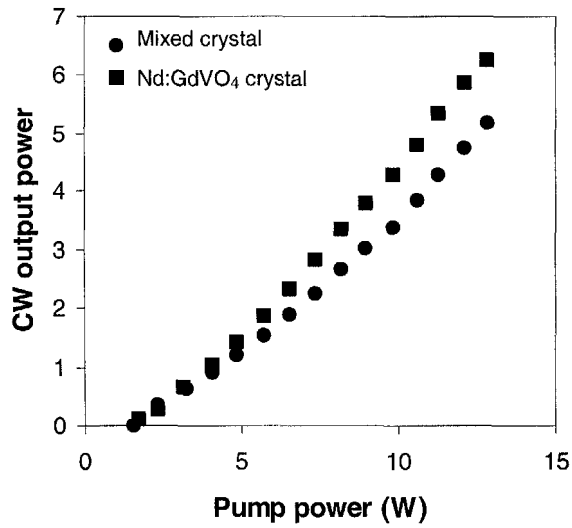

Fig. 3.20: Optimum CW power of the Nd:$Gd_{0.64}Y_{0.36}VO_4$ and Nd:$GdVO_4$ lasers, respectively measured with the output coupler of $T = 20\%$.

On the other hand, laser beam quality of Nd:$Gd_{0.64}Y_{0.36}VO_4$ was analyzed using the same moving knife-edge method as stated above. The results further confirm that the laser operation was in a TEM_{00} condition. M^2 parameter at full pump power was found to be 1.53 for the Nd:$GdYVO_4$ laser. The far field spatial beam at 0.1 m away from the cavity output coupler was estimated to have a radius of about 0.43 mm. Fig. 3.21 illustrates the experimental and Gaussian fitted spatial beam profile.

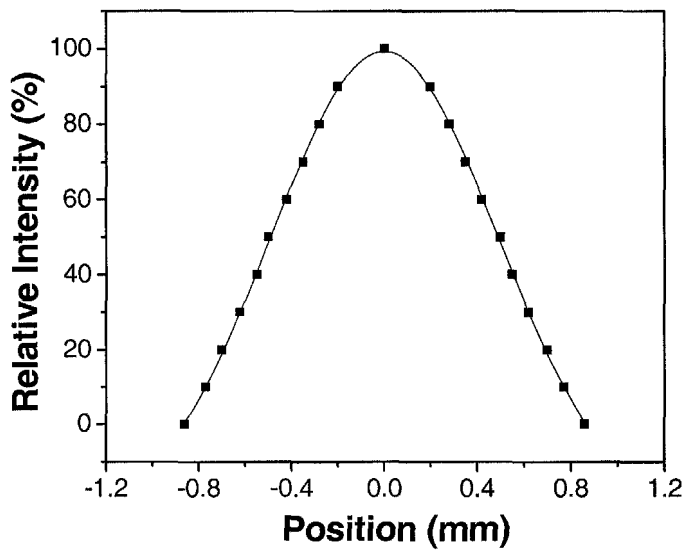

Fig. 3.21: Gaussian fitted (line) and experimental determined (dot) spatial beam spot of the Nd:$Gd_{0.64}Y_{0.36}VO_4$ laser.

3.5 Summary

In this chapter, diode-pump CW laser performance of Nd:$GdVO_4$ and Nd:$GdYVO_4$ crystals have been investigated. The overall study began by characterizing the laser diode pump source performance, and identifying the absorption coefficient and thermal focal lengths of laser materials for efficient cavity design. Investigation of the influences of laser properties to CW laser efficiency was further conducted together with the characterization on laser beam quality. It was found that doping concentration is the governing factor in increasing the pump absorption coefficient and the laser thermal lens effect. As a result, the 1.61 at.% doped Nd:$GdVO_4$ showed a strong thermal focal length of less than 150 mm at the full pump power, whereas the 0.5 at.% lightly doped crystal formed a thermal lens with focal length of about 200 mm at the same pumping level. Mixed crystal Nd:$Gd_{0.64}Y_{0.36}VO_4$ with its higher thermal conductivity is favorable with

its weaker thermal effect than the same doping level of the pure Nd:$GdVO_4$ crystal. In identifying the measured thermal lens results of the mixed crystal, temperature-induced refractive index change of Nd:$Gd_{0.64}Y_{0.36}VO_4$ crystal is estimated to be 3.5×10^{-6} K^{-1} in the experiment.

As has been found, the lasing action was strongly influenced by the thermal induced effect accordingly with the cavity design. Low doping concentration of laser is more favorable in producing high efficient CW output power. In the two mirror plano-concave resonator, a proper cavity length is indeed necessary to achieve a proper mode matching for the highest laser efficiency. The average CW laser slope efficiency for three different doping levels of Nd:$GdVO_4$ (0.5 at.%, 1.14 at.% and 1.61 at.%) was respectively found to be about 62.6%, 56 and 53.4%. At the optimum cavity transmission of T = 20%, 50% optical-to-optical conversion efficiency was achieved at the limited pump power of 12.81 W. The beam quality factor measured at the full pump power was determined to be M^2 = 1.5, suggesting the laser was in a low order transverse mode.

Through the comprehensive studies on the Nd:$GdVO_4$ laser birefringent and crystal cutting in CW laser operation, laser performance has been experimentally found to be dependent on the polarization accordingly with its light dependent absorption and emission cross section, as well as the thermal property. The c-polarized Nd:$GdVO_4$ laser with its larger gain cross section has shown the highest efficiency of CW laser output performance. On the other hand, due to the exemption from the polarization loss, the unpolarized c-cut Nd:$GdVO_4$ laser has a lower lasing threshold and higher laser slope efficiency than the a-polarized component, as both would have the similar emission cross

section. In the experiment, it is also confirmed that c-polarized emission cross section is about double of the a-polarized component.

For the Nd:$Gd_{0.64}Y_{0.36}VO_4$ crystal laser operation, the highest slope efficiency of 56.4% was achieved in the laser with an optimal cavity transmission of 20%. The slightly lower output power in the mixed crystal laser as compared to the Nd:$GdVO_4$ is in good agreement with its lower emission cross section. From the characterization of the spatial laser beam propagation, low-order transverse-mode laser output with M^2 = 1.53 was obtained at the full pump power. All these results reveal that the combined effects of the laser properties and the proper cavity design are determinant to achieve the high efficient CW laser output.

CHAPTER 4

Experimental study on passively Q-switched operations

Despite the fact that Nd:$GdVO_4$ laser has advantage of large gain cross section, which allows it to achieve high efficient CW operation, this property, on the other hand, is an obstacle for obtaining large passively Q-switched pulse energy. The first experimental study on the passively Q-switched Nd:$GdVO_4$ laser reported inferior passively Q-switched result of pulse energy of merely 20 μJ, and peak power of 625 W, which was thought to be caused by the too large stimulated emission cross section of the crystal [102]. In this thesis, intensive research has been conducted on the passive Q-switching of Nd:$GdVO_4$ and mixed crystal Nd:$Gd_{0.64}Y_{0.36}VO_4$ using Cr^{4+}:YAG saturable absorber.

From the derived analytical rate equations for passive Q-switching, it is shown the selection of laser parameters crucially affects the quality of the passively Q-switched laser operation, and this includes the gain medium doping level, saturable absorption strength, emission cross section, and cavity reflectivity. It is important to appropriately combine the laser parameters to achieve the optimized passively Q-switched laser performance. Nd:$Gd_{0.64}Y_{0.36}VO_4$ mixed laser crystal which has smaller emission cross section than Nd:$GdVO_4$ crystal, has been shown to have better passively Q-switched performance than the Nd:$GdVO_4$ laser. Apart from the gain medium features, the property of the saturable absorber also plays a crucial role in the optical pulse energy and peak power of the passively Q-switched laser. In this chapter, a detailed investigation on the effects of the above stated laser parameters is carried out to have an overall understanding in giving optimal passively Q-switched output. A novel approach using the

nonlinearity of GaAs as a nonlinear output coupler has been conducted to further narrow the passively Q-switched pulse duration for higher pulse peak power.

4.1 Experimental details

The essential part of the passively Q-switched operation is the insertion of a saturable absorber in the cavity. The stronger light intensity with a smaller beam spot size on the passive Q-switch relative to the gain medium is dominated to the Q-switched performance. Within the stable cavity condition, this criterion can easily be achieved in a simple concave-plano two-mirror cavity configuration or in a hybrid plane parallel laser cavity configuration with the occurrence of the thermal lens. The cavity lengths were selected based on the consideration of cavity stability and the highest achievable CW output power, in which the mode matching of the laser was found optimum in the studies in Chapter 3. Due to the concave input mirror and thermal lens in the gain medium, the position of the smallest cavity mode size for putting the passive Q-switch in the cavity is therefore near the output coupler.

The Cr^{4+}:YAG crystals used in the experimental study are <111>-oriented, respectively with initial transmission T_0 of 90% ($5 \times 5 \times 0.82$ mm^3) , 80% ($5 \times 5 \times 1$ mm^3), and 60% ($5 \times 5 \times 1.74$ mm^3). The saturable absorbers are anti-reflection coated both sides to reduce the insertion loss in the cavity. Due to the flexibility of Cr^{4+}:YAG crystal in controlling the saturation strength for optimum Q-switched parameter, Cr^{4+}:YAG passive Q-switch is mainly used in most of the experiments. In the final section of this chapter, GaAs semiconductor mirror is introduced for advancement on the passive Q-switching technique. The GaAs wafer was grown along <100>-axis and cut

with a cross-section of 10 mm × 20 mm and a thickness of 450 μm. One side of the GaAs wafer is optical polished, and its opposite surface was coated with a gradually varying transmission from T = 3% to 60% along the 20mm edge direction. In the Q-switched operation, cavity output coupling with lower reflectivity R was selected for optimal cavity energy extraction in the passive Q-switching. Depending on the laser condition, cavity output mirror with reflectivity of either 70% or 60% at 1.06 μm was mainly used in the experiments. The Q-switched laser output was detected with a high speed InGaAs photon detector (New Focus 1611-AC). A digital storage oscilloscope (Tektronix TDS 360) and a power meter were used to display and measure the Q-switched pulses and their average power.

4.2 Passively Q-switched performance of Nd:$GdVO_4$ laser

Proper combination of the laser parameters is crucial for achieving the optimized laser Q-switching performance. As shown in the previous chapter that the Nd-ion doped crystal with higher doping level has higher pump absorption strength. According to Eq. (2.14) where stronger laser absorption is proportional to higher pumping rate, a higher doping concentration could therefore provide larger amount of population inversion for generating larger single pulse energy in the passively Q-switched operation. Besides, heavily doped laser crystals may also able to avoid the pump saturation in the continuous pumping process. On the other hand, lower output coupling reflectivity and higher saturation strength are also factors in enhancing the passively Q-switched performance. In practice, there is an optimal parameter for each factor corresponding to their

interactive influences. Appropriate combination of the laser parameters is the criterion to be achieved experimentally for the good passively Q-switched laser output.

Three a-cut Nd:$GdVO_4$ crystals with doping concentration of 0.5 at.% (3.5 × 3.5 × 6 mm), 1.14 at.% (3.5 × 3.5 × 4 mm), 1.61 at.% (3.5 × 3.5 × 3.5 mm), respectively represents the lightly, mildly and heavily doped crystal. All the passively Q-switched lasers were built in the previous determined CW laser concave-plano cavity, with Cr^{4+}:YAG as a passive Q-switch. For Nd:$GdVO_4$ crystals with 0.52 at.% and 1.14 at.%, a cavity length of 60 mm was selected. While for the crystal of high doping concentration (1.61 at.%) the cavity length was reduced to 30 mm to avoid the thermal lens effect induced cavity instability. The experimental setup is shown in Fig. 4.1.

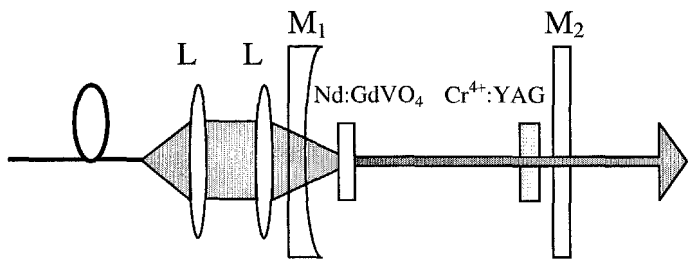

Fig. 4.1: Schematic of the laser setup. M_1: concave mirror, M_2: output coupler. L: coupling lens.

Fig. 4.2a shows a comparison of the average output power of the Nd:$GdVO_4$ laser of different doping concentration when passively Q-switched by the Cr^{4+}:YAG crystal of 80% initial transmission. In all the experiments an output coupler of 70% reflectivity was used. Under the experimental condition the laser with the 1.14 at.% doping concentration emitted the highest average power. Q-switched output power of 2.4 W was obtained with the pump power of about 14 W, giving a slope efficiency of 23%. Despite the lightly

doped crystal having a similar laser threshold and a slope efficiency of almost comparable with the 1.14 at.% doped laser, its average output power is inferior in the Q-switched operation. Comparatively, the laser with the 1.61 at.% doping concentration has a fairly low maximum output power. With a pump power of about 12.5 W the laser already reached its maximum output of about 1.3 W. Further increasing the pump power caused a decrease of the laser output. The reduction in the laser output power is attributed as a consequence of the strong thermal lens induced cavity instability in the high doping concentration of the laser crystal.

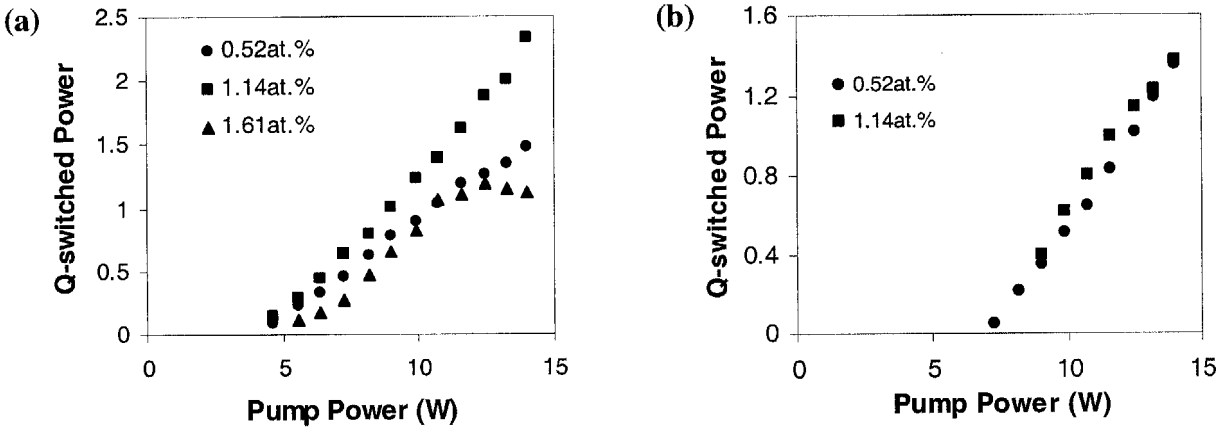

Fig. 4.2: Average output power of the Q-switched Nd:$GdVO_4$ laser under different doping levels. (a) Output coupler transmission: 30%, Cr^{4+}YAG initial transmission: 80%; (b) Output coupler transmission: 40%, Cr^{4+}YAG initial transmission: 60%.

The passively Q-switched operation was further studied by decreasing the output coupling reflectivity to 60%, and increasing the Cr^{4+}:YAG saturation strength to initial transmission of 60%. In such a high cavity loss condition Q-switched operation was failed to achieve in the heavily doped Nd:$GdVO_4$ laser. Comparison was made between

the 0.5 at.% and 1.14 at.% crystals. Fig. 4.2b shows the average output of the lasers with an output coupling of 40% and a Cr^{4+}:YAG crystal of 60% initial transmission. In this case the highest average output power achieved was 1.37 W for both the laser crystals of 0.52 at.% and 1.14 at.% doping concentrations. The 1.14 at.% laser output initially raised with a higher slope efficiency, but slightly declined its slope efficiency at 13.28 W. This phenomenon is also attributed to the onset of the thermal focal lens at the high pump power. Actually the higher average Q-switched output power does not indicate the proportion to single pulse energy. The essential judgment on the Q-switched laser performance is its achievable optical pulse energy and peak power. Based on this concept, the laser was further investigated to determine the effect of saturable absorption strength to the Q-switched pulse properties. The studies were carried out on the 1.14 at.% Nd:$GdVO_4$ laser by using Cr^{4+}:YAG crystals with either 60% or 80% initial transmission. The output coupler transmission was kept as low as 40%. Fig. 4.3 shows the Q-switched pulse width, pulse energy, repetition rate and peak power changes with the pump power. The results demonstrated that with the Cr^{4+}:YAG crystal of 60% initial transmission, a maximum single pulse energy of 130.1 μJ and pulse width of 7 ns can be achieved, giving Q-switched pulse peak power of 18.6 kW. Even with the Cr^{4+}:YAG crystal of 80% initial transmission in the cavity, Q-switched pulses with single pulse energy as high as 76 μJ and peak power of 4.8 kW could be obtained. Fig. 4.4 shows a stable Q-switched pulse train with pulse amplitude jitter less than 2% as observed in the experiment.

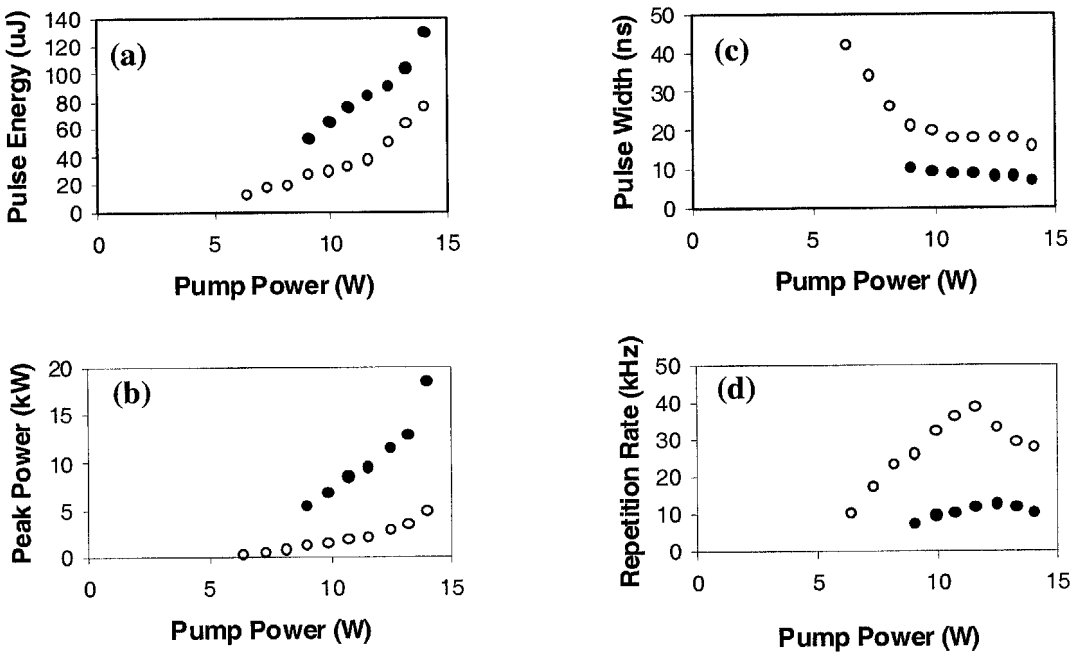

Fig. 4.3: Passively Q-switched 1.14 at% Nd:$GdVO_4$ lasers. Pulse properties under different Cr^{4+}:YAG initial transmissions: full circles: Cr^{4+}:YAG with 60% initial transmission; open circles: Cr^{4+}:YAG with 80% initial transmission. (a) Pulse energy; (b) Peak power (c) Pulse width; (d) Repetition rate.

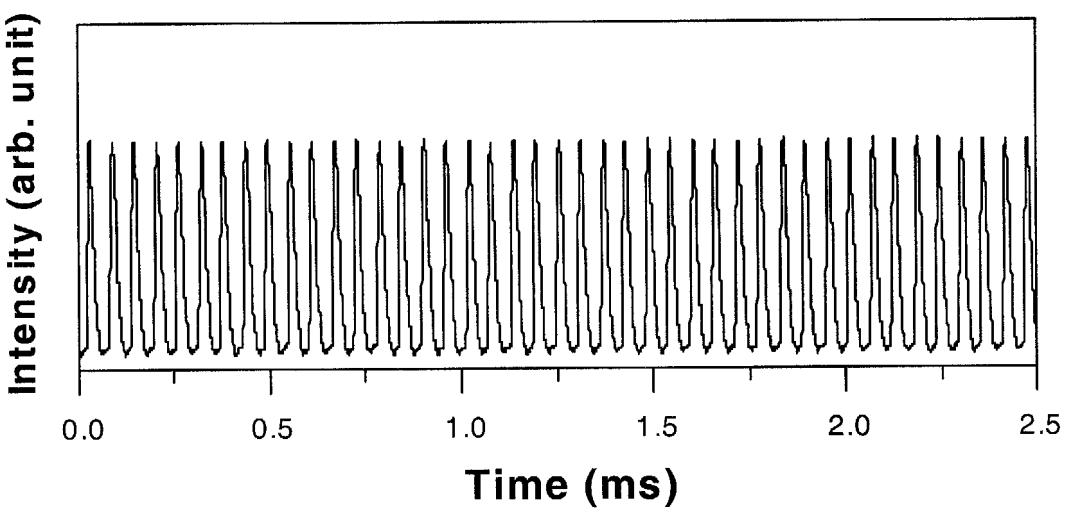

Fig. 4.4: Example of a stable Q-switched pulse train. Nd:$GdVO_4$ doping concentration: 1.14 at.% , Cr^{4+}:YAG initial transmission: 60%, output coupler transmission: 40%.

It may be noted that in the experiment as the pump power increased beyond a certain value, Q-switched pulse repetition rate started to decrease. The decrease point started at the pump power of 13.28 W, which is the same as the variation of average output power in Fig. 4.3b. This effect is explicable with the cavity diffraction loss induced from the thermal lens effect. An increased cavity loss also means an increased effective threshold pump power, and consequently a decreased Q-switched pulse repetition rate. However, a less significant pulse repetition rate drop was observed when the Cr^{4+}:YAG saturable absorber of 60% initial transmission was used. This could be understood as being that the cavity loss in this case was very strong before the occurrence of the thermal induced loss. Therefore, a drastic dropping tendency of the pulse repetition rate could not be seen. The influence of the thermal lens introduced diffraction loss hence becomes less significant.

On the other hand, the 0.5 at.% laser under the same passively Q-switched condition was found not to be able to achieve the result compared with the 1.14 at.%. Fig. 4.5 shows the experimental results of the passively Q-switched lightly doped Nd:$GdVO_4$ lasers. The maximum achievable pulse energy and peak power are merely 24.3 μJ and 1.06 kW, respectively under the operating conditions of T = 40%, T_0 = 60%. Amplitude and repetitive pulse jitters were found to be significant in the 0.5 at.% doped laser, particularly at high pump power. This poor result is most probably because of the inability to fulfil the Q-switched second threshold. The reasons may include the low absorption coefficient in the lightly doped crystal, and low laser net gain with the finite ions number in ground state. From the cavity design, weaker thermal focal lens in the

lightly doped crystal could also result a weak intracavity focusing on the saturable absorber that obstruct the laser to hold the inequality of Eq. (2.6).

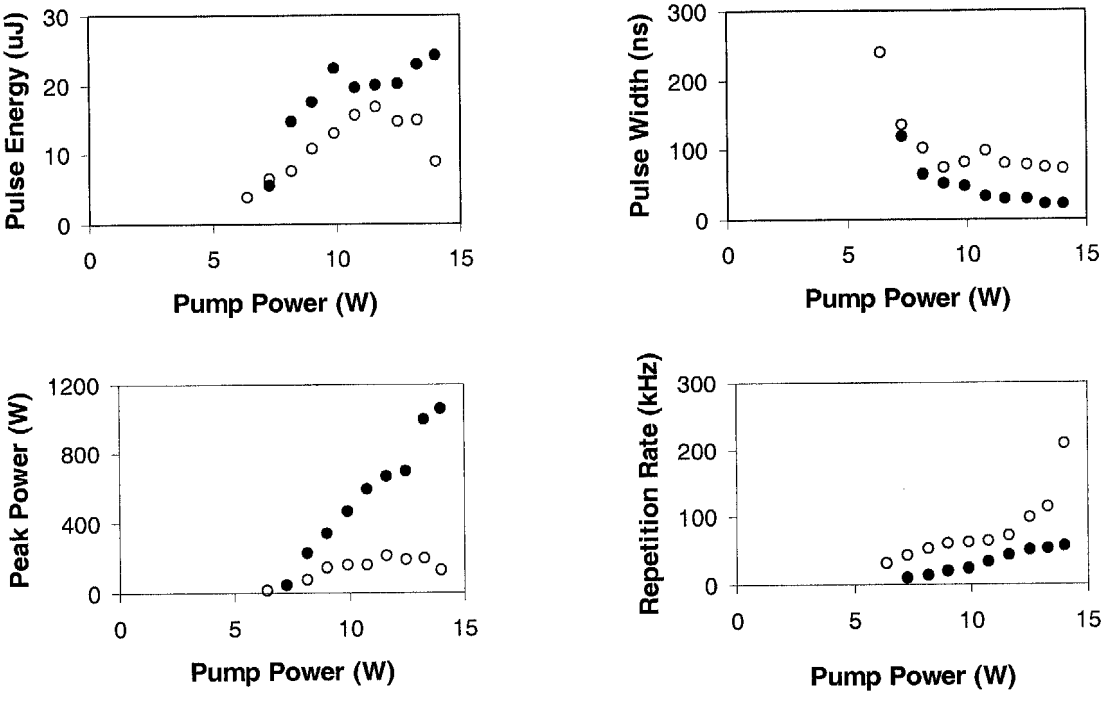

Fig. 4.5: Pulse properties of the passively Q-switched 0.5 at.% Nd:$GdVO_4$ lasers. Full circles: Cr^{4+}:YAG with 60% initial transmission; open circles: Cr^{4+}:YAG with 80% initial transmission. (a) Pulse energy; (b) Peak power (c) Pulse width; (d) Repetition rate.

The Q-switched pulse properties of the laser under cavity output coupling transmission of 20% have also been compared. As expected, due to the low energy extraction from the cavity, the pulse energy and peak power were inferior compared to the cavity of 40% transmission. It was found in practice that high average output is from experimental condition with low round trip losses (saturation strength and coupling transmission). Since laser gain is unable to store up to higher value, pulse energy is

consequently low. However, with lower losses, the laser can thus achieve higher average output power. Therefore, the combination of all the cavity gain and loss in the passively Q-switched regime is crucial to passively control the laser performance. The higher doping level of laser crystal is better for high gain, while the best combination of the cavity output coupling and the saturable absorber initial transmission in the experiments is the 40% output coupling transmission and 60% saturable absorber initial transmission.

Because of its higher lasing threshold and higher diffraction loss, the suitable cavity output transmission for the heavily doped 1.61 at.% laser is 30% by passively Q-switched with the T_0 = 60% of Cr^{4+}:YAG crystal. In such a short cavity the laser with the 1.61 at.% Nd:$GdVO_4$ could achieve the highest single pulse energy of 158.2 μJ with a repetition rate of 6.3 kHz at the pump power of 12.5 W. Fig. 4.6 shows as example a Q-switched laser pulse with 6ns pulse width, and peak power of 26.4 kW. When the Cr^{4+}:YAG crystal of 80% initial transmission was used, the achievable maximum pulse energy and peak power dropped about half to 95.2 μJ and 13.6 kW, respectively. This demonstration shows that the doping concentration of the Nd:$GdVO_4$ crystal is more dominant for the larger single Q-switched pulse energy and peak power with the optimized selections of the cavity output coupling and saturable absorber strength. The experimental results show that crystals with higher doping concentration are beneficial for the passive Q-switching, provided that the laser cavity is appropriately designed to avoid thermal induced cavity instability. Further shortening the cavity length is obstructed by the bulky laser system.

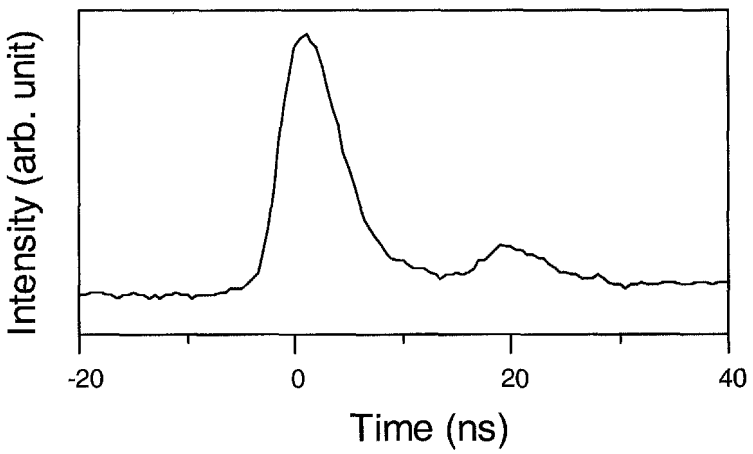

Fig. 4.6: Pulse profile of single Q-switched pulse with the pulse width of 6 ns.

For the passive Q-switching was conducted in the optimized cavity configuration of the CW lasers, laser beam quality with the insertion of the Cr^{4+}:YAG was further checked with the knife-edge method as which applied in the CW laser emission. The Q-switched beam diameter was found to be slightly smaller compared to the free-running laser output. The stronger the saturable absorption strength, the more effective the beam diameter to be apertured. This implies that the saturable absorber acts as an effective aperture to the laser and cut off the higher order mode. From the measurement, beam quality number of the passive Q-switching the experiments at the full pump power of about 14 W is in the range of about 1.3 ~ 1.4.

4.2.1 Effects of crystal anisotropy

The a-cut Nd:$GdVO_4$ with large emission cross section is advantageous for the CW power scaling with low threshold. By contrast for the passively Q-switched operation, large gain cross section obstructs the energy storage at laser upper energy level and results in an inefficient passive Q-switching. One alternative to enhance the passive Q-

switching performance in the crystals of tetragonal group space is to utilize the smaller laser gain cross section to increase the energy store capacity. Nonetheless, this does not absolutely imply that the smaller emission cross section is better in the passively Q-switched operation. There might have other influences more dominant to affect laser performance. In this section, laser operation under two different light polarizations (gain cross sections) is investigated. Comparisons of laser performance are made between the natural resolved birefringence of an a-cut Nd:$GdVO_4$ crystal, and also with a c-cut Nd:$GdVO_4$ laser of the same parameters. The advantages and drawbacks of each laser polarization operation are analyzed experimentally.

A flat-wedged (3 degrees) surface of a-cut Nd:$GdVO_4$ laser crystal was used to separate the two naturally polarized radiations from the crystal. Both a-cut and c-cut laser crystals are mildly doped at 1.0 at. % with dimensions of $3.5 \times 3.5 \times 4$ mm^3. The laser operations were conducted with simple two-mirror laser cavity with the insertion of a Cr^{4+}:YAG saturable absorber closely to the output coupler as in Fig. 4.7. Passive Q-switching of the a-polarized laser and the c-cut Nd:$GdVO_4$ was carried out in the same cavity conditions. An optimized Q-switched operation of the lasers was obtained with the laser output coupling transmission T = 30% and initial transmission of the Cr^{4+}:YAG saturable absorber of T_0 = 90%. Because of the small stimulated emission cross-section of the lasers, Cr^{4+}:YAG saturable absorbers of lower initial transmission could not be used.

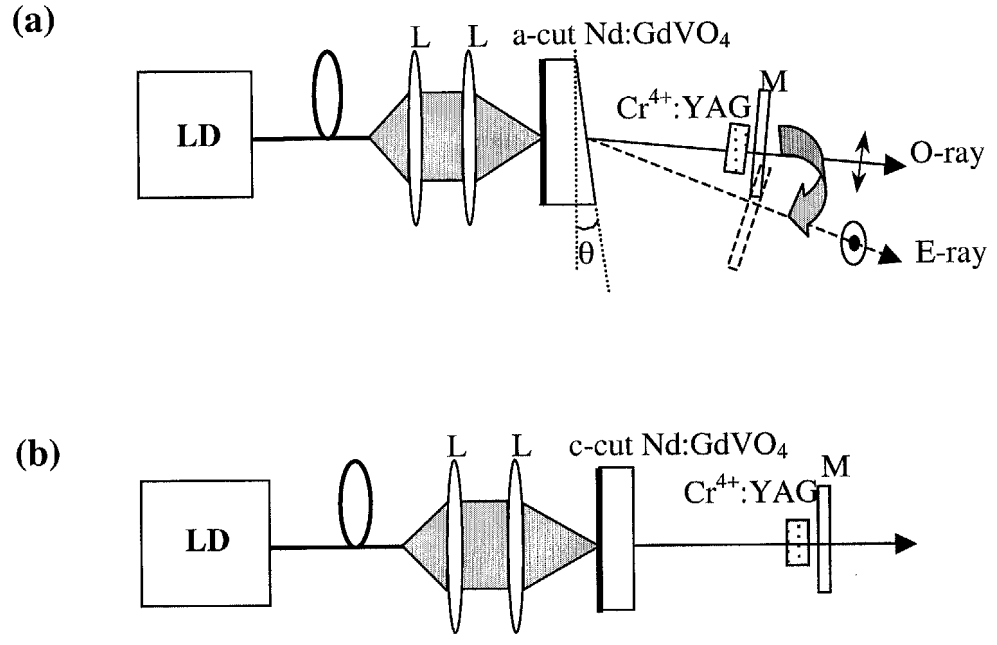

Fig. 4.7: Schematic experimental setups. (a) The a-cut Nd:$GdVO_4$ laser, where the a- or c-polarized emission were selected by the orientation change of the output coupler. (b) The c-cut Nd:$GdVO_4$ laser. L: coupling lens; LD: laser diode. M: output coupler.

Fig. 4.8 shows the comparison of the Q-switched performance between the a-cut a-polarized laser and the c-cut laser. As a reference, passively Q-switched operation of the a-polarized light under the output coupling of T = 20% is also given in the figure. As expected, higher cavity loss is better for extracting higher pulse energy from the cavity. It is clear to see that the c-cut Nd:$GdVO_4$ laser had a better performance than the a-cut a-polarized laser under the same pump power. However, the operation of the c-cut laser suffered from strong influence of the pump-induced cavity losses and instability. When the pump power exceeded 11.3 W no stable Q-switched operation could be obtained. The

stable passively Q-switched operation of the a-cut a-polarized laser could extend to the maximum incident power of 12.4 W. Similarly, its Q-switched operation was unsteady and ceased with the further increasing of the pump after 12.4 W. In the experiment, the Q-switched pulse energy and peak power obtained on the a-cut a-polarized laser and the c-cut laser are comparable, they are 99.4 μJ and 97.5 μJ, and 9.47 kW and 9.75 kW, respectively for the a-cut laser at the pump power of 12.4W and the c-cut laser at the pump power of 11.3 W.

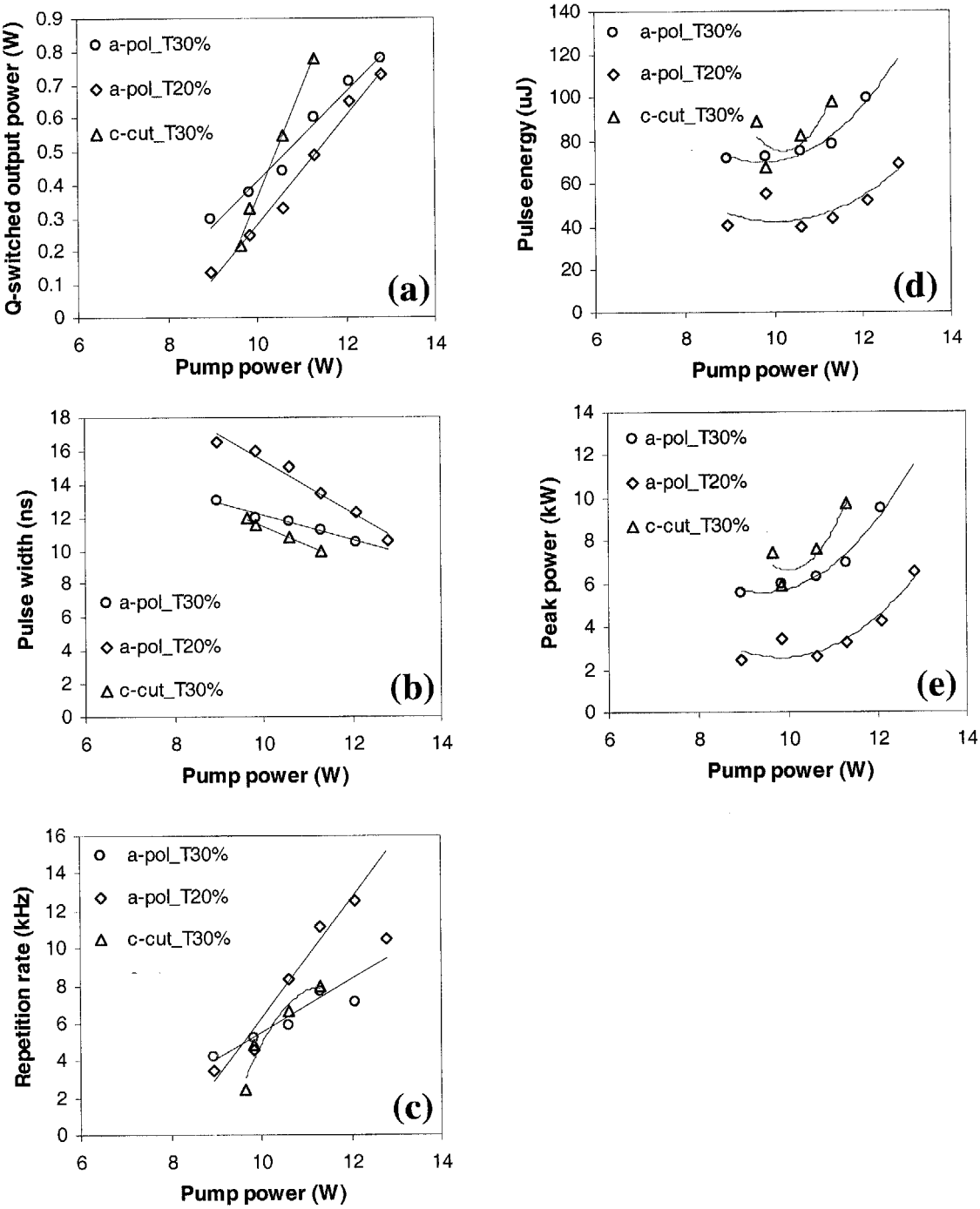

Fig. 4.8: Comparison between the passively Q-switched operation of the c-cut and the a-cut a-polarized lasers. (a) Average Q-switched output power, (b) pulse width, (c) pulse

repetition rate, (d) single pulse energy and (e) peak power. Cr^{4+}:YAG initial transmission $T_0 = 10\%$, output coupler transmission $T = 30\%$.

A typical Q-switched pulse train for the a-cut a-polarized Nd:$GdVO_4$ laser is shown in Fig. 4.9, where the inset is the single pulse profile measured.

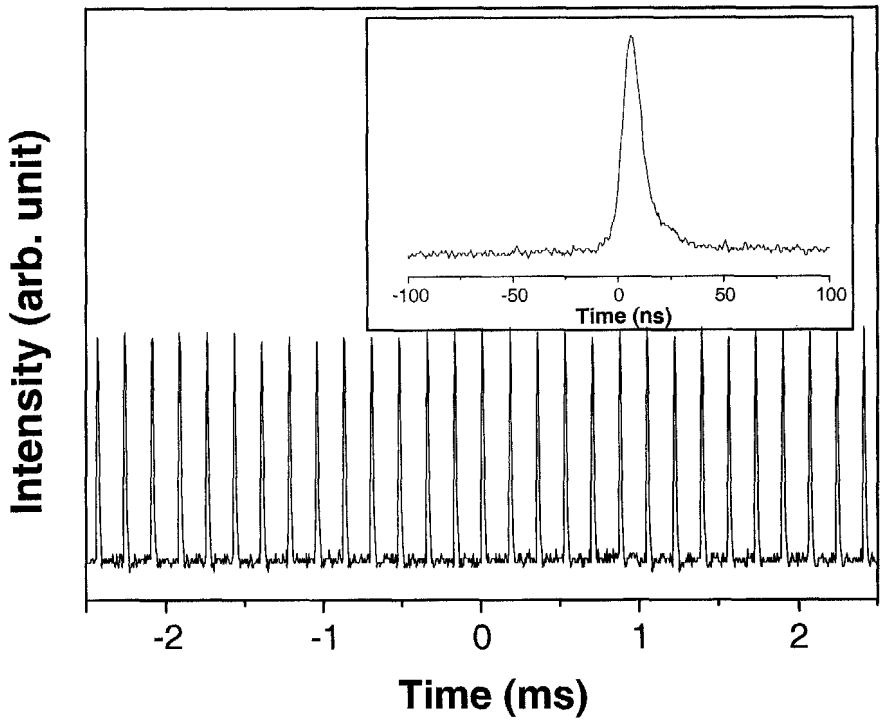

Fig. 4.9: A stable Q-switched pulse train of the a-cut a-polarized Nd:$GdVO_4$ laser. The inset is a typical Q-switched pulse shape.

Experimental data clearly revealed that Nd:$GdVO_4$ lasers with low emission cross section were limited at the high pumping regime. Despite the thermal induced cavity, losses and instability could cause a decline to laser output, based on the fact of the drastic cease of Q-switched laser operation, and the observed strong visible luminescence in the crystal in the high pumping region. It is strongly believed that the nonlinear absorptions

might exist in the a-polarized and c-cut Nd:$GdVO_4$ lasers at the high pump power. As mentioned in Chapter 2, Nd:$GdVO_4$ laser tends to have excited state absorption (ESA) and energy transfer upconversion (ETU). When more ions are populated at the upper energy level of the laser, the phenomenon becomes more obvious. Therefore, this effect is believed to be stronger in that passively Q-switched operation of the mildly doped a-polarized and c-cut Nd:$GdVO_4$ lasers, which both have a lower emission cross section.

When the population in the excited state is high, upconversion rate is also higher than the laser radiative rate and multiphonon decay rate, and directly affects the laser output. Therefore, the luminescence spectrum was checked in the visible range using a wide range optical spectrum analyzer (Ando AQ-6315B) for the passively Q-switched low gain lasers at the pump power of about 10 W. Fig. 4.10 shows the strong fluorescence centered at the wavelength of 401 nm and another two emission bands found at 532 nm and 617 nm. This evidence confirms the existence of the ETU in Nd:$GdVO_4$ laser. From this spectrum, the higher lying stark levels of Nd:$GdVO_4$ laser that responsible for the nonlinear absorptions can be identified and correspondingly with other fluorescent manifolds in the common Nd^{3+} lasers (Fig. 4.11).

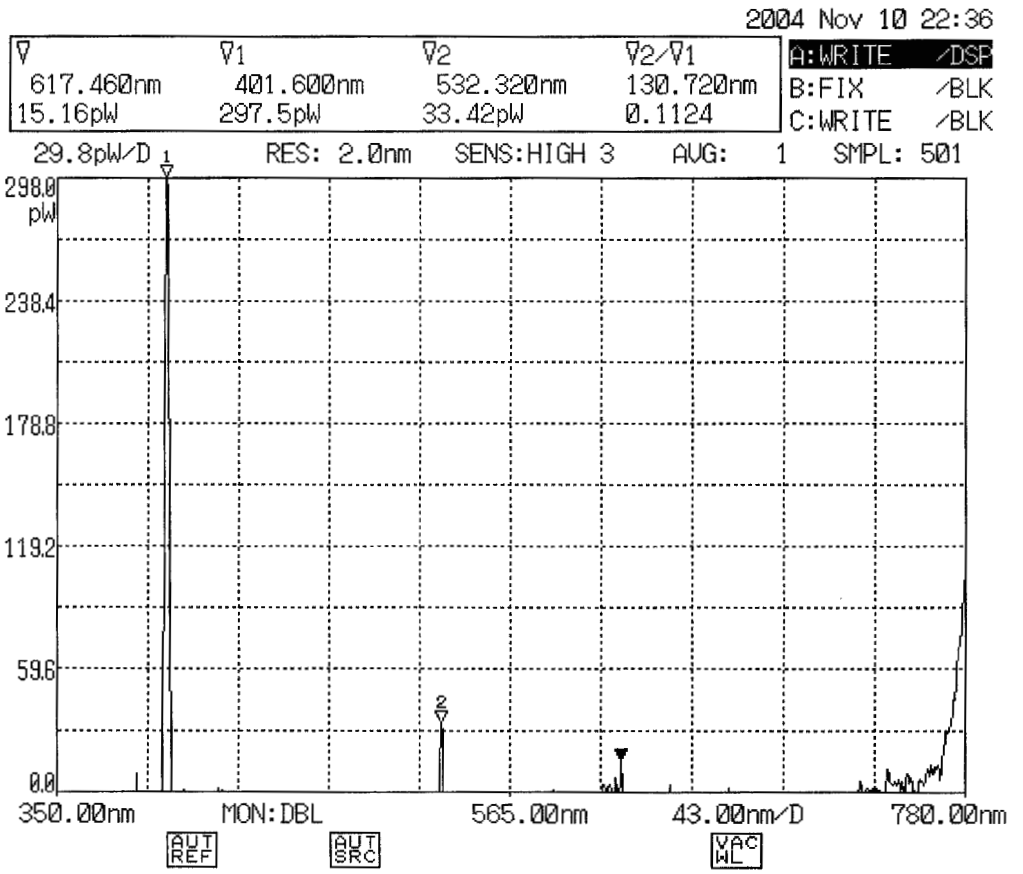

Fig. 4.10: Visible luminescence observed during the passively Q-switched c-cut Nd:$GdVO_4$ laser.

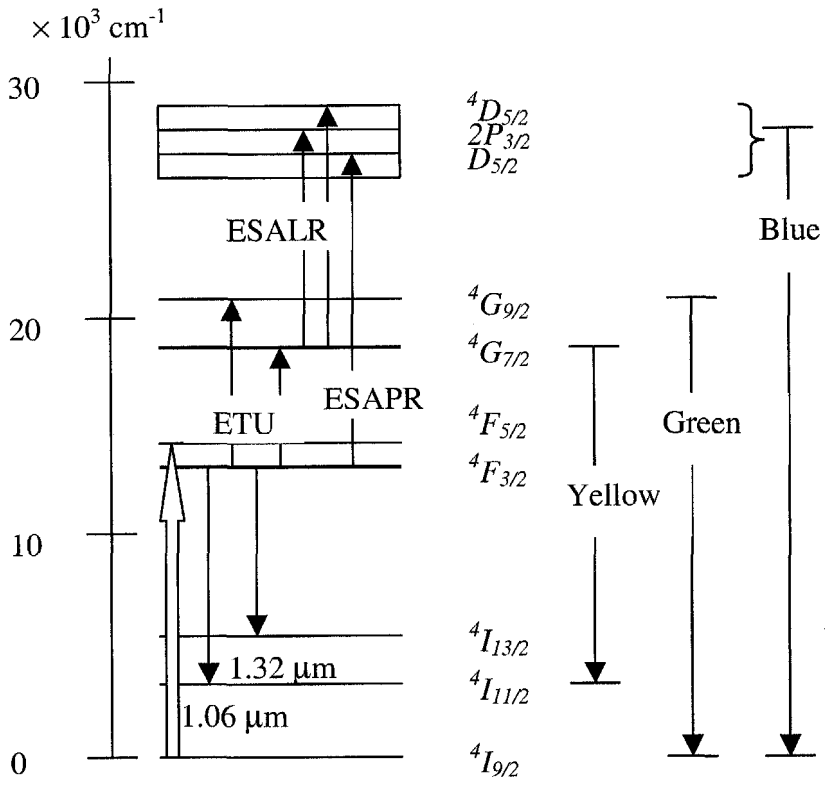

Fig. 4.11: The surmised energy diagram of the Q-switched a-oriented Nd:$GdVO_4$ laser with low emission cross section. The thick arrow indicates the pump photon energy, and the nonradiative decays are not depicted in the diagram.

In fact, when the excited ions density is high at metastable $^4F_{3/2}$ level, besides ETU process, ESA can take effect through the pump light resonance. Under strong laser cavity intensity, the accumulated ions through ETU at $^4G_{7/2}$ level (19000 cm^{-1}) will be further promoted to the higher lying multiplets with Stark energy of about 29000 cm^{-1}. The radiation decay will hence produce the UV spectrum. The yellow luminescence is insignificant as observed in the experiment because of the ESA at the $^4G_{7/2}$ level. The depopulation of the inversion at the upper laser energy level is considered as a loss mechanism to the main laser emission at infrared. The nonradiative energy decay from

the multipletes can also induce heat generation to increase the thermal focal lens. The drastic drop of the repetition rate observed in the low gain Q-switched lasers at the high pump power could well explain the starting of this dissipative phenomenon where the cavity optical loss increased because of the depopulation and additional heating. The increasing of the pump power after the onset of the obvious depopulation would further decrease the optical efficiency and enhance the thermal focal lens, and consequently perturbed and stopped the Q-switching process.

The passively Q-switched performance of the a-cut c-polarized and a-polarized lasers was further compared. As under the c-polarization the laser has large gain coefficient, with the Cr^{4+}:YAG crystal of initial transmission T_0 = 90% in cavity, the absorber was easily saturated. Consequently, the energy stored in the upper energy level of the Nd:$GdVO_4$ crystal was limited. Based on the previous studies on the passively Q-switched a-cut Nd:$GdVO_4$ laser, laser operation was optimized with the output coupling of T = 40% and the Cr^{4+}:YAG saturable absorber initial transmission of T_0 = 60%. Under such operating condition, stable Q-switched pulses were successfully achieved, giving the maximum Q-switched pulse energy of 106 μJ, peak power of 20 kW at pulse duration of 5.4 ns. Without the several percentage of the input mirror loss, the pulse peak power is slightly higher than the previous result which used the same passive Q-switch and output coupler. Fig. 4.12 shows the comparison between the best Q-switched operations of the a-cut a-polarized and the c-polarized lasers. Compared with the same pump power, it is clearly seen that the a-polarized laser is able to store more energy in the upper level, and therefore the Q-switched pulses have large pulse energy, corresponding to the low Q-

switched pulse repetition rate. The high gain c-polarized laser has the advantages of generating narrower pulse width and higher peak power.

A laser with a small stimulated emission cross-section could easily satisfiy the conditions for good passive Q-switching and produce passively Q-switched pulses with larger pulse energy. As if simply based on the fundamental laser viewpoint without considering any other nonlinear absorption influence, small emission cross section is equivalent to small gain coefficient. This means the Q-switched laser needs a longer build-up time, and consequently longer Q-switched pulse duration and lower peak power.

Based on the experimental results it can be seen that in order to achieve the best passive Q-switched operation in the laser, it is very important to select the appropriate combination of laser parameters such as the saturable absorber strength, and laser output coupling. These parameters are dominant to affect the passively Q-switched laser performance once the saturable absorber recovery time and the gain medium upper level lifetime are fixed in the passive Q-switching. As far as the second laser threshold could be fulfilled, lasers with large stimulated emission cross-section are preferred for achieving narrower Q-switched pulse and higher peak power.

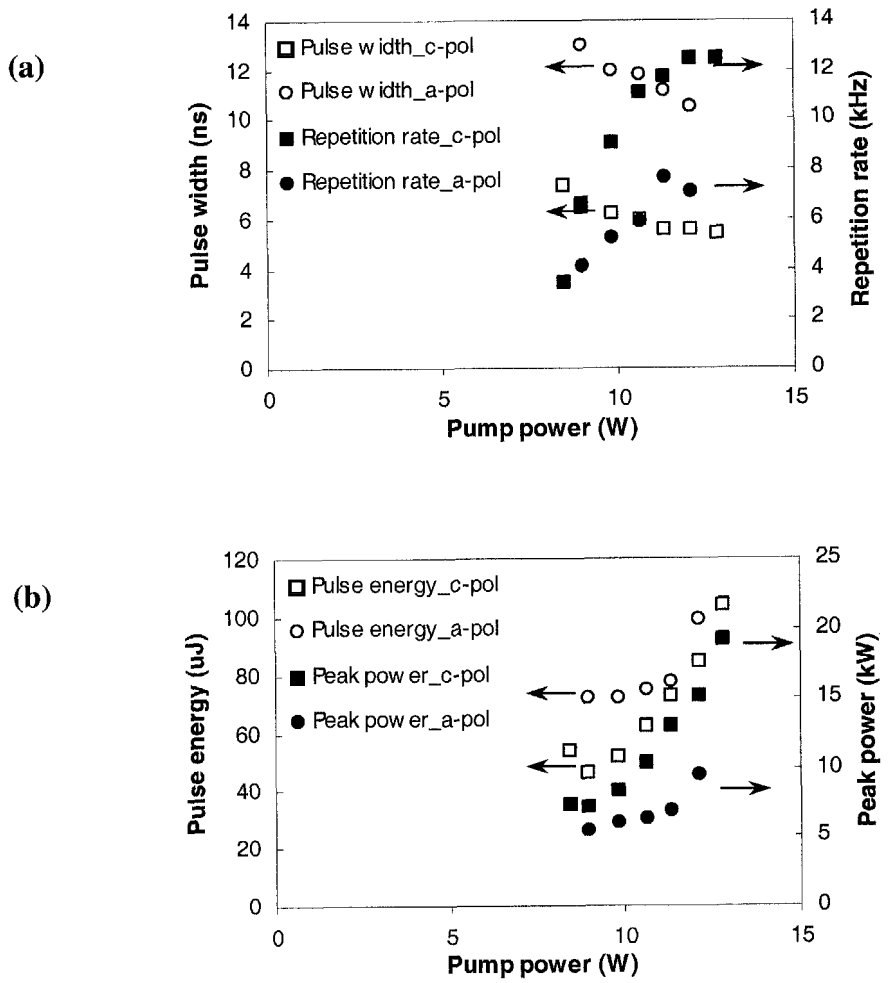

Fig. 4.12: Comparison between the passively Q-switched operation of the a-cut c-polarized (square) and the a-polarized (circle) Nd:$GdVO_4$ lasers. (a) Pulse width and repetition rate, (b) pulse energy and peak power, versus pump power.

The large emission cross section of the c-polarized laser may avoid the strong excited state concentration, and thus weakened the ESA and ETU. The c-polarized Q-switched laser could operate steadily up to the maximum pump power. However, it is believed that a similar deficiency will occur, if the Q-switched laser is attempted under even higher pump power.

4.3 Passively Q-switched performance of Nd:$GdYVO_4$ laser

As found experimentally in the previous studies, the c-polarized Nd:$GdVO_4$ laser is more favorable for the passive Q-switching if the second threshold can be satisfied. The unpleasant Q-switched results of the lightly doped a-cut Nd:$GdVO_4$ laser might be the result of difficulties in fulfilling the Q-switched criterion. Since the excessively small gain cross section of the a-polarized light can cause certain limitation to the Q-switched laser output and pulse properties, improvement on the laser gain medium properties is more effective.

Nd:$Gd_xY_{1-x}VO_4$ mixed crystal with different Gd/Y composition % has been reported showing different optical and physical properties than either of the Nd:YVO_4 and Nd:$GdVO_4$ crystals. As also stated in Chapter 2, Nd:$Gd_{0.64}Y_{0.36}VO_4$ crystal has a slightly smaller c-polarized emission cross section (4.8×10^{-19} cm^2) and longer upper-level lifetime (138 μs) than Nd:YVO_4 and Nd:$GdVO_4$ lasers. These two characteristics of Nd:$GdYVO_4$ are important to enhance the energy storage capacity with certain extent of improvement to passive Q-switching.

4.3.1 Comparative study of Nd:$GdYVO_4$ and Nd:$GdVO_4$ lasers

The performance of the passively Q-switched 0.5 at% Nd:$Gd_{0.64}Y_{0.36}VO_4$ was studied under the same experimental parameters (cavity length is 60 mm, cavity coupling loss, T = 40%, and saturable absorption strength, T_0 = 60%) as the lightly doped Nd:$GdVO_4$ laser. The cavity design is the same as illustrated in Fig. 4.1. The pump power dependence of average Q-switched output power and pulse properties is given in Fig. 4.13. Apparently, the mixed crystal gave an improvement in the pulse quality when

compared to the 0.5 at.% Nd:$GdVO_4$ laser. Because of the capability of large energy storage, the Nd:$GdYVO_4$ laser shows a slower Q-switched pulse repetition rate. The emitted single pulse energy can therefore achieve five times higher energy than the conventional Nd:$GdVO_4$ laser. As a result of the intense pulse energy, peak power of the passively Q-switched Nd:$GdYVO_4$ laser was consequently enhanced. The laser diode after long-term use has shown a gradual degradation of the pump power. In running this experiment, the launching power from the diode has reduced about 9% from 14 W to the maximum pump power of 12.81 W. Limited by the available pump power, the highest pulse energy of 111 μJ and peak power of 14.6 kW for a 7 ns Q-switched pulse was obtained using the neodymium mixed-gadolinium-yttrium vanadate crystal.

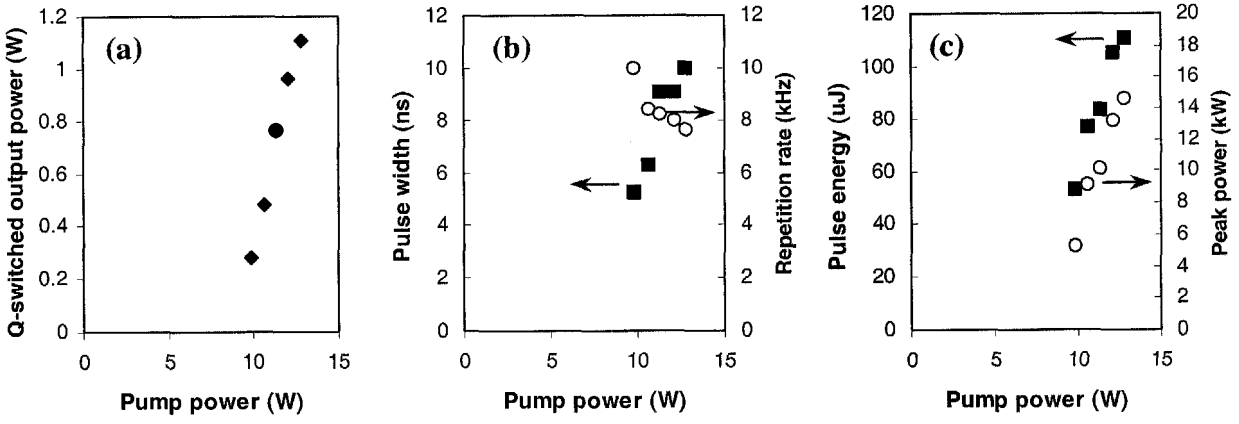

Fig. 4.13: Summary of the passively Q-switched Nd:$Gd_{0.64}Y_{0.36}VO_4$ results. (a) Q-switched average output power. (b) Q-switched pulse width and repetition rate. (c) Single pulse energy and peak power.

According to the linear increase of the Q-switched pulse repetition rate, the nonlinear absorption-induced effect is not appreciable in the mixed crystal. Despite the upper energy transfer rate being undetermined so far in the laser, the moderate gain cross

section, low doping concentration, and the better thermal quality could be responsible for minimizing the upper state depopulation effect. This result confirms the promising features of Nd:$Gd_{0.64}Y_{0.36}VO_4$ laser for the passive Q-switching. It shows that contrary to the common understanding that smaller laser stimulated emission cross section is better for passive Q-switching of a laser. Through the experimental results, it should be noted that a comprehensive consideration of all laser parameters is required to achieve the best performance of the laser operation. Experimental evidence shows that the high laser doping concentration is favorable for the passive Q-switching. It is predictable that with a mildly doped Nd:$Gd_{0.64}Y_{0.36}VO_4$ crystal which has stronger absorption and the expected larger inversion, better passively Q-switched laser performance could be achieved in the Nd:$GdYVO_4$ than that in the same doping level of Nd:$GdVO_4$ laser.

4.3.2 Q-switched pulse narrowing with GaAs output coupler

Referring to the theoretical analysis, it should be noted that besides the strength of saturable absorption, laser cavity length for the bulky crystal system is the main restriction on the shortest passively Q-switched pulse width attainable. The approach of further narrowing the pulse duration would be favorable in the current laser system for higher pulse peak power. Directly increasing the saturation loss is a way of reducing the pulse build up time, however, the loss might also increase the lasing threshold. In the previous experimental studies, passive Q-switching with GaAs wafer has demonstrated narrow Q-switched pulses under suitable experimental conditions [91, 92]. In order to further enhance the achievable Q-switched peak power from the existing laser system, the function of GaAs wafer in narrowing the Q-switched pulse duration is investigated.

The passively Q-switched Nd:$GdYVO_4$ experiment is continued by replacing the normal cavity output coupler with a flat GaAs semi-insulating semiconductor. In this case, the optimum absorption strength of Cr^{4+}:YAG crystal (T_0 = 60%) as proved in the previous experiments was selected. The GaAs wafer was <100>-cut into the dimensions of 20 × 10 × 0.450 mm^3 and was coated with gradually varying transmission at 1.06 μm from about T = 3% to 60% along the 20mm edge direction. The incorporated variation transmission coatings onto a GaAs wafer, allow ease of optimization on the cavity coupling parameter. The laser setup is schematically shown in Fig. 4.14. In order to properly extract the pulse energy from the cavity, GaAs mirror was mounted on a linear translation stage for free adjustment to the cavity transmission through shifting the wafer along its 20 mm edge. The GaAs mirror was translated down from its highest transmission portion to avoid the strong pulse fluence optical damage on the intracavity element caused by the high coupling reflectivity.

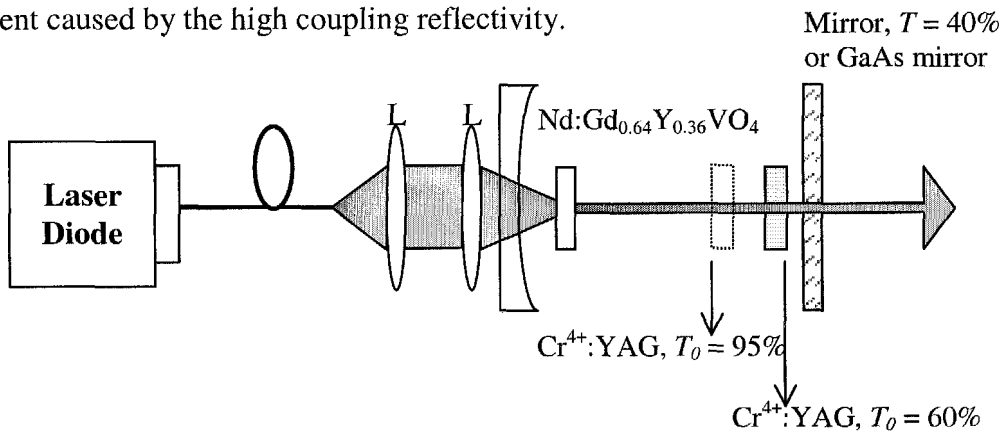

Fig. 4.14: Schematic diagram of experimental setup. L: Coupling lens. The arrangement of the optical elements is explained in details in text.

Fig. 4.15 shows the relationship of the average laser output power to the pump power obtained under the optimized GaAs wafer transmission. The Q-switched operation

of the laser has a pump threshold of 8 W and a slope efficiency of about 20%. For comparison, the average output power of the Q-switched laser with the flat mirror of T = 40% used as the output coupler is also shown in the figure.

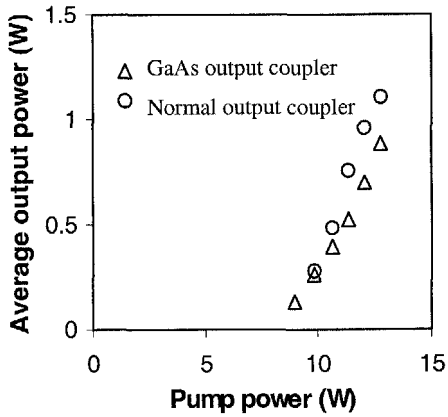

Fig. 4.15: Average Q-switched output of the lasers. Triangle: GaAs wafer used as output coupler. Open circle: flat mirror used as output coupler.

Fig. 4.16 compares the Q-switched pulse properties before and after the GaAs wafer was used as the output coupler. Clearly, under exactly the same other laser operation conditions, with the GaAs wafer used as the output coupler the Q-switched pulse width is significantly narrowed, a compression factor of more than three has been achieved. Experimentally it was observed that when the pump power increased beyond 11.3 W, the Q-switched pulse width remained at a fixed value of 2.2 ns. Fig. 4.16 also shows that at the same pump strength the Q-switched pulse repetition rate has become slightly higher. Correspondingly, the single pulse energy is smaller. However, as the factor of pulse width narrowing is larger than that of the pulse energy decrease, the peak power of the Q-switched pulse is still increased. A peak power of 26.3 kW was obtained at the maximum

pump power of 12.8 W in the experiment. Since no pulse energy saturation was observed, even higher peak power could be obtained with larger pump power.

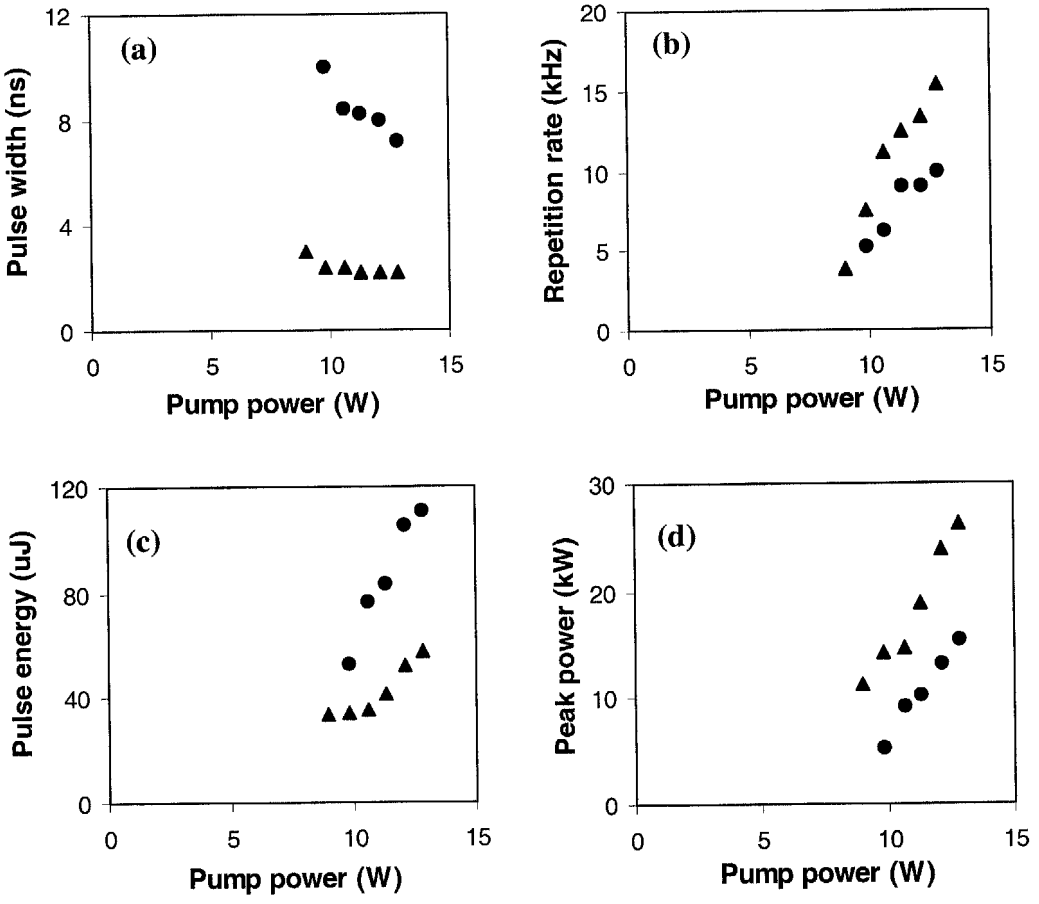

Fig. 4.16: Comparison of the Q-switched pulse properties of the lasers. Triangle: With the GaAs wafer used as output coupler. Open circle: With the flat mirror used as output coupler.

Fig. 4.17 compares the Q-switched pulse profiles of the lasers. It can be seen that, with the GaAs wafer as the output coupler, both the rising and trailing sides of the pulse become steeper, which consequently results in the pulse width narrowing. It was also

noticed experimentally that with the GaAs wafer as the output coupler, the overall Q-switching performance of the laser becomes relatively more stable.

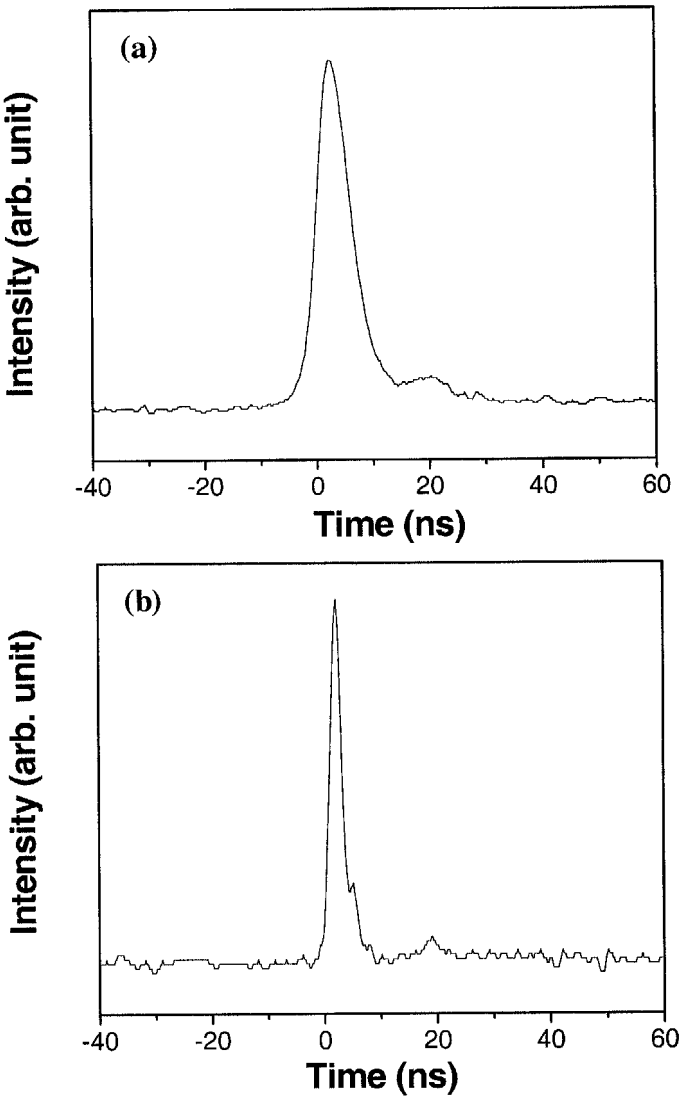

Fig. 4.17: Comparison of the Q-switched pulse profiles when the laser was with (a) a flat mirror output coupler; (b) a GaAs wafer as output coupler.

Fig. 4.18 shows for example a typical Q-switched pulse train obtained. The Q-switched pulse train is found not only has amplitude-to-amplitude jitters of less than 5 %, but also such a pulse train remains even as the pump power increases to the maximum.

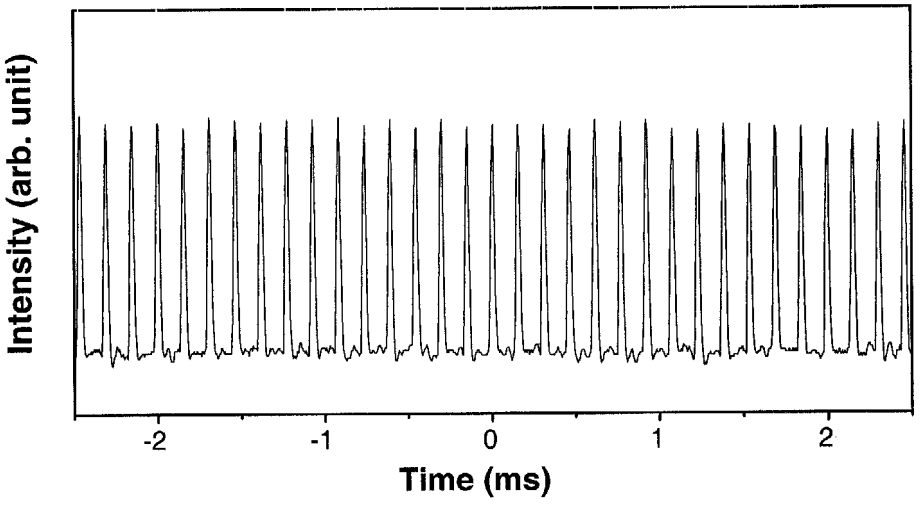

Fig. 4.18: A typical Q-switched pulse train of the laser with the GaAs wafer as output coupler.

The pulse narrowing mechanism of the passively Q-switched Nd:$GdYVO_4$ laser with GaAs output coupler was further studied. To check whether the observed pulse width narrowing is caused by the extra linear saturable absorption of the GaAs wafer, the Q-switched pulse property change of the Nd:$Gd_{0.64}Y_{0.36}VO_4$-Cr^{4+}:YAG laser was observed by adding another Cr^{4+}:YAG absorber in the cavity. The additional Cr^{4+}:YAG crystal has similar linear saturable absorption strength (T_0 ~ 95%) as the GaAs wafer. As expected, the Q-switching threshold increased with the double Cr^{4+}:YAG crystals in cavity. Compared to the single Cr^{4+}:YAG Q-switching, the shortest Q-switched pulse width indeed decreased slightly due to the stronger cavity saturation loss. However, the narrowest pulse width obtained is still larger than 6.5 ns. The intense laser pulse was

obtained just for a short moment after the bleaching of the saturable absorbers, implying that the laser was insufficient to overcome the total cavity loss continuously. The result of double Cr^{4+}:YAG passive Q-switching is shown in Fig. 4.19.

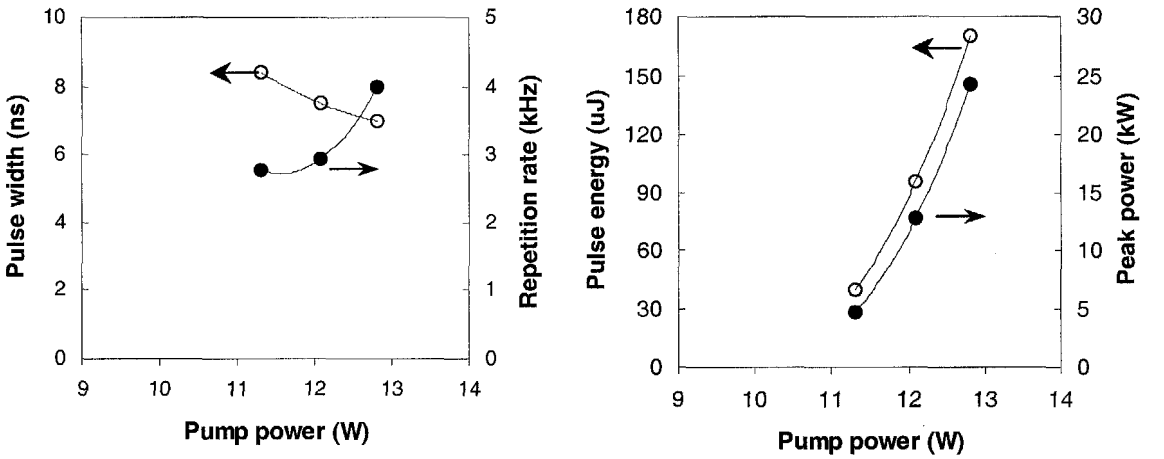

Fig. 4.19: Q-switched pulse properties obtained from the double Cr^{4+}:YAG saturable absorbers.

In addition, the passively Q-switched laser performance by using the GaAs wafer simultaneously as saturable absorber and output coupler was investigated. This was done by just moving away the Cr^{4+}:YAG from the laser cavity. In such a case only the long and broad, weak Q-switched pulses with few tens to hundreds of ns could be obtained. This causes a very poor result to the laser, giving the highest pulse energy of several μJ and peak power of less than 50 W at the maximum pump power (Fig. 4.20). In particular, the Q-switched pulse from the GaAs absorber exhibited large amplitude and frequency pulse jitters following the increase of pump power. Fig 4.21 shows one example for the typical Q-switched pulse train by using the simultaneous GaAs saturable absorber and cavity output coupler. Therefore, all these experimental results suggested

that the nonlinear effect of the GaAs wafer is a possible cause of the observed pulse width narrowing.

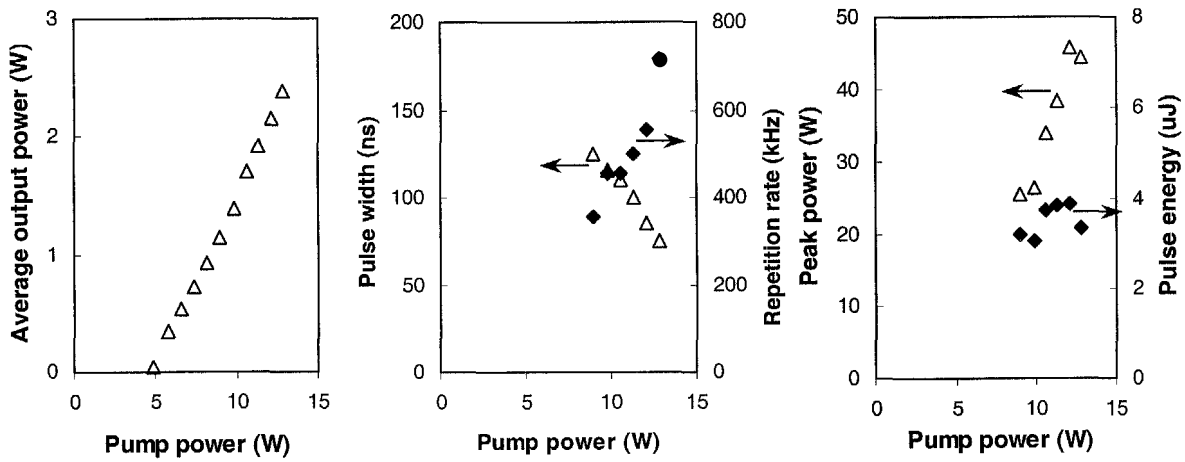

Fig. 4.20: Passively Q-switched Nd:$Gd_{0.64}Y_{0.36}VO_4$ laser outputs by the GaAs saturable absorber mirror.

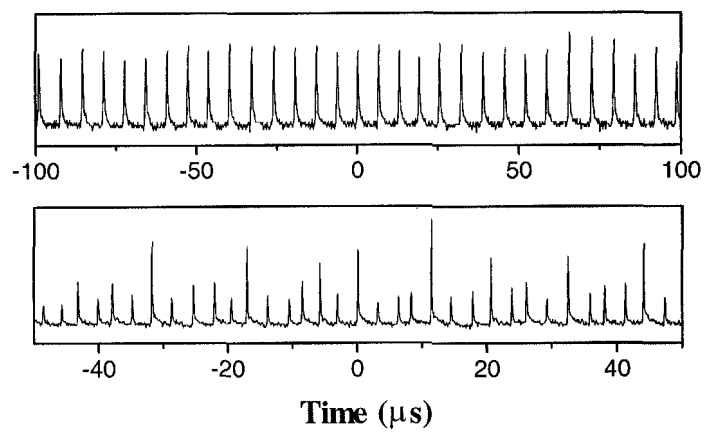

Fig. 4.21: Observed Q-switched pulse trains. Upper trace: at pump power of 6 W. Lower trace: at pump power of 10 W.

For Nd:$GdYVO_4$-Cr^{4+}:YAG Q-switched laser with the GaAs as output coupler, the intracavity pulse fluence is estimated as in the range of 84 - 156.4 mJ/cm^2 from the threshold to the maximum pump power. The Q-switched pulse formed initially by the

Cr^{4+}:YAG before the compression in GaAs is energetic and in several ns pulse duration. Both the TPA and the FCA of the GaAs is believed to exist in the laser under the high intracavity pulse fluence. To determine how strong these nonlinear absorptions affect the Q-switched pulse width narrowing, the Q-switched laser performance was further studied by changing the position of the GaAs wafer in the laser cavity. Instead of using the GaAs wafer as the output coupler, a GaAs wafer of the same thickness and property but with both its surfaces AR coated at the lasing wavelength was inserted in the cavity at the position just in front of the Cr^{4+}:YAG crystal. Experimentally it was found that no obvious pulse width narrowing could be observed if GaAs wafer were not used as an output coupler. In this case the laser just behaved in a similar way as was the case with the two Cr^{4+}:YAG crystals in the cavity described above. This means that in order to obtain pulse width compression it is critical to use the GaAs wafer as an end-mirror. Based on this experimental result it is therefore concluded that the observed pulse width narrowing should not be directly caused by the nonlinear absorptions of the GaAs wafer.

Through carefully analyzing the experimental results, a new intensity dependent loss mechanism in the GaAs wafer is then proposed. When using the GaAs wafer as the output coupler, the incident and the reflected light by the outer surface of the wafer generate strong interference within the wafer. Under existence of strong nonlinear absorption of the GaAs wafer, this further causes free-carrier index grating and absorption grating in the GaAs wafer. These grating induced diffraction losses are believed to introduce a sufficiently strong intensity dependent loss to the laser cavity, which affect the passive Q-switching process and generates narrow pulse width of Q-switched pulses. Indeed, previous experimental studies have also shown that the

influence of the nonlinear absorption of the GaAs on the pulse intensity is far less significant than those caused by the refractive index changes [103].

This demonstration revealed that the combination of an appropriately coated GaAs wafer as output coupler and an intracavity Cr^{4+}:YAG absorber is efficient to enhance the passive Q-switching. This simple and low cost technique is suitable to be applied in all Nd-doped solid-state lasers to generate more reproducible Q-switched pulses with higher peak power and narrow pulse width.

4.4 Investigation of passively Q-switched Nd:$GdVO_4$ lasers pulse profile

In certain experimental conditions, a small secondary pulse was generally found subsequent to the main Q-switched pulse in both Nd:$GdVO_4$ and Nd:$GdYVO_4$ lasers. The significance of this satellite pulse varied depending on the laser parameters used, such as the cavity reflectivity, laser and absorber doping concentration as was investigated in Nd:$GdVO_4$ lasers. Basically the observed Q-switched satellite pulse in nanoseconds range has no influence to the stability of the pulse train. Nevertheless, it is necessary to understand and identify the dependence of pulse profile on the experimental conditions. In this investigation, different doping concentrations of Nd:$GdVO_4$ samples were selected to provide more parameters in comparison. Focusing on the evolution of a single Q-switched pulse, it is understood that the rising edge of pulse is determined by laser energy storage, while pulse decay is controlled by the cavity photon decay loss. In other word, saturable absorption strength plays a role in enhancing the laser gain during the high cavity Q-factor, and the cavity coupling transmission has the function of controlling the round trip loss in a given resonator length.

The observation was initially conducted in the mildly (~ 1 at.%) doped Nd:$GdVO_4$ laser using a strong Cr^{4+}:YAG saturable absorber of T_0 = 60%. At a given pump power of 9.83 W, the influence of the coupler reflectivity to the pulse pattern was investigated. According to the experimental results as in Fig. 4.22, the Q-switched pulses show a broader pulse width associated with the reduction of cavity transmission loss. This is in good agreement with the relation of pulse width and cavity decay rate as given in Eq. (2.18). At the decay tail of each Q-switched pulse, a small pulse envelope was observed at about few tens ns following the main Q-switched pulse. The significance of this satellite pulse increased following the decrease of the cavity coupling reflectivity. At the optimized extraction of cavity energy in generating the narrow pulse duration as such in the condition of R = 60%, the small Q-switched pulse profile shows the most distinctive satellite pulse compared to the rest at the pulse trailing edge.

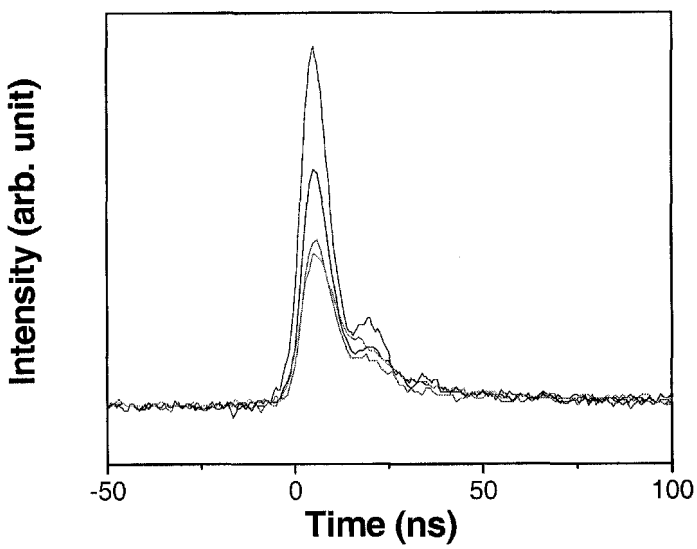

Fig. 4.22: Influence of coupling reflectivity to the pulse shape. From the highest to the lowest amplitude of Q-switched pulses, cavity reflectivity varied from R = 60% to 70%, 80%, and 90%.

On the other hand, at a fixed output coupler reflectivity of 60%, the Q-switched laser pulse shape was studied by varying the Cr^{4+}:YAG absorption strength in terms of its initial transmission. Fig. 4.23 shows the experimental observation on the mildly doped Nd:$GdVO_4$ laser when it was passively Q-switched by Cr^{4+}:YAG crystal with either T_0 = 80% and 60% at the pump power of 9.83 W. As expected, the weaker saturable absorption generated a broader pulse without the obvious appearances of the satellite pulse. Strong Q-switched pulse with clear secondary pulse was obtained using the lower initial transmission Cr^{4+}:YAG crystal. This implies that the Q-switched satellite pulse is proportional to the energy stored in the upper laser energy level during the Q-switching.

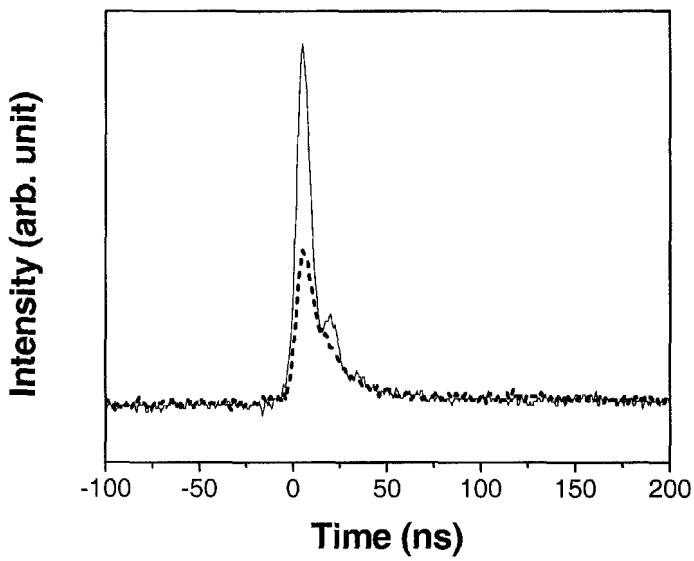

Fig. 4.23: The observed passively Q-switched pulse shapes in different initial transmission of Cr^{4+}:YAG crystals. Solid line: T_0 = 60%, dash line: T_0 = 80%. The experiment conducted under coupling reflectivity R= 70% and the pump power of 9.83 W.

Therefore, based on the relation of laser doping concentration to the laser gain in passively Q-switched lasers, it is to be expected that the lightly doped passively Q-switched Nd:$GdVO_4$ laser will have less obvious satellite pulse generation due to its weak ability to store energy. This is confirmed experimentally by the Q-switched pulses of a 0.52 at.% Nd:$GdVO_4$ laser, though a strong saturable absorber was used. Fig. 4.24 shows for example a single pulse at the condition of T_0 = 60% and R = 60%. With its lower pulse energy, the pulse profile is more symmetrical on both rising and decaying edges.

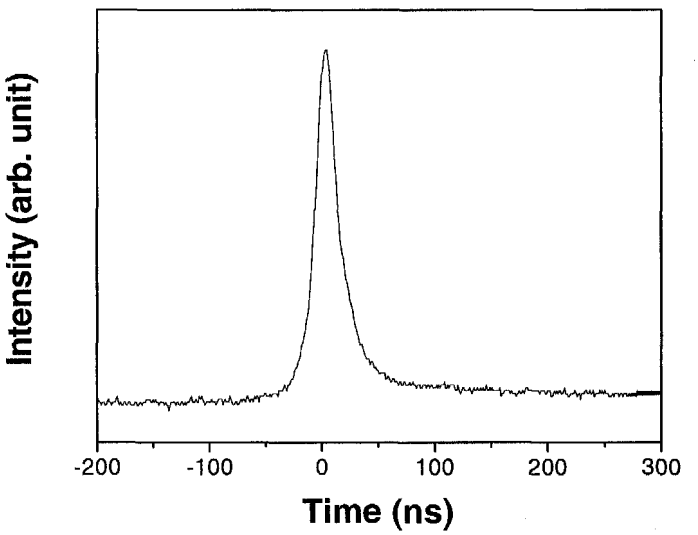

Fig. 4.24: Experimental Q-switched pulse obtained from the lightly doped Nd:$GdVO_4$ under the parameters of T_0 and R = 60%.

In contrast, in the case of the heavily doped laser crystal of 1.61 at.%, strong Nd^{3+} ion concentration with higher pump absorption coefficient yielded larger population inversion in Q-switching. Hence at the decay tail of the intensive narrow Q-switched pulse there was a significant satellite pulse, despite the fact that the Cr^{4+}:YAG absorption

strength and cavity transmission were low. Fig. 4.25 depicts the experimental 1.61 at.% laser at pump power of 12.48 W when passively Q-switched with a Cr^{4+}:YAG of T_0 = 80% under the coupling reflectivity of R = 70%.

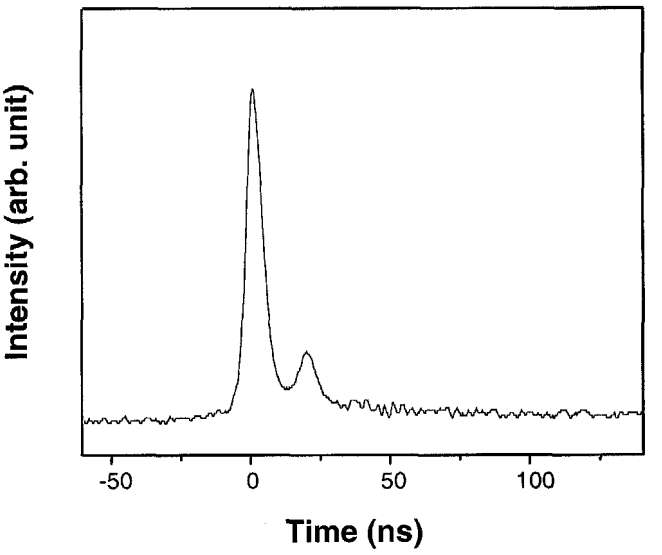

Fig. 4.25: Experimental Q-switched pulse for the 1.61 at.% Nd:$GdVO_4$ laser with the output coupler of R = 70% and a Cr^{4+}:YAG crystals with T_0 = 80%.

The experimental results revealed that the significance of Q-switched secondary pulse is dependent on the laser pulse energy. Under experimental conditions of low cavity reflectivity, strong saturable absorber and laser dopants that result in the tendency of satellite pulse to the passively Q-switched laser, the laser doping concentration is obviously the most detrimental factor.

4.5 Summary

Based on the analytical description of the passive Q-switching that shows the relation of the experimental parameters with the Q-switched pulse properties, appropriate selection

of the coupling loss, saturation strength with respect to the laser emission cross section has been studied in practice. In order to achieve the best performance of the passively Q-switched operation of the laser, an overall consideration of the laser parameters is important.

The experimental results demonstrated that crystals with higher doping concentration are beneficial for the passive Q-switching, provided that influence of the thermal lens effect is considered in the cavity design. It is in contrast to the CW operation of the laser, where a low doping concentration is preferred for higher laser output efficiency. By using the natural birefringence of an a-cut Nd:$GdVO_4$ crystal, laser operation has been experimentally investigated under different light polarizations. Their laser performance was further compared with that of a c-cut Nd:$GdVO_4$ laser using the same experimental parameters. It was found experimentally that though the c-cut Nd:$GdVO_4$ laser has a good passively Q-switched performance in the low pump power region, the a-polarized and c-cut Nd:$GdVO_4$ lasers could be influenced by other nonlinear absorptions at the upper energy level. The intrinsic laser effects increase the thermal induced cavity losses and severely degrade the laser performance under the high pump power. The best passively Q-switched performance is obtained in the experiments on the a-cut c-polarized Nd:$GdVO_4$ laser though it has a larger stimulated emission cross section. Stable Q-switched pulses with pulse width of 5.4 ns, single pulse energy of 106 μJ and peak power of 20 kW were achieved under the laser operation condition of T = 40%, T_0 = 60%. It is confirmed that once the Q-switched second threshold is reached, proper combination of the coupling transmission and saturation strength is more dominant to affect the laser performance. In particular, laser crystal and saturable

absorbers with high doping concentration are favorable for achieving large single pulse energy and high peak power of the passively Q-switched pulses. With a heavily doped 1.61 at.% Nd:$GdVO_4$ laser, the highest single pulse energy of 158.2 μJ at a repetition rate of 6.3 kHz could be obtained. Maximum peak power of 26.4 kW was achieved at its narrowest pulse width of 6 ns.

For the unpleasant passive Q-switching of the lightly doped Nd:$GdVO_4$ laser, a great enhancement was found in the Q-switched performance with the used of Nd:$Gd_{0.64}Y_{0.36}VO_4$ crystal. Compared to the same lightly doped Nd:$GdVO_4$ laser, Nd:$Gd_{0.64}Y_{0.36}VO_4$ has a slightly smaller emission cross section, and longer upper energy level lifetime. The better laser quality of the mixed crystal has significantly increased the pulse energy to 111 μJ by about five times than that in the lightly Nd:$GdVO_4$ laser. It is believed that mildly doped Nd:$GdYVO_4$ will have better performance than the same doping level of conventional Nd:$GdVO_4$ laser to achieve even higher pulse energy and peak power in passive Q-switching. By using an appropriately coated GaAs wafer as output coupler, the passively Q-switched pulse width of the Nd:$GdYVO_4$ mixed crystal laser with the Cr^{4+}:YAG saturable absorber could be narrowed by a factor of three. Stable passively Q-switched pulse train with pulse width of about 2.2 ns, pulse energy of 57.85 μJ and peak power of 26.3 kW has been obtained at an absorbed pump power of 8.54 W. In addition, experimental studies on the pulse narrowing physical mechanism in GaAs have showed that the observed pulse narrowing is not caused by the direct nonlinear absorptions of the GaAs wafer, but possibly by a free-carrier index grating induced self-diffraction loss mechanism. This simple combination of the Cr^{4+}:YAG saturable absorber

and the low cost nonlinear GaAs output coupler would be plausible to generate Q-switched pulses with higher peak power for practical interest in numerous applications.

Besides the exploit of passively Q-switched laser performance corresponding to the appropriate laser designs, the single Q-switched pulse profile of Nd:$GdVO_4$ laser in nanosecond range has been particularly investigated under different cavity parameters. Results show that the observed Q-switched secondary pulse is a dependence of cavity coupling transmission, Cr^{4+}:YAG saturable absorption strength, and laser doping concentration. It has been found that the significance of the satellite pulse is proportionate to the laser gain during passive Q-switching according to the parameters selection, at which the laser doping level is dominant among all factors. In fact, the occurrence of the satellite pulse implies the division of total laser energy generated from the passive Q-switching, which should be contained by the main Q-switched in the ideal case. It is significantly shown in experiments that the existing Q-switched secondary pulse is a characteristic of the laser system, whose physical cause will be analyzed quantitatively in the next chapter.

CHAPTER 5

Numerical simulation of passively Q-switched Nd:$GdVO_4$ lasers

Although the satellite pulse phenomenon has been observed in the passive Q-switching process of several Nd-doped lasers [104, 105], there has been no consistent analysis to its mechanism so far. A quantitative study of the passively Q-switched Nd:$GdVO_4$ lasers pulse profile is presented in this chapter to comprehend the generation of secondary pulse in the Q-switched lasers. Generally, passive Q-switching is described analytically by using the rate equations on the basis of the perfect laser system. In such ideal conditions, population in lower energy level is negligible for its fast emptying. Laser spontaneous emission and pumping terms are also ignored in the analytical model for ease of analysis. In fact, the analytical rate equations provide good descriptions of the general characteristics of Q-switched lasers, especially for those generated by active Q-switching approach. Nonetheless, for the passive Q-switching, where complicated nonlinear interaction between light with the gain medium and the saturable absorber exists, an analytical description is difficult to express appropriately the laser behavior. Numerical simulation by directly solving the equations becomes necessary.

Through numerical simulation, the physical mechanism of the Q-switched satellite pulse generation is firstly explained using a generalized two-level rate equations model, where the finite ions decaying lifetime of the lower energy level has been considered. The effects of the thermally induced change of the cavity mode size and

pump rate estimate are further considered in the model for a more detailed and accurate simulation of the experimentally measured Q-switched pulse properties.

5.1 Secondary Q-switched pulse

The Nd:$GdVO_4$ laser is a four-level system whose ion transitions are illustrated in Fig. 5.1. In the ideal case of laser transition, the decay of Nd^{3+} ion at the lower laser level to the ground state is on an infinitely short time scale, and thus it is usually negligible in theoretical analysis. However, in the real case, this assumption has been proved invalid, as ions require a certain time to relax to the ground state before being excited. According to Tso in his numerical study on the Nd:YAG passively Q-switched laser [106], delay of the ions transition from the lower energy level to the ground state could influence the Q-switched pulse shape and laser extraction efficiency. For the Nd:$GdVO_4$ laser which has a large emission cross section, this effect would be even stronger because of the drastic population change between the two lasing levels during the Q-switching process. In addition, this relaxation would have greater impact on the Q-switched pulse profile when a slow saturable absorber suchlike Cr^{4+}:YAG is used. This is because the slow response of Cr^{4+} ions is unable to further shape the pulse after the saturation of Cr^{4+}:YAG crystal. Any dynamic change of laser inversion after the bleaching of Cr^{4+}:YAG is thereby directly reflected on the Q-switched pulse profile.

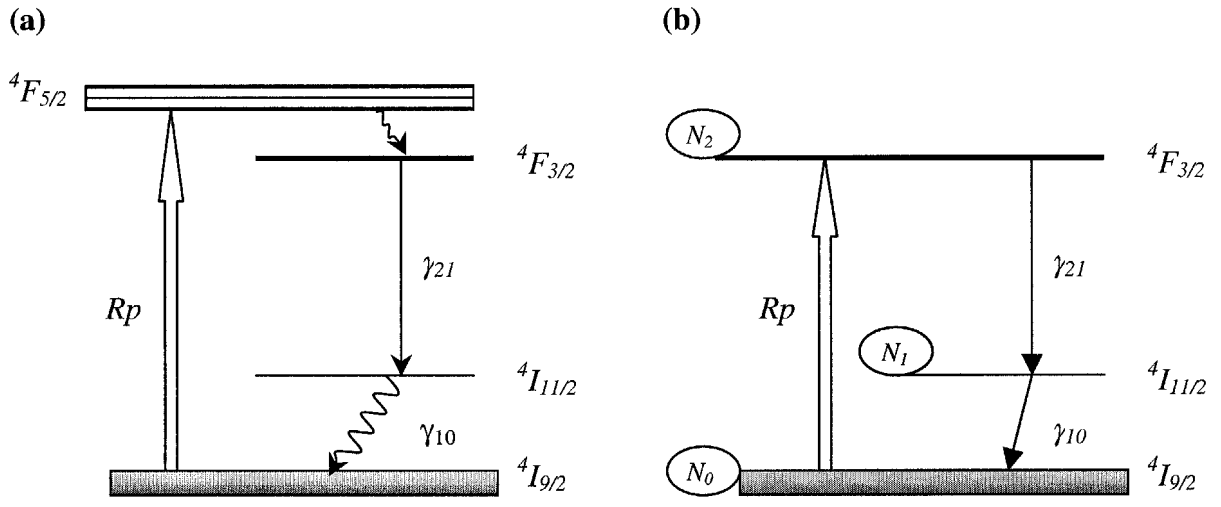

Fig. 5.1: Energy diagram of the Nd:$GdVO_4$ laser. (a) Ideal case in the four-level energy system with a rapid transition between $^4F_{5/2}$ - $^4F_{3/2}$ and $^4I_{11/2}$ – $^4I_{9/2}$. (b) Slow decaying of $^4I_{11/2}$ level is considered in the model. Laser diagram is simplified with the fast non-radiant decay from the higher-lying energy band.

A simple, coupled rate equation model was used to simulate the dynamics of the single Q-switched pulse. Because of the fast non-radiant relaxation from laser pump band to the metastable state $^4F_{3/2}$, Fig. 5.1a is simplified to Fig. 5.1b following the assumption that the ions are directly pumped to the upper level. In order to study the effect of the slow ions relaxation on the pulse profile, ideal continuous pumping of infinite ions in the ground state is assumed. The rate equations model is written as follows:

$$\frac{d\phi}{dt} = \frac{\phi}{t_r}\left[2\sigma_g l_g (N_2 - N_1) - 2\sigma_s l_s N_s - 2\sigma_{es} l_s (N_{s0} - N_s) - \left(\ln\frac{1}{R} + L\right)\right] \tag{5.1}$$

$$\frac{dN_2}{dt} = Rp - (\gamma_{20} + \gamma_{21})N_2 - \sigma_g c\phi(N_2 - N_1) \tag{5.2}$$

$$\frac{dN_1}{dt} = -\gamma_{10}N_1 + \gamma_{21}N_2 + \sigma_g c\phi(N_2 - N_1) \tag{5.3}$$

$$\frac{dN_s}{dt} = \gamma_s(N_{s0} - N_s) - \sigma_s c\phi N_s \tag{5.4}$$

The first differential equation describes the laser output in term of the photon density ϕ through the gain and loss in the cavity, where R is the cavity mirror reflectivity and L is the cavity dissipative loss. As differs to the ideal laser, spontaneous emission from N_2 to N_1 and the ion relaxation from N_1 to ground state are taken into account in the model. Rp is the volumic excited ions density in unit $cm^{-3}s^{-1}$ and σ_g is the stimulated emission cross section. The length of the laser gain medium, the light velocity in the vacuum, and the cavity round trip transit time are represented by l_g, c, and t_r, respectively. The last equation is for the saturable absorber that controls the modulation of cavity loss. In the model, the ground state energy transition in Cr^{4+}:YAG which takes effect to the passive Q-switching is described by the Cr^{4+} ions population change N_s, with saturable absorption cross section σ_s and recovery rate γ_s, while the residual absorption at the excited state with population of $(N_{s0} - N_s)$ is included as an unsaturated loss to the laser, in which N_{s0} is the total Cr^{4+} dopants. Since the passive Q-switching process is based on the modulation of cavity gain and loss, the Q-switched laser performance can be illustrated through the relation of the laser population inversion and the laser system loss. Based on the thinking that the laser Q-switched gain is equal to loss, and the cavity photon number is equal to zero in Eq. (5.1), the Q-switched system loss is defined as

$$Loss \approx \frac{2\sigma_s l_s N_s - 2\sigma_{es} l_s (N_{s0} - N_s) - \left(\ln\frac{1}{R} + L\right)}{2\sigma_g l_g} \tag{5.5}$$

In the model the sum of the spontaneous emission rate γ_{21} and the decay rate of the terminal lasing level to ground state γ_{20} is actually the laser fluorescence rate $\gamma_f = \gamma_{20} + \gamma_{21}$. It is also equivalent to $\frac{1}{\tau_f} = \frac{1}{\tau_{20}} + \frac{1}{\tau_{21}}$. Based on the Judd-Ofelt theory that the atomic relaxation rate from the upper laser energy level corresponds to its transition probability $A(J'' \rightarrow J')$, laser spontaneous transition rate γ_{21} in the model can be estimated through the upper level fluorescent lifetime once the corresponding transition branch ratio B is known.

$$\tau_f = \frac{1}{\sum_{J'}(J'' \rightarrow J')}, \quad B = \frac{A(J'' \rightarrow J')}{\sum_{J'}(J'' \rightarrow J')} \text{ and } \gamma_{21} = \frac{1}{\tau_f} \times B$$

According to the experimental measurement of Jiang *et al.* [107], the branch ratio of Nd:$GdVO_4$ laser at 1.06 μm is 51.95%, and the measured τ_f value is 109.8 μs. Based on this result, ion relaxations of the laser metastable were calculated for the purpose of simulation. Through the calculation, γ_{21} is about 4731.33 s^{-1}, whereas, pertaining to the relaxation ratio of 36.89%, γ_{20} is hence to be 3359.74 s^{-1}. However, the unknown τ_{10} in Nd:$GdVO_4$, which would be determined in the numerical calculation was taken to be in the same range of that of in Nd:YAG laser [108]. τ_{10} = 20 ns is the value taken as trial for the simulation. It was selected to be consistent with the experimental results in sense of the closely similar pulse shape and the sequences of the pulse width and the repetition rate with pump power.

Based on the assumption of uniform pumping, the number of excited active ions of a longitudinal end-pumping configuration is estimated as a ratio of the absorbed pump power to a unit volume of the incident pump energy.

$$Rp = PN_0 = \frac{P_{in}}{h\nu_p}\left[\frac{(1-\exp(-\alpha_g l_g))}{\pi\omega_p^{\,2} l_g}\right], \tag{5.6}$$

where P_{in} is the input pump power, ω_p is the pump beam radius on the laser crystal and ν_p is the frequency of the pump light. α_g is the absorption coefficient of the laser gain medium which was determined experimentally for different doping concentration of laser crystals. P is the pump rate, while N_0 is the ground state population density.

Despite the fact that some of the material parameters are uncertain in the reported experimental measurements, such as stimulated emission cross section of Nd:$GdVO_4$ (7.6×10^{-19} [29] and $14.76 - 16.4 \times 10^{-19}$ cm^2 [109]), and widely discrepant absorption cross section of Cr^{4+}:YAG ($\sigma_{gs} = 8 \times 10^{-19} - 8 \times 10^{-18}$, $\sigma_{es} = 2 \times 10^{-19} - 2 \times 10^{-18}$ [82 - 84]), in the numerical simulation, if possible, the parameters whose simulation is close to the experimental results are taken. The used value for σ_g, σ_{gs} and σ_{es} is respectively 7.6×10^{-19} cm^2, 4.3×10^{-18} cm^2, and 7.8×10^{-19} cm^2.

Calculation has also been made to ensure certain constants in the simulation are in accordance with the experimental parameters. The total number of active ions N for different doping concentration of Nd:$GdVO_4$ crystal is calculated from

$$N = xat.\% \times \frac{AtomicDensity}{MolecularWeight} \times N_{Avogrado}. \tag{5.7}$$

x at.% indicates the doping concentration of Nd:$GdVO_4$ crystal, $N_{Avogrado}$ is Avogrado's number = 6.022×10^{23} ions/mol. The value N following the doping concentration of 0.52 at.%, 1.14 at.% and 1.61 at.% are 6.29×10^{19}, 1.38×10^{20} and 1.95×10^{20} cm^{-3}, respectively.

On the other hand, for the ion-doped passive Q-switch, total Cr^{4+} ions number N_{s0} in Cr^{4+}:YAG saturable absorber is dependent on the preset initial transmission T_0 and the thickness of the crystal. The relation is given as

$$N_{s0} = \frac{\ln T_0}{-\sigma_{gs} l_s}. \tag{5.8}$$

According to the real conditions, N_{s0} for the Cr^{4+}:YAG with T_0 = 80% and 60% is respectively about 5.19×10^{17} cm^{-3} and 6.83×10^{17} cm^{-3}.

The rate equations model was solved by using ODE 45 in Matlab, which operates on a basis of the nonstiff fourth and fifth-order Runge-Kutta method. Numerical simulation shows that the existence of the satellite pulse is closely dependent on the laser parameters. The level of the satellite pulse is found to be stronger when the stored energy is higher in the laser. The simulated pulse profile was firstly checked in the optimal passive Q-switching conditions. Fig. 5.2 shows the experimental and simulated passively Q-switched pulse for the 1.14 at.% Nd:$GdVO_4$ laser with cavity coupling reflectivity R = 40%, and Cr^{4+}:YAG initial transmission T_0 = 60% at a given pump power of 14 W. The secondary pulse is found significant in this Q-switched pulse, which has a high pulse energy. As compared to the experimental result, the simulation shows a good agreement on the temporal pulse profile particularly the reproducible pattern of satellite pulse even though the simulated pulse width is slightly broader.

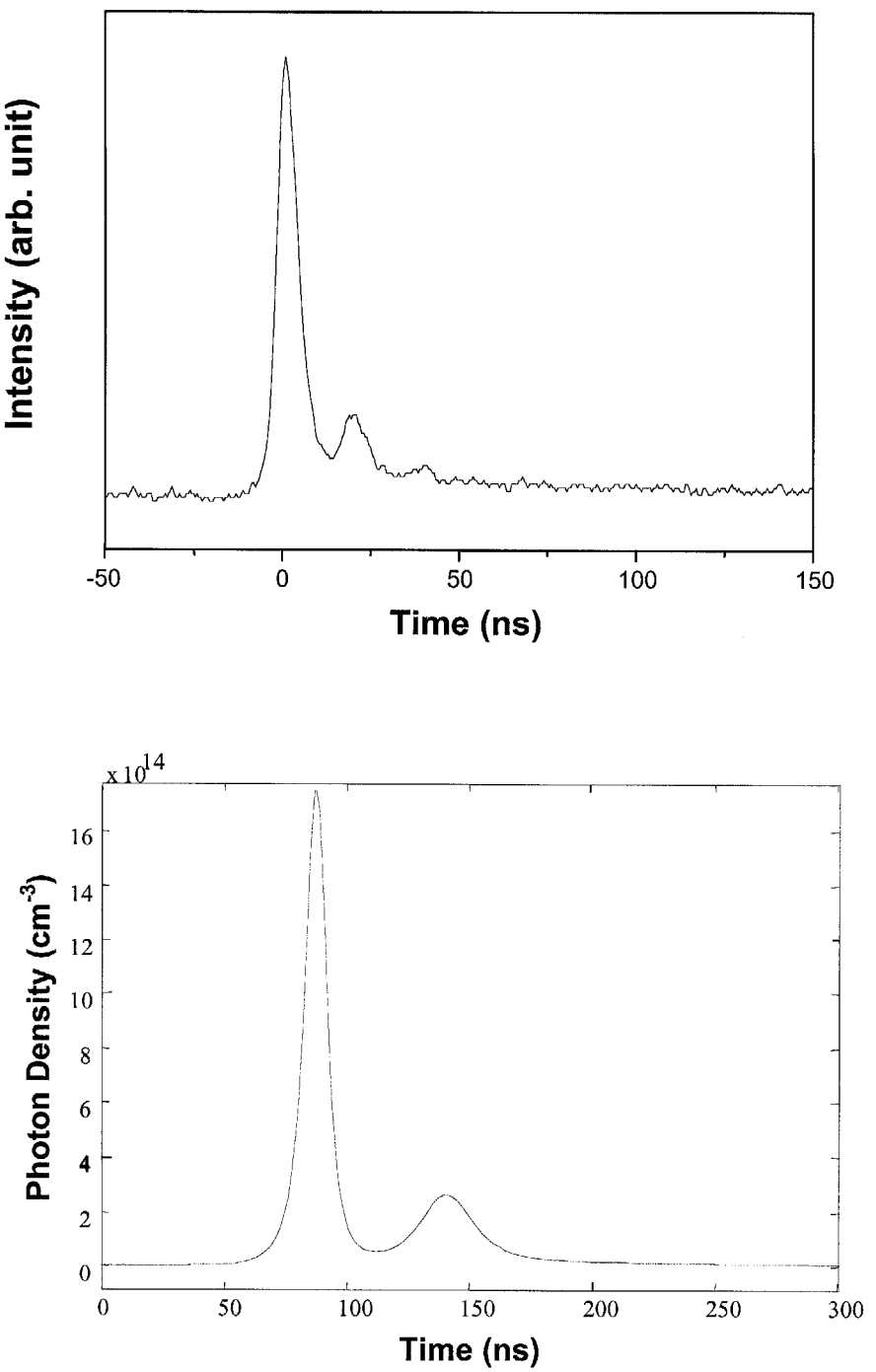

Fig. 5.2: (a) Observed and (b) calculated Q-switched pulse profile obtained with the parameters T_0 = 60% and R = 60% in the 1.14 at.% Nd:$GdVO_4$ laser.

In cases where a low dopant saturable absorber and a low coupling transmission are used, multiple Q-switched pulses do not exist. The Q-switched pulse energy in such conditions is weak and with a broad pulse duration. Fig. 5.3 shows the observed and the calculated pulses of the 1.14 at.% doped Nd:$GdVO_4$ passively Q-switched laser by a Cr^{4+}:YAG of T_0 = 80%. The cavity output coupling was set at R = 70%.

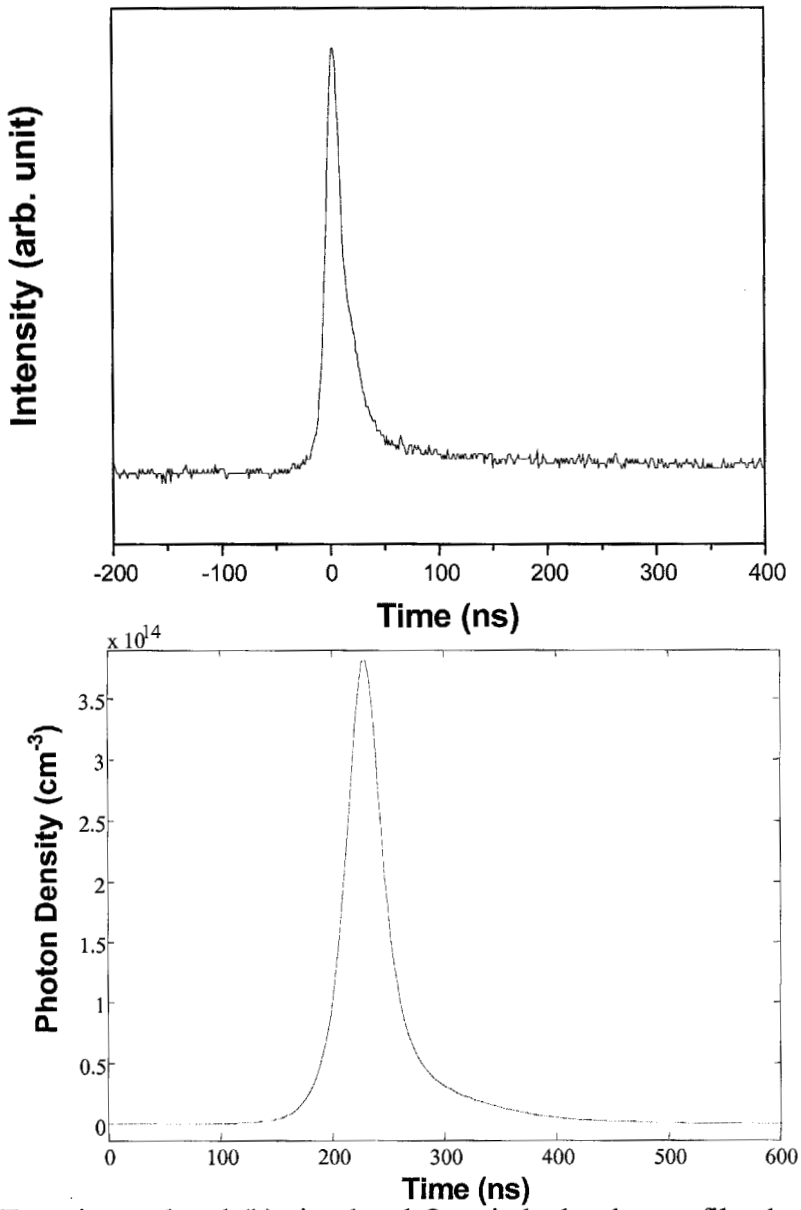

Fig. 5.3: (a) Experimental and (b) simulated Q-switched pulse profile obtained in the 1.14 at.% Nd:$GdVO_4$ laser with the parameters of T_0 = 80% and R = 70%.

In order to understand the influence of the finite lifetime of the lower energy level on satellite Q-switched pulse, the ions population density change in each laser energy level is explicitly enlarged associated with the Cr^{4+} ions change during the Q-switched pulse interval. The time-extended numerical diagram is given in Fig. 5.4. Numerical comparison is made at a given cavity reflectivity of 70% with excited ions density of 8.4 $\times 10^{22}$ $cm^{-3}s^{-1}$. Fig. 5.4a and Fig. 5.4b respectively show for the case that is with and without the secondary pulse corresponding to the use of either a strong (T_0 = 60%) or a weak (T_0 = 80%) saturable absorber. At the initial pulse build up period in which the weak absorber is used (Fig. 5.4a), population in the lower laser energy level N_1 is low, and laser inversion N_g is equivalent to ion density in the upper energy level N_2. As a result of the saturation of Cr^{4+}:YAG passive Q-switch, N_2 decays simultaneously with the reduction of Cr^{4+} ions N_s in the ground state of the saturable absorber. The slow transition of the lower laser energy level to the ground state results in the accumulation of ions in the lower energy level, which consequently reduces the laser population inversion. Following the relaxation of N_1, laser gain N_g is no longer the same as N_2 but it decreases further to the value below the total cavity loss. At the condition when N_g is lesser than the system loss, laser gain starts to increase slightly while N_2 continues to reduce below the loss. Even so, there is no secondary pulse observed because the laser gain rests at the value below loss.

Instead in the condition of employing a strong saturable absorber as in Fig. 5.4b, higher value of N_2 and N_g are achieved in the laser. The accumulated N_1 in lower energy level from ions decay of the higher energy level becomes larger at the minimum of loss. As a consequence of the increase of N_1 population, extraction of N_2 for laser energy is

retarded. The ion population in the higher level is consequently restrained from the entire release at the opening of the Q-switch. This implies that the laser has a poor extraction of the stored energy because of the slow ion transition from the lower energy level to the laser ground state. At the onset of N_1 relaxation, N_g drops below the loss and further triggers the upper energy level to dump out the residual ion density and build up the gain. This is noticed from the drastic increase of N_g until it overcomes the loss once again. At that moment when the gain equals the loss, cavity photon density achieves its second peak and forms a satellite pulse subsequent to the main Q-switched pulse. From the relation between the change of population density and loss, it is realized that the slow passive Q-switch has no effect in causing the secondary pulse, yet the slow ion transition of the lower laser energy level is the main cause for the generation of multiple Q-switched pulses in the laser. The higher the laser stored energy, the stronger the satellite pulse incurred.

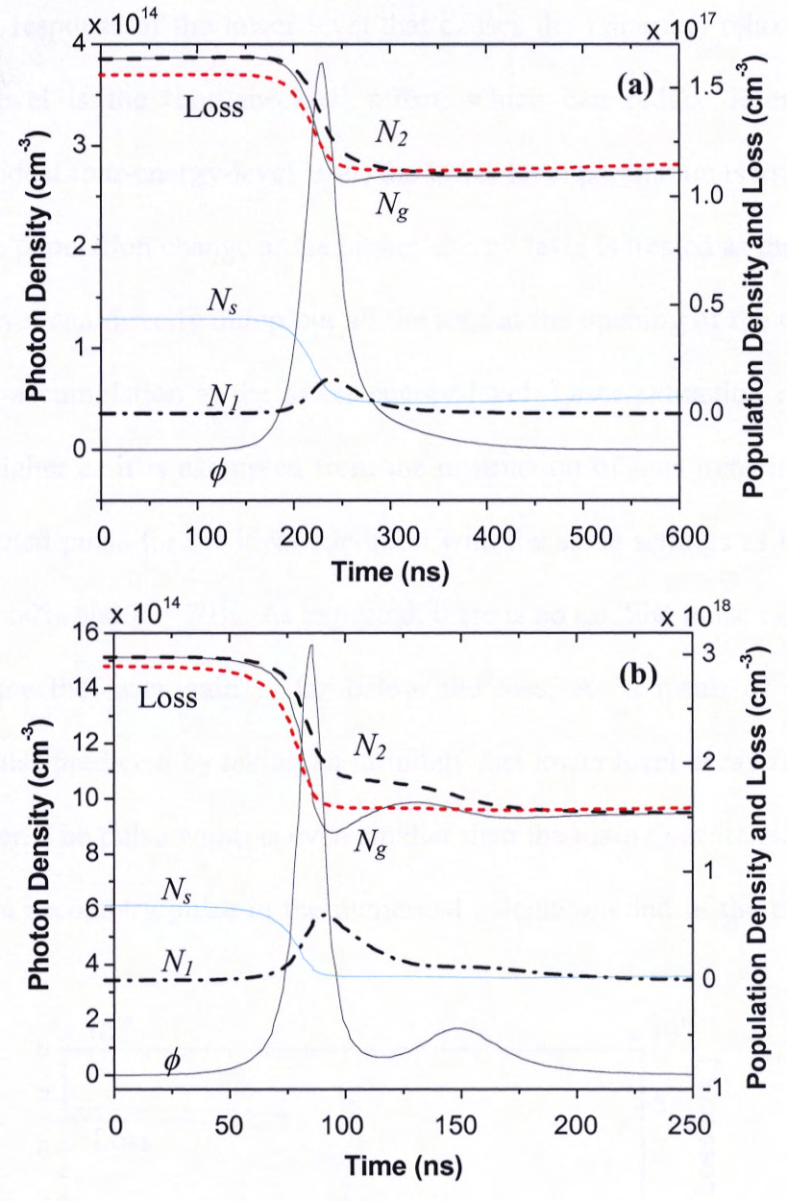

Fig. 5.4: Numerical time expanded plot for the Q-switched pulse evolution ϕ, population density change in the laser (N_1, N_2, and induced inversion, N_g) and in the saturable absorber (N_s). Q-switched laser loss is depicted with short dash line. Parameters in calculation: Nd:$GdVO_4$ crystal with doping concentration of 1.14 at.%, output coupler reflectivity R = 70%, and Cr^{4+}:YAG initial transmission of (a) T_0 = 80%, and (b) T_0 = 60%.

The slow response of the lower level that causes the imperfect relaxation of the higher energy level is the 'bottlenecked' effect, which can reduce laser extraction efficiency. In an ideal four-energy-level laser, the lower level population is low enough to be negligible; the population change at the higher energy level is treated as the laser gain. Higher energy level can directly dump out all the ions at the opening of the Q-switching without the ions accumulation at the lower energy level. Laser extraction efficiency is expected to be higher as it is exempted from the obstruction of ions transition. Fig. 5.5 shows the calculated pulse for the ideal condition with the same settings as in Fig. 5.4b, that is when $T_0 = 60\%$ and $R = 70\%$. As expected, there is no satellite pulse existing at the decay tail because the laser gain is far below the loss. As a result of better laser extraction, the pulse predicted by taking an infinitely fast lower level decay time is much higher and sharper. The pulse width is even smaller than the main Q-switched pulse with the existence of a secondary pulse in the numerical calculation and in the experimental result.

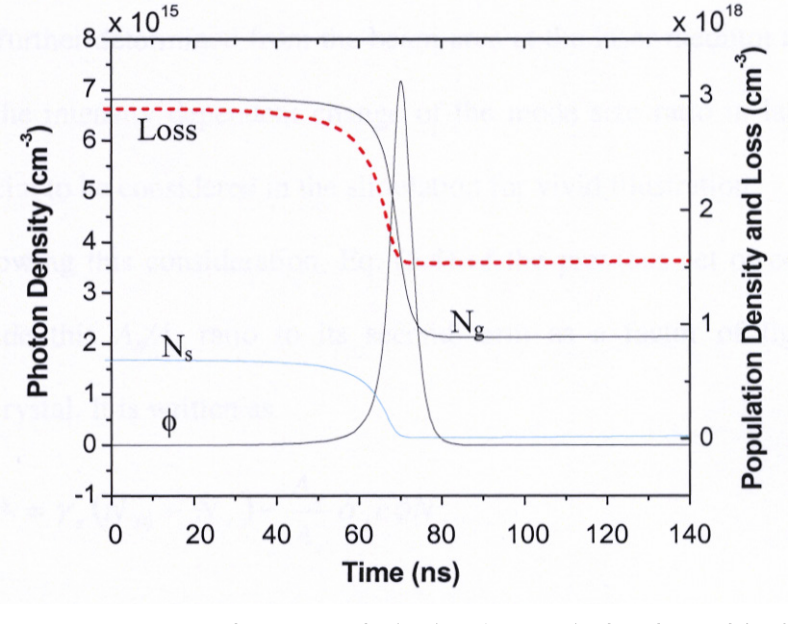

Fig. 5.5: Time expanded plot of the Q-switched pulse evolution in an ideal laser system.

The Q-switched secondary pulse profile clearly shows that Nd:$GdVO_4$ laser has a slow ions emptying lower energy level that could separate the fully extraction of upper level stored energy into two stages. This result also indicates that ideal laser assumption is not suitable for modelling the pulse properties in a real case.

5.2 Pulse properties

Viewing back the calculated pulse profile as described previously, though the secondary pulse trend is successfully explained, there is a discrepancy on the exact pulse duration. In the real laser system that has been discussed, thermal lens effect is essential to change the cavity mode size, which varies with the pump strength. This will result in different effective laser cross sections and different energy fluences on the saturable absorber. As found from Eq. (2.16), the principle of the passively Q-switched outputs is basically dependent on the optical material properties, and the light interactions between gain medium and saturable absorber. Interaction between the light with gain and saturable absorber is further determined from the beam area at the laser medium and the absorber. Therefore, the intensity dependent change of the mode size ratio in laser and absorber A_g/A_s is crucial to be considered in the simulation for vivid illustration.

Following this consideration, Eq. (5.4) of the previous set of coupled equations hence include this A_g/A_s ratio to its second term as a factor of light saturation in Cr^{4+}:YAG crystal. It is written as

$$\frac{dN_s}{dt} = \gamma_s (N_{s0} - N_s) - \frac{A_g}{A_s}\sigma_s c \phi N_s . \tag{5.8}$$

The cavity mode size ratio is estimated using the experimental thermal lens and the *ABCD* law. The increase of thermal lens effect with respect to the pump power leads to an increase in the ratio. The value is then slightly adjusted within the calculation for accurate simulation of pulse properties. The change of A_g/A_s in relation with the pump power used in the simulation is shown in Fig. 5.6

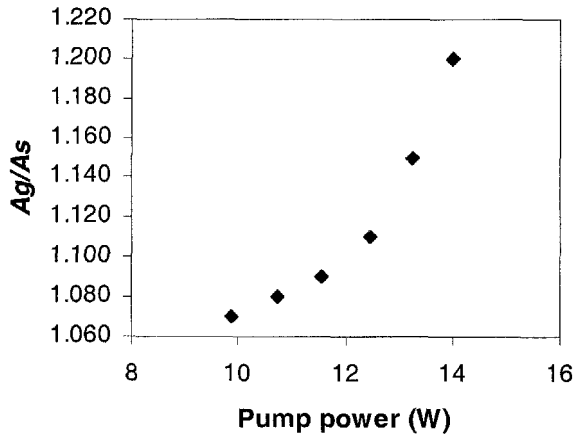

Fig. 5.6: Mode size ratio of the gain medium and the saturable absorber used in the simulation.

In addition, the effective laser pump rate also affects the stored energy. Instead of using the directly calculated *Rp* value as given in Eq. (5.6), an effective pump rate was experimentally estimated and fitted according to the experimental results. Since Rp term represents the total excited ions from the ground state, and the ground state population N_0 is related to the total active ions N_{total} change ($N_{Total} = N_0 + N_1 + N_2$), Eq (5.2) can be described as

$$\frac{dN_2}{dt} = P(N_{Total} - N_2 - N_1) - \gamma_f N_2 - \sigma_g c\phi(N_2 - N_1). \tag{5.9}$$

At the steady state condition where $dN_2/dt \approx 0$ *and* $\phi \approx 0$, the laser pump rate has a relation of

$$P(N_{Total} - N_1) = N_2(\gamma_f + P),$$

$$\frac{N_2}{(N_{Total} - N_1)} = \frac{P}{\gamma_f + P} = \frac{P\tau_f}{1 + P\tau_f}. \tag{5.10}$$

$N_{total} >> N_1$, *and* $P\tau_f << 1$ Eq. (5.10) is simplified to

$$\frac{N_2}{N_{Total}} \approx P\tau_f. \tag{5.11}$$

As is already known, laser signal gain coefficient is the product of stimulated emission and population inversion. By multiplying both sides of Eq. (5.11) with σ_g, a small signal gain coefficient is then obtained for the inhibited laser condition, which is excited above threshold.

$$g_0 = \sigma_g P\tau_f N_{Total}, \tag{5.12}$$

and the relationship between the single pass gain and the pump input power is [60]

$$g_0 l_g = KP_{in}, \tag{5.13}$$

where P_{in} is the input pump power and l_g is the laser crystal length. $K = \eta_{Total}/A_p I_s$ is the pump to laser radiation conversion factor, in which A_p is the pump beam area and I_s is the saturation flux. The total conversion efficiency η_{Total} consists of the pump absorption ($\eta_\alpha = (1\text{-}exp(-\alpha_g l_g))$, upper state efficiency ($\eta_u = \eta_{Quantum} + \eta_{Stroke}$), mode match between pump beam size ω_p and cavity mode size ω_p ($\eta_B = 2\omega_g^2/(\omega_g^2 + \omega_p^2)$), and laser extraction efficiency (η_E). The combination of Eq. (5.12) and Eq. (5.13) yields

$$P = \frac{KP_{in}}{\sigma_g \tau_f N_{Total}} \tag{5.14}$$

This gives a more realistic pump rate parameter to the real laser system because K is a measurable parameter for the laser at lasing threshold through Findlay-Clay analysis [60]. For the experimental parameters of laser doping concentration of 1.14 at.%, T_0 = 60% and R = 60%, the measured K parameter is about 0.12 at the Q-switched lasing threshold. The value is adjusted slightly for a proper pump rate fitting to the laser output.

A_g/A_s value was found to have a strong influence on the pulse width, while the pump rate is dominant to determine the pulse repetition rate. In the simulation, pulse energy is obtained from the area under pulse. The fitting result of the Q-switched pulse outputs is shown in Fig. 5.7. The simulation successfully shows a good agreement with the experimental results.

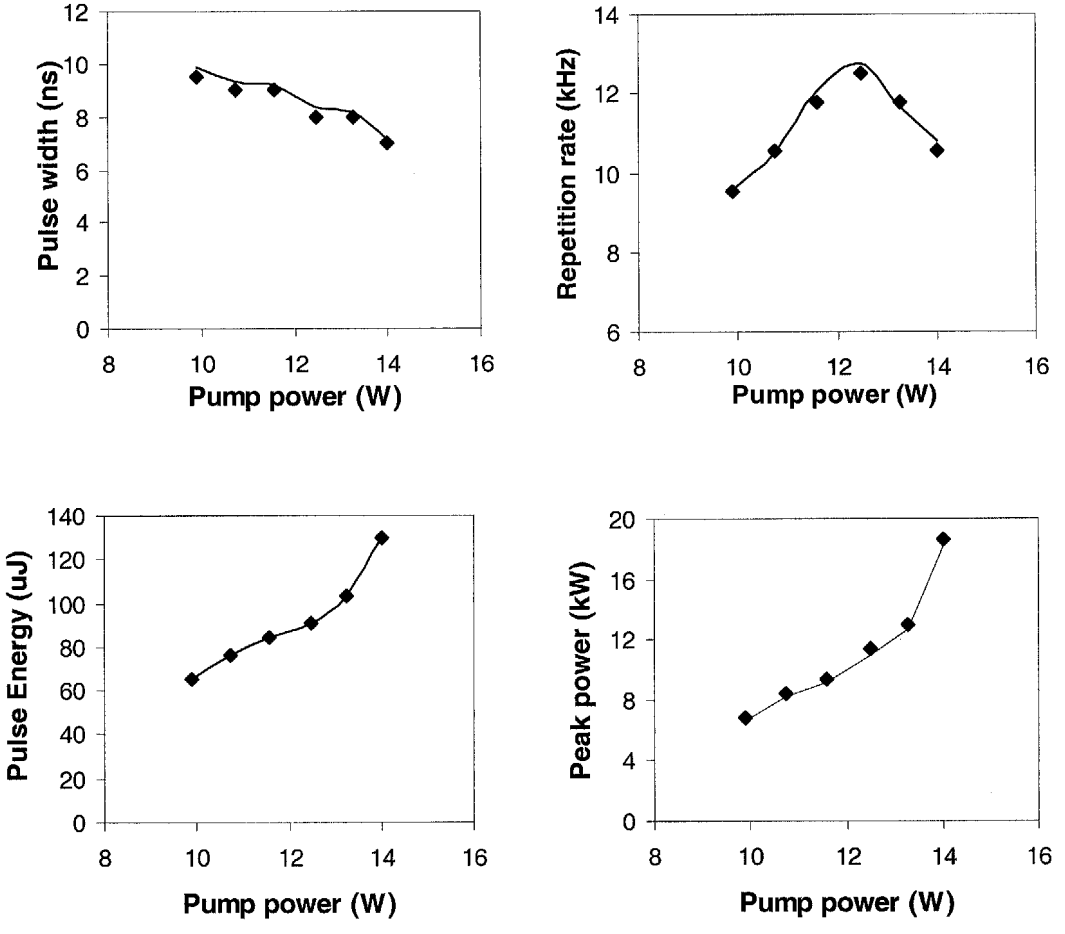

Fig. 5.7: Experimental (diamond) and simulated (line) Q-switched pulse properties. Laser doping concentration: 1.14 at.%, Cr^{4+}:YAG initial transmission T_0 = 60% and coupling reflectivity R = 60%.

The K value used for this excellent fitting is essential to reveal the condition that occurred in the real system. K is related to the cavity single pass gain G_0 through

$$G_0 = \exp(KPin) = \exp(g_0 l_g), \tag{5.14}$$

In this relation, g_0 is the small signal gain, and K is proportional to the effective gain. It is supposed that at higher pump strength, the increase of photon density in the cavity will

cause a smaller signal gain g_0, and so to the K. However, according to Fig. 5.8, the excessive decline of K value from 0.1116 W^{-1} to 0.093 W^{-1} corresponding to the pump power of 12.48 W and above implies that there is not only the gain saturation, but also a drastic increase of cavity losses that affect the laser gain. Similar to the experimentally observed dip tendency of the Q-switched output power and the pulse repetition rate as discussed in Chap. 4, the simulation result further confirms that cavity loss would be dominated at high pumping regime. This additional loss might be mainly attributed to the thermal induced beam diffraction with stronger thermal lens formed in the crystal at high pump power.

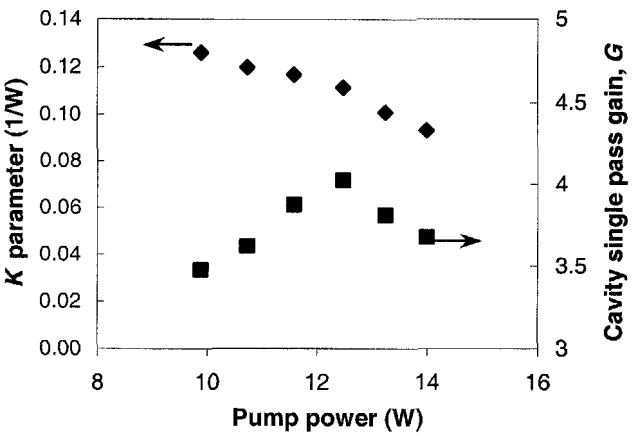

Fig. 5.8: The pump power dependent K parameter and the effective gain G in the simulation.

When a laser pulse is further zoomed into its evolution interval at pump power of 14 W, the simulated pulse as shown in Fig. 5.9 has a similar pulse profile as the experimental Q-switched pulse. The secondary Q-switched pulse is reproduced well in the simulation.

This indicates that the estimated time relaxation of the lower energy τ_{l0} in the simulation is close to that in the real laser system.

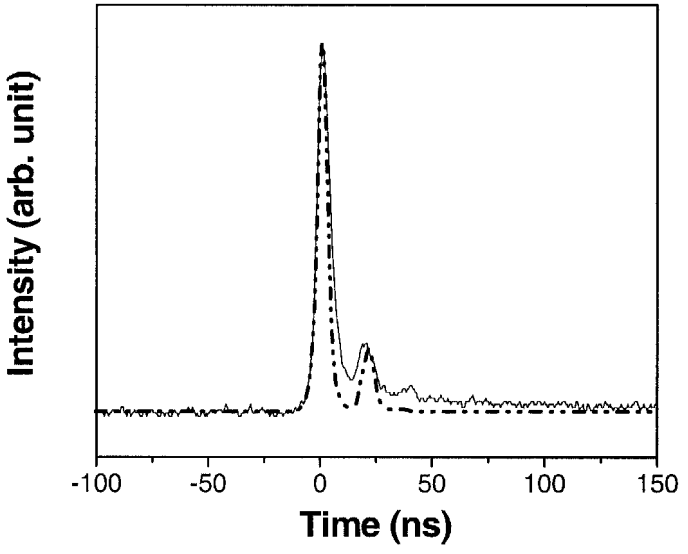

Fig. 5.9: Single Q-switched pulse profile. Solid line: Experimental data; Dash-dot line: simulated result.

5.3 Summary

The Q-switched secondary pulse has been numerically studied according to the experimental observation in the passively Q-switched Nd:$GdVO_4$ lasers by Cr^{4+}:YAG crystal. Based on a coupled rate equations model that takes into account the effect of the finite lower level lifetime, the observed Q-switched satellite pulse was well demonstrated.

The numerical results explicitly show that the finite relaxation lifetime of the lower laser level is a determinant of the observed pulse pattern. As a result of the slow ions emptying in the lower laser energy level to the ground state, the accumulated population becomes an obstruction to the laser extraction from the upper energy level.

The laser requires two stages to fully release the upper laser state stored energy and hence forms a satellite pulse subsequent to the main Q-switched pulse. With further consideration of the effect of thermally induced mode size change and the effective pump rate change on the Q-switched pulse properties, such as Q-switched pulse width, repetition rate, energy and peak power have been numerically studied, which are well in agreement with the experimental observations. As a result of a more consistent calculated pulse profile compared to the experimental pulse, the result suggests that the lower energy level would have a relaxation time of about 20 ns in the Nd:$GdVO_4$ laser.

CHAPTER 6

Dynamics of passively Q-switched Nd^{3+} doped lasers

The essence of all passive Q-switching techniques is, through inserting a saturable absorber in the laser cavity, to use the mutual interaction of the light with the gain medium and the saturable absorber to achieve a stable pulsed laser emission. As noted, such a laser system is in principle a nonlinear dynamic system.

In this chapter, the investigation of the continuously pumped Q-switched laser dynamics is expanded from the nanoseconds pulse profile to the Q-switched pulse train, which is in the repetitive period of microseconds. In order to confirm the dynamical behaviors of the repetitively passive Q-switching, besides the Nd:$GdVO_4$ and Nd:$GdYVO_4$ lasers, different types of passively Q-switched Nd-doped lasers such as Nd:YAG and Nd:YVO_4 have also been demonstrated in the study. As far as is known, the intrinsic nonlinear dynamics nature of the passively Q-switched solid-state lasers, which had not so far been clearly addressed, was firstly observed in the experiments. By considering the ion transition within each energy level, the chaotic behavior of the laser has been qualitatively reproduced with an extended rate equation model.

6.1 Population dynamics associated with Q-switched pulse generation

The energy levels involved in a passively Q-switched Nd-ion doped laser with a Cr^{4+}:YAG saturable absorber can be schematically shown in Fig. 6.1. The Cr^{4+}:YAG crystal is illustrated as a four-energy level system, as has been stated in Chapter 2.

Although the effective passively Q-switched operation only involves the ground state absorption of the Cr^{4+}:YAG, the two upper energy levels are indicated to show that excited state absorption of Cr^{4+}:YAG is a cause of nonsaturable loss in the passive Q-switching.

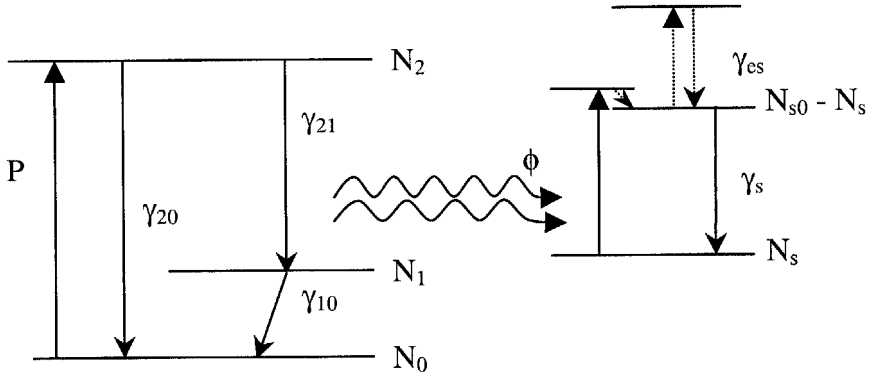

Figure 6.1: Simple energy-level scheme for passively Q-switched laser. N_0, N_1 and N_2: energy levels in Nd^{3+} doped laser. N_s and N_{s0}-N_s: energy levels in Cr^{4+}:YAG saturable absorber. ϕ is laser stimulated emission, and γ indicates the relevant ion relaxations.

When pump light interacts with gain medium, the active Nd^{3+} ions absorb energy and make a transition to a higher energy state. While the excited ions relax down by emitting photons, the light beam intensively increases, and bleaches the saturable absorber. The difference between the number of ions in the higher and lower energy level determines the cavity gain and output laser intensity. The light interaction between gain and saturable absorber for the Q-switched pulse evolution is a nonlinear process. When the saturable absorber is saturated, the following pulse build up process occurs to evolve a Q-switched pulse. Population inversion drops to a value below threshold after the pulse emission, and builds up to its initial value again within the cavity high Q period through the repumping process. The repetitive relation of the gain, loss and photon number in the

Q-switching cycle is shown in Fig. 6.2. The gain build up duration is equivalent to the Q-switched pulse repetition time. Compared to the repumping period that usually in several tens to hundreds microseconds, the Q-switched pulse width in nanosecond range is very short. Therefore, the pumping term is always ignored in the Q-switched analytical model.

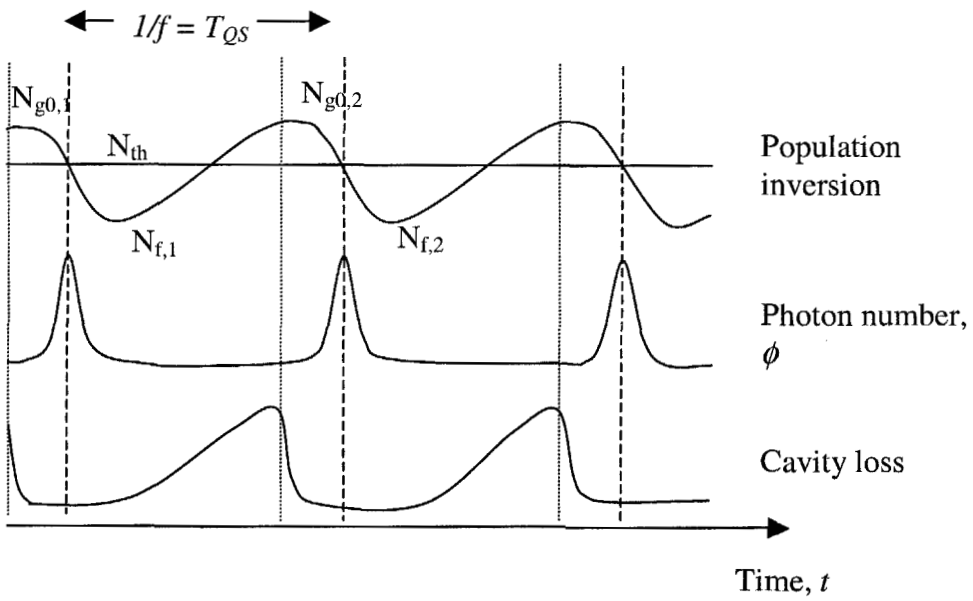

Fig. 6.2: Relation of population inversion, loss and photon number in the repetitively Q-switching.

Under the continuous pump, N_{g0} and N_f is the population inversion just before and after the Q-switched pulse. The achievable value of $N_{g0,2}$ is closely related to the previous $N_{f,1}$ and the pumping rate. If the pump power is high, the residual $N_{f,1}$ can be easily driven to the next $N_{g0,2}$. Eq. (6.1) shows the relation of the new initial inversion $N_{g0,n+1}$ to the repumping rate, residual $N_{f,n}$ value and the fluorescent relaxation time.

$$N_{g0,n+1} = R_p\tau_f + N_{f,n}\exp(-\frac{T_{QS}}{\tau_f}) - R_p\tau_f\exp(-\frac{T_{QS}}{\tau_f}). \qquad (6.1)$$

The pump power and laser fluorescent lifetime can directly determine the change of population inversion.

At the time when N_f is obtained, photon density is far below its peak value, and the stimulated emission can hence be neglected. By referring to Fig. 6.1, the change of population inversion in the absence of stimulated emission can be written as

$$\frac{dN_2}{dt} = PN_0 - \frac{N_2}{\tau_{20}} - \frac{N_2}{\tau_{21}}$$

$$\frac{dN_1}{dt} = \frac{N_2}{\tau_{21}} - \frac{N_1}{\tau_{10}}$$

$$\frac{d(N_2 - N_1)}{dt} = PN_0 - \frac{2N_2}{\tau_{21}} - \frac{N_2}{\tau_{20}} + \frac{N_1}{\tau_{10}}. \qquad (6.2)$$

Physically, the pump light, laser spontaneous emission, and the fast emptying function of the lower laser energy level primarily affect the time variation of gain between two Q-switched pulses. Under continuous pumping, the mechanism of ion excitation and relaxation can be illustrated as an ion movement within the energy levels. This ions movement is equivalent to the ion circulation within the ground state and the higher energy levels in a steady state operating condition. For an ideal system, ion circulation can continuously provide the same gain to each pulse emission. This condition can only be satisfied in a perfect laser with fast-emptying lower level, and a constant excited number of ions. Nevertheless, in the real system, delays due to the finite lower energy level lifetime and pump saturation of the ground state can severely affect ion circulation within the energy levels. This is detrimental to influencing the dynamics of passively Q-switched laser, which has a periodic modulation of intensity dependence of saturable loss. For the Nd^{3+} lasers with nanoseconds relaxation delay in lower energy level, the slow-

emptying process may not become the main effect. However, at a high power laser operation, where the ion population in the ground level might be saturated under the continuous pumping process, the delay of the ions in lower energy level to the ground state could strongly affect the ion circulation. The effect of insufficient ions being excited up from ground state is to reduce the number of ions at the upper energy level and decrease the initial gain value N_{g0} and output energy of the Q-switched pulses. The high pulse energy will be obtained again once the ground state condition is restored.

In the continuous nonlinear optical saturation process, the dynamic phenomenon is impossible to be predicted analytically. As far as the N_{g0} at the opening of passive Q-switch is disturbed, Q-switched pulse train will exhibit change in pulse amplitude. The stronger the pump power, the more sensitive Q-switched laser with higher repetitive pulses is to show dynamic behavior due to the perturbation of ion circulation within the laser energy levels. Chaotic dynamics are strongly dependent on the change of experimental control parameters. Underlying the apparent randomness, the pulse Q-switched amplitude shows the general features of deterministic chaos. This phenomenon is an intrinsic nature of the system, regardless of the external noise or uncontrolled outside effects such as mechanical vibration.

6.2 Brief overview of deterministic chaos

The property of a nonlinear dynamical system, which is sensitive dependent on initial conditions, is identified as deterministic chaos. The history of chaos is rooted in the mathematical study of nonlinear dynamics, about a century ago by Poincaré on the mutual gravitational attraction [110]. Poincaré found that there could be orbits, which are

nonperiodic, and yet not forever increasing nor approaching a fixed point. Chaos studies attracted great attention when the linear theory first became evident that could not explain the observed behavior of certain experiments like the turbulence in fluid motion and nonperiodic oscillation in radio circuits. The main catalyst for the development of chaos theory was the electronic computer. The pioneer of chaos theory was Edward Lorentz whose interest in chaos came about accidentally through his simple mathematical model for atmospheric convection in early 60's. Lorentz discovered the extreme sensitivity on initial conditions in his weather simulation, showing that chaos might be important in a real physical system [111]. In 1975, Haken recognized the isomorphy between the laser equations and the Lorenz model, and concluded that lasers should exhibit chaotic emission [112]. Interest in laser instabilities arose in the 80's. The widespread notion of the laser as an intrinsic dynamic system started from the two clear experimental observations: one is on a simple loss-modulated CO_2 laser [113] and the other is on a multimode infrared He-Ne laser [114]. It was then followed by intensive experimental and theoretical investigations on laser dynamics to achieve better understanding and control over lasers. However, the laser dynamics in passively Q-switched solid-state laser was so far unaddressed.

In all branches of dynamic systems, including the atmosphere, solar system, turbulent fluids, economics, biological population and the biomedical, deterministic chaos shows quantitative and qualitative universal features underlying the complexities. Period-doubling cascade as firstly analyzed by Feigenbaum [115] is one of the commonest routes to chaos. The observation of period-doubling cascade is now a fingerprint of deterministic chaos in a system. Generally the transition to chaos is

evidenced with the peak heights in time series data. In the experiment, chaos can be easily distinguished from noisy behavior by looking at that divergence of nearby trajectories. The key feature of nonlinear behavior can be recognized through the sudden changes of the reproducible periodic to chaotic behavior at slow change of the control parameter. Within the chaotic regime odd number of periodic windows might smear out, in which period-3 window is usually the largest.

6.3 Deterministic chaos in passively Q-switched operations

Actually in all the passively Q-switched lasers, both the Nd:$GdVO_4$, Nd:$GdYVO_4$ that discussed previously, Q-switched pulses with a stable pulse amplitude could only be observed at certain laser parameters. Generally, relatively regular and reproducible Q-switched pulses are obtained at weak pump power, as the pump power increases, fluctuations on pulse amplitude and repetition rate easily become random. The chaotic Q-switched pulses could be observed under certain pump power following the period-doubling transition in the laser.

For instance, in the 1.14 at.% Nd:$GdVO_4$ laser passively Q-switched with the Cr^{4+}:YAG of 80% initial transmission, under the condition of output coupling transmission T = 30%, and cavity length of 60 mm, the bifurcation diagram of the Q-switched laser versus the pump power change was measured by controlling the laser diode pumping current. The Q-switched operation of the laser has a pump threshold of about 5.5 W. After the Q-switching threshold, a stable period-1 Q-switched pulse train was immediately obtained. The Q-switched pulse repetition rate and pulse energy increased following the increase of the pump power. At a pump power of 7.7 W the laser

suddenly became chaotic, characterized by the strong pulse amplitude and repetition rate jitters. Further increased the pump power to about 8.75W, a period-4 state then suddenly appeared. By slightly increasing the pump power, the Q-switched pulse train became chaotic again, and subsequently at the pump power of about 9.80W, a period-2 state appeared. The period-2 state evolved into a period-1 state at the pump power of about 9.89 W. The period-1 state remained a short while with the pump power increase. It then quickly returned to a chaotic state. The chaotic state remained all the way to the maximum pump power limit of the pump laser. This result implies that the passively Q-switched system exhibited the chaotic dynamics. However, because the bifurcation to chaos only occurs in a very narrow pumping parameter range, limited by the power changing resolution of the laser pump source, these period-doubling bifurcations to chaos could not be resolved. Therefore, some of the periodic states observed were randomly selected by the pump power value, where the mixture of different regime of the periodic and the chaotic pulses along the increase of pump power is generally observed.

As slightly tuning the cavity alignment is physically equivalent to fine changing of the pump power with the slightly increase of the cavity loss, this approach was employed to understand the complicated bifurcation diagram with the pump power. The laser emission was firstly zoomed into the periodic states. Clear period-doubling bifurcations could be obtained when the pump power was fixed at 9.89 W and the cavity alignment was finely tuned at the position. From a stable Q-switched state (Fig. 6.3a), the careful laser cavity detuning yielded a Q-switched pulse train with period-doubled energy pattern (Fig. 6.3b). The period of the pattern was further doubled (Fig. 6.3c) with continuous change of the cavity alignment, and eventually to an aperiodic state (Fig.

6.3d). Note that in order to measure a long train of the pulse pattern and display them on the oscilloscope, a low speed detection system was selected. Therefore, the pulse shapes shown in the figure are actually limited by the responses of the detection system, which are not exactly those of the real Q-switched pulses. Nevertheless, the relative pulse heights shown do directly relate to the actual relative Q-switched pulse energy variations.

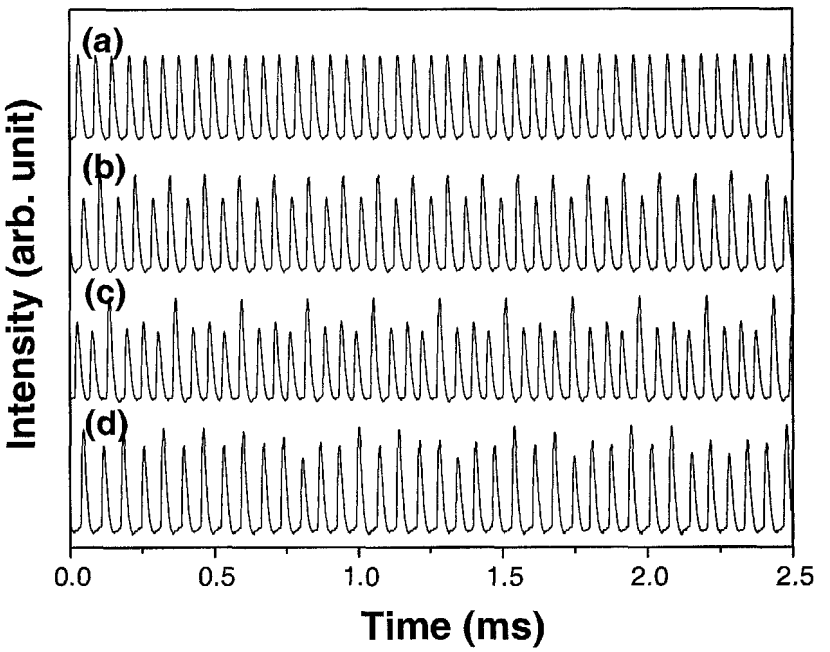

Fig. 6.3: Period-doubling route to chaos in the laser output. From (a) to (d) the cavity alignment was slightly tuned.

This experimental result suggests that the laser might have a period-doubling route to chaos at the position of each of these periodic states. Such observation was found as well in passively Q-switched mixed Nd:$GdYVO_4$ laser. It is worth mentioning that because of the narrow parameter range of the transition to chaos, the unavoidable experimental parameter drift might sometimes result in random switches between different states. Figure 6.4 shows as an example of such case. The laser pulses switched

from a period-2 state to a period-4 state, and then to a period-1 state. As no laser parameters were changed, it is believed that the drift might be generated purely due to the experimental noise and the sensitive dependence of the laser dynamics on the pump parameter. This property of the laser may well explain the general complicated pulsations observed on the passively Q-switched solid-state lasers.

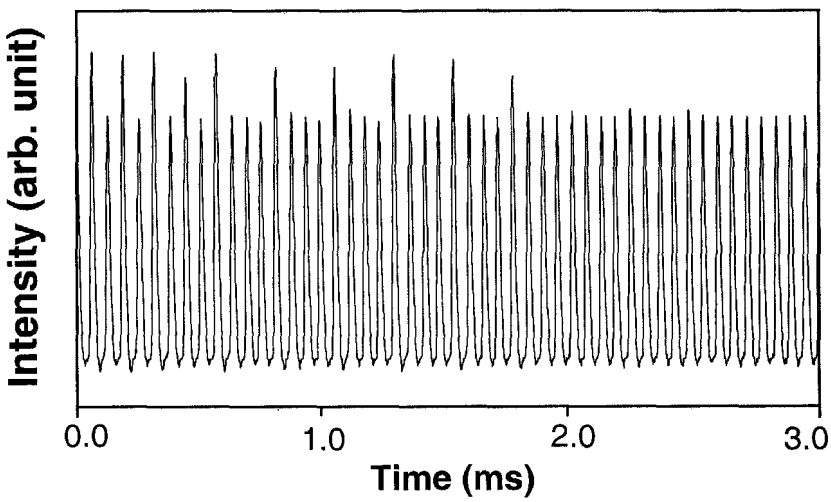

Fig. 6.4: Random switches of various periodic states due to the sensitive dependence of the laser output on the experimental parameters.

A similar bifurcation diagram with respect to the pump power could also be obtained by using different saturation strength of Cr^{4+}:YAG crystals. The main feature of the Q-switched laser under different kind of saturation losses could only show the difference of Q-switched output properties, such as energy, pulse width as discussed in Chapter 4. It is noted that though the concrete Q-switched pulse amplitude and repetition rate jitters could be different depending on the laser operation conditions, the general features of the lasers always remain. This result further confirms that the laser dynamics has basically no direct relation to the saturation strength.

For the 0.5 at.% lightly doped Nd:$GdVO_4$ crystal, the Q-switched pulse was found having comparatively higher fluctuations, and lower signal to noise ratio. 1% to 2% of the jittering in the period-1 pulse state was difficult to realized in the lightly doped Nd:$GdVO_4$ laser. Although the Q-switched performance of the 0.5 at.% Nd:$GdYVO_4$ laser is comparatively better, it was also prone to show the pulse jitters under certain pump power. This indicates that the lightly doped crystal may have stronger effect for dynamics. It is most probably the bleachable characteristics of the low doping concentration crystal under the high power pumping. This phenomenon was surmised that when the laser ground state is saturated, pump power would transmit through the gain medium without being absorbed. In order to prove this experimentally, the leakage of pump light from the cavity was observed during the passively Q-switched operation. A 0.5 at% Nd:$GdVO_4$ crystal combined with a T_0 = 80% Cr^{4+}:YAG passive Q-switch in a cavity with coupling transition of 40% was selected.

As shown in Fig. 6.5, the transmitted pump power and Q-switched output power were separated with a dichroic mirror (HR at 1064nm, and HT at 808 nm), and observed simultaneously with an oscilloscope. Optical spectrum analyzer was used firstly to ensure the detecting wavelength of both signals after the splitter. Two photoreceivers were placed at the same optical length for the detection of the output laser beams.

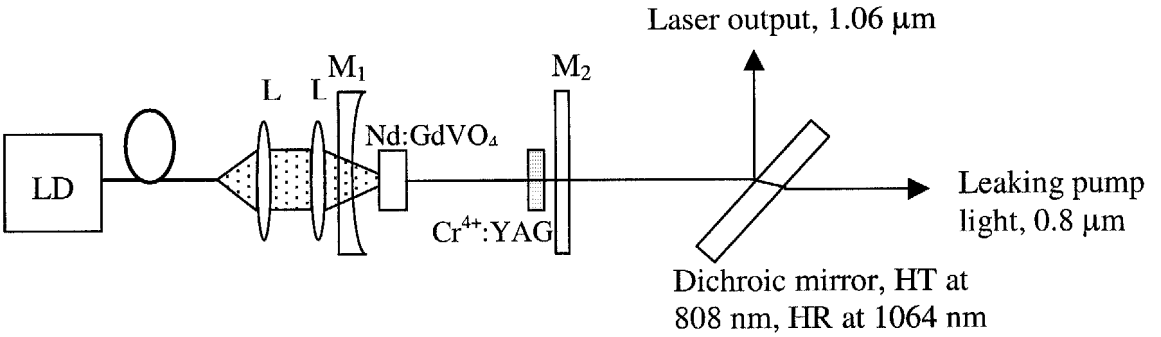

Fig. 6.5: Experimental setup for the observation on leaked pump light from the passively Q-switched laser cavity. LD: Laser diode. L: coupling lens. M_1: Concave mirror, M_2: output coupler.

The results revealed surprisingly the existence of the dynamic feature in the leaked pump light. This evidence shows that the ion population change in the laser ground state indeed occurring in the passively Q-switched laser. Fig. 6.6 shows the leaked pump light at the power of 7.25 W and 13.25 W. The higher peak of the leaked pump light indicated the lower ions number in the ground level. Obviously the ground state population varied unevenly during the passive Q-switching. At stronger pumping level, the variation of the leaked pump has higher repetition rate, showing that the pump saturation of the ground level was significant.

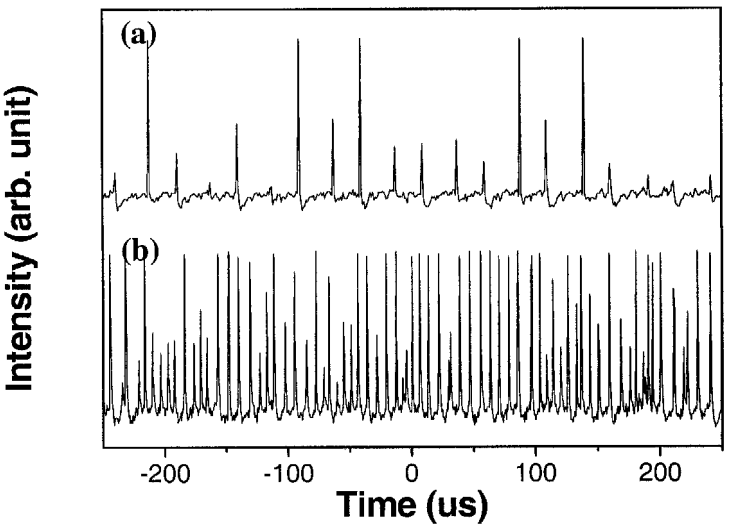

Fig. 6.6: Dynamic changes of the leaking pump light showing the equivalent changes of ion population in the laser ground state. Oscilloscope trace recorded at pump power of (a) 7.25 W, (b) 13.25 W.

When the Q-switched pulse and the leaked pump light were enlarged on screen as in Fig. 6.7, it could be seen that there was a small time difference between the peaks of both signals, where the Q-switched pulse peak was several ns preceding the maximum of the leaked pump light. Logically for the Q-switched operation when cavity photon is at its peak, the population inversion is at the minimum, and thus the ground state should fill with the relaxed ions. However, as shown in Fig. 6.7, the leaked pump light at that moment was reaching its maximum. This means that at this stage the laser ground state is depleted. The reduction of the ground state population at the peak of the Q-switched pulse implies that there is a delay between the ions which jump to the lower energy level that relax to the ground state. Following the continuous pumping, ions in the ground level

will be depleted. This strong ground state depletion and the delay of ions relaxation are believed could be the reasons that result in the dynamical laser output.

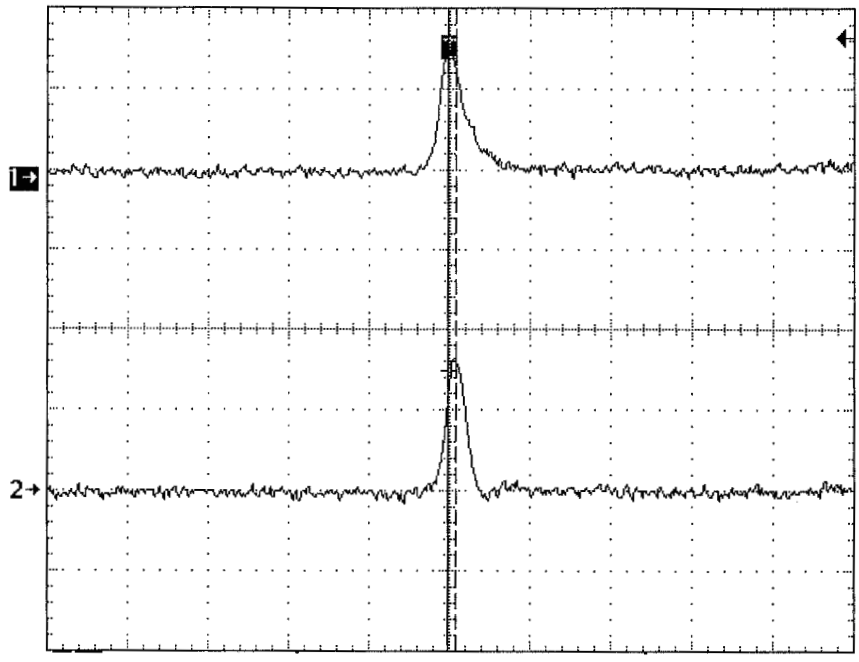

Fig. 6.7: Oscilloscope trace of the enlarged single Q-switched pulse (upper) and its simultaneous leaked pump light signal (lower).

At the opening of passive Q-switch, interaction of cavity photons with saturable absorber reduces the cavity loss nonlinearly, and Q-switched pulse builds up from the background noise, which is the random phase oscillating spontaneous emission in the cavity. More dynamic laser behaviors would be expected in accordance with a longer nonlinear saturation process for pulse evolution. Since the saturation process is dependent on the light intensity, the beam spot area on the saturable absorber is crucial in practice. It has been shown in Eq. (2.6) in Chap. 2 that a small beam spot size on saturable absorber is necessary to achieve intense Q-switched pulses. This criterion is also important to

enhance the Q-switched pulse stability and reduce the chaotic dynamics in a laser. For a plano-concave laser, which the saturable absorber is placed closely to the output coupler, changing the cavity length is equivalent to varying the ratio of the laser beam size on the gain medium and on the saturable absorber if the thermal lens effect in the laser crystal could be ignored. In that condition, longer cavity length is possibly good to achieve smaller beam size on the saturable absorber, which can hence quickly saturate the absorber. Similarly, with thermal lens formed in the laser crystal at a given pump power, operating the laser at the lens focusing point, or at the boundary of cavity stability (longer cavity) should also have a smaller beam size compared to a shorter cavity length. Therefore, the strength of the nonlinear interaction between the gain and the absorber becomes different in relation with the quick or slow saturation in the saturable absorber.

Experimentally, the 1.14 at.% of Nd:$GdVO_4$, and both absorption loss T_0 and cavity transmission T = 40% were selected to investigate its passively Q-switched operation under different cavity lengths at the pump power of 9.85 W. With the cavity length of 85 mm, the laser could emit Q-switched pulses overall with weaker amplitude fluctuations than the laser in cavity length of 60 mm. There was no complete route to chaos observed despite the fact that some of the period-doubling bifurcations could still be observed. Fig. 6.8 shows the output pulses from the system, some parts of the pulse energy patterns still exhibited period-2 feature, which suggests that the laser could still be a chaotic system. Generally, the Q-switched emission of the laser was found to be more "chaotic" at a short cavity length of 40 mm compared to that at 60 mm. Very clear period-doubling bifurcations could be easily observed. This experimental result indicates that the chaotic nature of the system is less significant if the saturable absorber could be

quickly saturated. The passive Q-switching of the solid-state lasers should preferably work under such a condition. Nonetheless, since the thermal lens varies with the pump power, it is impossible to change the laser cavity length for each pump level during the Q-switched operation. Therefore in practice, the proper cavity length is selected for the overall optimized laser performance within the studied pump range. This proper selection of laser parameters was carried out in the previous passively Q-switched demonstrations.

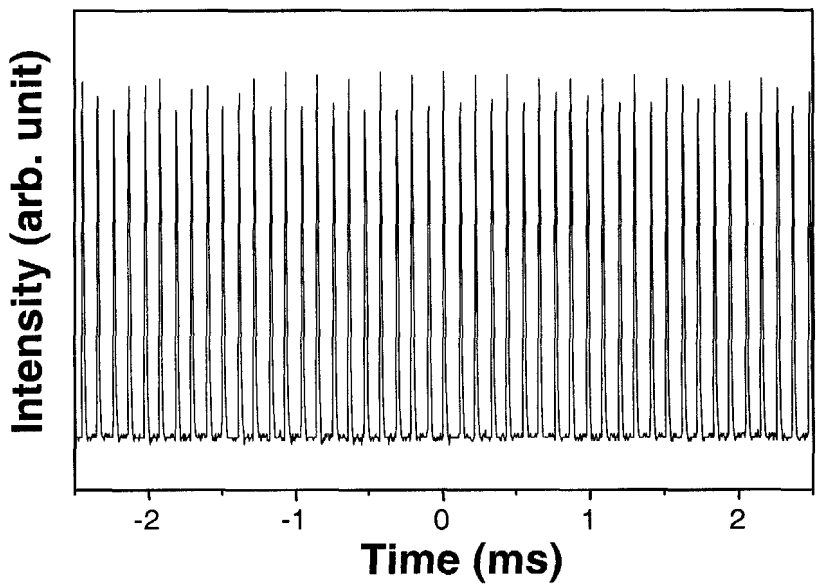

Fig. 6.8: A typical Q-switched pulse train of the Nd:$GdVO_4$ laser under the cavity length of 85 mm.

In order to confirm the dynamic behavior in the passively Q-switched operation as observed in the Nd:$GdVO_4$ and Nd:$GdYVO_4$ lasers, the commercial available Nd:YAG (1 at.%, dimensions: $\phi 3 \times 8$ mm) and Nd:YVO_4 (0.5 at.%, dimensions: $3 \times 3 \times 6$ mm^3) crystals were further employed to repeat the experiments. The laser was ensured to operate at its optimized Q-switched condition using a plano-concave cavity configuration as shown in Fig. 6.9. Nd:YAG laser has a cavity length of 75 mm, and Nd:YVO_4 was

kept in a length of 45 mm.

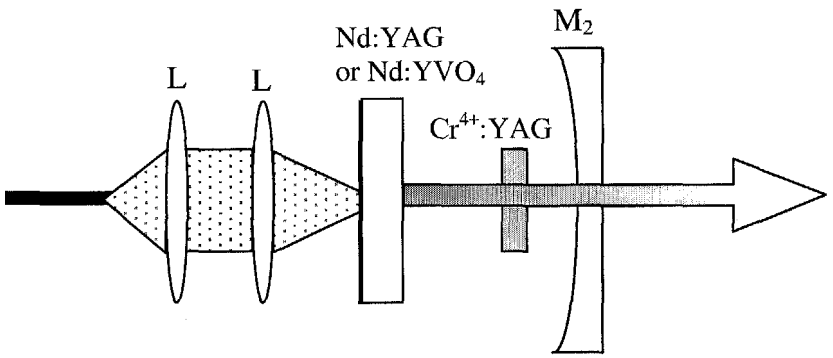

Fig. 6.9: Schematic configuration of the laser. L: coupling lens. M_2: Concave output coupler.

The radius of curvature of the concave output coupler (T = 40%) is 900 mm for Nd:YAG laser and 500 mm for Nd:YVO_4 laser, whereas, Cr^{4+}:YAG crystals with T_0 of 70% and 60% was used respectively for the Nd:YAG and Nd:YVO_4 passive Q-switching. Besides the period-doubling transition being observed clearly in both lasers, periodic windows with various odd periodicities such as period-3, periodic-5 could also be experimentally observed as an additional evidence of the deterministic chaos nature of the lasers. Fig. 6.10 shows as example those observed in the Nd:YVO_4 laser. These periodic windows were simply obtained through the fine-tuning on the cavity alignment when the laser is operating in a chaotic state.

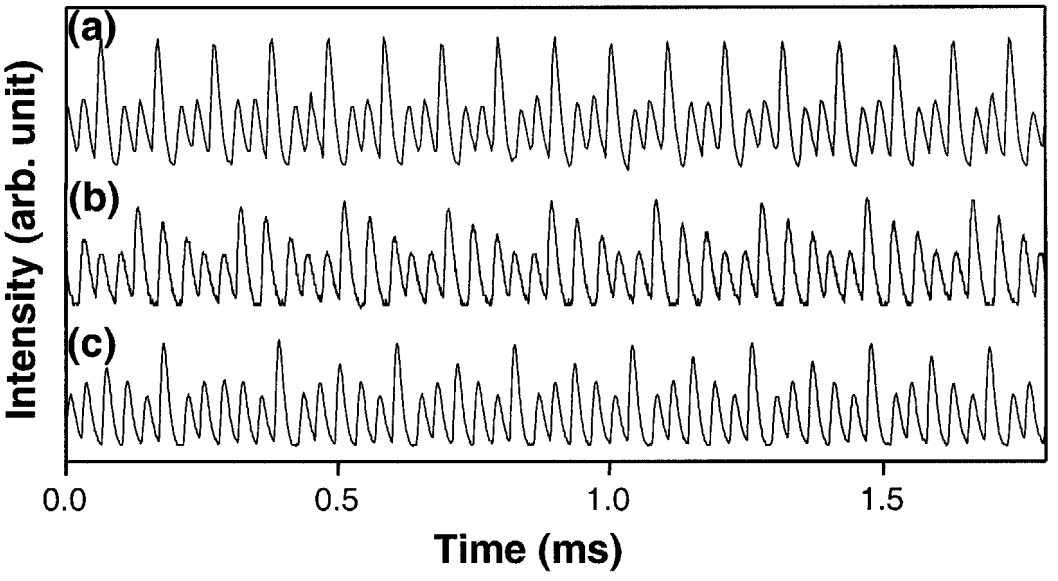

Fig. 6.10: States of periodic windows observed experimentally. (a) Period-3 window. (b) Period-5 window. (c) Period-6 window.

The existence of these periodic windows within the chaotic regime is well in agreement with the low-dimensional chaos theory, which further confirms that those conventionally called unstable Q-switched states could be a state of the low dimensional deterministic chaos. This experimental observation not only uncovers the chaotic nature of the lasers, but also confirms that the observed chaotic dynamics is independent of the laser host materials. It could be a general feature of all the passively Q-switched Nd^{3+}-doped solid-state lasers under strong interaction between the saturable gain and losses.

6.4 Analysis of observed chaotic data

6.4.1 Power spectrum

When a period-doubling bifurcation occurs in a system, the dynamics not only can be detected from the time evolution of a system variable, but can also be measured in the frequency domain from the power spectrum. This method is particularly useful for studying dynamic oscillating systems. Purely periodic signals have only sharp spectral lines, while a noise signal has broader spectra exhibited as the continuous background. Thus signal and noise can be easily distinguished. Power spectrum is used to study dynamical systems. One can see the peaks correspond to the fundamental frequency and its harmonics from the power spectra. When a system changes from period-1 to period-2 state, the main harmonic frequency peaks remain, but a sub-harmonic frequency spectrum appears. Similar to the period-doubling in time domain, further bifurcation results in the frequency quadrupling, octupling, and eventually to chaos.

Fig. 6.11 shows the spectrum analysis of a period-doubling process observed in the experiment. The recorded time series data of the period-doubling route to chaos as shown in Fig. 6.3 is converted to the frequency domain using the Fast Fourier Transform (FFT) technique. The data are sampled at 5.01 MHz, which is 250 times higher than the fundamental oscillation frequency of the laser dynamics. When the laser is in a period-1 state (Fig. 6.11a) the spectrum fundamentally consisted of the frequency of 20 kHz. While in period-2 (Fig. 6.11b) a sub-harmonic of the fundamental frequencies at 10 kHz appeared. Following the further bifurcation, further sub-harmonic components at frequencies at 5 kHz, 10 kHz, and 15 kHz are seen in period-4 state (Fig. 6.11c). Lastly in the chaotic condition (Fig. 6.11d), the background level in the power spectrum clearly

rises and with a broad peak near the frequency of 23 kHz, is indicative of a chaotic pulsation. All these frequency values are closely in agreement with the recorded pulse repetitive rate in the time series experimental data.

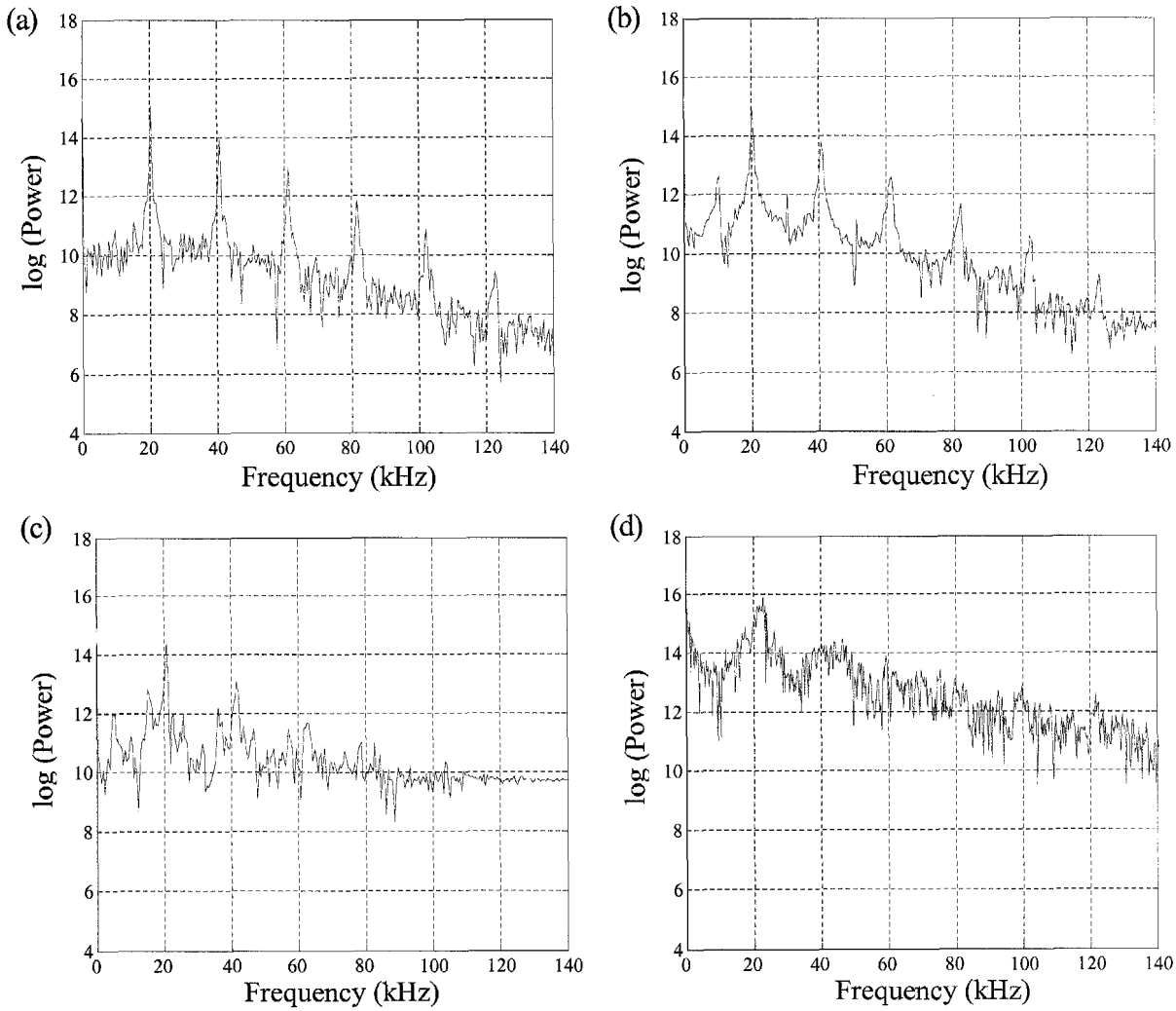

Fig. 6.11: Power spectrum of the period-doubling transition. (a) – (d): Period-1, 2, 4, and chaos.

6.4.2 Phase space

The passively Q-switched laser is a multidimensional system. Among the multi interaction factors of light with ions population change in the laser and that in the saturable absorber, Q-switched laser intensity is the only variable observed in the experiment. Mathematically, it has been proven that one can recreate a topologically equivalent picture of the original multidimensional system behavior by using the time series of a single observable variable. This method can be done through the time delay embedding method. From an established vector space, the trajectory of space dictates the state of the system. For the periodic sequences of bifurcations, the trajetory closes on itself, and forms limit cycles as an attractor in the phase space. This is another approach to visualize the period-doubling cascade instead of observing it in time domain. When a periodic state changes, one can identify it from the change of trajectory.

Phase space reconstruction is technically solved by decomposing series into delay vectors. Each observation in the one-dimensional signal *I(t)* is established into a vector which contains the observed *I(t)*, and time delays of τ.

$$s(n) = [I(n), I(n+\tau), I(n+2\tau), ..., I(n+(M_D-1)\tau], \tag{6.3}$$

where n is the time index, M_D is the embedding dimension and τ is the time delay. As a result, the series of vectors is:

$$S = [s(1), s(2), s(3), ..., s(N_D+(M_D-1)\tau], \tag{6.4}$$

where N_D is the length of the data series.

In order to be pragmatic in showing a proper shape of the attractor by occupying a large region of the reconstructed state, values of the time delay were optimized through the average mutual information technique as proposed by Fraser *et al.* [116]. As if the

time delay τ is too large, $I(t)$ and $I(t+\tau)$ are essentially random to each other, but if τ is too short, the measurement is not independent of each other. The ideal selection of τ is how maximum a given state $I(t)$ can predict about $I(t+\tau)$ state. In such estimation, the mutual information $I(t)$ will show the decrease, and then rise following the increase of τ. It is suggested to form the state space by using the τ value from the first minimum average mutual information. The same experimental period-doubling route to chaos (Fig. 6.3) is selected for the analysis. Through one of the functions of a shareware Visual Recurrence Analysis v 4.6, the time delay can be easily estimated. Fig. 6.12 shows one example of the average mutual information for the chaotic time series as in Fig. 6.3d. The first minimum data point is at the time unit of 100, which is equivalent to 20 μs.

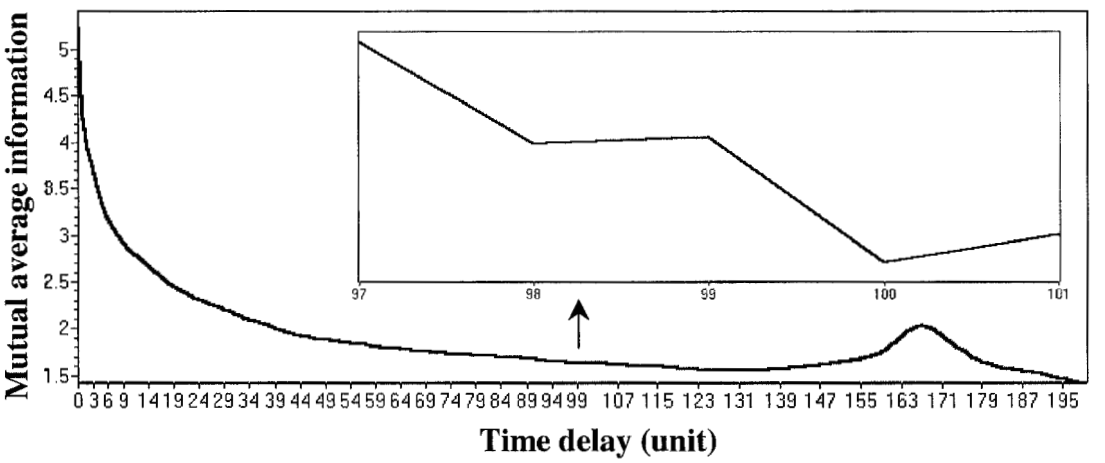

Fig. 6.12: Estimate of average mutual information for the time delay parameter. The inset graph is the enlarged curve for the first minimum data point.

Using this method, the estimated time lag for each data set is taken as a reference for reconstruction. The time delay τ used for all the phase diagrams shown in Fig. 6.13 is 20 μs. A loop like attractor, which is the so-called limit cycle is found from the established

phase plot. This experimental trajectory shows that the laser system approaches a periodic motion. Following the transition to chaos from Fig. 6.13a - d, the limit cycle changes from one cycle in period 1 to various cycles in the chaotic condition. The thickness of the curve is related to the noise in the experiment, as well as the finite sampling of the data.

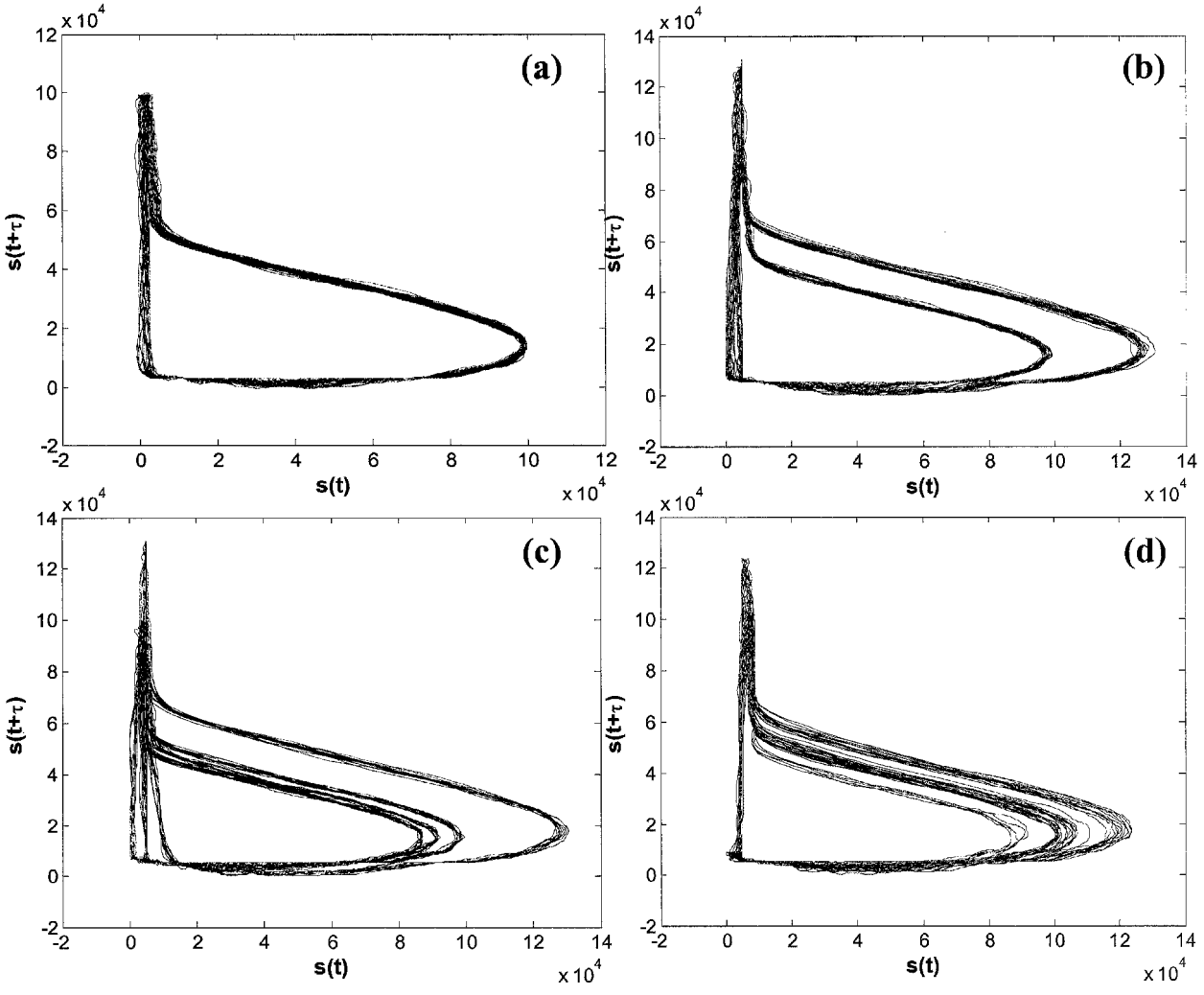

Fig. 6.13: Phase portrait reconstruction for period-doubling route to chaos from (a) – (d). Time delay used $\tau = 20$ μs.

6.5 Modelling and simulation

Changes in continuous variables are expressed with differential equations. For the laser system, time dependent changes can be expressed by a set of coupled first-order differential equations. The functions of the first derivations depend on the variables and control parameters in the equations.

As investigated above, laser dynamics are closely related to ion movement within energy levels. The dynamic phenomenon of the pump induced ground state depletion, and the delay of ions relaxation to ground state are believed as the causes to result in chaotic dynamics in passively Q-switched lasers. Therefore, the common rate equations model is extended to include these considerations for simulation. The interaction factors that describe the laser conditions are respectively the cavity photon density ϕ, laser population inversion M, laser ground state population N_0, and the population change in saturable absorber N_s. The laser ground state population change is explicitly described with a time dependent equation. This extended model with four degree of freedoms (variables) is shown as followings to describe the laser dynamics.

$$\frac{d\phi}{dt} = \frac{\phi}{t_r}\left[2\sigma_g l_g (N_2 - N_1) - 2\sigma_s l_s N_s - 2\sigma_{es} l_s (N_{s0} - N_s) - \left(\ln\frac{1}{R} + L\right)\right] \tag{6.5}$$

$$\frac{dM}{dt} = PN_0 + \gamma_1 (N - N_0) - (\gamma_2 + \gamma_g \sigma_g c\phi) M \tag{6.6}$$

$$\frac{dN_0}{dt} = \gamma_{20} N_2 + \gamma_{10} N_1 - PN_0 \tag{6.7}$$

$$\frac{dN_s}{dt} = \gamma_s (N_{s0} - N_s) - \sigma_s c\phi N_s \tag{6.8}$$

where the relations of the laser relaxation are represented by $\gamma_1 = \frac{\gamma_{10} - \gamma_{20} - 2\gamma_{21}}{2}$, and $\gamma_2 = \frac{\gamma_{10} + \gamma_{20} + 2\gamma_{21}}{2}$. σ_g is the laser gain emission cross section. $\sigma_{(s,\ es)}$ is either the saturation absorption cross section of ground state or excited state. Whereas, $l_{(g,\ s)}$ the crystal length for gain medium or saturable absorber. $\alpha_L = (ln1/R + L)$ is the total cavity losses.

The variables in model were normalized by using the following dimensionless parameters: $s = \frac{\alpha_L}{t_r} t$, $I = \frac{\sigma_g c \phi}{\gamma_2}$, $U_m = \frac{2\sigma_g l_g}{\alpha_L} M$, $U_s = \frac{2\sigma_s l_s}{\alpha_L} N_s$, $U_0 = \frac{2\sigma_g l_g}{\alpha_L} N_0$, $U_n = \frac{2\sigma_g l_g}{\alpha_L} N$, $w_s = \frac{2\sigma_s l_s}{\alpha_L} N_{s0}$, $\alpha = \frac{\gamma_2 \sigma_s}{\gamma_s \sigma}$, $d = \frac{\gamma_{21}}{\gamma_2}$, $\varepsilon = \frac{t_r \gamma_2}{\alpha_L}$, $\varepsilon_s = \frac{t_r \gamma_s}{\alpha_L}$, $b = \frac{\gamma_1}{\gamma_2}$, $\beta = \frac{\sigma_{es}}{\sigma_s}$, and this transformed the above model to:

$$\frac{dI}{ds} = I[U_m - U_s - \beta(w_s - U_s) - 1] \tag{6.9}$$

$$\frac{dU_m}{ds} = -\varepsilon\left[(1 + \gamma_g I)U_m - \left(\frac{P}{\gamma_2} - b\right)U_0 - bU_n\right] \tag{6.10}$$

$$\frac{dU_0}{ds} = \varepsilon\left[(1-d)U_n - (b+d)U_m - \left(1 - d + \frac{P}{\gamma_2}\right)U_0\right] \tag{6.11}$$

$$\frac{dU_s}{ds} = \varepsilon_s[w_s - U_s - \gamma_s \alpha I U_s] \tag{6.12}$$

The model was further simplified to make it existing in the simple form of the differential equations. By defining $W = \frac{P}{\gamma_2} U_0 + b(U_n - U_0)$, Eq. (6.10) thus becomes:

$$\frac{dU_m}{ds} = \varepsilon\left[W - \left(1+\gamma_g I\right)U_m\right]. \tag{6.13}$$

Since $\frac{dW}{ds} = \frac{(P-\gamma_1)}{\gamma_2}\frac{dU_0}{ds}$, substitution of Eq, (6.11) into this equation yields

$$\frac{dW}{ds} = P(1-d+b)\frac{U_n}{\gamma_2} - \left(\frac{Pb}{\gamma_2} - b^2\right)U_m - \left(1-d+\frac{P}{\gamma_2}\right)W .$$

As $\frac{Pb}{\gamma_2}, d, b << 1$, and can be ignored in certain terms under comparison, this equation is written in the simple form as below.

$$\frac{dW}{ds} = \varepsilon\left[A + b^2 U_m - W\right], \tag{6.14}$$

where A is defined as $A = \frac{PU_n}{\gamma_2}$ (6.15)

The final dimensionless rate equations are summarized as below.

$$\frac{dI}{ds} = I\left[U_m - U_s - \beta(w_s - U_s) - 1\right] \tag{6.16a}$$

$$\frac{dU_m}{ds} = \varepsilon\left[W - \left(1+\gamma_g I\right)U_m\right] \tag{6.16b}$$

$$\frac{dW}{ds} = \varepsilon\left[A + b^2 U_m - W\right] \tag{6.16c}$$

$$\frac{dU_s}{ds} = \varepsilon_s\left[w_s - U_s - \gamma_s \alpha I U_s\right] \tag{6.16d}$$

The set of Eq (6.16) was numerically solved by fourth-order Runge-Kutta to simulate dynamic laser behaviors. Time evolution of laser photon density in Eq. (6.16a), which is proportional to laser intensity as observed in experiment, was given focus in simulation. The numerical solutions show a good qualitative agreement with the observations on laser dynamics. In the simulation, period-doubling route to chaos is

obtained by changing the A value, which is proportional to the pumping rate P stated in Eq. (6.15). The transition from Q-switching to chaos is found to occur in a very narrow control parameter range in the calculation. This explains why high resolution of pump power is required to observe the complete period-doubling route to chaos in practice. Fig. 6.14 shows the period-doubling transition obtained with a slight change on A. State space trajectory for the system is shown together in the figure. Compared to the experimental phase plots, which exhibited measurement noise, clean limit cycles with fine lines are found in the simulation. Parameters for this generation are: Cr^{4+}:YAG with initial transmission $T_0 = 60\%$, cavity output coupling $R = 70\%$ and laser doping concentration of 1.14 at.%. The dimensionless parameters used for calculation are respectively $\gamma_1 = 16.49 \times 10^6$, $\gamma_2 = 16.506 \times 10^6$, $w_s = 2.5542$, $\beta = 0.1907$, $\varepsilon = 0.03614$, $\varepsilon_s = 0.00054188$, $b = 0.999$, and $\alpha = 377.34$.

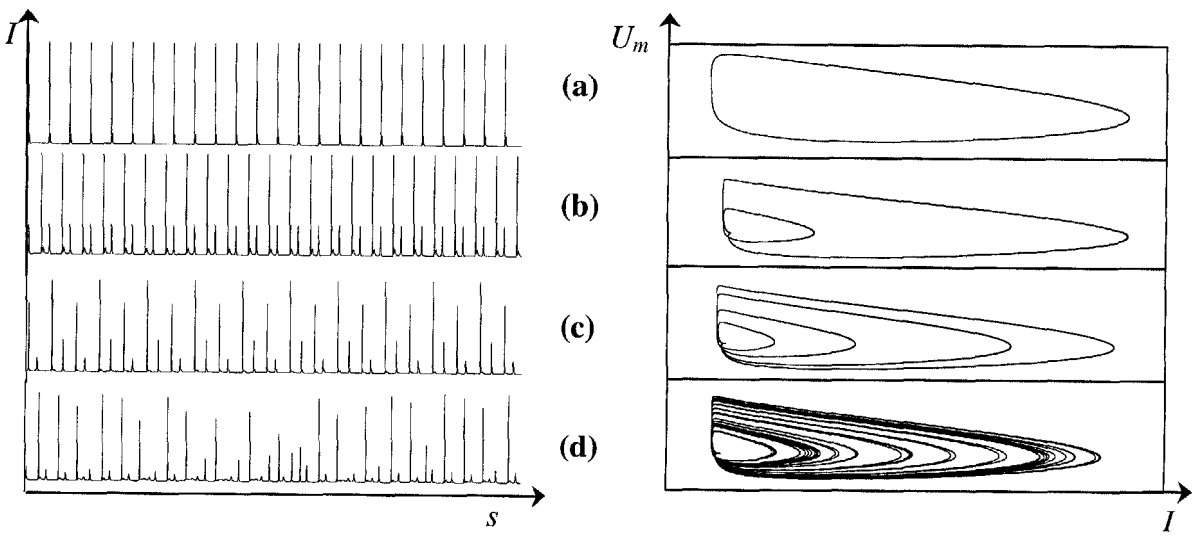

Fig. 6.14: The period doubling route to chaos and the respective phase plots obtained in the simulation. A is slightly increased for the period-doubling transition. (a) Period-1: $A = 0.068065$. (b) Period-2: $A = 0.06810$. (c) Period-4: $A = 0.06815$. (d) Chaos: $A = 0.06865$.

It was observed in the numerical simulation, there is a threshold value of A, showing the onset of the laser transformation from stable period-1 state to chaotic condition. This qualitatively implies that under certain pumping level ions saturation occurs in ground state and results in dynamic behavior by disturbing the balance of ions movements within energy levels. Below this value, the Q-switched pulses are in a stable period-1 condition. In this case, the threshold value of $A = 0.064$. Exceeding this value, a large chaotic regime is obtained together an odd number of periodic windows. As a consequence of chaos, there is a starting of a descending periodic transition and then following with an ascending period-doubling route to chaos again. The bifurcation sequence is apparently reproduced to show the self-similarity as a universal feature of dynamics. The replicating sequence is schematically shown in Fig. 6.15.

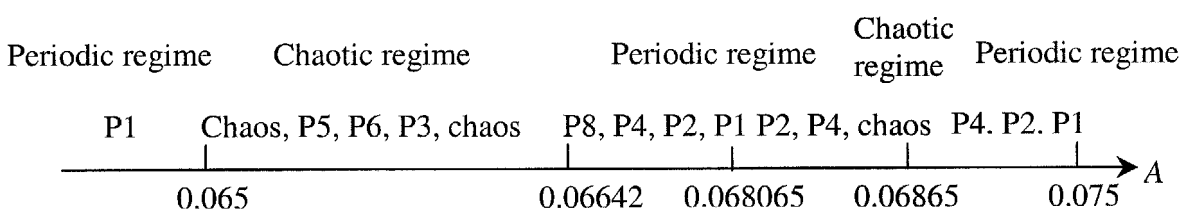

Fig. 6.15: Schematic diagram for the periodic and chaotic regimes associated with the varying of A parameter in the simulation.

While zoom into the chaotic regime, odd numbers of periodic windows, period-3, 5, and 6 are able to see as correspondingly to the experimental observation. Fig. 6.16 shows the time series periodic windows as well as their phase state.

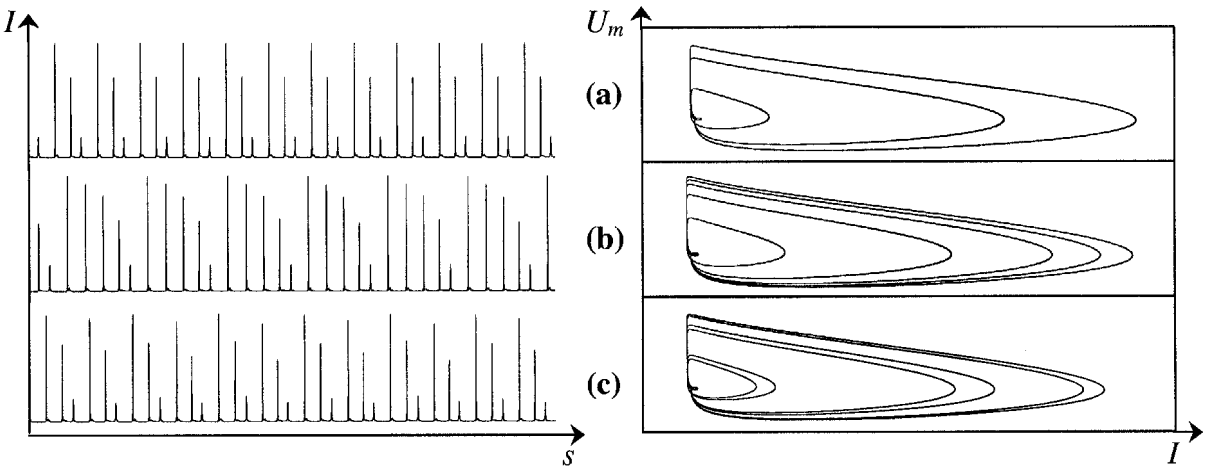

Fig. 6.16: The simulated odd numbers of periodic windows in time series and phase plot. (a) Period-3, A = 0.0658. (b) Period-5, A = 0.06504. (c) Period-6, A = 0.06574.

6.6 Summary

In this chapter, the dynamics of the CW pumped passively Q-switched Nd-ion doped lasers has been investigated. Perturbation of the ions movement within the laser energy levels during the passive Q-switching is the main reason for the nonlinear behavior in the laser. Based on the experimental investigation, it is believed that the laser dynamics are due to the pump saturated ions population in the laser ground state, and the slow emptying of the lower laser energy level during the laser actions.

Experimentally, the period-doubling route to chaos and odd numbers of periodic windows are the general nonlinear phenomena observed in the diode-pumped passively Q-switched Nd:$GdVO_4$ and Nd:$GdYVO_4$, Nd:YAG and Nd:YVO_4 lasers. These demonstrations reveal that the chaotic dynamics are independent of the laser gain medium used, are a general property of all passively Q-switched solid-state lasers under a strong light interaction between the saturable gain and losses. Through the nonlinear time

series analysis, the existence of the clear complete period-doubling route to chaos in the lasers were further interpreted and visualized in frequency domain and state space. By considering the finite lifetime of the lower energy level and the population change in the ground state, the common rate equations model is extended to simulate the observed chaotic nature of the laser. Period-doubling route to chaos and odd periodic windows were qualitatively reproduced.

The deterministic chaos in the laser actually suggests that the strong pulse-to-pulse amplitude and repetition rate jitters frequently observed in the diode pumped solid-state lasers could be an intrinsic nature of the system. Therefore, chaos control techniques should be the most appropriate way to efficiently suppress these Q-switched pulse instabilities rather than the conventional laser engineering techniques.

CHAPTER 7

Passively mode-locked Nd:$GdYVO_4$ lasers

As discussed in detail in the previous chapters, duration of a Q-switched laser pulse may vary from several hundred nanoseconds to several nanoseconds, depending on the laser parameters. The selected parameters can also affect the cavity build-up energy, and restrict the pulse repetition rate at most kHz rates. Through the mode-locking technique, the optical pulse duration can be further narrowed from nanoseconds to picoseconds or subpicoseconds, at MHz repetition rates corresponding to the cavity round trip. In contrast to the Q-switched laser whose whole cavity is filled with energy, in a mode-locked laser the energy is compacted into a pulse that oscillates in the resonator. The duration of the mode-locked pulses depends mainly on the laser gain bandwidth and the effectiveness of mode-locker. The greater the laser emission bandwidth, the narrower the mode-locked pulse can be.

Basically, temporal characteristics of the passive mode-locking can be distinguished as being continuous-wave mode-locking, and Q-switched mode-locking. According to Eq (2.21) as discussed in Chapter 2, the passively mode-locked feature is closely related to the laser conditions, such as the saturable absorption loss, pumping strength, cavity reflectivity, laser fluorescent lifetime, cavity length, and the stimulated emission cross section. Significantly, the property of the gain medium plays the dominated role in suppressing pulse energy and maintaining intracavity fluence for achieving the continuous-wave mode-locking. Among all the criteria, laser material with a large stimulated emission cross section or a non-homogenously broadened gain is

absolutely crucial to achieving the stablility of mode-locking in the operating condition that is far above threshold, and which is common to every passively mode-locked laser. As stated in Chapter 2, the mixed-gadolinium-yttrium vanadate crystal is excellent with its good thermal property, a slightly longer upper state lifetime and a broad inhomogenously broadened emission linewidth, so it is believed that Nd:$GdYVO_4$ might show a plausible performance in ultrashort pulse generation, with the ease in achieving the stable continuous-wave mode-locking.

In this chapter, passively mode-locked Nd:$GdYVO_4$ laser is experimentally demonstrated. The mode-locking laser performance is studied by either using Cr^{4+}:YAG crystal or GaAs wafer as a saturable absorber. As discussed in Chapter 2, Cr^{4+}:YAG crystal is conventionally used as saturable absorber in Nd-doped lasers for passive Q-switching. This saturable absorber also exhibits a saturable excited state absorption (ESA) under strong intracavity intensity, which enables passive mode locking to occur. The semi-insulating bulk GaAs crystal, on the other hand, has been selected to passively mode-lock several Nd-doped lasers for its lower cost and robustness. This polar GaAs semiconductor exhibits a significant TPA and FCA nonlinear process under the illumination of strong irradiance. The TPA process will photo-generate free carriers in the conduction band and induce the free carrier nonlinearity to the absorption and refraction in GaAs. When the GaAs saturable absorber is used to build a standing wave cavity, the interference of two plane waves within the GaAs causes a spatially non-uniform intensity pattern and yields the photorefractive grating diffraction loss to the cavity. As a result of the varying of irradiance on the GaAs, photorefraction effect is altered simultaneously for a continuous loss modulation to the laser.

A Z-folded cavity is explicitly selected to reduce the effective cavity beam spot on the saturable absorber. This configuration is to increase the light interactive nonlinearity and hence the modulation depth in the saturable absorber for better mode-locked laser performance. This chapter begins with the simulation of fold-mirror cavity design based on the consideration of the previous measured thermal lens. Experimental results are presented in the ensuing sections for the laser with above-mentioned saturable absorbers.

7.1 Z-folded laser cavity design

Commonly, folded cavity configuration is used to achieve a tightly focused beam spot on the saturable absorber and simultaneously have a good mode matching between the cavity mode and pump beam. Based on the Gaussian beam *ABCD* method as employed in Chapter 3, the folded-mirror cavity stability and the effective beam size are estimated. As it differs to the linear two-mirror cavity that used in the CW and passive Q-switching, the Z-folded configuration has four mirrors for cavity confinement, in which two mirrors are for the tilted arms, and the other two mirrors are respectively to begin and complete the resonator (Fig. 7.1). The ray transfer matrices of each cavity mirror used in *ABCD* simulation are given also in the Fig. 7.1.

9

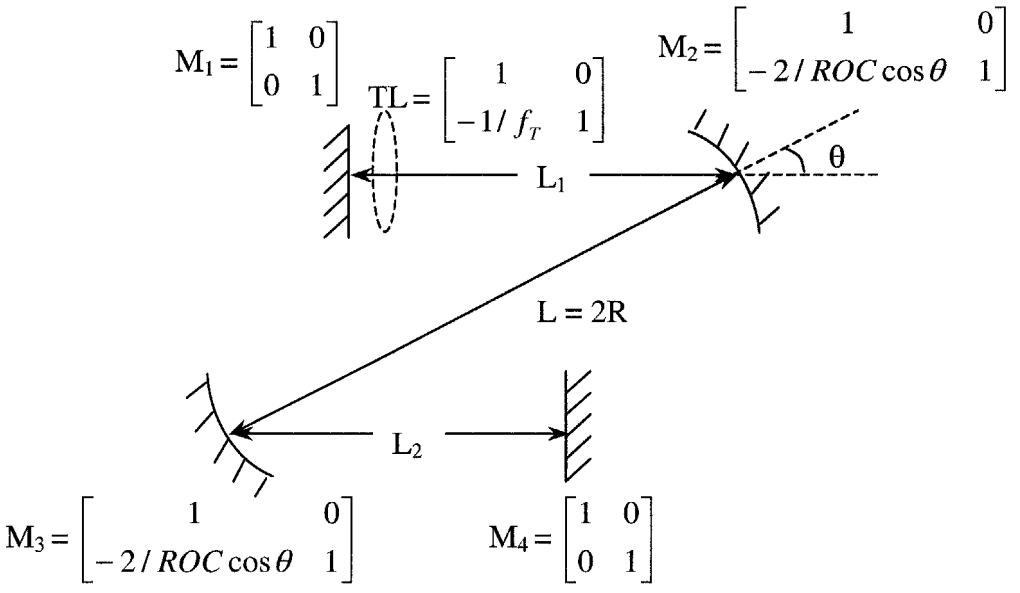

Fig. 7.1: The four mirror Z-folded cavity.

In the experiment, M_2 and M_3 are two concave mirrors with the same radius of curvature (*ROC*) of 300 mm, and separated at L = 600 mm with each other. Normally in practice, the cavity-tilted angle θ with respect to the optical axis is kept small in order to avoid the cavity astigmatism. This angle was determined in the experimental setup as about $\theta = 5$ degrees.

Based on the experimental result obtained in the two-mirror cavity as given in Chapter 3, thermal lens has been found to be detrimental to the laser performance. Therefore, pump power dependent thermal focal length was also taken into account in the design of the folded-cavity. Cavity stability under varying length of L_1 and L_2 was firstly calculated under the strongest thermal lens of f_T = 200 mm in Nd:$GdYVO_4$ as was measured at the maximum pump power of 13 W. Fig. 7.2 shows the stability diagram for the folded-cavity by varying the lengths of L_1 and L_2.

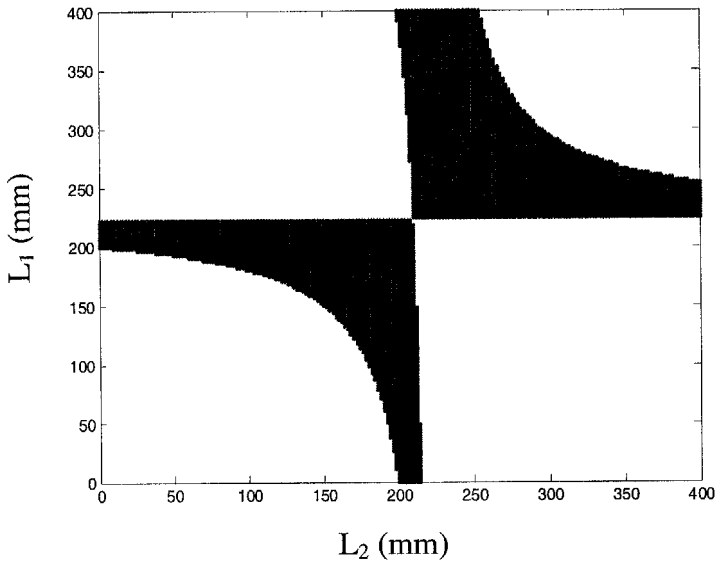

Fig. 7.2: The calculated stability diagram of Z-folded cavity upon the consideration of thermal lens in the gain medium measured at maximum pump power.

Laser operation is stable within that marked area as shown in the diagram above. However, following the change of thermal lens with respect to the pump power, mode matching between pump beam and cavity mode is another factor to be considered in laser if it is necessary to obtain a steady output along the increase of pump power. Based on the cavity mode size of about 200 μm in the previous optimum two-mirror CW laser, the lengths of L_1 and L_2 particularly are estimated in simulation and confirmed practically. Under such optimal condition upon the consideration of laser mode matching, L_1 and L_2 are found to be about 120 mm and 200 mm, respectively. Fig. 7.3 shows the relationship of cavity beam waist, and mode size in gain medium with respect to the pump power. It can be seen that the effective mode radius in gain medium does not have a significant change following the increase of pump power. Following the variation of thermal focal

lens in the gain medium, the resonator mode size at the laser crystal and the saturable absorber was computed ranging from 202.4 – 228.7 μm and 86 – 66 μm, respectively for the change of pump power from 6 W to 13 W.

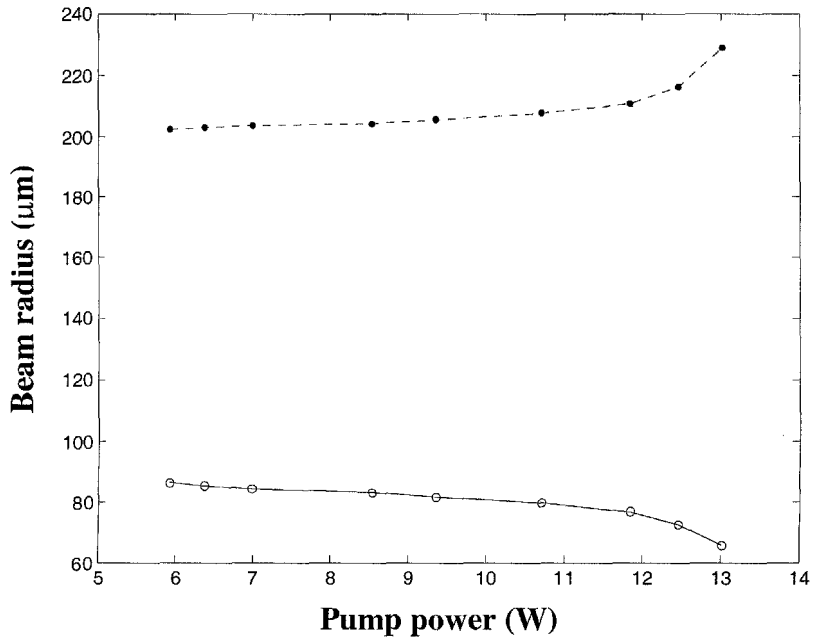

Fig. 7.3: Dependence of cavity beam size on the pump power. ω_g: cavity mode radius in laser crystal; ω_0: cavity beam waist radius.

Fig. 7.4 shows the mode size variation within the laser resonator of total length of 920 mm. The calculation is made based on the thermal focal length of 200 mm in the gain medium.

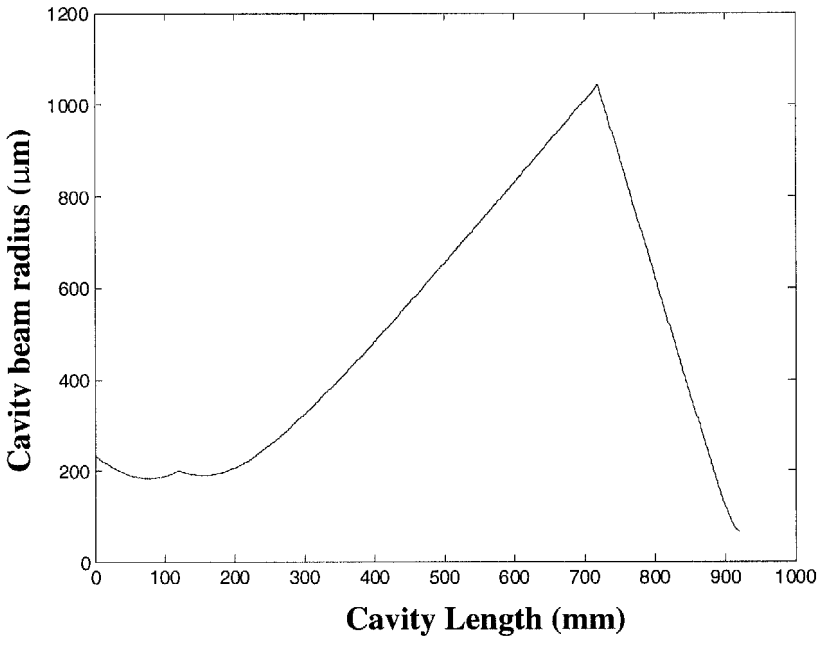

Fig. 7.4: The calculated mode propagation in laser cavity.

7.2 Nd:GdYVO$_4$ – Cr^{4+}:YAG mode-locking

The laser layout is shown in Fig. 7.5. The resonator was built according to the cavity design as shown above. It consists of a flat dichroic input mirror (M_1) coated at the pump and the fundamental wavelengths, two highly reflective concave mirrors (M_2 and M_3) at 1064 nm both with a radius of curvature of 300 mm, and a flat output coupler (M_4). L_1 was kept at 120 mm, L_2 at about 200 mm, and the distance between the two concave mirrors M_2 and M_3 was 600 mm.

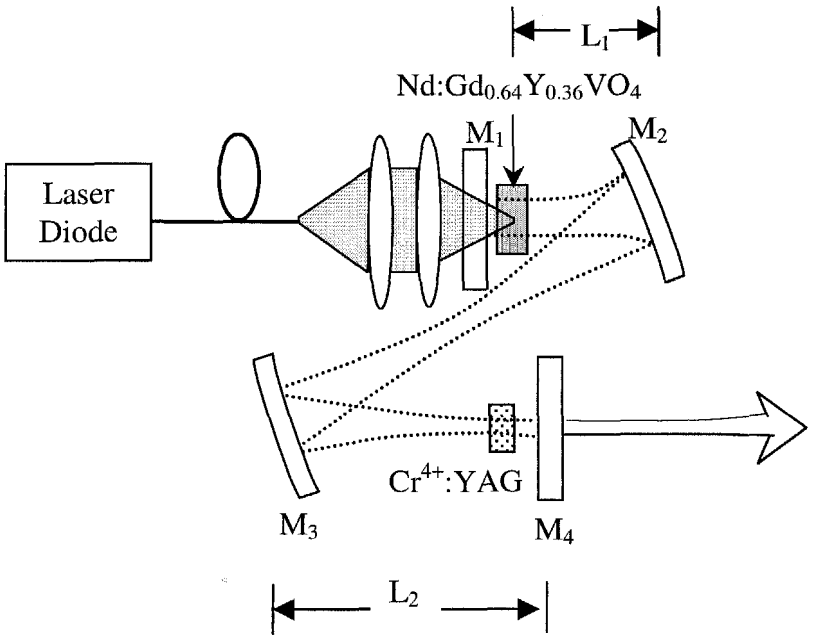

Fig. 7.5: Schematic diagram of the passive mode-locking experimental setup.

The light from the fiber end was collimated and focused onto the Nd:$Y_{0.36}Gd_{0.64}VO_4$ crystal through the flat input mirror. The laser crystal is a-cut to a dimension of 3.5 × 3.5 × 5 mm^3 and doped with 0.5 at.% of the Nd^{3+}. Both surfaces of the Nd:$GdYVO_4$ crystal are antireflection coated at 808 nm and the lasing wavelength of 1064 nm. As an approach to protecting the crystal from the heat influence, the crystal was wrapped properly with a layer of 0.1 mm-thick indium foil and mounted within a water-cooled copper holder at 18 ^{0}C during the experiment.

In order to examine the mode matching in the laser crystal, laser cavity alignment was initially optimized under its CW operation with different transmission of a flat output coupler. In the optimized condition where the cavity coupling loss is T = 6%, the laser achieved a maximum CW power of 4.86 at the launching pump power of 12.81 W, giving a slope efficiency of 46%. The laser slope efficiency is about the same for other cavity

coupling transmission of T = 10% and 40%. A maximum CW output power of 3.1 W was successfully obtained in the laser, in spite of the high cavity coupling loss of 40%. This good CW laser performance indicates that the current Z-folded cavity configuration is in a good mode matching condition. Fig. 7.6 shows the CW output laser with the output coupler of T = 6%, 10%, and 40%.

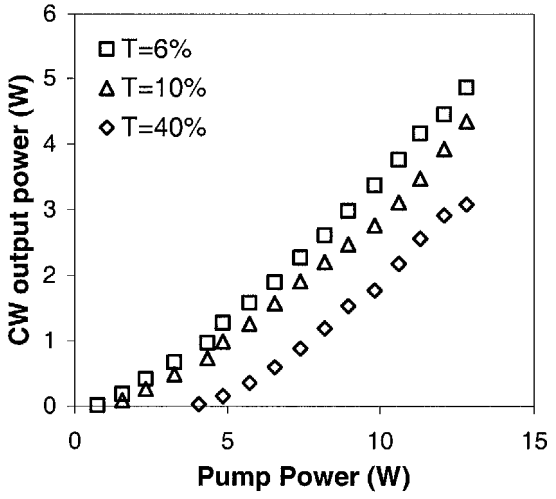

Fig. 7.6: Average output power for the laser operated in CW operation with cavity coupling transmission of T = 6% (square), T = 10% (triangle) and T = 40% (diamond).

Because a high transmission coupler is able to shorten the cavity build-up time to generate an efficient passive Q-switching according to the analytical model and experimental practice in Q-switching, the cavity coupling for optimized pulsed laser performance has been appropriately examined. In agreement with the previous Q-switched experimental parameters, output coupler with transmission of T = 40% was found to be optimized also for the Q-switched pulse energy and mode-locking in the experiment.

In order to increase the Q-switched energy and hence the intracavity energy fluence for better mode-locking, high doping concentration of Cr^{4+}:YAG saturable absorber is selected. These included two antireflection coated Cr^{4+}:YAG crystals with initial transmission of either T_0 = 60% and T_0 = 50%. The Cr^{4+}:YAG with I_0 = 50% is <001>-cut with dimensions of 5 × 5 × 3.7 mm^3, while the weaker one is <111>-cut with the same cross-section but a thickness of 1.74 mm. These two absorbers are antireflection coated at 808 nm and 1064 nm on their incident surfaces. In the laser operation, the Cr^{4+}:YAG crystal was wrapped with indium foil and mounted on an aluminum holder to dissipate the heat induced from the strong intracavity intensity. According to the calculation, the large ratio of mode size between the gain medium and the absorber is sufficient to achieve an efficient Q-switching. In the experiment, the mode-locked pulse repetition rate was detected by a high-speed photoreceiver (New focus, 1611-FS), while to further resolve the mode-locked pulses, a standard commercial autocorrelator (Femtochrome, FR-103XL) using a BBO nonlinear crystal was used. The detected pulse characteristics were observed with a digital oscilloscope (TDS 360).

Laser with the Cr^{4+}:YAG crystal of 60% initial transmission was firstly studied. After proper alignment of the Cr^{4+}:YAG, passively Q-switched mode-locking was observed immediately, starting from the laser threshold. Fig. 7.7 shows the average output power of the laser at the QML operation together with the Q-switched pulse energy in relation to the pump power. A maximum output power of 1.85 W was obtained at the maximum available pump power of about 12 W. The slope efficiency of the passively Q-switched mode-locked laser of about 31.9% is about 10% lower than the CW operation. In such conditions, Q-switched pulses with a maximum single pulse energy of

94.8 μJ were obtained in the laser, which further confirms the potential of $Nd:GdYVO_4$ laser for the passively Q-switched operation.

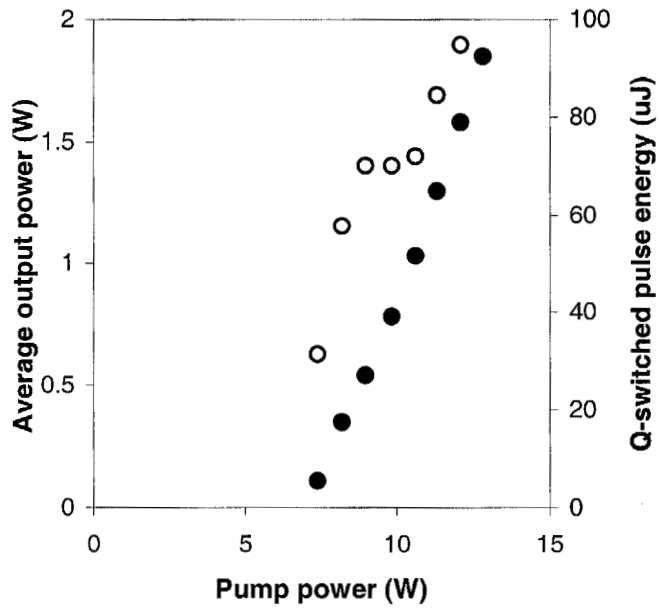

Fig. 7.7: Dependence on pump power of Q-switched average output power (solid circle) and pulse energy (open circle) for the QML laser.

The corresponding Q-switched pulse width and pulse repetition rate are given in Fig. 7.8. Based on the calculated mode size, the light fluence in the Cr^{4+}:YAG crystal was estimated to be 0.5 J/cm^2 near the threshold of the Q-switching. This is far above the calculated excited state saturation fluence for the Cr^{4+}:YAG of about 0.1 J/cm^2 if 8.2×10^{-19} cm^2 is taken as the excited state absorption cross section. Hence it suggests that the excited state of the Cr^{4+}:YAG crystal is saturated all the time. Generally, a considerably stable Q-switched pulse train could be observed in the experiment.

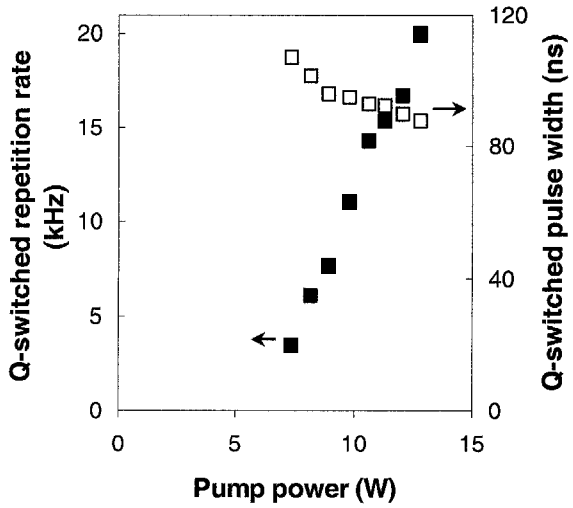

Fig. 7.8: Q-switched pulse width and pulse repetition rate with respect to pump power.

Fig. 7.9 shows one example of the Q-switched pulse train, which has a pulse jitter of less than 5%.

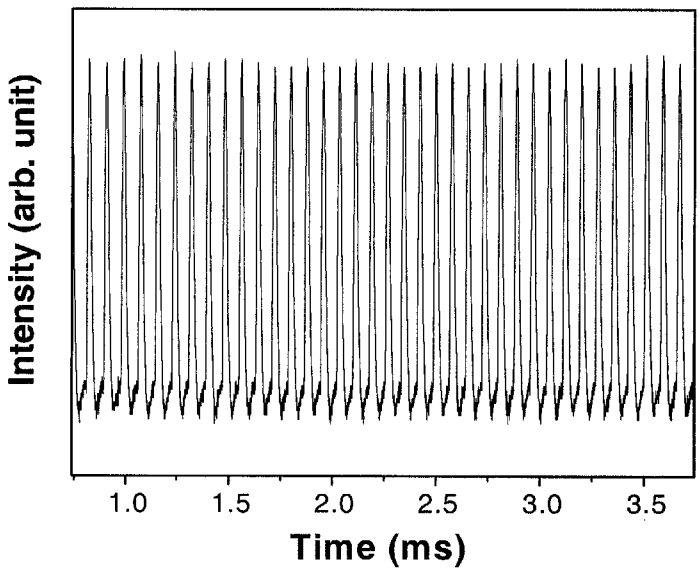

Fig. 7.9: A typical Q-switched pulse train detected with the slow detection channel of the photoreceiver.

With a high-speed photoreceiver and an oscilloscope the mode-locking nature of the Q-switched pulses was clearly seen. Such a typical oscilloscope trace is shown in Fig. 7.10. The mode-locked pulses have a repetition rate of 161.3 MHz, which corresponds to the cavity length.

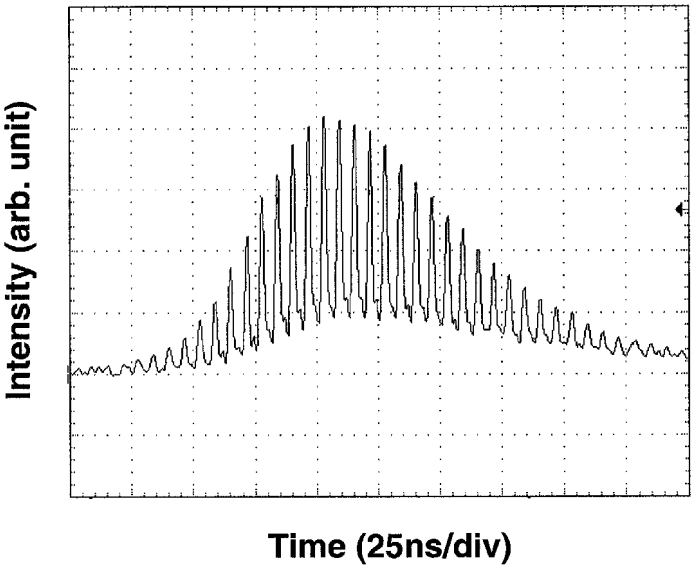

Fig. 7.10: Oscilloscope trace of a typical QML pulse profile.

With the increase of the pump power from the threshold to the maximum level, the modulation depth of the mode-locked pulses was found to have slightly increased from 80% to 90%. The peak power of the mode-locked pulses near the maximum of the Q-switched envelope was estimated to be about 1.7 MW at the pump power of 12 W. This high peak power of mode-locked pulses near the Q-switched envelope peak makes the laser attractive for a number of applications such as nonlinear optical wavelength conversion, micro-machining, and spectroscopy.

The intrinsic dynamics of the passive Q-switching was further confirmed in the passively Q-switched mode-locking operation. The periodic and chaotic regimes

appeared alternately following the ascending change of the pump power. Similarly the laser was prone to show chaotic pulsation at the high pump power, and period-doubling route to chaos could be obtained with the fine-tuning of the cavity alignment. It is noted that this dynamic at the Q-switching regime has no influence on the narrow mode-locked pulses within the Q-switched pulse envelope. Using a spectrum analyzer (HP 4396B), the Q-switching and cavity resonant mode were illustrated in frequency domain as given in Fig. 7.11. The frequency scanning range is from 0 Hz to 200 MHz. As observed, there are two frequency groups in the diagram respectively for the Q-switching in few tens of kHz, and the mode-locking with the centre pulse repetitive frequency at 161 MHz. Due to the resolution of 300 kHz, the Q-switched frequency is unresolved.

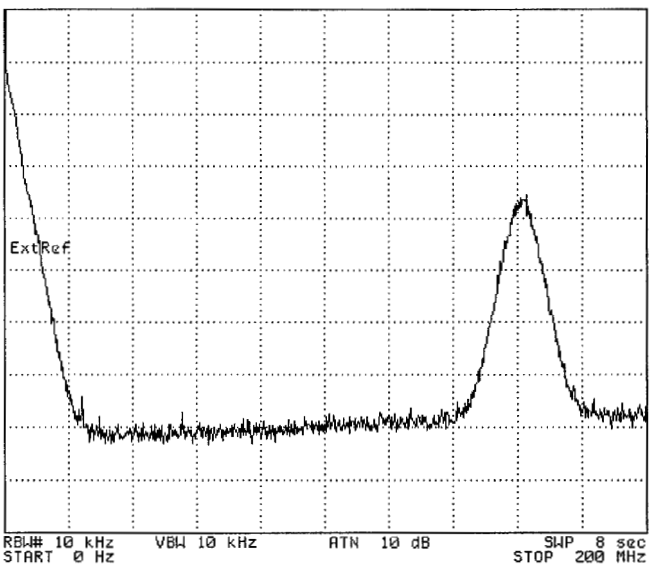

Fig. 7.11: Frequency spectrum of the passively Q-switched and mode-locked operation.

The spectrum range was zoomed particularly into the first 50 kHz of Q- switched regime for the periodic and chaotic Q-switching in relation to the change of pump power. As in Fig. 7.12, clear frequency spectra of periodic and chaotic QML were observed in laser

with the increasing of the pump power from 8.76 W to 12.31 W. At a pump power of 8.76 W, the sharp Q-switched frequency is at about 9.64 kHz correspondingly to the period-1 pulsation. The frequency of Q-switched laser operation became double at pump power of 9.64 W with its main frequency of 10 kHz in accordance with the increasing of pump power. Further increase of the pump power resulted in period-4 at pump power of 10.34 W, and chaotic operation at pump power of 12.31 W.

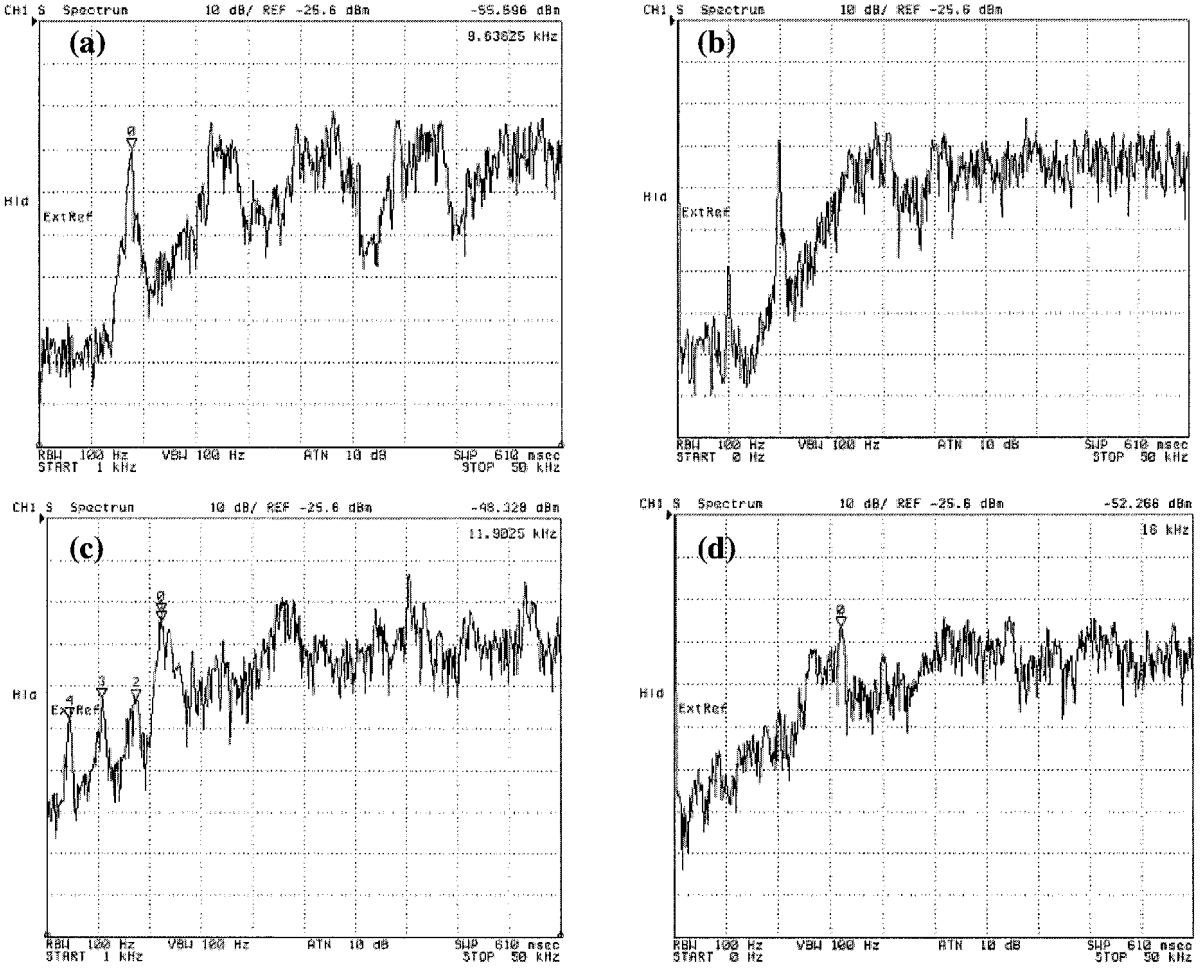

Fig. 7.12: Frequency spectra of the passively Q-switched mode-locked laser in periodic and chaotic regimes. (a) – (d) is spectrum of period-1, 2, 4, and chaos, respectively.

The odd number of periodic windows was observed within the chaotic Q-switched regime. After the period-4 laser operation at 10.34 W, a period-3 was obtained when pump power increased to 10.61 W before the pulsation became totally aperiodic. Fig. 7.13 shows one example of the period-3 frequency spectrum. These observations further confirmed the chaotic nature of the diode-pumped solid-state lasers in Q-switched regime.

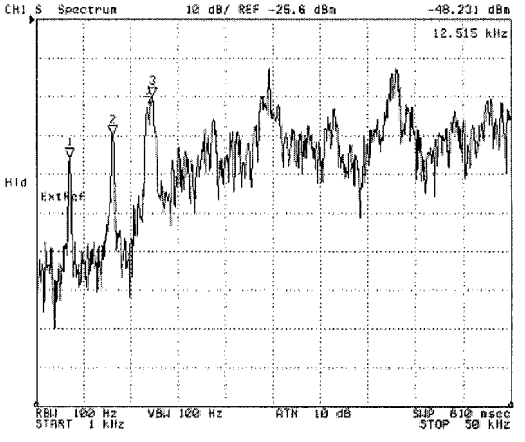

Fig. 7.13: Frequency spectrum of the Q-switched mode-locked pulses in period-3 regime.

Further investigation was carried out by replacing the current Cr^{4+}:YAG (T_o = 60%) with the stronger one (T_0 = 50%). As observed at the lasing threshold of the laser, a series of strongly fluctuating narrow pulses was obtained instead of the Q-switched and mode-locked pulses. The stability of the pulse train and the average output power was enhanced with increasing of the pump power. A fairly stable CWML pulse train was obtained at the pump power of about 12 W, giving an output power of 1.23 W. Limited by the available pump power of 12.48 W, the maximum achievable CWML average power was 1.36 W, at the laser slope efficiency of 29.2% (Fig. 7.14).

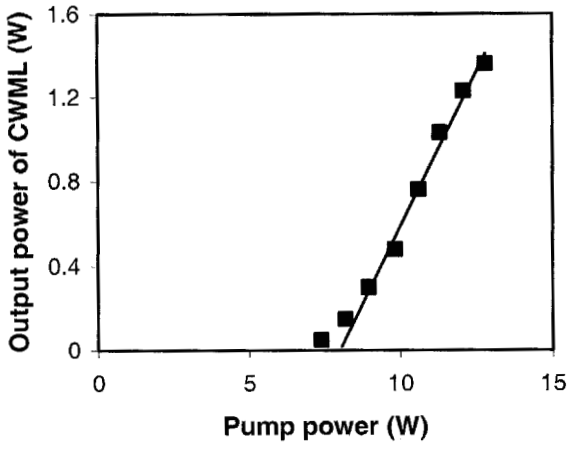

Fig. 7.14: Average output power in relation to the pump power for the CWML laser.

Fig. 7.15 shows the CWML pulse train observed in the experiment. The temporal pulse separation is 6.2 ns as in the case of QML. The mode-locked pulse duration was further measured with a commercial autocorrelator.

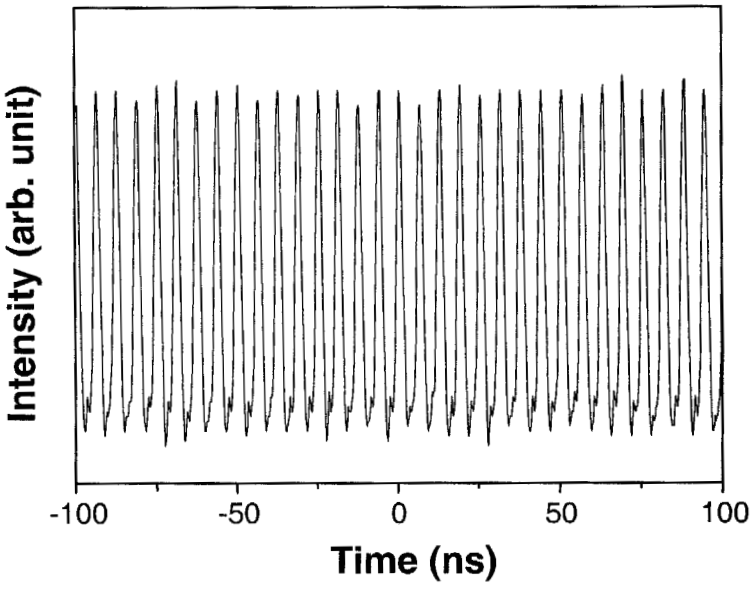

Fig. 7.15: A typical CWML pulse train at the pump power of 12 W.

Fig. 7.16 shows the measured autocorrelation trace fitted with a Gaussian pulse profile. The full width at the half maximum (FWHM) of the autocorrelation trace is about 4.19 ps. Assuming a Gaussian pulse profile the mode-locked pulse width is therefore estimated as about 2.96 ps. Similar pulse duration was also obtained when the QML pulse was detected with the same system.

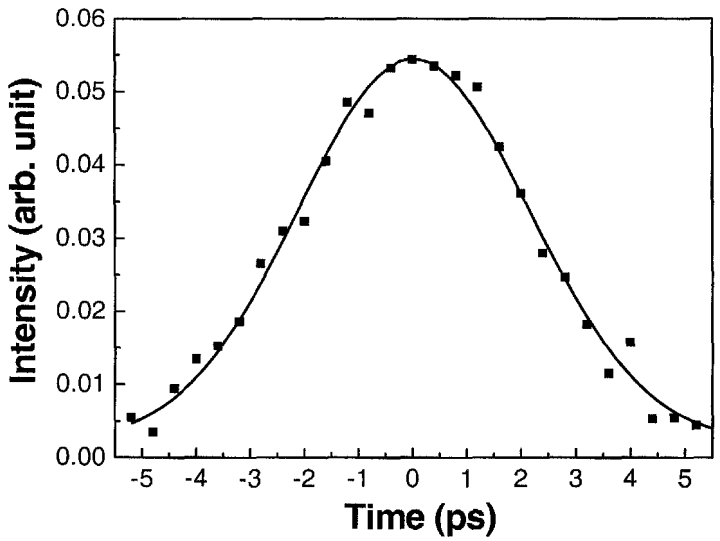

7.16: Autocorrelation trace of the mode-locked pulses. Dot: experimentally measured autocorrelation trace; solid-line: Gaussian fitting curve.

Besides the large emission cross section and relatively long fluorescent lifetime of the Nd:GdYVO$_4$ helping to reduce the gain saturation fluence for the ease to achieve the CW mode-locked pulses, it is believed that the realization of CWML in the laser could be due to the high energy pulse fluence achieved in the cavity by using the stronger Cr^{4+}:YAG absorber. As the ground state of the Cr^{4+}:YAG crystal is fully bleached during the laser operation, majority of the Cr^{4+} ions are practically depopulated to the first excited state. Therefore, the ground state saturation becomes insignificant and the ESA

plays the dominating role in the laser dynamics. ESA absorption in the sub-nanosecond range of recovery time will then result in the CWML of the laser. Nevertheless, it is to be pointed out that the decay of the Cr^{4+} ions to the ground state could cause a slow pulse peak modulation to the CW mode-locked pulse train. Using an rf spectrum analyzer (HP 4396B), the CWML pulse peak modulation caused by the ground state absorption was further identified in frequency domain. Fig. 7.17 shows for example a typical measured result. As a result of the pulse peak modulation two sidebands appeared to the pulse repetition frequency with a separation of about 200 kHz. This modulation frequency corresponds well with the lifetime of the first excited state in Cr^{4+}:YAG crystal. The strength of the sidebands is more than 20 dB weaker than that of the main peak, which gives an indication of the peak modulation strength. It was experimentally found that if the intracavity light fluence was not sufficiently strong, a significant decay of the ions to the ground state could occur, which further induced strong absorption of the ground state and large peak power fluctuations of the CWML pulse train. Indeed, in the experiment, mode-locked pulse train with large intensity modulation was always observed in the low pump power regime.

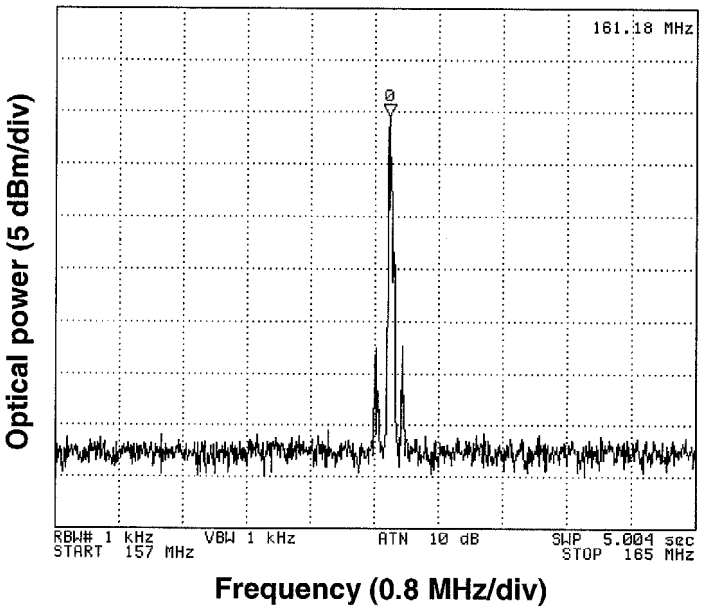

Fig. 7.17: Rf-spectrum of the CWML pulse train measured at the pump power of 11 W with a resoluation of 1 kHz.

7.3 Nd:$GdYVO_4$ – GaAs mode-locking

For the strong illumination on the GaAs wafer, the same cavity configuration and experimental conditions of the passively mode-locked Nd:$GdYVO_4$-Cr^{4+}:YAG laser was employed. In this case, a GaAs semiconductor mirror was used to replace the flat output coupler M_4 of the resonator. The system setup is given in Fig. 7.18.

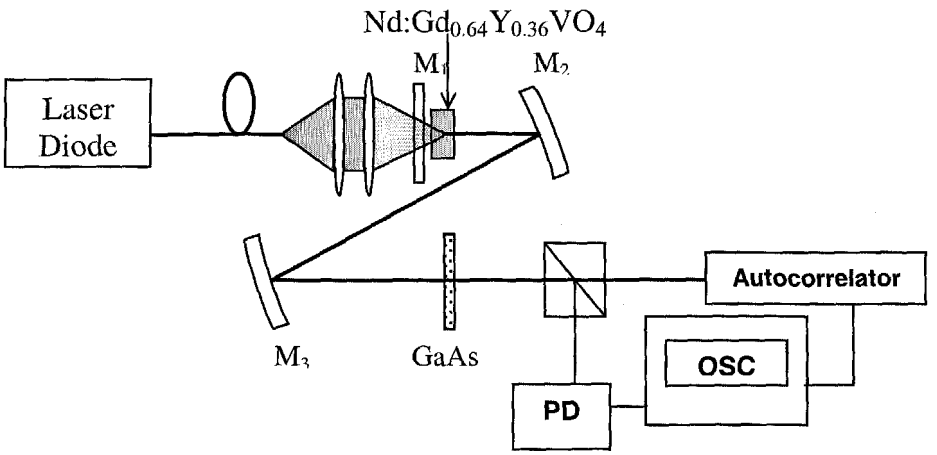

Fig. 7.18: Schematic diagram of the experimental setup. PD: Photodiode. OSC: Osilloscope.

The GaAs wafer is <100>-cut and has a cross-section of 10 mm × 20 mm and a thickness of 450 μm. One side of the GaAs wafer was anti-reflection coated at 1 μm, and the other side was coated to have a continuously varying transmission from T = 3% to 60% along the 20 mm edge direction. The GaAs wafer was simply mounted on a heat sink without extra water-cooling.

With appropriate alignment of the laser cavity, mode-locking of the laser was easily obtained. Fine adjustment on the distance between GaAs mirror and M_3 was made to optimize the mode-locked pulses. By linearly translating the GaAs wafer along the 20mm edge, mode locked operation of the laser under different reflectivity coating of the wafer was experimentally investigated. The quality of the mode-locked pulse train differs with the change of reflectivity on the GaAs wafer. A very unstable mode locked pulse train was observed with the used of the low transmission GaAs wafer coating (T ≈ 6%). While with the high cavity transmission of 20%, the Q-switched mode-locking was

predominately obtained, where the intracavity pulse energy could be too weak to support the CW mode-locking [58]. Only at an appropriate GaAs wafer transmission coating, which in the laser was about T ≈ 10%, a stable CW mode-locked pulse train could be obtained. The CW mode-locking was achieved immediately after the pump strength was beyond the lasing threshold at 3.12 W and increased with respect with pump power to 2.47 W, at a sloping efficiency of 26.6%.

However, as shown in Fig. 7.19, it was observed that a lower lasing threshold resulted from using the relatively higher wafer transmission coating (T ≈ 20%), whereas a slightly higher mode-locked lasing threshold was obtained in contradiction with a lower wafer transmission coating (T ≈ 6%). This might be from different intensity dependent absorption mechanisms coexisting in the GaAs wafer that directly affected the mode-locked laser operation. The nonlinear interaction between the light with the gain medium and the wafer during mode-locking process might be explained based on the viewpoint of the grating induced loss. In a low transmission cavity, because of the high energy fluence, photorefractive grating formed in the GaAs is strong. The induced loss could hence be higher than that of the high transmission cavity to achieve the mode-locking operation.

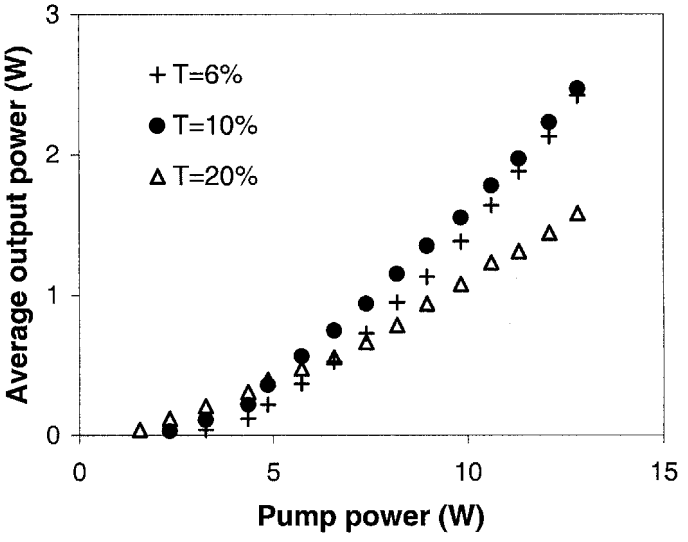

Fig. 7.19: Average output power versus pump power at different GaAs wafer transmission.

Fig. 7.20 shows the oscilloscope trace of a CW mode-locked pulse train. The pulse repetition rate is about 161.3 MHz, which corresponds to the mode spacing of the laser cavity length. Due to the bandwidth limitation of the detection system, the actual mode-locked pulse cannot be resolved by the oscilloscope trace.

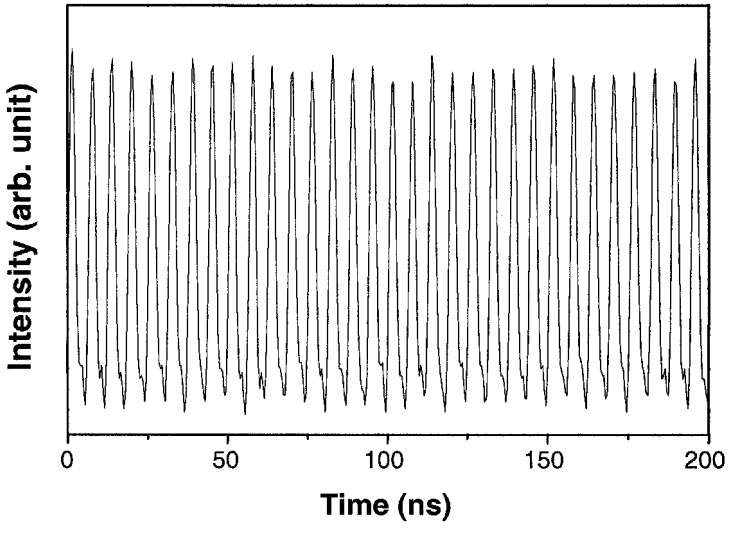

Fig. 7.20: The observed CW-mode-locked pulse train.

Therefore, the commercial autocorrelator was further used to characterize mode-locked pulses. A typical measured autocorrelation trace is shown in Fig. 7.21. The full width at the half maximum (FWHM) of the autocorrelation trace is about 12.5 ps. If a Gaussian pulse profile is assumed, the pulse width of the mode-locked pulses is then estimated as about 8.8 ps. It was noted that the obtained pulse width is a few times narrower than that achieved on the Nd:$GdVO_4$ laser mode-locked with the same GaAs absorber mirror [117]. The narrower pulse width is deduced from two factors. One is that the nonlinearity in the GaAs was enhanced in the current folded-mirror cavity design through the smaller focus beam size compared to that in the two-mirror cavity; the other may be attributed accordingly to the broader gain bandwidth of the neodymium mixed-gadolinium-yttrium vanadate crystal.

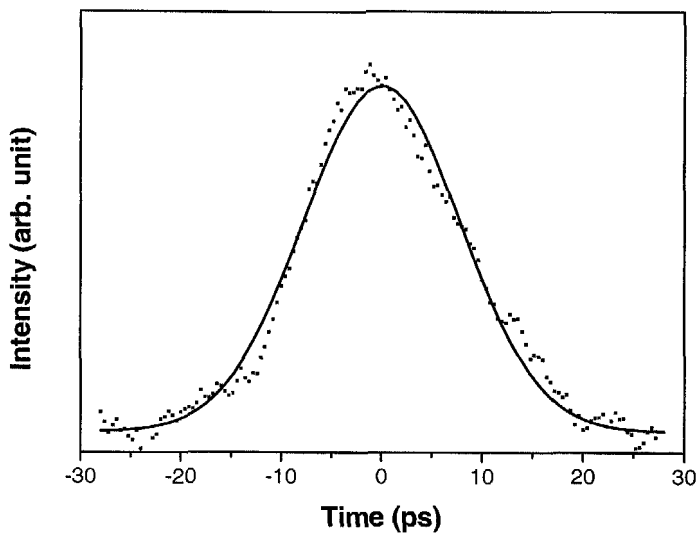

Fig. 7.21: Autocorrelation trace of the CW mode-locked pulses. Dots – Experimental data; Solid line – Gaussian fit.

The corresponding optical spectrum of the mode-locked pulses was measured using an optical spectrum analyzer (ANDO, AQ6317). Under a scanning resolution of 0.01 nm, the optical spectral bandwidth of the mode locked pulses was measured as about 0.336nm centered at the 1063 nm. This then gives the time-bandwidth product of the mode-locked pulses of about 0.785. This time-bandwidth product value is far greater than that of a Gaussian transform-limited pulse, which suggests that the mode-locked pulses are strongly chirped. Considering that the mode-locked pulses obtained in the Nd:$GdVO_4$-GaAs laser are not transform-limited either, the strong chirp should be due to the material properties of the GaAs. It was believed that with proper selection of the saturable absorber, shorter mode-locked pulses are potentially obtainable with the Nd:$GdYVO_4$ laser.

7.4 Summary

In conclusion, passively mode-locked Nd:$GdYVO_4$ lasers have been firstly demonstrated using the material properties of the Cr^{4+}:YAG crystal and GaAs semiconductor output mirror. In the Nd:$GdYVO_4$-Cr^{4+}:YAG mode-locking operation, besides the Q-switched mode-locked pulses, a continuous-wave mode locking was also experimentally realized, for the first time to our knowledge in the laser, under a strong intracavity pulse energy fluence. This shows that passive mode-locking with Cr^{4+}:YAG laser is not only restricted to the conventional QML operation as reported so far, whereas, the condition to achieve the CWML in this laser depends mainly on whether the excited state absorption is dominant to control the laser dynamics. This is only possible when the Cr^{4+}:YAG

saturable absorber is fully bleached and hence, there has been no significant change of cavity Q-factor induced by the ground state absorption.

In practice, the Nd:$GdYVO_4$ laser has successfully achieved the CWML when passively mode-locked by a Cr^{4+}:YAG crystal with the initial transmission of 50%. Average output power of 1.36 W at a slope efficiency of 29.2% was obtained in the experiment. On the other hand, Cr^{4+}:YAG with initial transmission of 60% is able to mode-lock the Nd:$GdYVO_4$ laser to a modulation depth of 90%. The peak power of the mode locked pulse near the maximum of the Q-switched envelope was estimated to be about 1.7 MW at the pump power of 12 W. At such launching power, the QML has achieved a maximum average output power of 1.85 W at a slope efficiency of 31.9%. Basically, both CWML and QML lasers have a same mode-locked pulse width of about 2.96 ps with a repetition rate of 161.3 MHz. In the passively QML laser operation, chaotic dynamics were observed once again in the Q-switching regime. The nonlinear light interactions in the microsecond range of dynamic laser relaxation has essentially no influence on the few ns of mode-locked pulse train, and so to the ps of narrow mode-locked pulses. Nevertheless, this phenomenon has further confirmed the intrinsic nature of the laser in the passive Q-switching.

Under the similar cavity conditions, passively mode locked Nd:$GdYVO_4$ laser has been conducted using a GaAs saturable absorber mirror. The mode-locking mechanism in the GaAs may be attributed to the nonuniform spatial charge distribution. The induced photorefractive gratings cause light diffraction and hence cavity loss modulation. Despite the nonlinear properties of GaAs not being ideal to achieve excellent performance in mode-locking, mode locked pulses with pulse width of about 8.8 ps were obtained

experimentally at a pulse repetition rate of 161.3MHz. A maximum average output power of 2.47 W was obtained with a slope efficiency of 26.6%. Compared to the reported results of the Nd:$GdVO_4$-GaAs mode-locked laser, the narrower pulse width is arrived at two factors, corresponding to the broader gain bandwidth of the Nd:$GdYVO_4$ laser. Based on the fact that mode locking is possible only when a laser operates stably on a single transverse mode with diffraction-limited beam quality, M^2 parameter of the lasers during mode-locking is not further determined in the experiment.

The experimental results show that Nd:$GdYVO_4$ could be used for high power ultrashort pulse lasers. In particular, its broader emission spectrum bandwidth enables it to be favorable over other Nd-doped gain media for the purpose. The simplicity, low cost and robustness of the mode-locked laser with either its high peak power or ultrashort rapid pulses would be ideal for many applications.

CHAPTER 8

Conclusion and recommendations

8.1 Conclusion

This thesis details the investigation of the lasing characteristics of the newly developed neodymium gadolinium vanadate Nd:$GdVO_4$ and neodymium mixed-gadolinium-yttrium vanadate Nd:$Gd_{0.64}Y_{0.36}VO_4$. Lasers operating in continuous wave, Q-switching and mode-locking have been demonstrated.

The thermal effect in Nd:$GdVO_4$ which is proportional to the laser doping level was considered carefully in the optimal laser cavity design to avoid the drastic cavity diffraction loss and the decrease of pump efficiency. The experimental results revealed that lightly doped Nd:$GdVO_4$ is potentially efficient for high power continuous-wave laser output. However, the heavily doped Nd:$GdVO_4$ laser with stronger pump absorption coefficient is more favorable for generating higher peak power of passively Q-switched pulses provided that the thermal effect is well taken into account in the cavity design. High doping level determines the achievable population inversion, which is essential for energy storage for Q-switched lasers. In addition, thermal focal lens in the gain medium could be used to enhance the saturation of saturable absorber.

The characteristics of the laser passive Q-switching are basically determined by the interaction of light with gain medium and saturable absorber in the laser cavity. Through the comprehensive investigation of the effective laser parameters, such as laser doping concentration, saturable absorption loss, cavity coupling transmission and the crystal anisotropic effect, the optimum passively Q-switched Nd:$GdVO_4$ laser has been

achieved. Contrary to the common understanding that higher Q-switched pulse energy is determined by the smaller laser emission cross section, experimental results show that the c-polarized Nd:$GdVO_4$ laser is more efficient in generating high peak power pulses in spite of its large gain cross section. In such laser condition, an appropriate combination of doping concentration in gain medium and saturable absorber as well as the cavity transmission loss is more important to achieve the optimum Q-switched output.

Despite the fact that the c-cut Nd:$GdVO_4$ laser without the polarization loss showed better performance at the low pumping regime, the attainable Q-switched output was limited under certain pump power. The same phenomenon was observed in the a-polarized Nd:$GdVO_4$, which is also with the small stimulated emission cross section. Based on the existence of the strong luminescence at 401 nm in this case, it is believed that the degraded laser performance could be a result of the nonlinear interactions such as the excited state absorption, energy upconversion transfer in the excited laser energy level. The detected visible spectra were found to be compatible with the quantum energy level in Nd- ion doped lasers.

Detailed studies on the nanosecond Nd:$GdVO_4$ Q-switched pulse profile show that there is a small secondary pulse ensuing the Q-switched main pulse. The appearance of the satellite pulse is dependent on the laser parameters, such as the pumping power, doping level of laser and absorber, and cavity coupling transmission. On the other hand, for the lightly doped Nd:$GdVO_4$ laser, which is able to produce intense Q-switching compared to the Nd:$GdVO_4$, a weak satellite pulse is observable in the generated Q-switched pulses, while none is found in the same doping level of Nd:$GdVO_4$ laser. This fact implies that the laser energy storage is essential to determine the appearance of Q-

switched satellite pulse in the lasers. The results of the coupled rate equations model, after considering the finite relaxation rate of the lower laser energy level, show that the Q-switched secondary pulse results from the slow ion relaxation to the laser ground state. The slow relaxation of the ions in the lower energy level obstructs the decay of the stored laser energy, and further reduces the energy extraction for the main Q-switched pulse. Based on the numerically reproduced Q-switched pulse profile, the relaxation time of the lower energy level of Nd:$GdVO_4$ is found to be about 20 ns.

The dynamics of passively Q-switched laser under the repetitive pumping process were explicitly studied. It was found that stability of the Q-switched pulse train is related to the ion circulation within the energy levels. Under the strong pumping, the active ions transition within the laser energy levels could be affected by the finite number of ions in the ground state, associated with the delay of ions decay to the ground state from the lower laser energy level. The observed unstable Q-switched pulse train has so far been described as the cause of external noise and perturbation. Nevertheless, the deterministic chaos revealed during the passive Q-switching in experiments strongly suggests that the laser dynamic behavior is an intrinsic feature of the diode-pumped passive Q-switched lasers. Besides Nd:$GdVO_4$ and the Nd:$GdYVO_4$ laser, period-doubling route to chaos was observed in all major kind of Nd-ion doped lasers, such as Nd:YAG and Nd:YVO_4. By taking into account the finite ion population in the laser ground state, the feature of period-doubling route to chaos was successfully reproduced in the numerical simulation based on an extended rate equations model.

Excellent performance of the Nd:$Gd_{0.64}Y_{0.36}VO_4$ laser was found under the pulsed laser operation of either Q-switching or mode-locking. For the passively Q-

switched operation which was carried out under the same experimental conditions, Q-switched pulses generated in the 0.5 at.% Nd:$GdYVO_4$ laser possessing three times higher energy than that obtained in the lightly doped Nd:$GdVO_4$ laser. In the existing passively Q-switched Nd:$GdYVO_4$ laser, an appropriately coated GaAs output coupler was explicitly used to replace the normal cavity output mirror. Based on this simple approach, a pulse-narrowing effect on the Q-switched pulses was successfully obtained.

Benefiting from the broad emission linewidth and prominent ability of energy storage, the passively mode-locked Nd:$GdYVO_4$ laser in a Z-fold cavity has generated pulses of about three picoseconds by using a Cr^{4+}:YAG saturable absorber. As a result of the Cr^{4+}:YAG excited state absorption, both the conventional Q-switched mode-locking and continuous-wave mode-locking were realized in the Nd:$GdYVO_4$ laser. CWML is found to be feasible by using Cr^{4+}:YAG as saturable absorber, provided all the ground state Cr^{4+} ions are practically excited to the first excited state. This laser can provide either high peak power or ultrafast stable pulse train, which will find more laser applications. In the Q-switched mode-locking regime, the feature of deterministic chaos was also observed, which further confirms that laser dynamic behavior is an intrinsic nature of the passively Q-switched Nd ion-doped lasers. Under the same cavity configuration, Nd:$GdYVO_4$ was also passively mode-locked by GaAs wafer. As it is believed that the loss modulation mechanism in GaAs may be attributed to the nonlinear photorefractive grating formed in the GaAs output coupler. In such operation, CWML was easily achieved in the laser by using the GaAs wafer as an output coupler.

From the experimental evidences, it is found clearly that Nd:$GdVO_4$ and Nd:$GdYVO_4$ crystals exhibiting excellent crystal properties and good lasing

characteristics. Their strong pump beam absorption and high gain emission over Nd:YAG together with the considerably large heat susceptibility are undeniable the important elements to the development of solid-state lasers. In addition, feasibility of the lasers incorporated with the low cost Cr^{4+}:YAG and GaAs saturable absorbers for high peak power pulsed operations further shows the significant commercial implication of the lasers. Although efforts are still needed to transfer the experimental prototypes to mass produced systems as which in the semiconductor lasers industry, however, from this point of view, it is believed that Nd:$GdVO_4$ and Nd:$GdYVO_4$ are potential to become another substitution to the versatile Nd:YAG laser as a low-cost but high-reliable lasing source.

8.2 Future work

Comprehensive investigation of the potential of mixed gadolinium-yttrium vanadate crystal is constrained by the availability of samples. It is believed that there would have different characteristics for different mixing composition of Y^{3+} and Gd^{3+} ions in the vanadate crystal. The Gd/Y concentration could greatly affect the optical and thermal features of the laser materials. For instance, high Gd/Y yields a broader emission linewidth, while low Gd/Y is good in thermal quality. Therefore, good characterization and development of this newly developed Nd:$Gd_xY_{1-x}VO_4$ will be crucial in determining optimum laser performance corresponding to the laser applications.

Since higher laser doping concentration was found to be favorable in passive Q-switching. It is suggested increasing the doping level of Nd:$Gd_{0.64}Y_{0.36}VO_4$ crystal to mildly or heavily doped for fully exploiting the potential in achieving high pulse energy

and peak power. Good thermal property of the laser will make it preferable to operate with its high doping concentration under the strong pumping regime.

From the experimental and numerical results, it is believed that pulse jitter observed in the passive Q-switching is from the physical nature of laser systems. Instead of using continuous-wave pumping approach, it would be feasible to apply a rapid modulation pulsed pump source to avoid the laser ground state saturation, which might be able to avoid the perturbation on ion circulation during the Q-switched interval. In addition, chaos control techniques such as optoelectronic feedback control will be able to properly suppress the pulse fluctuations in the passive Q-switching, and make it attractive in applications. On the other hand, based on the customized ability of semiconductor saturable absorber mirror (SESAM) in giving the rapid switching modulation, the Q-switched secondary pulse in the current laser would be avoided to enhance the pulse energy extraction.

The ultrafast laser technology with femtosecond pulses is an extension of the mode-locking concept. For this purpose, the picoseconds mode-locked pulses achieved in the experiments by using the Cr^{4+}:YAG absorber and GaAs can be further narrowed with the use of dispersion control element in the cavity. This enhancement can be done through the implementation of intracavity prism-pair which exhibits negative dispersion. As the pulse passes through the prisms, the short-wavelength components being refracted at greater angle will travel faster to catch up the long-wavelength components and result in pulse compression. Corresponding to the broad gain bandwidth of the Nd:$Gd_{0.64}Y_{0.36}VO_4$ laser, the useful subpicosecond pulses could be feasibly achieved in the laser with this added dispersion compensation technique. Chirped mirror designs in

the recent technology that incorporate saturable absorber layers for mode-locking is also another potential alternative to provide simultaneously Fourier-limited femtosecond pulses over more bandwidth without any special cavity design. On the other hand, by using the fabricated quantum well semiconductor saturable absorber mirror, which is able to provide proper control and designation for the optimal laser performance, the mode-locked laser can be further improved to the generation of subpicosecond optical pulses. Apart from the experimental work, theoretical analysis is actually necessary to study the interaction of gain medium with Cr^{4+}:YAG or GaAs saturable absorber and to further explore the physical mechanism of mode-locked lasers.

In fact, potential of Nd:$GdVO_4$ and Nd:$GdYVO_4$ crystals is significant according to the lasers performance achieved experimentally. For the starting point of technical progress and innovative concept on the laser technology is from the reliable laser sources, the following step should focus on exploiting the mature and marketable applications. Based on the good lasing properties and high peak power obtained in the investigation, implementation of physical ideas on nonlinear wavelength conversion to other optical spectra is greatly desirable. By using the intense near infrared radiation, frequency doubling and tripling to the green and ultraviolet visible regions can be easily done for material processing. Wavelength extension of the high peak-power Nd:$GdVO_4$ and Nd:$GdYVO_4$ lasers to the mid infrared is also plausible through optical parametric oscillation for molecular spectroscopy and remote LIDAR application. Generally conversion efficiency of generating higher harmonics of frequency components goes down by increasing multiplication factor. Moreover, some of these spectra are accessible by the inexpensive, direct electrical pumped semiconductor lasers. However, replacement

of solid-state lasers by semiconductor laser source is still impossible for those applications that require high optical coherence and monochromicity, such as holography, and interferometry. Combining with the nearly diffractive limited beam, the pulsed operations of Nd:$GdVO_4$ and Nd:$GdYVO_4$ solid-state lasers are particularly more practical and efficient than the broad spectra diode lasers in micromachining. Nonetheless, compared to the semiconductor lasers, solid-state laser systems are relatively big in size, and costly with the related pump source, optics, nonlinear crystals, and control systems. Tedious laser alignment and optical design are also the factors to increase the difficulties in operations. For the practical consideration, simplification of the laser systems to table top design, and reduction of maintenance cost might be obtained by replacing water chiller to thermo-electric cooler. Active Q-switch components like acousto-optics and electro-optics would be also preferred to facilitate the control and increase the efficiency in laser applications.

AUTHOR'S PUBLICATIONS

1. D. Y. Tang, **S. P. Ng**, L. J. Qin, X. L. Meng, "Deterministic chaos in a diode-pumped Nd:YAG laser passively Q-switched by a Cr^{4+}:YAG crystal," Opt. Lett. **28**, 325-327 (2003).
2. **S. P. Ng**, D. Y. Tang, L. J. Qin, X. L. Meng, "High power passively Q-switched Nd:$GdVO_4$ lasers," Opt. Commun. **229**, 331-336 (2004).
3. **S. P. Ng**, D. Y. Tang, J. Kong, L. J. Qin, X. L. Meng, Z. J. Xiong, "Passive mode-locking of a diode pumped Nd:$Gd_{0.64}Y_{0.36}VO_4$ laser with a GaAs saturable absorber mirror," Appl. Phys. B **80**, 475-477 (2005).
4. **S. P. Ng**, D. Y. Tang, J. Kong, Z. J. Xiong, T. Chen, L. J. Qin, X. L. Meng, "Quasi-cw diode-pumped Nd:$GdVO_4$ laser passively Q-switched and mode-locked by Cr^{4+}:YAG saturable absorber," Opt. Commun. **250**, 168-173 (2005).
5. **S. P. Ng**, D. Y. Tang, L. J. Qin, X. L. Meng, Z. J. Xiong, "Q-switched and continuous-wave mode-locking of a diode pumped Nd:$Gd_{0.64}Y_{0.36}VO_4$-Cr^{4+}:YAG laser," Appl. Phys. B **81**, 511-515 (2005).
6. **S. P. Ng** and D. Y. Tang, A. Q. Liu, L. J. Qin, X. L. Meng, "Short pulse passively Q-switched Nd:GdYVO4 laser using a GaAs mirror," Opt. Commun (DOI information: 10.1016/j.optcom.2005.08.056).
7. **S. P. Ng** and D. Y. Tang, L. J. Qin, X. L. Meng, Z. J. Xiong, "Period-doubling route to chaos in diode-pumped passively Q-switched Nd:$GdVO_4$ and Nd:YVO_4 lasers," Int. J. Bifurcat. Chaos **16** (to be published in 2006).

8. **S. P. Ng**, D. Y. Tang, L. J. Qin, X. L. Meng, "Polarization resolved study on the diode pumped passively Q-switched Nd:$GdVO^4$ lasers," submitted to Appl. Opt.
9. **S. P. Ng**, D. Y. Tang, L. J. Qian, L. J. Qin, "Satellite pulse generation in diode-pumped passively Q-switched Nd:GdVO4 lasers," submitted to IEEE J. Quantum Electron.
10. **S. P. Ng**, D. Y. Tang, L. J. Qin, X. L. Meng, "High power diode-pumped Nd:$GdVO_4$ lasers passively Q-switched by Cr^{4+}:YAG crystals," in *The 5th Pacific Rim Conference on Lasers and Electro-Optics*, 763-764 (2003).
11. **S. P. Ng**, D. Y. Tang, L. J. Qin, X. L. Meng, "Deterministic chaos in passively Q-switched solid-state lasers," in *Dynamics Day '04* (2004).
12. **S. P. Ng**, D. Y. Tang, J. Kong, L. J. Qin, X. L. Meng, Z. J. Xiong, "Diode-pumped passively Q-switched and continuous-wave mode-locked Nd:$Gd_{0.64}Y_{0.36}VO_4$ - Cr^{4+}:YAG laser," **Outstanding paper award** in *Symposium on Technology Fusion of Optoelectronics and Communications (STFOC '05) — International Conference on Photonics*, 112-113 (2005).
13. J. Kong, D. Y. Tang, **S. P. Ng**, "GaAs wafer for passive mode locking and compression of energetic Q-switched pulses," in *3rd International Conference on Materials for Advanced Technologies (ICMAT 2005)*, 3-8 (2005).
14. **S. P. Ng**, D. Y. Tang, L. J. Qin, X. L. Meng, Z. J. Xiong, "Q-switched and continuous-wave mode-locked Nd:$Gd_{0.64}Y_{0.36}VO_4$ - Cr^{4+}:YAG laser," **Invited book chapter** for *Modern Technology of Optoelectronics and Communications*.

REFERENCES

[1] Albert Einstein, "Zur quantentheorie der strahlung," Mitt. Phys. Ges. **18**, 47-62, Zurich, (1916). An English translation is in B. L. van der Waerden, ed., *Sources of Quantum Mechanics* (North-Holland, Amsterdam, 1967).

[2] J. Weber, "Amplification of microwave radiation by substances not in thermal equilibrium," Transactions IRE Professional Group on Electron Devices **3**, 1-4 (1953).

[3] T. H. Maiman, "Stimulated optical radiation in ruby lasers," Nature **187**, 493-494 (1960).

[4] Richard C. Powell, *Physics of solid-state laser materials* (Springer-Verlag, New York, 1998), Chap. 9.

[5] T. Kushida and J.E. Geusic, "Optical refrigeration in Nd-doped yttrium aluminum garnet," Phys. Rev. Lett. **21**, 1172-1175 (1968).

[6] P. P. Yaney, L. G. DeShazer, "Spectroscopic studies and analysis of the laser states of Nd^{3+} in YVO_4," J. Opt. Soc. Am. **66**, 1405-1414 (1976).

[7] A. W. Tucker, M. Birnbaum, C. L. Fincher, J. W. Erler, "Stimulated-emission cross section at 1064 and 1342 nm in Nd:YVO_4," J. Appl. Phys. **48**, 4907-4911 (1977).

[8] T. S. Lomheim, L. G. DeShazer, "Optical absorption intensities of trivalent neodymium in the uniaxial crystal yttrium orthovanadate," J. Appl. Phys. **47**, 5517-5522 (1978).

[9] R.A. Fields, M. Birnbaum and C.L. Fincher, Appl. Phys. Lett. "Highly efficient Nd:YVO_4 diode-laser end-pumped laser," **51**, 1885-1886 (1987).

[10] A. I. Zagmennyi, V. G. Ostromov, I. A. Shcherbarkov, T. Jensen, J. P. Meyn, and G. Huber, "The Nd:$GdVO_4$ crystal: new material for diode pumped lasers," Sov. J. Quantum Electron. **22**, 1071-1072 (1992).

[11] J. Liu, Z. Shao, H. Zhang, X. Meng, L. Zhu, M. Jiang "Diode-laser-array end-pumped 14.3 W CW Nd:$GdVO_4$ solid-state laser at 1.06 μm," Appl. Phys. B **69**, 241-243 (1999).

[12] C. Wang, Y. T. Chow, L. Reekie, W.A. Gambling, H. J. Zhang, L. Zhu, X. L. Meng "A comparison study of the laser performance of diode-laser-pumped Nd:$GdVO_4$ and Nd:YVO_4 crystals," Appl. Phys. B **70**, 769-772 (2000).

[13] D. Y. Shen, H. R. Yang, J. G. Liu, S. C. Tam, Y. L. Lam, W. J. Xie, J. H. Gu, K. Ueda, "Efficient and compact intracavity-frequency-doubled Nd:$GdVO_4$/KTP laser end-pumped by a fiber-coupled laser diode," Appl. Phys. B **72**, 263-266 (2001).

[14] V. V. Kochurikhin, K. Shimamura, T. Fukuda, "Czochralski growth of gadolinium vanadate single crystals," J. Cryst. Growth **151**, 393-395 (1995).

[15] L. J. Qin, X. L. Meng, J. G. Zhang, L. Zhu, H. J. Zhang, B. C. Xu, H. D. Jiang, "Growth and defects of Nd:$GdVO_4$ single crystal," J. Cryst. Growth **242**, 183-188 (2002).

[16] L. J. Qin, X. L. Meng, L. Zhu, J. H. Liu, B. C. Xu, H. Z. Xu, F. Y. Jiang, C. L. Du, X. Q. Wang, Z. S. Shao, "Influence of the different Gd/Y ratio on the properties of Nd:$Y_xGd_{1-x}VO_4$ mixed crystals," Chem. Phys. Lett. **380**, 273-278 (2003).

[17] L. J. Qin, X. L. Meng, C. L. Du, L. Zhu, B. C. Xu, Z. S. Shao, Z. Q. Liu, Q. Fang, R. F. Cheng, "Growth and properties of mixed crystal Nd:$YGdVO_4$," J. Alloy. Compd. **354**, 259-262 (2003).

[18] J. H. Liu, X. L. Meng, Z. S. Shao, M. H. Jiang, B. Ozygus, A. Ding, and H. Weber, "Pulse energy enhancement in passive Q-switching operation with a class of Nd:$Gd_xY_{1-x}VO_4$ crystals," Appl. Phys. Lett. **83**, 1289-1291 (2003).

[19] J. Isasi, M. L. Veiga, Y. Laureiro, R. Saez-Puche, C. Pico, "Synthesis, structural determination and magnetic behaviour of $Y_xGd_{1-x}VO_4$ phases (x = 0.25, 0.50, 0.75)," J. Alloy. Compd. **177**, 143-147 (1991).

[20] F. G. Anderson, H. Weidner, P. L. Summers, R. E. Peale, X. X. Zhang, B. H. T. Chai, "Effect of Gd^{3+} substitution for Y^{3+} in $YLiF_4$, $KLiYF_5$, and YVO_4, X. X. Zhang, B. H. T. Chai, J. Lumin. **60/61,** 150-153 (1994).

[21] K. Byrappa, B. Nirmala, M. Yoshimura, "Crystal growth of Nd:RVO_4 (where R = Y, Gd) under mild hydrothermal condition," Mat. Sc. Forum **315-317**, 506-513 (1999).

[22] L. H. Zhang, Y. Hang, D. L. Sun, X. B. Qian, S. F. Li, S. T. Yin, B. Li, B. M. Wu, "Growth and basic properties of Nd^{3+}:$Y_{0.5}Gd_{0.5}VO_4$ crystal," Journal of Functional Materials and Devices **9**, 143-146 (2003).

[23] D. R. Lide (ed.), *CRC Handbook of chemistry and Physics* (CRC Press, Boca Raton, 1991, 72nd ed.), 4-121.

[24] H. J. Zhang, J. H. Liu, J. Y. Wang, C. Q. Wang, L. Zhu, Z. S. Shao, X. L. Meng, X. B. Hu, M. H. Jiang, "Characterization of the laser crystal Nd:$GdVO_4$," J. Opt. Soc. Am. B **19**, 18-27 (2002).

[25] http://www.itieo.com/data/NdYVO4datasheet.pdf

[26] M. Higuchi, H. Sagae, K. Kodaira, T. Ogawa, S. Wada, H. Machida, "Float zone growth of Nd:$GdVO_4$ single crystals along [110] direction and their laser performance," J. Cryst. Growth **264**, 284-289 (2004).

[27] H. Y. Shen, X. L. Meng, G. Zhang, J. J. Qin, W. Liu, L. Zhu, C. H. Huang, L. X. Huang, M. Wei, "Sellmeier's equation and the expression of the thermal refractive-index coefficient for a $Nd_{0.007}Gd_{0.993}VO_4$ crystal," Appl. Opt. **43**, 955-960 (2004).

[28] H. J. Zhang, X. L. Meng, L. Zhu, H. Z. Zhang, P. Wang, J. Dawes, C. Q. Wang, Y. T. Chow, "Investigations on the growth and laser properties of Nd:$GdVO_4$ single crystal," Cryst. Res. Technol. **33**, 801-806 (1998).

[29] T. Jensen, V. G. Ostroumov, J.-P. Meyn, G. Huber, A. I. Zagumennyi, I. A. Shcherbakov, "Spectroscopic characterization and laser performance of diode-laser-pumped Nd:$GdVO_4$," Appl. Phys. B **58**, 373-379 (1994).

[30] A. I. Zagumennyi, V. G. Ostroumov, I. A. Shcherbakov, T. Jensen, J. P. Meyan, G. Huber, "Nd:$GdVO_4$ crystal. A new material for diode-pumped lasers," Sov. J. Quantum Electron. **22**, 1071-1072 (1992).

[31] J. H. Liu, Z. P. Wang, X. L. Meng, Z. S. Shao, B. Ozygus, A. Ding, H. Weber, "Improvement of passive Q-switching performance reached with a new Nd-doped mixed vanadate crystal Nd:$Gd_{0.64}Y_{0.36}VO_4$," Opt. Lett. **28**, 2330-2332 (2003).

[32] J. L. He, C. K. Lee, J. Y. J. Huang, S. C. Wang, C. L. Pan, K. F. Huang, "Diode-pumped passively mode-locked multiwatt Nd:GdVO4 laser with a saturable Bragg reflector", Appl. Opt., **42**, 5496-5499 (2003).

[33] M. L. Kliewer, R. C. Powell, "Excited state absorption of pump radiation as a loss mechanism in solid-state lasers," IEEE J. Quantum Electron. **27**, 1850-1854 (1989).

[34] L. Fornasiero, S. Kuck, T. Jesen, G. Huber, B. H. T. Chai, "Excited state absorption and stimulated emission of Nd^{3+} in crystals. Part 2: YVO_4, $GdVO_4$, and $Sr_5(PO_4)_3F$," Appl. Phys. B **67**, 549-533 (1998).

[35] V. Ostroumov, T. Jensen, J.-P. Meyn, G. Huber, M. A. Noginov, "Study of luminescence concentration quenching and energy transfer upconversion in Nd-doped $LaSc_3(BO_3)_4$ and $GdVO_4$ laser crystals," J. Opt. Soc. Am. B 15, 1052-1060 (1998).

[36] A. I. Zagumennyi, G. B. Lutts, P. A. Popov, N. N. Sirota, I. A. Shcherbakov, "The thermal conductivity of YAG and YSAG laser crystals," Laser Phys. **3**, 1064-1065 (1993).

[37] H. J. Zhang, L. Zhu, X. L. Meng, Z. H. Yang, C. Q. Wang, W. T. Yu, Y. T. Chow, M. K. Lu, "Thermal and Laser Properties of Nd:YVO_4 Crystal," Crys. Res. Technol. **34**, 1011-1016 (1999).

[38] Z. Xiong, Z. G. Li, N. Moore, W. L. Huang, G. C. Lim, "Detailed investigation of thermal effects in longitudinally diode-pumped Nd:YVO_4 lasers," IEEE J. Quantum Electron. **39**, 979-986 (2003).

[39] L. J. Qin, X. L. Meng, H. Y. Shen, L. Zhu, B. C. Xu, L. X. Huang, H. R. Xia, P. Zhao, "Thermal conductivity and refractive indices of Nd:$GdVO_4$ crystals," Cryst. Res. Technol. **38**, 793-797 (2003).

[40] J. K. Neelnd, V. Evtuhov, "Measurement of the laser transition cross section for Nd^{3+} in yttrium aluminum garnet," Phys. Rev., **156**, 244-246 (1967).

[41] T. Kushida, H. M. Marcos, and J. E. Geusic, "Laser transition cross section and fluorescence branching ratio for Nd^{3+} in yttrium aluminum garnet," Phys. Rev. **167**, 289-291 (1968).

[42] Y. Sato, T. Taira, "Spectroscopic properties of neodymium-doped yttrium orthovanadate single crystals with high-resolution measurement," Jpn. J. Appl. Phys. **41**, 5999-6002 (2002).

[43] P. A. Studenikin, A. I. Zagumennyi, Y. D. Zavartsev, P. A. Popov, I. A. Shcherbakov, "$GdVO_4$ as a new medium for solid-state lasers: some optical and thermal properties of crystals doped with Nd^{3+}, Tm^{3+}, and Er^{3+} ions," Quantum Electron. **25**, 1162-1165 (1995).

[44] R. L. Byer, "Diode laser-pumped solid-state lasers," Science **239**, 742-747 (1988).

[45] *Laser Focus World* January, **32**, 62-63 (1996).

[46] K. J. Kuhn, *Laser Engineering* (Prentice-Hall, NJ, USA, 1998), Chap. 10.

[47] W. G. Wagner and B. A. Lengyel, "Evolution of the giant pulse in a laser," J. Appl. Phys. **34**, 2040-2046 (1963).

[48] A. Szabo and R. A. Stein, "Theory of laser giant pulsing by a saturable absorber," J. Apply. Phys. **36**, 1562-1566 (1965).

[49] R. B. Kay and G. S. Waldman, "Complete solutions to the rate equations describing Q-spoiled and PTM laser operation," J. Appl. Phys. **36**, 1319-1323 (1965).

[50] J. J. Degnan, "Optimization of passively Q-switched lasers," IEEE J. Quantum Electron. **31**, 1890-1901 (1995).

[51] X. Y. Zhang, S. Z. Zhao, Q. P. Wang, Q. D. Zhang, L. K. Sun and S. J. Zhang, "Optimization of Cr^{4+}-doped saturable absorber Q-switched lasers," IEEE J. Quantum Electron. **33**, 2286-2294 (1997).

[52] X. Y. Zhang, S. Z. Zhao, Q. P. Wang, B. Ozygus and H. Weber, "Modeling of passively Q-switched lasers," J. Opt. Soc. Am. B. **17**, 1166-1175 (2000).

[53] A. E. Siegman, *Lasers*, (Univ. Science, Mill Valley, CA, 1986), Chap. 26.

[54] Y. K. Kuo, M. F. Huang, M. Birnbaum, "Tunable Cr^{4+}:YSO Q-switched Cr:LiCAF laser," IEEE J. Quantum. Electron. **31**, 657-663 (1995).

[55] Y. K. Kuo, H. M. Chen, Y. Chang, "Numerical study of passive Q-switching of a tunable alexandrite laser with a Cr:Y_2SiO_5 solid-state saturable absorber," Appl. Opt. **40**, 1362-1368 (2001).

[56] Y. K. Kuo, Y. A. Chang, "Numerical study of passive Q-switching of a Tm:YAG laser with a Ho:YLF solid-state saturable absorber," Appl. Opt. **42**, 1685-1691 (2003).

[57] F. X. Kärtner, L. R. Brovelli, D. Kopf, M. Kamp, I. Calasso, U. Keller, "Control of solid-state laser dynamics by semiconductor devices," Opt. Eng. **34**, 2024-2036 (1995).

[58] C. Hönninger, R. Paschotta, F. Morier-Genound, M. Moser, U. Kellar, "Q-switching stability limits of continuous-wave passive mode-locking," J. Opt. Soc. Am. B **16**, 46-56 (1999).

[59] U. Keller, " Semiconductor nonlinearities for solid-state lasers modelocking and Q-switching," Semicond. Semimetals **59**, 211-287 (1999).

[60] W. Koechner, *Solid-state laser engineering*, 5th ed. (Springer-Verlag, Berlin, 1999), Chap. 8, 3.

[61] T. T. Kajava, A. L. Gaeta, "Intra-cavity frequency-doubling of a Nd:YAG laser passively Q-switched with GaAs," Opt. Commun. **137**, 93-97(1997).

[62] Ping Li, Qingpu Wang, Xinyu Zhang et al., "Analysis of a diode-pumped Nd:YVO_4 laser passively Q-switched with GaAs," Opt. & Laser Tech. **33**, 383-387 (2001).

[63] J. J. Zayhowski, C. Dill, "Diode-pumped passively Q-switched picosecond microchip lasers," Opt. Lett. **19**, 1427-1429 (1994).

[64] A. Agnesi, S. Dell' Acqua, C. Morello, G. Piccinno, G. C. Reali and Z. Y. Sun, "Diode-pumped neodymium lasers repetitively Q-switched by Cr^{4+}:YAG solid-state saturable absorbers," IEEE J. Selected Topics in Quantum Electron. **3**, 45-52 (1997).

[65] A. Agnesi, S. Dell'Acqua, G. C. Reali, Z. Sun, "High performance Cr^{4+}:YAG Q-switched CW diode pumped Nd:YAG laser," Opt. Quantum Electron. **29**, 429-433, (1997).

[66] Y. F. Chen, S. W. Tsai, and S. C. Wang, "High-power diode-pumped *Q*-switched and modelocked Nd :YVO laser with a Cr :YAG saturable absorber," Opt. Lett. **25**, 1442-1444, (2000).

[67] I. V. Klimov, M. Y. Nikol'skii, V. B. Tsvetkov, I. A. Shcherbakov, "Passive Q switching of pulsed Nd^{3+} lasers using Cr^{4+}:YSGG crystal switches exhibiting phototropic properties," Sov. J. Quamtum Electron. **22**, 653-656 (1992).

[68] J. Bartschke, V. I Klimov, K. J. Boller, R. Wallenstein, "Passive Q-switching of diode end-pumped Nd^{3+}:$GdVO_4$ and Nd^{3+}:YAB lasers by using Cr^{4+}:YAG and Cr^{4+}:YSGG as saturable absorbers," in *Conf. Laser and Electro-Opt.*, OSA Tech. Dig. Ser., Opt. Soc. Amer. Washington, DC, **15**, 126-127 (1995).

[69] R. Moncorge, H. Manaa, F. Deghoul, Y. Guyot, Y. Kalisky, S. A. Pollack, E. V. Zharikov and M. Kokta, "Saturable and excited state absorption measurements in Cr^{4+}:LuAG single crystals," Opt. Commun. **132**, 279-284 (1996).

[70] B. Braun, F. X. Kartner, U. Keller, J. P. Meyn, G. Huber, "Passively Q-switched 180-ps Nd:$LaSc_3(BO_3)_4$ microchip laser," Opt. Lett. **21**, 405-407 (1996).

[71] U. Keller, D. A. B. Miller, G. D. Boyd, T. H. Chiu, J. F. Ferguson, M. T. Asom, "Solid-state low-loss intracavity saturable absorber for Nd:YLF lasers: an antiresonant semiconductor Fabry-Perot saturable absorber," Opt. Lett. **17**, 505-507 (1992).

[72] U. Keller, K. J. Weingarten, F. X. Kärtner, D. Kopf, B. Braun, I. D. Jung, R. Fluck, C. Hönninger, N. Matuschek, J. Aus der Au, "Semiconductor saturable absorber mirrors (SESAMs) for femtosecond to nanosecond pulse generation in solid-state lasers," IEEE J. Sel. Top. Quantum Electron. Special Issue on Ultrafast Electronics, Photonics and Optoelectronics **2**, 435-453 (1996).

[73] B. G. Kim, E. Garmire, S. G. Hummel, P. D. Dapkus, "Nonlinear Bragg reflector based on saturable absorption," Appl. Phys. Lett. **54**, 1095-1097 (1989).

[74] P. Yankov, "Cr^{4+}:YAG Q-switching of Nd:host laser oscillators,"J. Phys. D. **27**, 1118-1130 (1994).

[75] K. Spariosu, W. Chen, R. Stultz, and M. Birnbaum, "Dual Q-switching and laser action at 1.064μm and 1.44μm in a Nd^{3+}:YAG-Cr^{4+}:YAG oscillator at 300 K," Opt. Lett. **18**, 814-816 (1993).

[76] S. Zhou, K. K. Lee, and Y. C. Chen, "Monolithic self-Q-switched Cr, Nd:YAG laser," Opt. Lett. **18**, 511-512 (1993).

[77] L. Lin, B. Ouyang, Y. Leng, X. Wan, "Mode-locked Nd:YAG laser using Cr^{4+}:YAG crystal at 1.064 μm," in *Tech. Dig. CLEO'99*, **Ctuk36**, 134 (1999).

[78] T. M. Jeong, C. M. Chung, H. S. Kim, C. H. Nam, C. J. Kim, "Generation of passively Q-switched and mode-lcked pulse from Nd:YVO_4 laser with Cr^{4+}:YAG saturable absorber," Electron. Lett., **36**, 633-634 (2000).

[79] Y. F. Chen, S. W. Tsai, "Simultaneous Q-switching and mode-locking in a diode-pumped Nd:YVO_4-Cr^{4+}:YAG laser," IEEE J. Quantum. Electron., **37**, 580-586 (2001).

[80] S. J. Zhang, E. Wu, H. P. Zeng, "Q-switched mode-locking by Cr^{4+}:YAG in a laser-diode-pumped c-cut Nd:$GdVO_4$ laser," Opt. Commun. **231**, 365-369 (2004).

[81] L. I. Krutova, N. A. Kulagin, V. A. Sandulendo, and A. V. Sandulenko, "Electonic state and position of chromium ions in garnet crystals," Sov. Phys. Solid State **31**, 1193-1196, (1989).

[82] Y. Shimony, Z. Burshtein, and Y. Kalisky, "Cr^{4+}:YAG as passive Q-switch and Brewster plate in a Nd:YAG laser," IEEE J. Quantum Electron. **31**, 1738-1741, (1995).

[83] X. Y. Zhang, S. Z. Zhao, Q. P. Wang, Q. D. Zhang, L. K. Sun, S. J. Zhang, "Optimization of Cr^{4+}-doped saturable absorber Q-switched lasers," IEEE J. Quantum. Electron. **33**, 2286-2294 (1997).

[84] Z. Burshtein, P. Blau, Y. Kalisky, Y. Shimony, M. R. Kokta, "Excited-state absorption studies of Cr^{4+} ions in several garnet host crystals," IEEE J. Quantum Electron. **34**, 292-299 (1998).

[85] G. C. Valley, A. L. Smirl, "Theory of transient energy transfer in gallium arsenide," IEEE J. Quantum Electron. **24**, 304-310, (1988).

[86] A. L. Smirl, G. C. Valley, K. M. Bohnert, T. F. Boggess, "Picosecond photorefractive and free carrier transient energy transfer in GaAs at 1 μm," IEEE J. Quantum. Electron., **24**, 289-303 (1988).

[87] A. Agnesi, G. P. Banfi, M. M. Costa, M. Ghigliazza, G. C. Reali, "Picosecond nonlinear optical characterization of GaAs at lamda=1.064 um," Proc. SPIE, **1282**, Ultrafast Laser Probe Phenomena in Bulk and Microstructure Semiconductors III, (Robert R. Alfano; Ed.), 50-58 (1990).

[88] J. H. Gu, F. Zhou, W. J. Xie, S. C. Tam, Y. L. Lam, "Passive Q-switching of a diode-pumped Nd:YAG laser with a GaAs output coupler," Opt. Commun. **165**, 245-249 (1999).

[89] L. Pan, X. Hou, Y. Li and Y. Sun, "Passively Q-switched Nd:$GdVO_4$ laser with GaAs saturable absorber" Opt. & Laser Tech. **36**, 121-124 (2004).

[90] Y. He, X. Y. Hou, L. J. Qin, Y. M. Sun, Y. F. Li, H. J. Qi, L. Pan, "Laser-diode pumped passively Q-switched Nd:$Y_xGd_{1-x}VO_4$ laser with a GaAs saturable absorber," Opt. Commun. **234**, 305-308 (2004).

[91] T. T. Kajava and A. L. Gaeta, "Q-switching of a diode-pumped Nd:YAG laser with GaAs", Opt. Lett. **21**, 1244-1246 (1996).

[92] J. Gu, F. Zhou, K. T. Wan, T. K. Lim, S. C. Tam, Y. L. Lam, D. Xu and Z. Cheng, "Q-switching of a diode-pumped Nd:YVO4 laser with GaAs nonlinear output coupler", Opt. Laser Eng. **35**, 299-307 (2001).

[93] T. F. Boggess, JR., A. L. Smirl, S. C. Moss, Ian W. Boyd and Eric W. Van Stryland, "Optical limiting in GaAs", IEEE J. Quantum Electron. **21**, 488-494 (1985).

[94] Z. Zhang, L. Qian, D. Fan and X. Deng, "Gallium arsenide: A new material to accomplish passively mode-locked Nd:YAG laser," Appl. Phys. Lett. **60**, 419-421 (1992).

[95] A. Hordvik, "Pulse stretching utilizing two photon induced light absorption", IEEE J. Quantum Electron. **6**, 199-203 (1970).

[96] T. T. Kajava and A. L. Gaeta, ''Intra-cavity frequency doubling of a Nd:YAG laser passively *Q*-switched with GaAs,'' Opt. Commun. **137**, 93-97 (1997).

[97] M. E. Innocenzi, H. T. Yura, C. L. Fincher, R. A. Fields, "Thermal modeling of continuous-wave end-pumped solid-state lasers," Appl. Phys. Lett. **56**, 1831-1833 (1990).

[98] F. Song, C. B. Zhang, X. Ding, J. J. Xu, G. Y. Zhang, M. Leigh, N. Peyghambarian, "Determination of thermal focal length and pumping radius in gain medium in laser-diode-pumped Nd:YVO_4 lasers," Appl. Phys. Lett. **81**, 2145-2147 (2002).

[99] S. C. Tidwell, J. F. Seamans, M. S. Bowers, A. K. Cousins, "Scaling CW diode-end-pumped Nd:YAG lasers to high average powers," IEEE J. Quantum Electron. **28,** 997-1009 (1992).

[100] J. T. Verdeyen, *Laser Electronics*, (Prentice-Hall Int. Inc., New Jersey, 1995), Chap. 2.

[101] N. Hodgson, H. Weber, *Optical Resonators, Fundamentals, Advanced Concepts and Applications*, (Springer-Verlag, London, 1997), Chap. 22.

[102] C. Li, J. Song, D. Shen, N. S. Kim, J. Lu and K. Ueda, "Diode-pumped passively Q-switched Nd:$GdVO_4$ lasers operating at 1.06 μm wavelength," Appl. Phys. B **70**, 471-474 (2000).

[103] A. Agnesi, A. Del Corno, P. Di Trapani, M. Fogliani,G. C. Reali, J. C. Diels, C. Y. Yeh, X. M. Zhao and V. Kubecek, "Generation of extended pulse trains of minimum duration by passive negative feedback applied to solid-state Q-switched lasers", IEEE J. Quantum Electron. **28**, 710-719 (1992).

[104] J. H. Liu, B. Ozygus, S. Hu. Yang, J. Erhard, T. Seelig, A. Ding, H. Weber, "Effcient passive Q-switching operation of a diode-pumped Nd:$GdVO_4$ laser with a Cr^{4+}:YAG saturable absorber," J. Opt. Soc. Am. B **20**, 652-661 (2003).

[105] A. Agnesi, S. Dell'acqua, "High-peak-power diode-pumped passively Q-switched Nd:YVO_4 laser," Appl. Phys. B **76**, 351-354 (2003).

[106] Y. F. Tso, "Effect of finite lower level lifetime on Q-switched lasers," Quantum Electron. Lett. **24**, 2345-2349 (1988).

[107] H. D. Jiang, H. J. Zhang, J. Y. Wang, H. R. Xia, X. B. Hu, B. Teng, C. Q. Zhang, "Optical and laser properties of Nd:$GdVO_4$ crystal," Opt. Commun. **198**, 447-452 (2001).

[108] http://www.redoptronics.com/Nd-YAG-crystal.html

[109] P.K. Mukhopadhyay, A. Nautiyal, P.K. Gupta, K. Ranganathan, J. George, S.K. Sharma and T.P.S. Nathan, "Experimental determination of the thermo-optic coefficient (dn/dT) and the effective stimulated emission cross-section (σ_e) of an a -axis cut 1.-at. % doped Nd:$GdVO_4$ crystal at 1.06 μm wavelength," Appl. Phys. B **77**, 81-87 (2003).

[110] H. Poincare, *Les meyhodes nouvelle de la mecanique celeste* (Gautheir-Villars, Paris, 1892).

[111] E.N. Lorenz, "Deterministic nonperiodic flow", J. Atmospheric Sciences **20**, 130-141 (1963).

[112] H. Haken, "Analogy between higher Instabilities in Fluids and Lasers," Phys. Lett. **53A**, 77-78 (1975).

[113] F. T. Arecchi, R. Meucci, G. P. Puccioni, J. R. Tredicce, "Experimental evidence of subharmonic bifurcations, multistability, and turbulence in a Q-switched gas laser,"Phys. Rev. Lett. **49**, 1217-1220 (1982).

[114] C. O. Weiss, A. Godone, A. Olafsson, "Routes to chaotic emission in a cw He-Ne laser," Phys. Rev. A **28**, 892-895 (1983).

[115] M. J. Feigenbaum, "Universal behavior in nonlinear systems," Los Alamos Science **1**, 4-27 (1980).

[116] A.M. Fraser, "Reconstructing Attractors from Scalar Time Series: A Comparison of Singular System and Redundancy Criteria," Physica D, **34** 391-404 (1989).

[117] J. Kong, D. Y. Tang, S. P. Ng, B. Zhao, L. J. Qin, X. L. Meng, "Diode-pumped passively mode-locked Nd:$GdVO_4$ laser with a GaAs saturable absorber mirror," Appl. Phys. B **79**, 203-206 (2004).